

MODELLING THE IMPACT OF TREES ON VEHICULAR  
EMISSIONS IN THE URBAN ENVIRONMENT USING  
COMPUTATIONAL FLUID DYNAMICS

Thesis Submitted for the degree of

Doctor of Philosophy

at the University of Leicester

By

Antoine Jeanjean

EARTH OBSERVATION SCIENCE GROUP

DEPARTMENT OF PHYSICS AND ASTRONOMY

The University of Leicester

*Supervisors:* Prof Roland Leigh, Prof Paul Monks, Dr Andrew McMullan

February 15, 2017

# MODELLING THE IMPACT OF TREES ON VEHICULAR EMISSIONS IN THE URBAN ENVIRONMENT USING COMPUTATIONAL FLUID DYNAMICS

Antoine Jeanjean

Abstract

This thesis focuses on the simulation of the impact of trees on vehicular emissions in the urban environment, using CFD (Computational Fluid Dynamics) simulations of air-pollutant concentrations performed under the OpenFOAM software platform (k- $\epsilon$  model). Special attention was paid to the evaluation of the CFD model, by assessing the model results against wind tunnel and tracer experiments, as well as against a road side monitoring station. An overall accuracy of 30 to 40% on simulated concentrations was found, which is comparable to the results of previous studies. Most of the statistical parameters were also found to lie within an acceptable range.

CFD models in the literature typically use idealised buildings to model wind flow and pollution dispersion. However, the methodology used in this thesis uses actual LIDAR data of buildings and trees to reconstruct a 3D representation of the different modelled scenes, such as Leicester City centre ( $2 \times 2$  km area). The modelled areas were on a scale larger than those usually used in other CFD studies. Furthermore, a special focus of this thesis details the interaction between trees and wind flow dynamics. In addition to the study of the aerodynamic effects of trees, the reduction of air pollution by deposition was investigated, which is something that has not yet been modelled at this scale.

A final focus of this thesis was the ranking of current and prospective NO<sub>2</sub> mitigation strategies including trees, building facades coated with photocatalytic paint and solid barriers. Trees were shown to be the most beneficial strategy when combining both economic and environmental effectiveness. With an attractive cost compared to other solutions, tree-planting policies could offer benefits to urban planning when funding is limited.

# Acknowledgments

It has been a great privilege to pursue a PhD at the University of Leicester where I have been honoured to work with my supervisors, Prof Roland Leigh, Prof Paul Monks and Dr Andrew McMullan. They have provided me with invaluable and continuous support for the past 3 years, generously taking time to meet, review, correct and guide me through the program. Doors have always been open (or been made open) to facilitate discussions or the direction of my research. Grateful for the unique opportunity to learn from highly skilled and established academics, I am proud to have had them as supervisors, thank you to all of them.

It has been a pleasure working with Dr. Joshua Vande Hey, especially on air quality related issues within the automotive industry. I express my thanks to the air quality group that meets every Monday afternoon and to the wider EOS family, especially Dr. Hannah Sonderfled and Dr. Hartmut Boesch for the landfill work. A special thank you to my office mates: Phil, Jas, Jordan, Kirsty, Amrita and Alex, for a stimulating work environment. My sincerest thanks to Mrs Colette Godfrey and Mrs Kiri Humphreys, who have sorted out so many administrative issues.

I would like to thank the University of Leicester, for funding part of this work alongside the European Space Agency (ESA) under the uTRAQ project. A special thanks to all the people that contributed to this thesis, in particular, Dr Grant Allen on the landfill work, Dr Riccardo Buccolieri for the Marylebone tree study, Dr John Gallagher for the Oxford Street study and Dr Jolanta Obszynska from Leicester City Council. Thank you Prof Ranjeet Sokhi and Dr Sandro Finardi, for granting me the Young Researcher Award 2016, during the 10<sup>th</sup> International Conference on Air Quality in Milan, Italy.

I want to express my gratitude to God who has been so good to our family. I dedicate this thesis to my wife Glose and two sons Michael and Raphael.

# Contents

<b>1</b>	<b>Air quality in urban atmosphere</b>	<b>1</b>
1.1	Urban atmosphere . . . . .	1
1.1.1	Urban air pollution context . . . . .	1
1.1.2	General introduction to the atmosphere . . . . .	2
1.1.3	Earth's atmosphere composition . . . . .	4
1.1.4	Air quality guidelines . . . . .	5
1.2	Air pollution sources . . . . .	5
1.2.1	Particulate matter . . . . .	5
1.2.2	NO <sub>x</sub> . . . . .	9
1.2.3	Dry deposition velocity . . . . .	12
1.2.4	Projections . . . . .	13
1.3	Air quality issues . . . . .	14
1.3.1	Health impacts . . . . .	14
1.3.2	Degradation of ecosystems and cultural heritage . . . . .	15
1.3.3	Climate change . . . . .	15
1.4	Air pollution mitigation measures . . . . .	16
1.4.1	Removing air pollutants once emitted . . . . .	16
1.4.2	Decreasing the emissions . . . . .	17
1.5	Thesis objectives . . . . .	18
<b>2</b>	<b>Model description and evaluation</b>	<b>20</b>
2.1	Air quality dispersion models . . . . .	20
2.1.1	Existing dispersion models . . . . .	20
2.1.2	Comparisons of dispersion models . . . . .	22
2.2	General considerations . . . . .	24
2.2.1	Generic Navier-Stokes equations . . . . .	24
2.2.2	Resolving the Navier-Stokes equations . . . . .	25

2.3	RANS simulations . . . . .	27
2.3.1	Derivation of RANS equations . . . . .	27
2.3.2	k- $\epsilon$ model equations . . . . .	28
2.3.3	Summary of guidelines for RANS simulations . . . . .	30
2.3.4	Tree modelling . . . . .	34
2.3.5	CFD software platform . . . . .	36
2.4	Model evaluation against wind tunnel measurements . . . . .	37
2.4.1	Wind tunnel description . . . . .	37
2.4.2	CFD parametrisation for the wind tunnel . . . . .	38
2.4.3	CFD comparison with wind tunnel measurements . . . . .	41
<b>3</b>	<b>Air quality affected by trees in real street canyons: the case of Marylebone neighbourhood in central London</b>	<b>48</b>
3.1	Introduction . . . . .	48
3.2	The study site . . . . .	49
3.2.1	Description of geometry and trees . . . . .	49
3.2.2	Description of the cases investigated . . . . .	50
3.2.3	Description of traffic data and pollutant concentration analysis	53
3.3	CFD modelling . . . . .	55
3.3.1	Flow modelling set-up . . . . .	55
3.3.2	Gaseous pollutant modelling set-up . . . . .	56
3.3.3	Modelling the effects of trees . . . . .	57
3.4	Results and discussion . . . . .	59
3.4.1	Comparison between simulations and 4 m height surface data monitored in the Marylebone site . . . . .	59
3.4.2	The influence of trees under different wind directions . . . . .	61
3.4.3	The influence of trees under different wind speeds . . . . .	63
3.4.4	Discussion . . . . .	64
3.5	Conclusions . . . . .	68
<b>4</b>	<b>The effectiveness of trees to disperse road traffic emissions in Le- icester</b>	<b>69</b>
4.1	Introduction . . . . .	69
4.2	Development of the CFD model for the Leicester urban area . . . . .	70
4.2.1	Description . . . . .	70
4.2.2	Numerical modelling . . . . .	72

4.3	City scale CFD results and discussion . . . . .	74
4.3.1	Comparison of a tree-free city to a city with trees . . . . .	74
4.3.2	Effectiveness of trees depending on the prevalent wind direction	80
4.4	Conclusions . . . . .	87
<b>5</b>	<b>The effectiveness of urban trees and grass on PM<sub>2.5</sub> reduction via dispersion and deposition in Leicester</b>	<b>88</b>
5.1	Introduction . . . . .	88
5.2	Experimental . . . . .	90
5.2.1	Model description . . . . .	90
5.2.2	Deposition velocities . . . . .	92
5.3	Results . . . . .	94
5.3.1	Reduction by trees and grass . . . . .	94
5.3.2	Generalisation between PM reduction and vegetation cover . .	96
5.3.3	Wind speed dependence . . . . .	101
5.3.4	Net flux of trees and grass in the summer season over Leicester	104
5.4	Discussion and links with previous studies . . . . .	104
5.4.1	Comparison with the i-Tree model . . . . .	104
5.4.2	Urban tree management . . . . .	105
5.5	Conclusion . . . . .	107
<b>6</b>	<b>Ranking current and prospective NO<sub>2</sub> mitigation strategies: a modelling investigation in Oxford Street, London</b>	<b>108</b>
6.1	Introduction . . . . .	108
6.2	Methods . . . . .	109
6.2.1	Case study: Oxford Street, London . . . . .	109
6.2.2	CFD modelling . . . . .	111
6.3	Modelled area dimensions . . . . .	111
6.4	Grid sensitivity analysis . . . . .	114
6.4.1	Pollution mitigation strategies . . . . .	115
6.4.2	Life cycle costing of mitigation strategies . . . . .	117
6.5	Results . . . . .	117
6.5.1	Ranking environmental performance of pollution mitigation measures . . . . .	117
6.5.2	Spatial visualisation . . . . .	120
6.5.3	Ranking life cycle costs of pollutant mitigation measures . . .	122

6.5.4	Mitigation at pollution hotspots . . . . .	126
6.6	Discussion . . . . .	128
6.6.1	Mitigation strategies strengths and weaknesses . . . . .	128
6.6.2	Pedestrian areas vs on-road pollution . . . . .	129
6.6.3	Child vs adult exposure . . . . .	129
6.6.4	Full street vs hotspots . . . . .	129
6.6.5	Ranking mitigation strategies . . . . .	130
6.7	Conclusions . . . . .	132
<b>7</b>	<b>Conclusion</b>	<b>133</b>
7.1	Model evaluation and performance . . . . .	133
7.2	The use of trees as a mitigation strategy . . . . .	133
7.3	Future work . . . . .	135
7.3.1	Improved tree modelling . . . . .	135
7.3.2	Other model improvements . . . . .	136
7.3.3	The role of CFD in the development of future mitigation strategies . . . . .	137
<b>A</b>	<b>Derivations of the Navier-Stokes equations</b>	<b>139</b>
A.1	Mass conservation . . . . .	139
A.2	Momentum equation . . . . .	140
<b>B</b>	<b>Wind averaged maps</b>	<b>144</b>
B.1	Wind averaged concentration maps . . . . .	144
B.2	Wind averaged concentration difference maps . . . . .	145
B.2.1	Processing steps . . . . .	145
B.2.2	Wind direction dependence . . . . .	145
<b>C</b>	<b>Model real scale application and validation over a landfill site</b>	<b>151</b>
C.1	Introduction . . . . .	151
C.2	Site description and survey . . . . .	153
C.3	Tracer release experiment . . . . .	153
C.3.1	Tracer release test . . . . .	153
C.3.2	Gas sampling . . . . .	153
C.3.3	Wind monitoring . . . . .	155
C.4	CFD modelling . . . . .	155
C.4.1	Method . . . . .	155

C.4.2	Additional modification of the method incorporated in Open-FOAM . . . . .	156
C.5	Results . . . . .	157
C.5.1	Experimental wind conditions . . . . .	157
C.5.2	Measured gas concentration . . . . .	159
C.5.3	CFD simulated concentrations and comparison with the measured data . . . . .	159
C.5.4	Model sensitivity analysis . . . . .	160
C.6	Conclusions . . . . .	163

# List of Tables

1.1	European and WHO guidelines on air quality levels for NO <sub>2</sub> , O <sub>3</sub> and PM. . . . .	5
1.2	Natural and anthropogenic sources of NO <sub>x</sub> worldwide (adapted from Wallace and Hobbs 2006; Jacob 1999). . . . .	10
2.1	Summary of the CFD parametrisation for the wind tunnel. . . . .	39
2.2	Correlation factors ( $R^2$ ) for normalised concentrations between CFD and wind tunnel measurements. . . . .	44
2.3	Wall average normalised concentration C+ comparison between the WT experiment and CFD for a tree-free street canyon and a street canyon with trees. . . . .	46
3.1	Scenarios investigated with different types of trees, seasons and meteorological data simulated. . . . .	52
3.2	Calculated NO <sub>x</sub> and PM <sub>2.5</sub> emissions from annual average daily flows (AADF, annual averaged number of vehicles per 24h). M stands for Marylebone Rd traffic counts, GP for Gloucester Place and BS for Baker Street. . . . .	53
3.3	Pressure loss coefficients of trees ( $\lambda$ ) of the modelled area across the seasons. . . . .	58
3.4	Literature values of deposition velocities of PM <sub>2.5</sub> on vegetation. . . . .	58

3.5	Influence of wind direction on PM <sub>2.5</sub> concentrations emitted by traffic at the Marylebone monitoring station, for a wind speed of 5 m s <sup>-1</sup> , without urban background concentrations. Total percentages (%) are calculated in comparison with seasonal average concentrations of PM <sub>2.5</sub> , corresponding to the wind speed of 5 m s <sup>-1</sup> . The 225° wind direction was not included in the calculation as the results were not satisfactory when compared to measurements. Highlighted numbers correspond to wind directions which result in a beneficial reduction in air pollution because of the aerodynamic dispersion of trees. Aerodynamic and deposition effects are calculated as shown in Fig. 2.6. . . . . .	63
3.6	Influence of wind speed on aerodynamic dispersion and deposition of trees on PM <sub>2.5</sub> concentrations emitted by traffic at the Marylebone monitoring site. . . . .	64
3.7	Effect of trees on average street concentrations of PM <sub>2.5</sub> emitted by traffic, for a wind speed of 5 m s <sup>-1</sup> , without urban background concentrations. Total percentages (%) are calculated in comparison with seasonal average concentrations of PM <sub>2.5</sub> corresponding to the wind speed of 5 m s <sup>-1</sup> . The 225° wind direction was not included in the calculation as the results were not satisfactory when compared to measurements. Highlighted numbers correspond to wind directions for which trees aerodynamic dispersion is beneficial. . . . .	67
4.1	Probability of the wind direction in Leicester from a local weather station. The probabilities have been aggregated every 30 ° ( + / - 15 ° around each wind direction). . . . .	81
5.1	Set of modelled scenarios and associated deposition velocities. . . . .	92
5.2	Coefficients of PM <sub>2.5</sub> reduction at different wind speeds expressed in Eq. 5.2 and Eq. 5.3. . . . .	101
5.3	Coefficients of the PM <sub>2.5</sub> reduction relations linearly interpolated from Table 5.2 between the wind speeds of 1 and 4.6 m s <sup>-1</sup> . . . . .	102

6.1	Installation and maintenance costs for life cycle cost analysis of different NO <sub>2</sub> mitigation strategies (one-off installation cost; annual maintenance costs; all costs in Pound sterling). Prices were taken from the UK Forestry Commission for London trees and woodlands (Forestry-Commission, 2009). . . . .	119
6.2	Relative differences in concentrations for different NO <sub>2</sub> mitigation strategies (represented as percentage reductions (-) or increases (+) to reference concentrations). Samples were taken all across Oxford St on a regular 2 x 2 m grid at both children height (1.0 m) and adults height (1.5 m). . . . .	121
6.3	Summary of Table 6.2 over the full street. Only trees and photocatalytic paint have a positive effect over the full street. . . . .	121
6.4	Ranking of mitigation strategies based on both their cost and ability in decreasing NO <sub>2</sub> concentrations (over pedestrian zone at 1.5 m height).130	
C.1	Distribution of wind speed classes observed during the tracer experiment. . . . .	158
C.2	PMCH sample bags coordinates . . . . .	159
C.3	Impact of the Sc <sub>t</sub> on the modelled concentrations. . . . .	161
C.4	Difference between modelled and measured tracer concentrations depending on the number of wind directions (WD) and wind speeds (WS). . . . .	162

# List of Figures

1.1	The atmospheric temperature profile (change of $dT/dz$ ) of the atmosphere with the different layer classification (Wayne, 1993). . . . .	2
1.2	The troposphere can be divided into two layers, the Atmospheric Boundary Layer (ABL) and the free atmosphere (Stull, 2012). . . . .	3
1.3	Recommended parameterisation for the CFD simulation of an ABL flow in an urban environment (Blocken et al., 2007). . . . .	4
1.4	PM formation (image credit: PennState University communication). . . . .	6
1.5	Sources of primary $PM_{2.5}$ and $PM_{10}$ for 2013 in the EU (image credit: EEA). . . . .	7
1.6	Average aerosol mass concentrations with associated chemical compositions at multiple locations in the northern hemisphere (from Zhu et al. 2012, adapted from Jimenez et al. 2009). . . . .	8
1.7	Idealised size distribution of ambient particulate matter showing fine and coarse modes (Wilson and Suh, 1997). . . . .	9
1.8	UK $NO_x$ traffic emissions projection are planned to decrease despite an increase of traffic (adapted from DfT 2015). Scenario 1 is a standard scenario (number of car trips remains constant). In scenario 2 the relationship between incomes and miles driven is removed (as higher income groups usually travel more). Scenario 3 takes into account a decline of car trip rates which was observed in the past decade. Scenario 4 and 5 are taking into account the volatility of the oil price from low and high demands respectively. . . . .	13
1.9	Trend of European emissions of primary $PM_{2.5}$ and $PM_{10}$ , according to the EEA. Colours are defined below the Figure. . . . .	14

2.1	Fitness for purpose matrix for dispersion models (adapted from Denby et al. 2011). Different colours indicate the fitness for purpose, green = <i>fit</i> ; orange = <i>conditionally applicable</i> (caused by difficult parameterisation or long processing time); red = <i>not fit</i> . <i>Aerodynamic</i> is defined as the modelling of the dispersive effects of trees and <i>Deposition</i> as the modelling of air pollution deposition on the leaf surfaces. . . . .	23
2.2	Simulations of flame produced by combustion a) from DNS modelling b) from LES modelling and c) from RANS modelling (image credit: ENEA, Italy). . . . .	25
2.3	Illustration of the Navier-Stokes approximation with the definition of an average $\bar{u}$ and transient term $u'(t)$ . . . . .	27
2.4	Specification of roughness parameters for the simulations of ABL flows (Blocken, 2015). Note that the Area 1 is outside the computational domain (used for inflow parameterisation). $z_0$ is defined as the surface roughness length (m), $k_s$ as the equivalent sand-grain roughness height (m) and $C_S$ is the roughness constant. . . . .	33
2.5	Assumption made for modelling tree: an average tree profile with a constant LAD over height. . . . .	35
2.6	Calculations of the aerodynamic and deposition effects of trees. . . . .	36
2.7	a) Sketch of the wind tunnel experiment. b) Dimensions of the street canyon. c) Wind tunnel model of idealised street canyon with trees (adapted from CODASC 2014). . . . .	38
2.8	Geometry and boundary conditions used for the simulation of an idealised street canyon (of aspect ratio $W/H=1$ ). a) For a wind direction of $90^\circ$ . b) For a wind direction of $45^\circ$ . c) For a wind direction of $0^\circ$ . Wide buffer conditions are used around the buildings to allow the inflow wind to change directions. . . . .	40
2.9	Normalised concentration ( $C^+$ ) at the walls of an empty street canyon for 3 wind directions of $0^\circ$ , $45^\circ$ and $90^\circ$ , for wind tunnel (WT) and simulated (CFD) experiments. Wind angles of incidence for the street canyon are defined in Figure 2.7. Wind tunnel concentrations data were collected up to the street canyon height ( $z/H = 1$ ) which explains why data are not shown above this height. . . . .	42

2.10	Normalised concentration (C+) for wind tunnel (WT) and simulated (CFD) experiments at the walls of a street canyon filled with porous tree for 3 wind directions of 0°, 45° and 90°. Wind tunnel data were collected up to the street canyon height ( $z/H = 1$ ) which explains why data are not shown above this height. . . . .	43
2.11	Comparison of the reference grid with a grid decreased by a factor of 1.5 (grid 2). Wind tunnel data were collected up to the street canyon height ( $z/H = 1$ ) which explains why data are not shown above this height. . . . .	45
2.12	Statistical analysis of the CFD against wind tunnel measurements. . .	46
3.1	Area of interest around the Marylebone monitoring site in London, UK. M stands for Marylebone, GP for Gloucester Place and BS for Baker Street. (a) GoogleEarth overview (b) 3D model of the scene using roads and buildings from Ordnance Survey UK and tree data from Bluesky International Ltd. . . . .	51
3.2	Wind Rose showing the wind directions (°) and wind speeds during the year 2014 in London (data: London City Airport weather station). The wind speed and direction were recorded every 30 minutes with a resolution of 10°. . . . .	52
3.3	Example of the wind rose plot showing the method used to average hourly NO <sub>x</sub> data over wind directions, here corresponding to the urban background pollution measured in Russell Square for the winter season at a wind speed of 5 m s <sup>-1</sup> . . . . .	54
3.4	Modelled area of interest inside the CFD OpenFOAM software. Coordinates are in British National Grid (UK coordinate system expressed in metres). Wide buffer conditions are used around the buildings to allow the inflow wind to change directions. . . . .	56
3.5	(a) View from the top and (b) View from the street canyon of the mesh used to carry out the CFD simulations. A maximum resolution of 1.25 m was used across the X and Y axis and 0.5 m along the Z axis. . . . .	57

3.6	Wind rose plots comparing modelled $\text{NO}_x$ and $\text{PM}_{2.5}$ for the cases CB (orange), CT1 (grey) and CT2 (yellow) against monitored data by Marylebone AURN site (blue) at a wind speed of $5 \text{ m s}^{-1}$ . The width of the wind rose plots is not fully reproduced by the CFD model for $\text{NO}_x$ , which could be caused by the Sct of 0.5 used here which could increase dispersion for wind directions parallel to the street canyon. . . . .	60
3.7	Statistical analysis of modelled pollutant concentrations when compared to the monitored data for the Marylebone site. . . . .	62
3.8	Street effects of trees in Marylebone Rd at pedestrian height over prevailing wind directions assuming a homogeneous spread of traffic. (a) Modelled $\text{PM}_{2.5}$ concentrations without trees (CB). (b) Modelled $\text{PM}_{2.5}$ concentrations with trees in summer (CT2). (c) Aerodynamic effects of trees in summer (%). (d) Loss of $\text{PM}_{2.5}$ via deposition on trees in summer. . . . .	66
4.1	Overview of the $2 \text{ km} \times 2 \text{ km}$ area of interest in Leicester showing the LIDAR data of the buildings, the road map and the national tree map (NTM <sup>TM</sup> ) from Bluesky. . . . .	71
4.2	Area of interest loaded into the paraView software, axes in British National Grid (BNG). (a) Overview from the top of the domain. (b) Mesh overview from the side of the domain with a zoom on a street canyon. Wide buffer conditions are used around the buildings to allow the inflow wind to change directions. . . . .	77
4.3	Modelling output of the normalised scalar concentration difference $\Delta C^*$ at a height of 1.5 m averaged uniformly over 12 wind directions. Trees increase traffic concentrations in street canyons but show a beneficial decrease of concentrations in open terrain configurations. . . . .	78
4.4	Difference in pollutant concentrations (%) induced by trees across the whole domain. Negative normalised concentrations indicate a decrease in pollutant concentrations and positive normalised concentrations indicate an increase. (a) Trees decrease pollutant concentrations at heights under 20-30 m and increase them at greater heights. (b) Greatest deviation in pollutant concentrations were observed at lower heights. . . . .	79

4.5	Difference in velocity ( $\text{m s}^{-1}$ ) induced by trees across the whole domain. (a) Plot of the difference in velocity ( $\text{m s}^{-1}$ ) depending on the wind direction ( $^\circ$ ) and height within the domain (m). Trees reduce the wind velocity across the domain with the greatest decrease observed at 12-15 m (corresponding to the average canopy height). (b) Distribution of difference in velocity ( $\text{m s}^{-1}$ ) averaged uniformly over 12 wind directions. Greatest deviation in velocity was observed around 12-15 m. (c) Map of the difference in velocity ( $\text{m s}^{-1}$ ) averaged uniformly over the 12 wind directions at $z = 1.5$ m. . . . .	82
4.6	Difference in vertical velocity ( $\text{m s}^{-1}$ ) induced by trees across the whole domain. (a) Plot of the vertical velocity difference ( $\text{m s}^{-1}$ ) depending on the wind direction ( $^\circ$ ) and height within the domain (m). Trees show a minor increase vertical velocities ( $0-5 \cdot 10^{-3} \text{ m s}^{-1}$ ). (b) Distribution of difference in vertical velocity ( $\text{m s}^{-1}$ ) uniformly averaged over 12 wind directions ( $x$ axis), height ( $y$ axis) and a number of CFD sampled points. The distribution of difference in vertical velocities is roughly constant over the heights of the domain. (c) Map of the difference in vertical velocity ( $\text{m s}^{-1}$ ) averaged uniformly over the 12 wind directions at $z = 1.5$ m. . . . .	83
4.7	Difference in eddy viscosity difference ( $\text{nut} - \text{m}^2 \text{ s}^{-1}$ ) induced by trees across the whole domain. (a) Plot of the eddy viscosity difference ( $\text{m}^2 \text{ s}^{-1}$ ) depending on the wind direction ( $^\circ$ ) and height within the domain (m). Trees are showing to increase turbulence, especially at heights over 20 m. (b) Distribution of difference in eddy viscosity ( $\text{m}^2 \text{ s}^{-1}$ ) uniformly averaged over 12 wind directions ( $x$ axis), height ( $y$ axis) and a number of CFD sampled points. The distribution of eddy viscosity difference shows that trees are only increasing turbulence. (c) Map of the difference in eddy viscosity ( $\text{m}^2 \text{ s}^{-1}$ ) averaged uniformly over the 12 wind directions at $z = 1.5$ m. . . . .	84
4.8	Yearly wind rose of the wind speed and direction in Leicester, averaged every hour from an anemometer placed on a 10 m mast in Leicester (data acknowledgement: Leicester City Council, 2013). . . .	85

4.9	Impact of the prevalent wind on the modelled average scalar concentration difference $\Delta C^*$ induced by trees: comparison of a uniform average over 12 wind directions with an average depending on the wind direction probability. . . . .	86
5.1	Leicester City $2 \times 2$ km area of interest. (a) Aerial photography of Leicester City in summer 2007. Urban structures are predominant with some green spaces located at the South East of the city. (b) Aerial photography combined with the LIDAR data of the buildings, the road map, the national tree map (NTM <sup>TM</sup> ) from Bluesky Ltd and the grass areas from the UK mapping agency (Ordnance Survey). (c) Mesh of the Leicester City area viewed from the CFD software OpenFOAM. More than 17 million cells were used with a resolution of 1 m for each individual building, 2 m for the trees and roads, and 4 m for the grass. . . . .	91
5.2	Subsets of Leicester city. These subsets were used to investigate the changes in PM <sub>2.5</sub> and their relation to tree and grass ground surface fraction (%). . . . .	92
5.3	Modelling output of the spatial change of PM <sub>2.5</sub> concentrations emitted from road sides at a height of 1.5 m. Tree aerodynamic effects for (a) a wind speed of 4.6 m s <sup>-1</sup> and (b) 1.0 m s <sup>-1</sup> . Tree deposition (aerodynamic effects of trees removed) calculated for an average deposition velocity of Vd = 0.64 cm s <sup>-1</sup> for (c) a wind speed of 4.6 m s <sup>-1</sup> and (d) 1.0 m s <sup>-1</sup> . Grass deposition calculated for an average deposition velocity of Vd = 0.64 cm s <sup>-1</sup> for (e) a wind speed of 4.6 m s <sup>-1</sup> and (f) 1.0 m s <sup>-1</sup> . Av is defined as average, med as median and std as standard deviation. . . . .	96
5.4	Probability distribution of the spatial change of PM <sub>2.5</sub> concentrations emitted from road sides at a height of 1.5 m (results from Figure 5.3). Tree aerodynamic effects for (a) a wind speed of 4.6 m s <sup>-1</sup> and (b) 1.0 m s <sup>-1</sup> . Tree deposition (aerodynamic effects of trees removed) calculated for an average deposition velocity of Vd = 0.64 cm s <sup>-1</sup> for (c) a wind speed of 4.6 m s <sup>-1</sup> and (d) 1.0 m s <sup>-1</sup> . Grass deposition calculated for an average deposition velocity of Vd = 0.64 cm s <sup>-1</sup> for (e) a wind speed of 4.6 m s <sup>-1</sup> and (f) 1.0 m s <sup>-1</sup> . . . . .	97

5.5	Modelled averaged change in traffic-emitted PM <sub>2.5</sub> concentrations induced by the tree aerodynamics, tree deposition and grass deposition for (a) a wind speed of 4.6 m s <sup>-1</sup> and (b) a wind speed of 1.0 m s <sup>-1</sup> (Note that grass us a consistent deposition sink). . . . .	98
5.6	Relation between the tree ground surface fraction (%) and the PM <sub>2.5</sub> reduction with the associated first order linear regression coefficients. The tree aerodynamics were included for the tree average (Vd = 0.64 cm s <sup>-1</sup> ) and high deposition (Vd = 30 cm s <sup>-1</sup> ) calculation (see choice of Vd in Table 5.1). The different spatial subsets of Leicester city are detailed in Figure 5.2. . . . .	99
5.7	Relation between the grass ground surface fraction (%) and the PM <sub>2.5</sub> reduction with the associated first order linear regression coefficients. The PM <sub>2.5</sub> deposition on grass were calculated for low (0.01 cm s <sup>-1</sup> ), average (0.64 cm s <sup>-1</sup> ) and high (8 cm s <sup>-1</sup> ) deposition velocities. The different spatial subsets of Leicester city are detailed in Figure 5.2. . . . .	100
5.8	Comparison of change in PM <sub>2.5</sub> concentrations (%) between the initial CFD model results (expressed in Figure 5.5) at pedestrian height and estimated changes through two linear relations (Eq. 5.2 and Eq. 5.3) based on trees and grass ground surface fraction (%). The aerodynamics of trees were added into the tree deposition calculation. 24 CFD cases (12 wind directions at two wind speeds) are compared to derived the relations. . . . .	102
5.9	PM <sub>2.5</sub> change dependence on the wind speed over Leicester City. (a) Tree aerodynamics, tree aerodynamics with deposition and grass deposition dependence on the wind speed (b) Tree deposition dependence on the wind speed (*) PM <sub>2.5</sub> estimated from linear relations (Eq. 5.2 and Eq. 5.3) with a linear interpolation between the two reference wind speeds of 1 and 4.6 m s <sup>-1</sup> . . . . .	103
5.10	CFD results of changes in PM <sub>2.5</sub> across the whole height of the simulation domain for a wind speed of 4.6 m s <sup>-1</sup> . All relative reductions (%) where calculated using the average ground concentrations of the reference scenario (see Table 5.1) as denominator. . . . .	106
6.1	View from Google Earth of the area of interest corresponds to Oxford Street within the City of Westminster in London (UK). The modelled area extend on 1.2 km between the Marble Arch and Oxford Circus. . . . .	111

6.2	Mesh used to carry out the CFD simulations which contains 3 million cells. A maximum resolution of 1.0 m was used across the X and Y axis and 0.5 m along the Z axis. . . . .	112
6.3	Modelled area of Oxford Street view from inside the CFD OpenFOAM software. Coordinates are in British National Grid (UK coordinate system expressed in meter). Wide buffer conditions are used around the buildings to allow the inflow wind to change directions. . . . .	113
6.4	Grid sensitivity analysis inside Oxford Street canyon, 100 points were sampled across the whole street at heights spreading between 1 to 20 m. . . . .	114
6.5	List of six scenarios examined for NO <sub>2</sub> mitigation potential. . . . .	118
6.6	Relative difference in NO <sub>2</sub> concentrations in comparison to an empty street canyon (scenario 1). Sampled were taken all across Oxford St on a regular 2 × 2 m grid at both 1.0 and 1.5 m height. Error bars correspond to the model accuracy of 40%. . . . .	122
6.7	Aerodynamic effects of existing trees (Sc. 2), narrow trees (Sc. 3) and solid barriers (Sc. 5) on vehicular emissions of NO <sub>2</sub> in Oxford St. The position of trees can be seen in Sc. 2 and Sc. 3. . . . .	123
6.8	Deposition effects of existing trees (Sc. 2), narrow trees (Sc. 3), painted buildings (Sc. 4), painted barriers (Sc. 6) and innovative barriers (Sc. 7) on vehicular emissions of NO <sub>2</sub> in Oxford St. . . . .	124
6.9	Life cycle costs of scenarios considered as feasible pollution mitigation measures in Oxford Street. . . . .	125
6.10	Hotspots locations in Oxford St for the reference scenario 1. Wind directions were averaged over the prevailing winds. . . . .	126
6.11	Aerodynamic and deposition effects of hotspot mitigation strategies on vehicular emissions of NO <sub>2</sub> in Oxford St. . . . .	127
7.1	Example of urban land surface temperature integration in a CFD model (Ketterer and Matzarakis, 2015). . . . .	137
A.1	Mass conservation principle applied to a control volume. . . . .	139
A.2	Force-momentum principle applied to a control volume (here for the U <sub>x</sub> component of the velocity). $g_x$ represents any forces exterior to CV.	141

B.1	Chronology followed to produce an averaged concentrations map (here NO <sub>2</sub> results from Chapter 6). 8 wind directions are averaged depending on the prevailing wind directions percentages and aggregated into a single average. . . . .	144
B.2	Steps showing how are obtained average difference maps. Percentages difference are obtained by dividing the difference of a tree-free city with a city with trees by the average scalar concentrations for the tree-free city. . . . .	146
B.3	Wind direction dependence on the normalised scalar concentrations difference (see Fig. B.6 for the averaged map). Here are shown the wind directions of 0°, 30°, 60° and 90°. . . . .	147
B.4	Wind direction dependence on the normalised scalar concentrations difference (see Fig. B.6 for the averaged map). Here are shown the wind directions of 120°, 150°, 180° and 210°. . . . .	148
B.5	Wind direction dependence on the normalised scalar concentrations difference (see Fig. B.6 for the averaged map). Here are shown the wind directions of 240°, 270°, 300° and 330°. . . . .	149
B.6	Modelling output of the normalised scalar concentration difference $\Delta C^*$ at a height of 1.5 m averaged uniformly over 12 wind directions (same Figure as Fig. 4.3). . . . .	150
C.1	(a) View of the landfill site (image credit: Bing Maps). (b) Combined LIDAR (1 m resolution) and OS MasterMAP terrain (50×50×5 m resolution) dataset used for the CFD simulations (British National Grid coordinates). . . . .	154
C.2	Distribution of wind directions divided every 7.5° observed during the tracer experiment. 15 wind directions were simulated between 127.5° and 232.5°. . . . .	158
C.3	PMCH modelled concentrations at ground level corresponding to the distributed wind classes of the tracer experiment. Measured tracer concentrations are compared to the modelled concentrations at each of the sampling locations (image credit: Bing Maps). . . . .	160
C.4	Summary of measured PMCH concentrations compared to modelled PMCH concentrations. Errors of a factor of 2.0 (FAC2) are represented in dashed lines. . . . .	161

# List of Acronyms

ABL	Atmospheric Boundary Layer
AURN	Automatic Urban and Rural Network
BC	Boundary conditions
BNG	British National Grid
BVOC	Biogenic Volatile Organic Compound
CFD	Computational Fluid Dynamics
DECC	Department of Energy and Climate Change
DEFRA	Department for Environment, Food and Rural Affairs
DfT	Department for Transport
DNS	Direct numerical simulation
ECD	Electron Capture Detection
EFT	Emissions Factors Toolkit
EPA	Environmental Protection Agency (United States)
LAD	Leaf Area Density
LAI	Leaf Area Index
LES	Large Eddy Simulation
LiDAR	Light Detection And Ranging
LPDM	Lagrangian Particle Dispersion Models
LST	Land Surface Temperature
NAN	Not a Number
NO <sub>x</sub>	Nitrogen Oxides
NSE	Navier-Stokes equations
NTM	National Tree Map
OECD	Organisation for Economic Co-operation and Development
PAN	Peroxyacyl nitrates
PET	Physiological Equivalent Temperature
PM	Particulate Matter

PM <sub>2.5</sub>	Particulate Matter smaller than 2.5 micrometers
PM <sub>10</sub>	Particulate Matter smaller than 10 micrometers
PMCH	Perfluoromethylcyclohexane
POA	Primary Organic Aerosol
PPQV	Particle per Quadrillion
RANS	Reynolds-averaged Navier-Stokes equations
RD	Relative Deviation
RSM	Reynolds stress model
Sc <sub>t</sub>	Turbulent Schmidt number
SOA	Secondary Organic Aerosol
UFORE	Urban Forest Effects Model
Vd	Deposition velocity
VOC	Volatile Organic Compound
WD	Wind Direction
WHO	World Health Organisation
WMO	World Meteorological Organisation
WS	Wind Speed
WT	Wind Tunnel

# Executive summary

## Main thesis findings

The results from this thesis suggest that trees are in general beneficial from a purely dynamic point of view, as they decrease the concentration of traffic emissions on average at pedestrian height. This decrease is primarily a result of an increase in turbulence that in turn increases the mixing of traffic emissions. Trees are however less effective in deep street canyons as they tend to trap emissions. The model used show that reduction is most effective when trees are placed in open areas, upwind from the emissions. The turbulence caused appears to propagate downwind where it increases the mixing of emissions. As a consequence, the worst effects of trees with respect to air quality was found for lower wind speeds, since the turbulent mixing was inhibited. A direct relationship between changes in air pollutant concentration and the presence of trees was found which suggests that there is level of geometry independence combining buildings and trees that is dominated by the aerodynamics of trees. The simulation of the effect of trees remains an area that requires further research, as the tree species and factors such as leaf area density (LAD) or tree canopy shape can play a significant role in the impact of trees on air pollution. The assessment of the local meteorology is of primarily importance, as both wind direction and wind speed distribution have a critical impact on the overall trees effect. Despite combined dispersion and deposition reductions, the findings of this study suggest that urban vegetation will not remove the problem of pollution. The urban background was found to be a large contributor of air pollution even within busy roads, which will additionally decreases the aerodynamic dispersive effects of trees on vehicular emissions.

## Conclusions

- Agreement with previous studies: The work completed in this study agrees with the fact that trees tend to trap emissions for most for the wind directions

in a street canyon.

- **Conflicting area of research:** While perpendicular winds to the street canyon orientation lead to larger pollution concentrations in street canyons in the presence of trees, research findings are divided on the effects of trees under parallel winds. Some modelling studies are finding beneficial effects of trees for parallel wind directions (such as in this thesis) and other studies are still finding a trapping effects of trees for parallel wind directions.
- **Overall assessment of green infrastructures:** Green infrastructures are beneficial but they do not represent a solution to completely remove air pollution from cities. It is clear that green infrastructure has a role to play at a city scale but only when co-ordinated with understanding of local implementation and traffic planning. Air quality is only one aspect of the importance of urban vegetation, other aspects such as their social benefits impacts (traffic noise reduction, improvement of mental wellbeing, etc.) must be considered as well.

# Journal Publications resulting from this work

Jeanjean, A. P., Hinchliffe, G., McMullan, W. A., Monks, P. S., & Leigh, R. J. (2015). A CFD study on the effectiveness of trees to disperse road traffic emissions at a city scale. *Atmospheric Environment*, 120, 1-14.

Jeanjean, A. P. R., Monks, P. S., & Leigh, R. J. (2016). Modelling the effectiveness of urban trees and grass on PM 2.5 reduction via dispersion and deposition at a city scale. *Atmospheric Environment*, 147, 1-10.

Jeanjean, A., Buccolieri, R., Eddy, J., Monks, P., & Leigh, R. (2017). Air quality affected by trees in real street canyons: The case of Marylebone neighbourhood in central London. *Urban Forestry & Urban Greening*, 22, 41-53.

Jeanjean, A. P., Gallagher, J., Monks, P. S., & Leigh, R. J. (2017). Ranking current and prospective NO<sub>2</sub> mitigation strategies: a modelling and life cycle investigation in Oxford Street, London. *Environmental Pollution*, under review.

# Chapter 1

## Air quality in urban atmosphere

### 1.1 Urban atmosphere

#### 1.1.1 Urban air pollution context

According to a report from the Organisation for Economic Co-operation and Development (OECD), by 2050, air pollution could account for the largest portion of environmental deaths if no precautions are taken, ahead of unsafe water supply and sanitation (OECD, 2012). This illustrates the challenge faced against air pollution in our modern society, where 80% of the world population lives in areas where the air pollution is not satisfactory (WHO, 2016). With more people now living in urban places than rural areas and with an increase in urban population (UNO, 2011), the problem is global. In low and middle income countries, 98% of cities with more than 100,000 inhabitants have air pollution levels above the safe recommended guidelines, this falls to 56% in developed countries (WHO, 2014). This results in an annual estimated 7 million premature deaths linked to air quality. The worldwide economic cost related bad air quality could reach up to \$2.6 trillion annually by 2060, if no measures are taken (OECD, 2016).

The application of vegetation as an air pollution mitigation strategy has been the recent focus of attention for urban planners (Janhäll, 2015; Gallagher et al., 2015). Urban greening, such as trees or grass, are known to improve air quality with the deposition of air pollutants on plant surfaces and occasionally via aerodynamic dispersive effects. The overall effects of trees, when combining both aerodynamic and deposition effects, has been the object of very few studies in the urban environment (Janhäll, 2015). Accurate modelling could help to design a new generation of streets

where the potential of trees as an air pollution mitigation strategy is maximised. This thesis focuses on the impact of trees on vehicular emissions, which are one of the main contributor of air pollution in the urban environment.

### 1.1.2 General introduction to the atmosphere

The atmosphere of the Earth is unbounded, but there is a critical level around 100 km that can be taken as the beginning of space. The Earth's atmosphere is formed by a succession of different layers which are the troposphere, stratosphere, mesosphere and thermosphere, each of these layers being located at an altitude where a temperature inflection is observed (see Figure 1.1). Around 99% of the atmospheric mass lies inside the stratosphere and troposphere, and 50% within the bottom 5 km of the troposphere. Tropospheric air is breathed by the majority of the life on Earth and is vital for its survival.

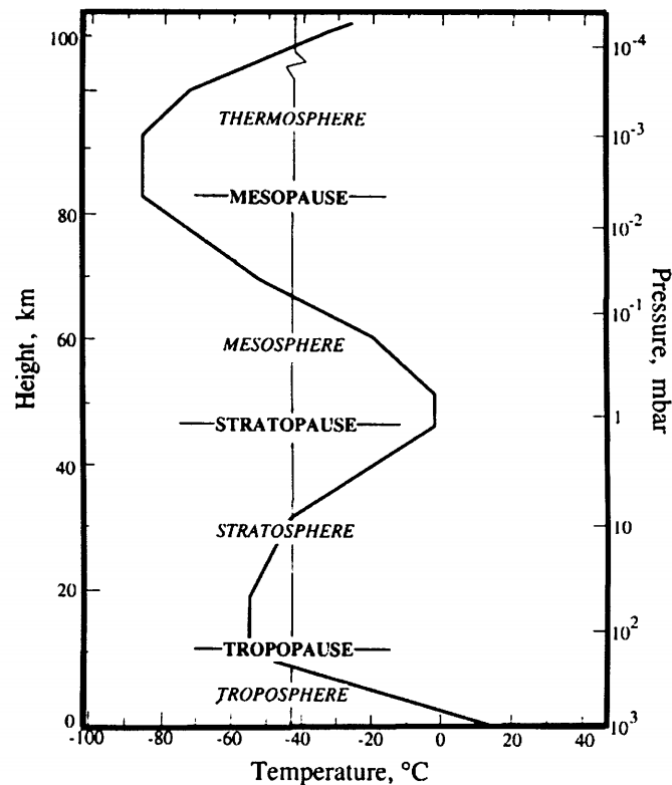


Figure 1.1: The atmospheric temperature profile (change of  $dT/dz$ ) of the atmosphere with the different layer classification (Wayne, 1993).

Transport processes that are directly influenced by the Earth's surface occur in the Atmospheric Boundary Layer (ABL), which typically ranges to altitudes of 100

## 1.1 Urban atmosphere

---

- 3000 m (Stull, 2012), although the Earth's surface can affect greater heights with the presence of mountain. Figure 1.2 illustrates the presence of the ABL near the Earth's surface. The ABL itself can be separated into two layers: the surface layer (surface to 50 - 100 m) where the wind structure is dependent on the surface friction and temperature change. Another region of the troposphere lies above the surface layer where the wind structure is dependent on the surface friction (although at higher altitudes the surface friction is less important), the temperature change and the Earth's rotation. The top height of the ABL changes across the time of day, typically with heights of a few hundred meters at night rising to 1 - 2 km during day time.

The urban canopy is composed of buildings, trees and other elements. The air enclosed between the ground and the top of the urban canopy forms the urban canopy layer, where most of the air pollution sources are emitted. For a  $2 \times 2$  km<sup>2</sup> area centred on the City of Leicester in the UK, the surface cover is divided between buildings (29%), grass (19%), trees (12%) and roads (9%) (see Chapter 5). Assuming that all buildings fully occupy the urban canopy and that porous trees do not significantly decrease the volume of air, the canopy air space in Leicester can be estimated to be at least 71% of the urban canopy layer. This number is variable depending on the cities and the area of focus (city centres, suburbs, etc.).

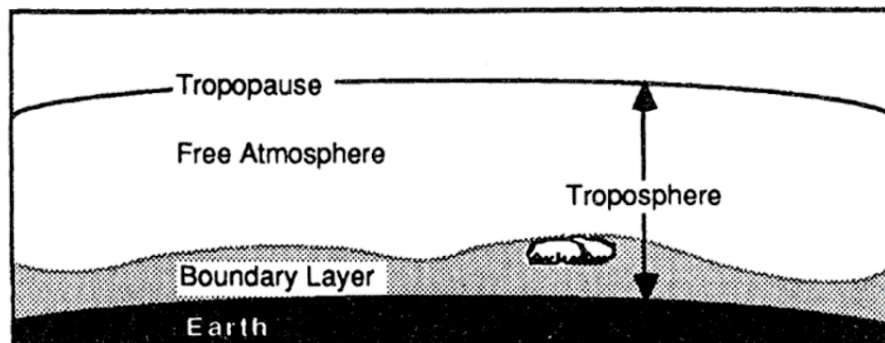


Figure 1.2: The troposphere can be divided into two layers, the Atmospheric Boundary Layer (ABL) and the free atmosphere (Stull, 2012).

City scale CFD (Computational Fluid Dynamics) dispersion model of air pollution focuses on the modelling of atmospheric boundary layer flow. At the inflow boundary conditions of the domain, the wind speed is modelled as a logarithmic law from the surface up to 100 m (see flow equation definition in Eq. 2.19). Above 100 m in height, a power law is usually used. Figure 1.3 illustrates the simulation of the

## 1.1 Urban atmosphere

---

ABL flow within a CFD model. The interaction of wind with urban structures which form the roughness of cities (such as buildings, trees, obstacles, etc) is then modelled at high resolution (around the meter scale), allowing a comprehensive simulation of air pollution dispersion.

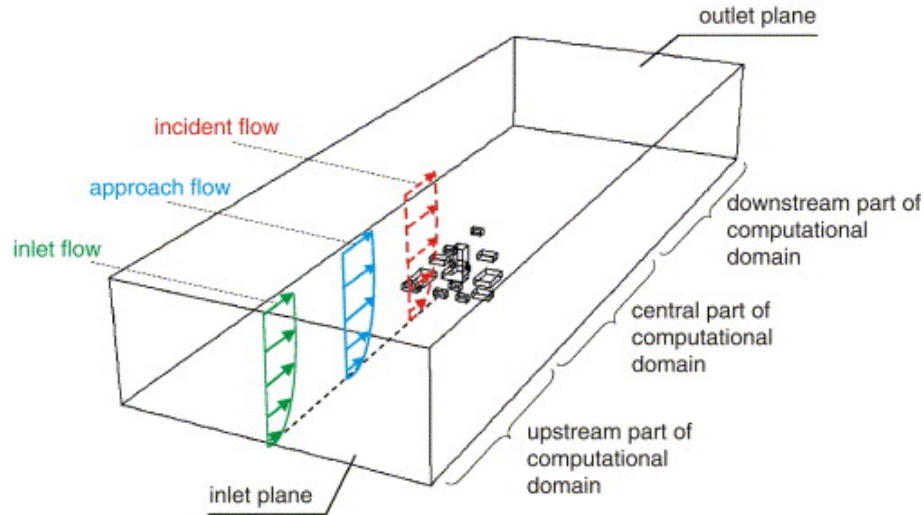


Figure 1.3: Recommended parameterisation for the CFD simulation of an ABL flow in an urban environment (Blocken et al., 2007).

### 1.1.3 Earth's atmosphere composition

The average chemical composition of the air in the Earth's atmosphere, in terms of volume, is known to be 78.09% nitrogen, 20.95% oxygen, 0.93% argon and small amounts of trace gases. Some gases have constant concentrations in the troposphere, such as nitrogen and noble gases including argon. The trace gases like carbon dioxide, water vapour and pollutants have variable concentrations within the atmosphere. When the concentration of pollutants reaches particular thresholds they can cause harmful effects on humans and natural ecosystems.

The six common air quality pollutants, as defined by the US Environmental Protection Agency (EPA) in 2016 are: particulate matter (PM), nitrogen oxides ( $\text{NO}_x$ ), ozone ( $\text{O}_3$ ), carbon monoxide (CO), sulfur dioxide ( $\text{SO}_2$ ) and lead (Pb) which can occur in gaseous and particulate forms. Nitrogen oxides, ground level ozone and particulate matter are today's most problematic outdoor pollutants in terms of health hazards in Europe (EEA, 2015). The origin of pollutants can be of natural sources or human sources (anthropogenic). There is a range of anthropogenically-produced pollutants from activities such as biomass burning, transport, factories

## 1.2 Air pollution sources

---

and residential sources. This thesis will focus on the dispersion of traffic emissions in the urban environment, which is one of the main source of air pollution within urban environment.

### 1.1.4 Air quality guidelines

In the European Union, each member state needs to adhere to air quality standards that are set by the European Commission (European Commission, 2015). The European and WHO guidelines for NO<sub>2</sub>, PM<sub>2.5</sub> (particle sizes which are less than 2.5 μm) and PM<sub>10</sub> (defined as the total mass of airborne particles with an aerodynamic diameter below 10 μm which passes with 50% efficiency through a 10 micrometre cut-off) are reported in Table 1.1.

Table 1.1: European and WHO guidelines on air quality levels for NO<sub>2</sub>, O<sub>3</sub> and PM.

Pollutant species	European guidelines	WHO guidelines
	Concentrations (μg m <sup>-3</sup> )	Concentrations (μg m <sup>-3</sup> )
NO <sub>2</sub>	200 (1h mean)	200 (1h mean)
	40 (annual mean)	40 (annual mean)
O <sub>3</sub>	120 (8h mean)	100 (8h mean)
PM <sub>2.5</sub>	25 (annual mean)	25 (1h mean)
		10 (annual mean)
PM <sub>10</sub>	50 (24h mean)	50 (24h mean)
	40 (annual mean)	20 (annual mean)

## 1.2 Air pollution sources

### 1.2.1 Particulate matter

PM consists of a complex mix of liquid droplets and particles from multiple origins, their composition being source-dependent. The chemical mechanisms responsible for the formation of PM are very complex and remain an area of ongoing research (Omidvarborna et al., 2015). In Figure 1.4, the main sources and sinks of PM

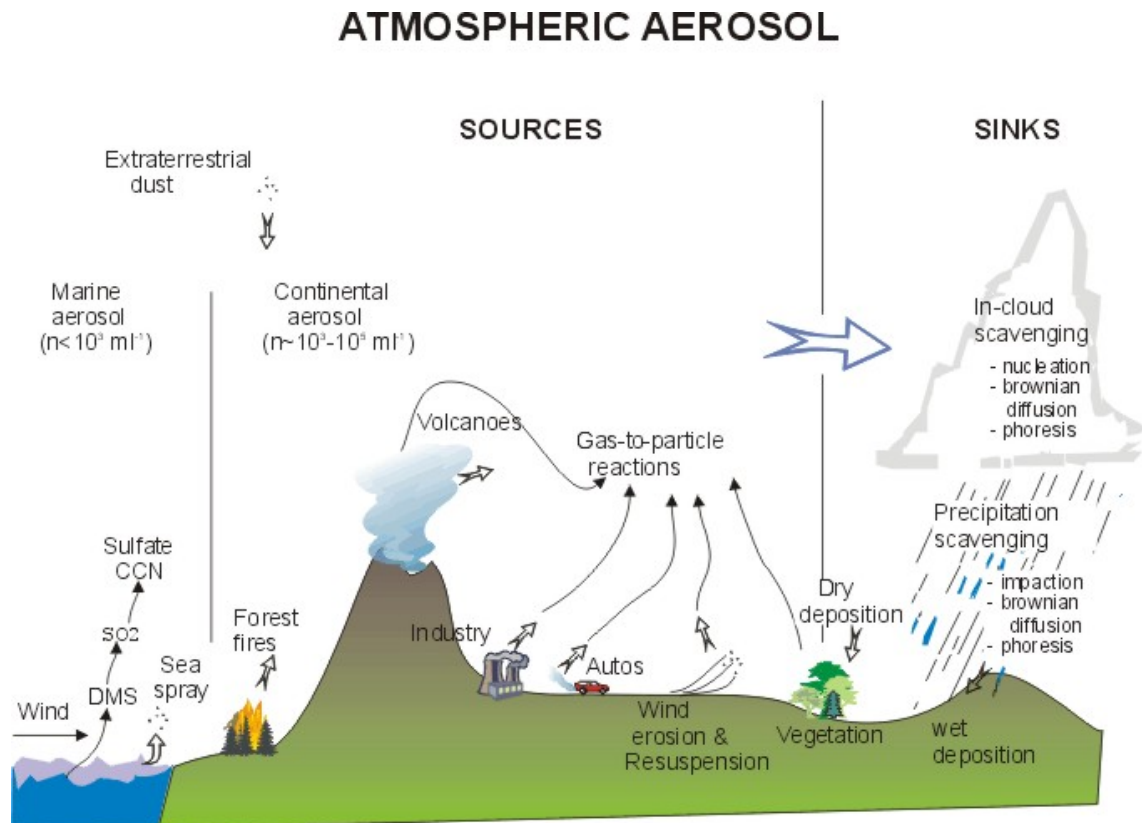


Figure 1.4: PM formation (image credit: PennState University communication).

are shown. Natural sources of PM include sea spray, forest fire, living vegetation (pollen), extraterrestrial dust or volcanoes, while anthropogenic sources include industries, vehicular emissions and others (see legend of Figure 1.5 for a more comprehensive list of human activities). Although natural sources of particles exist, anthropogenic sources are usually predominant in the urban environment. The main sinks of PM occur during rain events, but particles might be re-suspended once surfaces dry out. It has been shown that road dust suspension could account for as much PM emission concentrations as vehicular emissions (Lenschow et al., 2001). It is worth noting that in terms of mass, sea salt is the predominant aerosol in the atmosphere. However when considering fine and ultrafine fractions of particles, anthropogenic sources dominate (Seinfeld and Pandis, 2016).

Figure 1.5 shows the percentage PM emissions for primary (directly emitted) PM<sub>2.5</sub> and PM<sub>10</sub> for each contributory sector in 2013 in the EU, according to the European Environment Agency (EEA). Commercial, institutional and households are the major contributors of PM<sub>2.5</sub> emissions, with domestic heating being the biggest source of emissions (Cofala and Klimont, 2012). Road transport is an im-

## 1.2 Air pollution sources

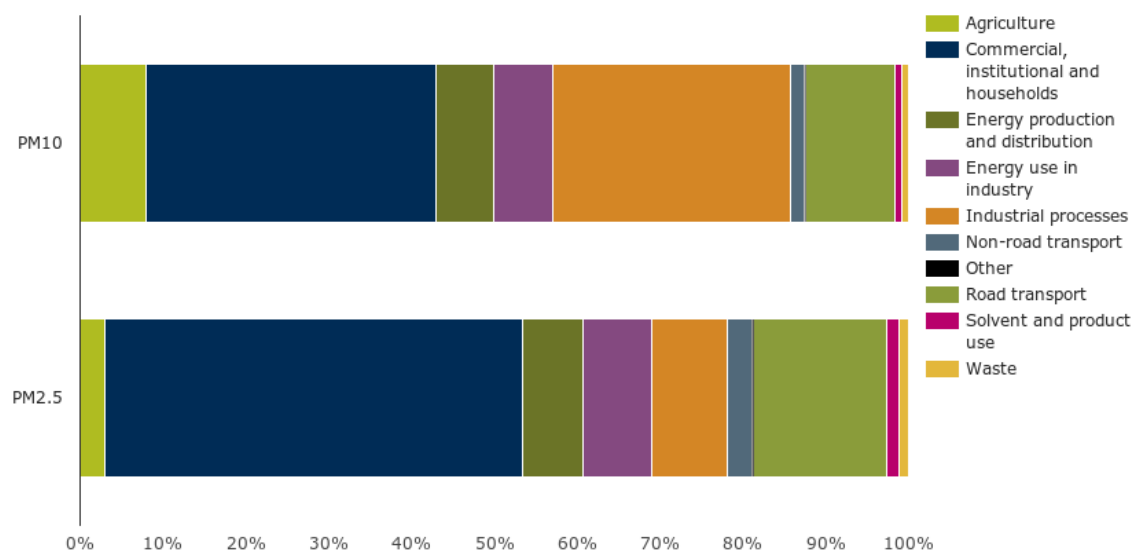


Figure 1.5: Sources of primary PM<sub>2.5</sub> and PM<sub>10</sub> for 2013 in the EU (image credit: EEA).

portant contributor although not the largest. In addition to tail pipe emissions, the emissions of road dust, tyre and brake wear are an important source of vehicular PM emissions (Rogge et al., 1993).

PM can also be formed within the atmosphere from chemical reactions (secondary aerosols) of precursor gases, such as NO<sub>2</sub> and SO<sub>2</sub> contributing to the formation of aerosols in the presence of ammonia (although often partially neutralised by ammonia, sulfuric acid can form aerosol without ammonia). These gases are usually emitted outside the urban environment via industries, agriculture or other sources. When emitted, sulfur is oxidised rapidly into sulfur dioxide (SO<sub>2</sub>) which is then transformed into sulfur trioxide (SO<sub>3</sub>). SO<sub>3</sub> reacts with water to produce sulfuric acid which is transformed into ammonium sulfate in the presence of ammonia (R1, R2, R3 and R4). If ammonia is in short supply, sulfuric acid can form ammonium hydrogen sulfate as an intermediate. The formation of ammonium nitrate is described in the following section (R14).



## 1.2 Air pollution sources

Although local emissions (primary PM) are usually the largest contributor of roadside concentrations and urban background concentrations, secondary aerosols can also affect the urban aerosols composition. During haze events recorded in China in 2013, secondary aerosols have been shown to contribute up to 30-77% of  $PM_{2.5}$  (Huang et al., 2014). Under cold weather and low wind speed conditions, such as in the Po Valley in Italy, it was found that secondary  $PM_{2.5}$  has a greater contribution than primary  $PM_{2.5}$  (Larsen et al., 2012). In Marylebone Rd, London, UK, it was found that haze events leading to high PM concentrations were essentially associated with long-range transport, in which the regional  $PM_{2.5}$  constituted most of the local concentrations (Charron and Harrison, 2005). In Figure 1.6, it can be seen that the average aerosol concentrations and their chemical compositions vary greatly depending on the location across the Earth, owing to different sources and meteorological conditions. Organic aerosols are formed both of primary organic aerosol (POA) and secondary organic aerosol (SOA). The formation of SOA remains poorly understood (Hallquist et al., 2009).

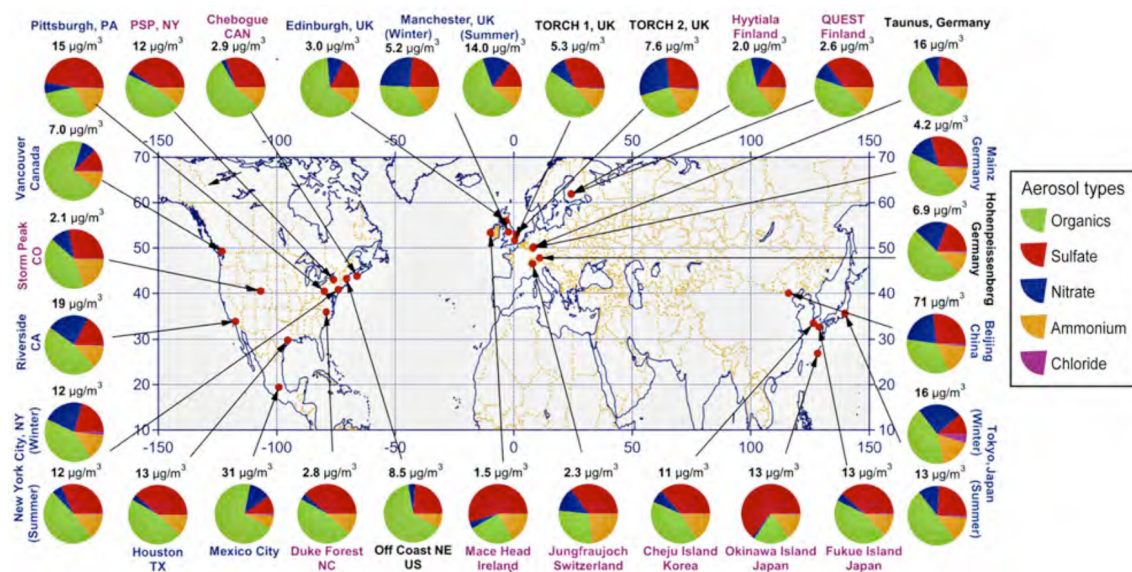


Figure 1.6: Average aerosol mass concentrations with associated chemical compositions at multiple locations in the northern hemisphere (from Zhu et al. 2012, adapted from Jimenez et al. 2009).

### $PM_{2.5}$ modelling approximations

In this thesis,  $PM_{2.5}$  concentrations are modelled (see Chapters 3 and 5). According to Janhäll (2015), an assumption can be made that  $PM_{2.5}$  behave like gases, which

## 1.2 Air pollution sources

is the case for diameters below  $\sim 0.1 \mu\text{m}$ . For particle sizes above  $1 \mu\text{m}$ , the particles impact on surfaces forces the air stream to bend and  $\text{PM}_{2.5}$  can no longer be considered to behave like a gas. In Figure 1.7, most of the mass of  $\text{PM}_{2.5}$  can be seen to lie between  $0.1$  to  $1.0 \mu\text{m}$ , which means that most of the  $\text{PM}_{2.5}$  particles are behaving between a gaseous and solid particle states. In this thesis, the assumption of Janhäll (2015) was used to consider that  $\text{PM}_{2.5}$  is dispersing like a gas. Modelling the formation of secondary aerosols inside a dispersion model requires the integration of precursor gases (such as  $\text{SO}_2$  and  $\text{NH}_3$ ), meteorological conditions that impact reaction rates, and reactive gases (such as  $\text{NO}_2$ ). Given that the focus of this thesis is vehicular emissions, the formation of secondary aerosols lies outside the scope of this thesis.

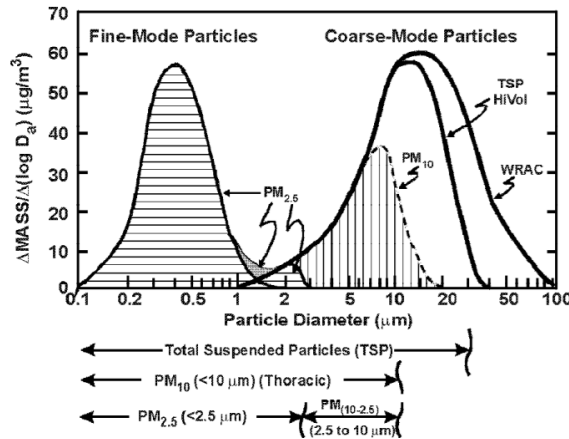


Figure 1.7: Idealised size distribution of ambient particulate matter showing fine and coarse modes (Wilson and Suh, 1997).

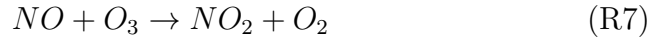
### 1.2.2 $\text{NO}_x$

Nitrogen oxides  $\text{NO}_x$  are formed of nitric oxide ( $\text{NO}$ ) and nitrogen dioxide ( $\text{NO}_2$ ). From a car exhaust, an approximated ratio of 80%  $\text{NO}$  and 20%  $\text{NO}_2$  is emitted, although this ratio is dependent on the type of engine (petrol or diesel), the type of vehicle and the temperature of the engine (Yao et al., 2005).  $\text{NO}$  and  $\text{NO}_2$  are in a constant reactive cycle with  $\text{O}_3$ , known as the Leighton relationship or photostationary state, mainly dominated by three reactions (R5, R6 and R7). Note that M is an inert molecule that absorbs the excess of energy during the reaction of

## 1.2 Air pollution sources

---

O<sub>2</sub> with an oxygen O (R6).



When other reactions are neglected (the oxidation of VOCs and the formation of peroxyacyl nitrates known as PANs are out of the scope of this thesis), relative concentrations of NO<sub>2</sub>, NO and O<sub>3</sub> can be expressed such that

$$\frac{[NO_2]}{[NO]} = [O_3] \frac{k_{1.1}}{k_{1.2}} \quad (\text{R8})$$

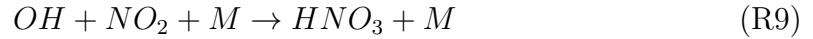
R8 shows that the concentration of O<sub>3</sub> is dependent on the ratio of NO<sub>2</sub> over NO. While sufficient O<sub>3</sub> is available, NO is quickly oxidised into NO<sub>2</sub> (R6). Via dissociation with sun light (R5), NO<sub>2</sub> can be dissociated to NO and lead on to the formation of tropospheric ozone (R7) that has harmful effects on ecosystems, especially on the photosynthetic activities of plants (e.g. Pye 1988).

Road transport account for 40% of the NO<sub>x</sub> emissions in urban areas in the EU (EEA, 2011). Table 1.2 lists the worldwide sources of NO<sub>x</sub>. It can be seen that anthropogenic sources largely dominate the emissions of NO<sub>x</sub>, being more 70 times greater than the natural sources.

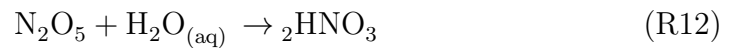
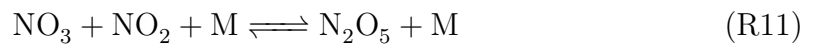
Sources	NO <sub>x</sub> (Tg/year)
Natural	
Soils	7 (5-12)
Lightning	5 (2-20)
Other	1.5 (0-5.7)
<b>Total natural</b>	<b>13.5 (7-38)</b>
Anthropogenic	
Fossil fuel combustion	21
Biomass burning	12
<b>Total anthropogenic</b>	<b>33</b>

Table 1.2: Natural and anthropogenic sources of NO<sub>x</sub> worldwide (adapted from Wallace and Hobbs 2006; Jacob 1999).

The main sink of nitrogen oxides is formation of nitric acid  $\text{HNO}_3$  (lifetime of 15 to 80 days), which occur mainly during the day through the reaction with OH radical and leads to the formation of nitric acid (Stavrakou et al., 2013).



During night time, nitrogen oxides are converted to nitric acid via the formation of a nitrate radical ( $\text{NO}_3$ ):



The change of  $\text{NO}_2$  concentrations over time can be expressed such that

$$\frac{d[\text{NO}_2]}{dt} = -j_{\text{NO}_2}[\text{NO}_2] + k_{\text{O}_3+\text{NO}}[\text{O}_3][\text{NO}] \quad (\text{R13})$$

where  $j_{\text{NO}_2}$  is the reaction rate representing the sinks of  $\text{NO}_2$  and  $k_{\text{O}_3+\text{NO}}$  is the reaction rate representing the source of  $\text{NO}_2$ .

In the presence of ammonia, nitric acid can form ammonium nitrate aerosols ( $\text{NH}_4\text{NO}_3$ ) and contribute to the formation of secondary aerosols (R14). The equilibrium is highly dependent on the temperature.



### **$\text{NO}_x$ modelling approximations**

In a real environment,  $\text{NO}_x$  species decrease over time by chemical reactions (reaction with OH radical, formation of PAN, reaction with water, etc.). The average atmospheric lifetime of  $\text{NO}_x$  has been estimated to range between 1.8 to 7.5 hours (Liu et al., 2016). In the modelled cases of this thesis, the maximum time  $\text{NO}_x$  would remain on the computational domains was estimated to be 0.17 hour in Leicester (Chapters 4 and 5) and 0.13 hour in Marylebone (Chapter 3), which is well under its atmospheric lifetime (the estimation was made considering the time it would take to cross the whole modelling domain at the lowest wind speed). This lead to the choice of omitting the integration of  $\text{NO}_x$  chemistry in the model. Modelling  $\text{NO}_2$  concentrations is a bit more complex, as  $\text{NO}_2$  is in a constant cycle with NO

and  $O_3$ . However, the introduction of the Leighton's cycle chemical reactions within a steady-state CFD model remains challenging, as  $O_3$  concentrations, sun light or temperature are affecting the reaction rates. The introduction of chemical reactions would have needed to run the model across a whole lot of meteorological conditions (seasons, sunlight, etc) which is too computationally demanding for CFD. As the lifetime of NO is a few seconds, this thesis takes the assumption that  $NO_2$  concentrations are modelled as a direct tail pipe emission (Chapter 6), supposing that NO already reached an equilibrium with  $NO_2$ .

### 1.2.3 Dry deposition velocity

The deposition velocity is often described as the sum of the inverse of the aerodynamic resistance ( $R_a$ ), boundary layer resistance ( $R_b$ ) and surface resistance ( $R_c$ ) such that:

$$Vd = \frac{1}{R_a} + \frac{1}{R_b} + \frac{1}{R_c} \quad (1.4)$$

$R_a$  represents the ability of turbulent diffusion to bring the air pollutant close to the surface of deposition. The aerodynamic resistance is often negligibly small compared to the other resistances, except for the case of large particles with diameters greater than  $10 \mu\text{m}$  (Hinds, 1999).  $R_b$  represents the resistance faced by the air pollutant to reach the area adjacent to the surface of deposition, which depends on the surface roughness and the species of pollutant.  $R_c$  is the affinity of the surface to absorb the air pollutant, which depends on the type of surface, its humidity and the species of pollutants.

The estimation of a deposition velocity for  $PM_{2.5}$  on vegetation is closely linked to the particle sizes and compositions. Variation up to two orders of magnitude are found within the literature (Litschke and Kuttler, 2008). For  $PM_{2.5}$  deposition on vegetation, an empirical relation was derived by Vong et al. (2010) to estimate the deposition velocity for particle diameters between  $0.2$  to  $0.5 \mu\text{m}$  (see Eq. 1.5). The deposition velocity is found to increase linearly with the friction velocity  $u^*$  and the particle diameter  $D_p$ .  $A$  represents an empirical constant (e.g. 1.35 over forests and 0.2 over grass) and  $L$  the Monin-Obukov length.

$$Vd = A \cdot u^* \cdot D_p \cdot \left( 1 + \left( -\frac{300}{L} \right)^{2/3} \right) \quad (1.5)$$

### 1.2.4 Projections

The following section was written with the assumption that newly manufactured vehicles were compliant with European regulations. However, recent attention has been drawn to the fact that vehicular emissions advertised by car manufacturers were not representative of the reality, leading to greater emissions (Holland et al., 2016). Following results shall then be treated with caution, especially the  $\text{NO}_x$  projections in Figure 1.8.

Despite an increase of the vehicle fleet which is planned to increase by 40% in the UK between 2010 and 2040 (DfT, 2015), the road transport emissions of  $\text{NO}_x$  and PM are planned to decrease significantly in the UK (see Figure 1.8). This decrease would also be seen for road emissions of PM, which according to DfT (2015) will be due to the enforcement of stricter European regulation. European trends are seeing a decrease in emissions which could be in 2020 less than half of what the emissions were in 1990 (see Figure 1.9). Other scenarios predict that urban air quality will continue to degrade worldwide, especially in Asia caused by an increase of the vehicle fleet (OECD, 2012).

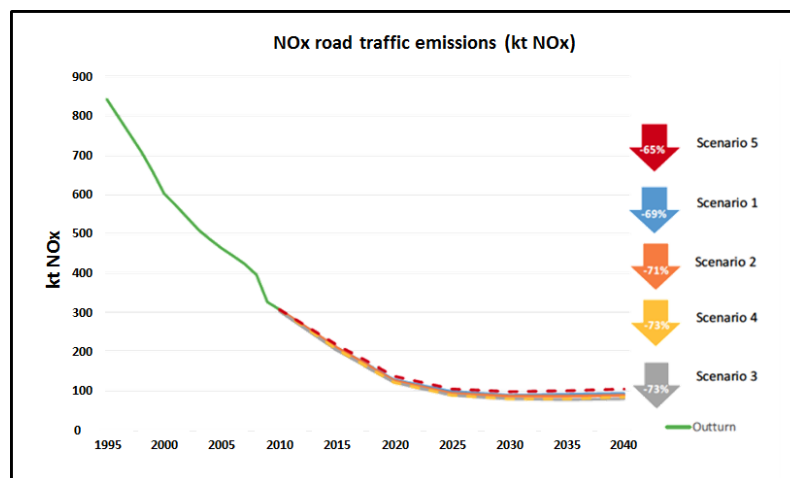


Figure 1.8: UK  $\text{NO}_x$  traffic emissions projection are planned to decrease despite an increase of traffic (adapted from DfT 2015). Scenario 1 is a standard scenario (number of car trips remains constant). In scenario 2 the relationship between incomes and miles driven is removed (as higher income groups usually travel more). Scenario 3 takes into account a decline of car trip rates which was observed in the past decade. Scenario 4 and 5 are taking into account the volatility of the oil price from low and high demands respectively.

## 1.3 Air quality issues

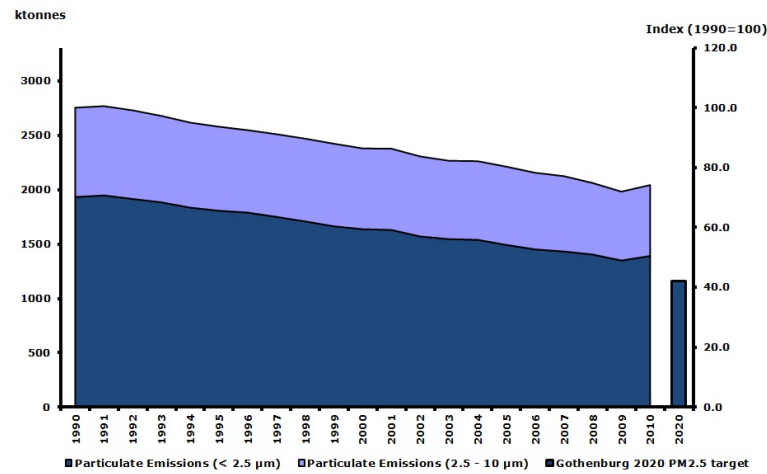


Figure 1.9: Trend of European emissions of primary  $PM_{2.5}$  and  $PM_{10}$ , according to the EEA. Colours are defined below the Figure.

## 1.3 Air quality issues

### 1.3.1 Health impacts

Statistical and epidemiological studies have consistently linked atmospheric pollution in urban environments to health problems (Latzka et al., 2009; Kim et al., 2015). Living along a busy street would be equivalent to smoking 10 cigarettes passively each day (van der Zee et al., 2016). WHO reported that for premature deaths caused by pollution, 80% were attributed to heart diseases and strokes, 14% to pulmonary diseases and 6% to lung cancers (WHO, 2014). Recent studies have estimated the economic cost of poor air quality to be around 20 billion euros per year in the UK (HoCEAC, 2011). In Germany, this figure is even higher, at 33 billion euros per year due to industrial emissions alone (Guerreiro et al., 2011). Correlations have been found between the atmospheric concentration of  $NO_2$  and respiratory symptoms, cardiovascular symptoms, and hospital admissions (Jon, 2011). Around 80% of the EU population is exposed to  $PM_{10}$  levels above the recommended guidelines, which consequences have been estimated to provoke around 400,000 premature deaths annually in the EU, bringing down the average life expectancy by approximately 6-12 months (Amann et al., 2013). Some studies have also demonstrated that it is economically beneficial to control air pollution to reduce its levels, the economic benefits being by far larger than the regulation enforcements costs (EPA, 1997, 2011). Nevertheless, it shall be noted that the gap in health metrics is important, especially

in developing countries suffering from inaccurate exposure assessment (Han and Naeher, 2006).

### 1.3.2 Degradation of ecosystems and cultural heritage

It is generally well known that high levels of ozone present risks for vegetation, decreasing the photosynthetic activities of plants with browning of the leaf (Pye, 1988). The related economic costs of crop yield loss due to ozone has also been shown to be important (Chuwah et al., 2015; Heagle, 1989). The deposition of PM on vegetation may also reduce the photosynthetic activities and cause leaf surface injury and its deposition on the ground can influence the pH of the soil (Grantz et al., 2003). PM is also associated with heavy metals concentrations, especially near road sides (Samara and Voutsas, 2005).

Atmospheric nitrogen dioxide dissolves with water to form nitric acid, which may present threat to any form of aquatic life. Excessive amounts of nitrogen can also lead to eutrophication which is the consequence of noxious aquatic plant growth, such as algae, which decrease levels oxygen when decomposing.

The emissions of  $\text{NO}_x$ , sulfur and carbon dioxide contribute to acid rain which can be very damaging for historical monuments. Materials such as zinc, bronze, nickel and natural stone are vulnerable to air pollution. The economic costs associated with the renovation of cultural monuments is far from being negligible. For example, the cost of cleaning white stone darkened with soot depositions, was estimated to be around £220 per metre square, which then add-up to a few billion pounds when considering all the affected surfaces in the EU (Watkiss et al., 2001).

### 1.3.3 Climate change

It has been recognised that climate change and air quality are linked together and can no longer be recognised as separate issues (Tai et al., 2010). Sources of air pollution are contributing to greenhouse gas emissions, the main global radiative force being of the Earth being  $\text{CO}_2$ .

Global warming has been to found to increase temperature over the mid-latitude continents (Jacob and Winner, 2009), leading to an increase in the number of heat waves which are associated to high pollution episodes. Less precipitation over some areas can also be attributed to global warming which consequently would decrease the washing out effects of aerosols (e.g. Trenberth 2011; Dai 2011). Climate mod-

els have also reported that a warmer climate could change atmospheric dynamic patterns, which subsequently could reduce the number of summer times cyclones in some areas leading to less venting and increased air pollution (Leibensperger et al., 2008), although other areas might see a strongest cyclonic activity (Knutson et al., 2010).

## 1.4 Air pollution mitigation measures

### 1.4.1 Removing air pollutants once emitted

One option for improving air quality consists of removing or decreasing specific levels of air pollutants after it has been emitted.

#### **Aerodynamic dispersion of vehicular emissions**

Improving aerodynamic dispersion can be achieved by altering street geometry, for example, roof shapes (Xie et al., 2005; Yang et al., 2016) or street canyon aspect ratios (Oke, 1988). However, modifying building geometry can be highly expensive and a detailed understanding of local meteorological conditions are required. Alternatively, Gallagher et al. (2015) suggested introducing solid and porous barriers to enhance pollution dispersion at street level in urban street canyons, although in some conditions these barriers can lead to increased concentrations. These barriers range from trees (Gromke and Ruck, 2007; Amorim et al., 2013b), hedgerows (Gromke et al., 2016), green roofs and facades (Speak et al., 2012; Perini et al., 2011; Pugh et al., 2012), solid barriers such as low boundary walls (McNabola et al., 2008; Gallagher et al., 2012), noise barriers (Baldauf et al., 2008; Finn et al., 2010) and parked cars (Abhijith and Gokhale, 2015; Gallagher et al., 2011).

#### **Dry deposition**

An alternative to physical barriers is offered by green infrastructures. Deposition of particulate matter depends on the species of tree, with deposition velocities that range from  $0.02 \text{ cm s}^{-1}$  for species such as *Picea* (Peters and Eiden, 1992) and *Ficus* (Freer-Smith et al., 2004) to  $30 \text{ cm s}^{-1}$  for the common Hazel (White and Turner, 1970). For grass, the dry deposition velocities range from  $0.01 \text{ cm s}^{-1}$  (Horbert et al., 1976) to  $8 \text{ cm s}^{-1}$  (Harrison et al., 1996). Vegetation is known to reduce  $\text{NO}_2$  concentrations via deposition (Smith et al., 2000), with deposition velocity

rates ranging from 0.007 - 0.042 cm s<sup>-1</sup> (Breuninger et al., 2013), to 0.12 cm s<sup>-1</sup> (Hereid and Monson, 2001) and 0.18 - 0.21 cm s<sup>-1</sup> (Rondón et al., 1993). The overall assessment of vegetation (not considered here), is a complex interplay between wind dynamics, deposition and chemistry, including biogenic volatile organic compounds (BVOCs). These can lead on to new particle formation as BVOCs play an important role in the atmospheric oxidation cycles (MacKenzie et al., 1991; Donovan et al., 2005).

For NO<sub>2</sub>, the application of photocatalytic paint on building and road surfaces has been shown to decrease NO<sub>2</sub> concentrations via deposition (Lasek et al., 2013), with literature suggesting the use of titanium dioxide (TiO<sub>2</sub>) as a photocatalyst to promote a deposition velocity of 0.002 - 0.02 cm s<sup>-1</sup> (Palacios et al., 2015) to 0.027 - 0.041 cm s<sup>-1</sup> (Boonen and Beeldens, 2014) and 0.24 cm s<sup>-1</sup> (DEFRA, 2016).

### 1.4.2 Decreasing the emissions

Another measure to improve air quality consists of decreasing emissions, to limit the amount of pollution released into the atmosphere.

#### Restrictive measures

Restrictive measures are a widely used option to decrease the emissions of air pollution.

- Congestion charging in central London was introduced to reduce the number of vehicles (Kelly et al., 2011).
- During pollution episodes, other cities have opted for alternate car circulation (Davis, 2008; Viegas, 2001). An emerging restrictive measure is to restrict the use of older vehicles known to be more polluting than other types of vehicle by imposing the display of an eco-pass (Invernizzi et al., 2011).
- The Cities of Paris, Mexico, Athens and Madrid have recently announced the full ban of diesel vehicles by 2025 (Guardian, 2016).
- For industries, the introduction of the carbon tax promises to limit the release of air pollution (in term of climate change) (Galinato and Yoder, 2010).

- Construction and demolition works, known to be an important source of particles, are now forced to use dust management plans, such as water-assisted dust sweeper (Holman and Consultants, 2014).

### **Incentive measures**

Incentive measures are mainly used to promote the use of less polluting transport. Government schemes and grants can for example target to increase rail transport, retrofit current bus fleet and promote cycling or walking (DEFRA, 2011a). The UK government road tax incentives encourage drivers to switch from petrol to diesel vehicles which decreases greenhouse gas emissions but increases the emissions of NO<sub>x</sub> and PM. This shows that some incentive measures can also lead to perverse air quality outcomes.

## **1.5 Thesis objectives**

Air quality has been shown to be a significant environmental problem, that affects most of the world's population. On top of serious health effects caused by air pollution, damages cultural heritage and ecosystems and the economic costs of poor air pollution are making it a crucial issue that needs to be tackled. Mitigation strategies have proved to be less successful than anticipated in recent years, with levels being measured above legal limits at over 40% of roadside air monitoring stations in 2010 in Europe (Guerreiro et al., 2013). Despite recent measures to reduce particulate matter (PM) levels, 92% of the European population was exposed to concentrations exceeding the WHO guidelines in 2012 (Guerreiro et al., 2014). In the City of Leicester, 80% of NO<sub>2</sub> is found to be emitted by traffic (DEFRA, 2011b). Leicester, along with many other cities in the UK, still fails to meet its European regulatory limits for urban air pollution (Evan, 2011).

Urban planners are constantly looking at solutions to improve air quality, mitigating strategies being one of them. Modelling the impact of existing or prospect mitigating strategies is appealing as these solutions are usually expensive to deploy. This thesis aims to model the effects of trees as a mitigating strategies on vehicular emissions. The structure of the thesis is as follow

- Chapter 2 describes the model used and a first evaluation exercise against wind tunnel measurements, including the evaluation of tree aerodynamic dispersion.

## 1.5 Thesis objectives

---

- Chapter 3 investigates the impact of trees in Marylebone Rd (London), where both aerodynamics and deposition effects of trees are modelled and compared against measurements of  $\text{NO}_x$  and  $\text{PM}_{2.5}$  from a monitoring site.
- Chapter 4 investigates the dispersive impact of trees in Leicester City Centre.
- Chapter 5 studies both the dispersive and deposition effects of trees in Leicester City Centre on  $\text{PM}_{2.5}$  concentrations.
- Chapter 6 includes a final simulation case in Oxford St (London) where trees are compared to other mitigation strategies from both an environmental and economic perspectives.

# Chapter 2

## Model description and evaluation

Predicting the concentration of air pollutants is essential for monitoring air quality. This chapter details the different types of air quality models, then introduces the physical background of the CFD model used in this thesis followed by a first evaluation against wind tunnel measurements.

### 2.1 Air quality dispersion models

#### 2.1.1 Existing dispersion models

A range of different urban dispersion models exist (see Figure 2.1), as presented in the review by Vardoulakis et al. (2003).

##### Gaussian dispersion models

For air quality modelling applications in an urban environment, Gaussian dispersion models are predominantly used, such as the Atmospheric Dispersion Modelling System ADMS-Urban (Carruthers et al., 1994) or the American Meteorological Society/Environmental Protection Agency Regulatory Model AERMOD (Cimorelli et al., 1998). These models assume that the dispersion of pollutant concentrations follow a Gaussian shape such that for steady state, non buoyant flow and a constant point source emission the dispersion of a gas is expressed as:

$$c(x, y, z) = \frac{Q}{2\pi\sigma_y\sigma_z u} \cdot \exp\left(\frac{-y^2}{2\sigma_y^2}\right) \cdot \left(\exp\left(\frac{-(z-h)^2}{2\sigma_z^2}\right) + \exp\left(\frac{-(z+h)^2}{2\sigma_z^2}\right)\right) \quad (2.1)$$

## 2.1 Air quality dispersion models

---

where  $c$  is the pollutant concentration ( $\text{kg m}^{-3}$ ),  $Q$  is the source emissions ( $\text{kg s}^{-1}$ ),  $x$  is the downwind distance from the source  $Q$  (m),  $y$  is the horizontal direction (m),  $z$  the vertical direction (m),  $u$  the flow speed ( $\text{m s}^{-1}$ ),  $h$  the height of release (m),  $\sigma_y$  is the horizontal cross-wind mixing of the pollutant (m) and  $\sigma_z$  is the vertical mixing of the pollutant (m). The dispersion coefficients  $\sigma_x$  and  $\sigma_y$  can be determined empirically or via theoretical formula (Hanna and Britter, 2010). A function is often used to express coefficients  $\sigma_x$  and  $\sigma_y$  as a distance away from the source such that  $\sigma_i^2 = \frac{2x \cdot D_i}{u}$ , where  $D_i$  is the turbulent diffusivity and  $i$  is  $y$  or  $z$ . The first term of Eq. 2.1 represents advection whereas the second and third term represent the turbulent diffusion. Eq. 2.1 neglects the impacts of molecular diffusion during convection (convection includes both advective and diffusive terms), which is often the case. However this assumption can lead to important errors at low wind speeds, when transport via molecular diffusion is no longer negligible. The integration of surface roughness has been found to have an important impact on the simulated pollutant concentrations (Barnes et al., 2014), showing the importance of estimating urban surface roughness properties in Gaussian dispersion models.

### **Lagrangian Particle Dispersion Models (LPDM)**

In LPDM models, the individual trajectories of thousands of particles are simulated across a mean wind flow velocity. In addition to the wind, a turbulent velocity and a random turbulent velocity are used to calculate the trajectories. LPDMs use time-dependent simulations and present similar results to Gaussian dispersion models over simple scenarios (Hanna and Britter, 2010). LPDMs are offering better accuracy in situations where Gaussian models are expected to poorly perform (e.g. when Gaussian model assumptions are no longer valid).

### **Computational Fluid Dynamics (CFD)**

Another modelling technique of gas dispersion relies on CFD applications. As they tend to be computationally demanding, owing to large computational grids (usually numbering a few million cells) and long computational times, CFD models are more frequently used for small scale scenarios (street canyon scale).

CFD models can resolve three-dimensional distributions of wind flow and pollutant concentration, making them an attractive choice for urban applications, where the structure of a city can be heterogeneous with streets and buildings of different sizes and shapes. CFD models are especially used for street canyon applications,

where the concentration of pollutants can reach high levels owing to vortices formed by wind flow and the subsequent recirculation of pollution between surrounding buildings. Depending on the kind of CFD model used, time-dependent simulations can be predicted.

### 2.1.2 Comparisons of dispersion models

In Figure 2.1 are listed different dispersion models and their applications depending on the scale of the modelling area (adapted from Denby et al. 2011). Gaussian models are generally used for urban applications but can model larger simulation domain if given a required homogeneous meteorology. However, Gaussian models are currently not able to model the aerodynamic effects of trees, and therefore, are not suitable for this thesis. Lagrangian models are able to model a whole wide range of scales, their accuracy depending on the number of trajectories of individual particles. Eulerian CFD models offer the benefit compared to Lagrangian models to provide space filling results. However, CFD models are perceived to be highly computationally expensive in modelling urban scale. Nevertheless, urban scale CFD models have already been the object of studies (Hanna et al., 2006; Parra et al., 2010) and theses (Gartmann, 2012; Philips, 2012) which investigated the dispersion of air pollutant around buildings structures. In this thesis, CFD dispersion simulations are used to model pollution concentrations in both street canyon and urban scales scenarios.

## 2.1 Air quality dispersion models

---

Model types and applications	Gaussian models	Lagrangian particle models	CFD models
Open roads			No obstacles, computationally expensive
Street canyon	In combination with parameterised wind field model	In combination with parameterised wind field model	Computationally expensive
Urban scale	Requires homogenous meteorology	Computationally expensive	Highly computationally expensive
Regional scale	Requires homogenous meteorology	Computationally expensive	Not computationally feasible
Integration of trees	✗ Aerodynamic ✓ Deposition	✓ Aerodynamic ✓ Deposition	✓ Aerodynamic ✓ Deposition

Figure 2.1: Fitness for purpose matrix for dispersion models (adapted from Denby et al. 2011). Different colours indicate the fitness for purpose, green = *fit*; orange = *conditionally applicable* (caused by difficult parameterisation or long processing time); red = *not fit*. *Aerodynamic* is defined as the modelling of the dispersive effects of trees and *Deposition* as the modelling of air pollution deposition on the leaf surfaces.

## 2.2 General considerations

### 2.2.1 Generic Navier-Stokes equations

The Navier-Stokes equations are used in Fluid Mechanics to describe the movements of fluids, their derivation are detailed in Appendix A. The general form of the Navier-Stokes Equations (NSE) can be expressed as

$$\frac{\partial \rho}{\partial t} + \nabla \cdot (\rho \cdot u) = 0 \text{ (conservation of mass),} \quad (2.2)$$

$$\frac{\partial(\rho \cdot u)}{\partial t} + \nabla \cdot (\rho \cdot u \cdot u) = -\nabla P + \nabla \tau + \rho \cdot g \text{ (momentum equation).} \quad (2.3)$$

where  $\rho$  is the fluid density ( $\text{kg m}^{-3}$ ),  $u$  the fluid velocity ( $\text{m s}^{-1}$ ),  $\tau$  the stress tensor ( $\text{kg m}^{-1} \text{s}^{-2}$ ) and  $g$  represents the external forces ( $\text{m s}^{-2}$ ). Eq. 2.2 is also called continuity equation. On the left of Eq. 2.3 are expressed the acceleration and convection of the fluid, which are equal to the sum of body forces expressed on the right side of the equation. Note that in these equations the divergence operator is used ( $\nabla \cdot A = \text{div } A = \frac{\partial A_x}{\partial x} + \frac{\partial A_y}{\partial y} + \frac{\partial A_z}{\partial z}$ ).

### Incompressibility

Wind flow simulations can be considered incompressible for Mach numbers that are lower than 0.3 (Anderson, 2005). Following Eq. 2.4, we can consider that wind flow simulations are incompressible for velocities that are lower than a  $100 \text{ m s}^{-1}$ .

$$M = \frac{u}{c}, \quad (2.4)$$

where  $M$  is the Mach number,  $u$  is the flow velocity (here the wind speed) in  $\text{m s}^{-1}$  and  $c$  is the speed of sound (in dry air at  $20 \text{ }^\circ\text{C}$ , the speed of sound is  $343.2 \text{ m s}^{-1}$ ).

### Incompressible Navier-Stokes equations

The incompressible Navier-Stokes governing equations are expressed with the conservation of mass (Eq. 2.5) and conservation of momentum (Eq. 2.6) equations (see full derivations of the Navier-Stokes equations in Appendix A):

$$\frac{\partial u_i}{\partial x_i} = 0, \quad (2.5)$$

$$\frac{\partial u_i}{\partial t} + \frac{\partial u_j u_i}{\partial x_j} = \frac{\partial}{\partial x_j} \left( \nu \frac{\partial u_i}{\partial x_j} \right) - \frac{1}{\rho} \frac{\partial p}{\partial x_i}, \quad (2.6)$$

where  $i$  and  $j$  represents either  $x, y$  and  $z$  (see Eq. A.18). The kinematic viscosity ( $\text{m}^2 \text{s}^{-1}$ ) is expressed as:

$$\nu = \frac{\mu}{\rho}, \quad (2.7)$$

where  $\mu$  is the dynamic viscosity ( $\text{N s m}^{-2} = \text{kg m}^{-1} \text{s}^{-1} = \text{Pa s}$ ) and  $\rho$  the fluid density ( $\text{kg m}^{-3}$ ).

### 2.2.2 Resolving the Navier-Stokes equations

The Navier-Stokes equations can be solved numerically using different CFD models know as Direct numerical simulation (DNS), Large Eddy Simulation (LES) and Reynolds-averaged Navier-Stokes (RANS). Figure 2.2 illustrates the modelling of a flame by each of the CFD models.

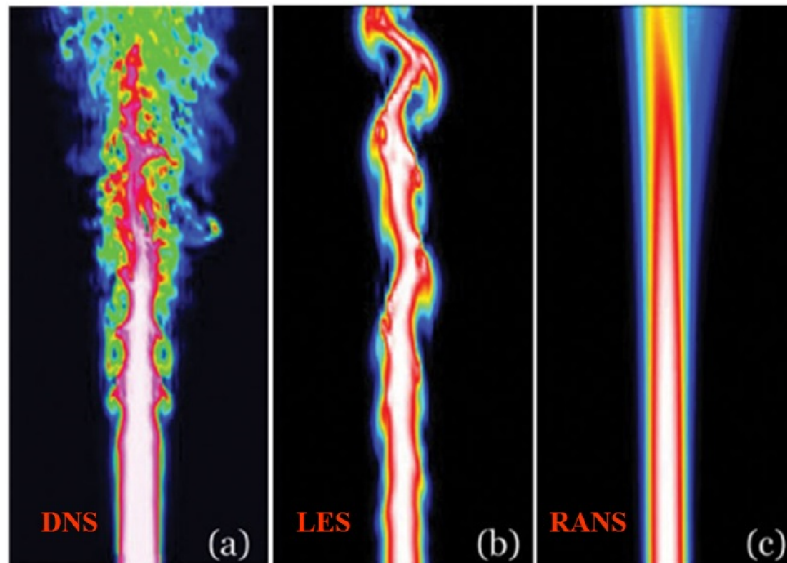


Figure 2.2: Simulations of flame produced by combustion a) from DNS modelling b) from LES modelling and c) from RANS modelling (image credit: ENEA, Italy).

#### DNS

Direct numerical simulations (DNS) fully resolve the Navier-Stokes equations. They, therefore, provide the most accurate simulations of CFD models, but are also extremely computationally expensive. They are primarily used in fundamental research to understand turbulence mechanisms.

### **LES**

Large Eddy Simulation models resolve the Navier-Stokes equations with the introduction of a turbulence model which solves the larger eddies and ignores the smaller eddies which are demanding to calculate. They are widely used in research and engineering domains such as combustion (Pitsch, 2006), acoustics (Wagner et al., 2007) or planetary boundary layer flows (Sullivan et al., 1994). LES model have been applied to street canyon simulations (Liu and Barth, 2002) and proved to provide increased accuracy compared to traditional Reynolds-averaged Navier-Stokes (RANS) models (Tominaga and Stathopoulos, 2011; Salim et al., 2011). Another reason leading for the choice of LES modelling is their ability to resolve intermittent flow structures. However, their computational costs are much greater than RANS simulations which prevent them from being used as dispersion model over large urban areas.

### **RANS**

RANS models are the most widely used CFD model, with a very large number of users across industries and fields of research. Their popularity can be explained by a much smaller computational cost than LES (and even more than DNS). This decrease in computational time (around an order of magnitude less) occurs as a result of providing a steady state (time-averaged) view of the flow without calculations of time-dependent fluctuations (see Figure 2.2). The RANS governing equations are solved with the introduction of the Reynolds stress term (last term in Eq. 2.13), which accounts for the modelling of turbulent fluctuations and has been the subject of intense modelling and interest over the past decades, known as the closure problem (Dewan, 2011; Hanjalic, 2004; Hanjalí, 1999).

Nevertheless, RANS simulations have been shown to perform better than Gaussian models in an urban environment, although both models prove to work reliably (Buccolieri and Sabatino, 2011). The review of Tominaga and Stathopoulos (2013) shows that the number of CFD applications in urban environments have been increasing recently. Regarding the FLACS RANS model, Hanna et al. (2004) have demonstrated that 86% of the predictions were within a factor of two of the observations, which is within the range of other dispersion models. Although no quantitative comparisons were made, Hanna et al. (2006) also shown that 5 different RANS models qualitatively present similar features when simulating a gas release in Manhattan

(New York city, United States).

The current literature shows an increased performance by using CFD simulation in urban environments rather than traditional Gaussian model. However, the parameterisation of CFD models remains a complex task (generation of the computational grid, boundary conditions (BC) parameterisation, etc.) which tends to make Gaussian dispersion models the preferred option for modelling simple geometry and point emission sources (Riddle et al., 2004).

## 2.3 RANS simulations

### 2.3.1 Derivation of RANS equations

The Reynolds decomposition method used to derive the Navier-Stokes equations is a mathematical operation which decomposes the time-averaged and fluctuating components from the steady state component (see Figure 2.3) such that:

$$u = \bar{u} + u' \quad (2.8)$$

$$p = \bar{p} + p' \quad (2.9)$$

where the steady state components  $u$  and  $p$  are on the left hand side of Eq. 2.8 and 2.9,  $\bar{u}$  and  $\bar{p}$  are time-averaged and  $u'$  and  $p'$  the fluctuating components ( $du'/dt = dp'/dt = 0$ ).

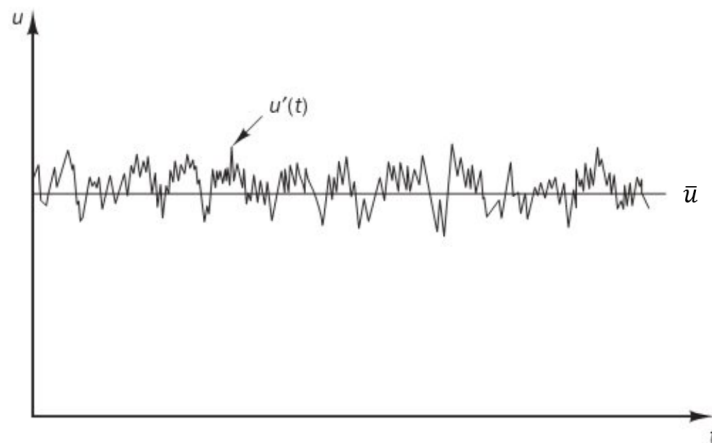


Figure 2.3: Illustration of the Navier-Stokes approximation with the definition of an average  $\bar{u}$  and transient term  $u'(t)$ .

Applying the Reynolds decomposition to Eq. 2.5 and 2.6, the RANS equations are obtained

$$\frac{\partial \bar{u}_i}{\partial x_i} = 0, \quad (2.10)$$

$$\frac{\partial \bar{u}_i}{\partial t} + \bar{u}_j \frac{\partial \bar{u}_i}{\partial x_j} = \frac{\partial}{\partial x_j} \left( \nu \frac{\partial \bar{u}_i}{\partial x_j} - \overline{u'_i u'_j} \right) - \frac{1}{\rho} \frac{\partial \bar{p}}{\partial x_i}, \quad (2.11)$$

Before applying the Reynolds decomposition to Eq. 2.6, it is worth noting that

$$\begin{aligned} \overline{u_i u_j} &= \overline{(\bar{u}_i + u'_i)(\bar{u}_j + u'_j)} \\ &= \overline{\bar{u}_i \bar{u}_j + \bar{u}_i u'_j + u'_i \bar{u}_j + u'_i u'_j} \\ &= \overline{\bar{u}_i \bar{u}_j} + \cancel{\overline{\bar{u}_i u'_j}} + \cancel{\overline{u'_i \bar{u}_j}} + \overline{u'_i u'_j} \\ &= \bar{u}_i \bar{u}_j + \overline{u'_i u'_j} \end{aligned} \quad (2.12)$$

Applying the Reynolds decomposition to the conservation of momentum (Eq. 2.6) leads to the equation

$$\frac{\partial \bar{u}_i}{\partial t} + \bar{u}_j \frac{\partial \bar{u}_i}{\partial x_j} = -\frac{1}{\rho} \frac{\partial \bar{p}}{\partial x_i} + \nu \frac{\partial}{\partial x_j} \left( \frac{\partial \bar{u}_i}{\partial x_j} \right) - \frac{\partial \overline{u'_i u'_j}}{\partial x_j} \quad (2.13)$$

As mentioned earlier, the real limitations with time-averaged RANS equation is the introduction of the Reynolds stress term which accounts for turbulent fluctuations (last term on Eq. 2.13). The time-averaged process implies a loss of information, and the methods used to solve the Reynolds stress term have been a very active area of research. Although not used in this thesis, it is worth mentioning the existence of the Reynolds Stress Model (RSM) which introduces additional equations to solve the Reynolds stress term. RSM models have been shown to provide more accurate results than other RANS models, which comes at the cost of more computationally intensive calculations (7 equations solved instead of 2 for the k- $\epsilon$  model). This comes from the fact that RANS simulations usually underpredict shear-layer gradient in space (Menter, 2009).

### 2.3.2 k- $\epsilon$ model equations

After a few mathematical operations on the incompressible and momentum Navier Stokes equations (see Furbo 2010 for the detailed derivation of the equations), the

equation for turbulent kinetic energy ( $k$ ) is obtained (Eq. 2.14).

$$\frac{\partial k}{\partial t} + \bar{u}_j \frac{\partial k}{\partial x_j} = - \frac{\partial}{\partial x_j} \left( \frac{1}{2} \overline{u'_i u'_i u'_j} + \frac{1}{\rho} \overline{u'_j p'} - \nu \frac{\partial k}{\partial x_j} \right) - \overline{u'_j u'_i} \frac{\partial \bar{u}_i}{\partial x_j} - \epsilon \quad (2.14)$$

In physical terms, the change of kinetic energy in Eq. 2.14 can be seen as: unsteady term + convection = -(turbulent transport + pressure diffusion - molecular diffusion of turbulence) - production - dissipation.

In order to solve this equation, a closure approximation is used to estimate the turbulent transport, pressure diffusion, production and dissipation which approximates the following model transport equation for the kinetic energy

$$\frac{\partial k}{\partial t} + \bar{u}_j \frac{\partial k}{\partial x_j} = \frac{\partial}{\partial x_j} \left[ \left( \nu + \frac{\nu_T}{\sigma_k} \right) \frac{\partial k}{\partial x_j} \right] + \nu_T \left( \frac{\partial \bar{u}_i}{\partial x_j} + \frac{\partial \bar{u}_j}{\partial x_i} \right) \frac{\partial \bar{u}_i}{\partial x_j} - \epsilon. \quad (2.15)$$

where  $\sigma_k$  is the turbulent Prandtl number and is usually taken as equal to one. The Prandtl number is defined as the dimensionless ratio between the viscous diffusion rate over the thermal diffusion rate.

The concept of energy cascade is used for the modelling of turbulence. It was first expressed by Richardson (1922) and considers that turbulence is composed of eddies of different sizes. Larger eddies that are unstable are decomposed by transferring their energy into smaller eddies. This process carries on until the molecular diffusivity prevails over inertial forces, which occurs at low Reynolds number

$$Re = \frac{uL}{\nu} \quad (2.16)$$

where  $L$  is the characteristic length scale of the flow and  $u$  the velocity scale of the eddies.

To avoid modelling a characteristic length scale of the flow, an additional transport equation for the dissipation can be solved on top of the  $k$  equation. These two equations for  $k$  and  $\epsilon$  forms the  $k$ - $\epsilon$  model which was first described by Jones and Launder (1972). The  $\epsilon$  equation is expressed as

$$\frac{\partial \epsilon}{\partial t} + \bar{u}_j \frac{\partial \epsilon}{\partial x_j} = \frac{\partial}{\partial x_j} \left( \frac{\nu_T}{\sigma_\epsilon} \frac{\partial \epsilon}{\partial x_j} \right) + C_{\epsilon 1} \frac{\epsilon}{k} \nu_T \left( \frac{\partial \bar{u}_i}{\partial x_j} + \frac{\partial \bar{u}_j}{\partial x_i} \right) \frac{\partial \bar{u}_i}{\partial x_j} - C_{\epsilon 2} \frac{\epsilon^2}{k} \quad (2.17)$$

The turbulent viscosity ( $\text{m}^2 \text{s}^{-1}$ ) in Eq. 2.17 and Eq. 2.17 is defined as

$$\nu_T = C_\mu \frac{k^2}{\epsilon} \quad (2.18)$$

and the Reynolds equations (Eq. 2.10 and 2.13) are solved for  $\overline{u_i}$  and  $\overline{p}$ . The standard constants as defined by Pope (2000) and used for the k- $\epsilon$  model are

$$C_\mu = 0.09, C_{\epsilon 1} = 1.44, C_{\epsilon 2} = 1.92, \sigma_k = 1.0, \sigma_\epsilon = 1.3$$

### 2.3.3 Summary of guidelines for RANS simulations

This paragraph summarises the guidelines and advises that have been produced for the use of RANS simulations within urban environments (Franke et al., 2007; Blocken, 2015).

#### Atmospheric stability

This thesis assumes a neutral condition of the atmosphere, which allows the neglect of buoyancy due to thermal effects within the ABL. Studies have confirmed the validity of a neutral atmosphere assumption for urban scale simulations (Lundquist and Chan, 2007). However for mesoscale and regional scale modelling, stable and unstable atmosphere needs to be considered.

#### Thermal effects

The introduction of thermal effects is challenging, as the temperature changes across the time of day (solar angle) by microphysics (clouds, precipitation, aerosols), topography (hills, buildings), etc. Although these effects are important for mesoscale atmospheric processes (meteorology), the introduction of temperature in CFD dispersion models remain a complicated task and is usually neglected. It should be noted that a branch of CFD studies focusing on urban heat island modelling, with the introduction of ground temperature gradients does exist, but these studies tend to be more focused on air flow simulations (Arnfield, 2003). Dispersion models usually neglect urban heat islands effects which are negligible on air pollution dispersion when the wind speed is greater than  $2 \text{ m s}^{-1}$  (Parra et al., 2010; Santiago et al., 2017).

### **Spatial resolution**

For wind flow simulations within street canyons, Franke et al. (2007) advised the use of at least 10 cells along the width of the canyon as a sufficient number of cells is needed to correctly reproduce the wind circulation. For a street canyon width of 10 m, these would lead to a horizontal resolution of 1 m minimum. For the study of pedestrians (1.5 m height), Blocken (2015) advises to have at least two cells on the vertical axis below 1.5 m. Therefore, the order of magnitude of vertical spatial resolution needed is 0.75 m minimum.

### **Temporal resolution**

RANS models provide steady state simulations, where the wind flow and concentrations are time-averaged (no fluctuations are modelled). An approach exists in modelling a large number of simulations to create an ensemble (such as in Parra et al. 2010) in order to take into account the meteorology conditions (wind speed, wind direction), and seasonality (spring, summer, autumn and winter for the UK) in the case of tree modelling. This technique has already been applied to estimate the potential of wind resources for wind-turbine applications, where the power output of a wind farm is calculated over different wind directions (see for example Barthelmie et al. 2010). In the case of air pollution concentrations from vehicular emissions, the limitations of RANS in temporal resolution necessitates the use of traffic averaged conditions. Traffic turbulence is known to affect the way vehicular emissions disperse, which is related to the speed of the vehicles, the street canyon aspect ratio and the road congestion (Vachon et al., 2002). Traffic turbulence has been successfully implemented in RANS models taking the assumption of different traffic densities (Di Sabatino et al., 2003).

### **Computational grid**

Different grid types exist, which are structured, unstructured and hybrid mesh. A structured mesh has many advantages in terms of code efficiency as the grid elements are identified by storage efficient coordinates (i, j and k), but is limited to conform to complicated shapes. Another advantage of structured mesh over unstructured mesh consists of better convergence and consequently greater accuracy (Castillo, 1991), but the quality of the mesh must be carefully controlled in order to simulate an accurate wind flow.

Unstructured meshes have a greater ability to conform to complicated shapes, however, the block structure is replaced by node numbers and a connectivity table connecting the nodes which leads to inefficient memory structures. Unstructured meshes are preferred to structured meshes when the structured mesh quality is unsatisfactory (e.g. the LES Fluidity model is based on unstructured mesh for volcanic ash modelling Jacobs 2014).

In this thesis, the computational resources needed for city-scale simulations were extremely demanding (up to 17 millions cells for Leicester City Centre in Chapter 5). The inefficiency of unstructured meshes led to the choice of using a structured mesh, with careful attention being paid, during the mesh generation, to key parameters such as the expansion ratio (growth between adjacent cell sizes  $\leq 20\%$ ) and the skewness (mesh quality indicator looking at optimum cell size  $\leq 0.85$ ) as recommended by best practice guidelines for CFD simulations (e.g. Jorg et al. 2007).

### **Boundary conditions**

In CFD, the term Boundary Conditions (BC) defines the parameterisation of the grid nodes on the external sides of the computational domain.

A distance of at least 5 H (H represents the height of the tallest buildings) is recommended between the inflow BC and the built area and of at least 15 H between the built area and the outflow BC. The vertical extension of the domain should be at least 5 H, where H is the tallest building in the computational domain (Jorg et al., 2007). The lateral extension of the domain should be placed further than 5 H from the side of the built area. Following the vertical and lateral positions of the domain, the blockage ratio of the built area should not exceed 3% (where the blockage is defined as the ratio of the projected area of the built area to the cross section of the computational domain).

The determination of appropriate roughness parameters is essential for accurate simulations of ABL flows. Blocken (2015) advises to split the computational domain into sub-domains, each of them having their own roughness (see Figure 2.4). The roughness values can be estimated using existing classifications (WMO, 2008; Wieringa, 1992).

In the ABL, the mean velocity boundary flow and the turbulent dissipation follow a logarithmic law (Hargreaves and Wright, 2007). The BC are then parameterised

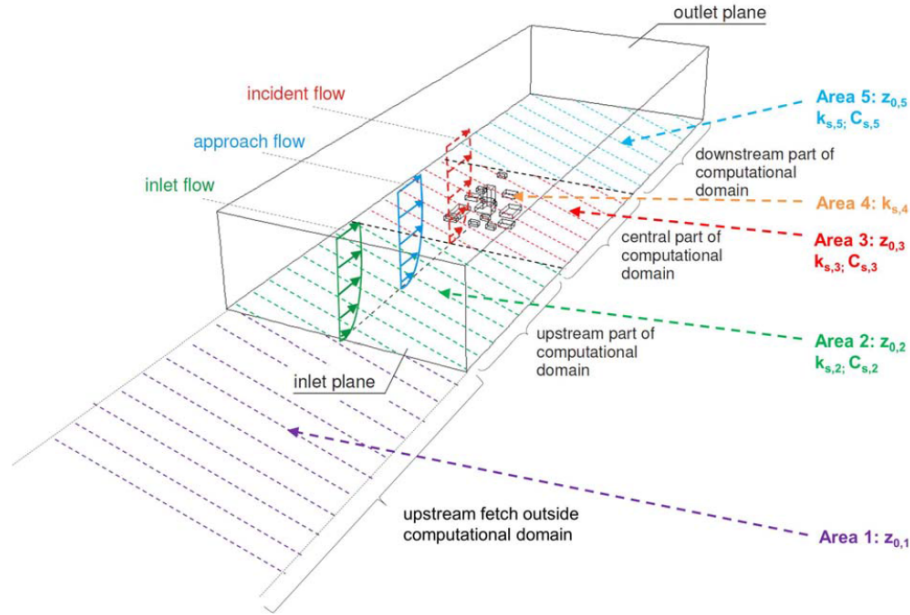


Figure 2.4: Specification of roughness parameters for the simulations of ABL flows (Blocken, 2015). Note that the Area 1 is outside the computational domain (used for inflow parameterisation).  $z_0$  is defined as the surface roughness length (m),  $k_s$  as the equivalent sand-grain roughness height (m) and  $C_S$  is the roughness constant.

accordingly such that

$$U = \frac{U^*}{K} \ln \left( \frac{z - z_g + z_0}{z_0} \right) \quad (2.19)$$

$$\epsilon = \frac{U^{*3}}{Kz} \left( 1 - \frac{z}{\delta} \right) \quad (2.20)$$

where  $U$  is the fluid velocity ( $\text{m s}^{-1}$ ),  $u^*$  is the frictional velocity ( $\text{m s}^{-1}$ ),  $K$  is the Karman's constant,  $z$  is the vertical co-ordinate (m),  $\delta$  is the boundary layer depth (m),  $z_0$  is the surface roughness length (m) and  $z_g$  is the minimum value in the  $z$  direction (m).

### Discretisation method

In CFD, the schemes represent a class of numerical discretisation methods for solving the RANS equations. Second order schemes are recommended, as first order are found to be too inaccurate (Franke et al., 2007; Blocken, 2015). Second order upwind schemes were followed for wind flow simulation.

In the case of RANS simulations, the iteration process continues until the solution converges and a solution is found (the difference of the flow solution between two

time step is less than the convergence criteria). A minimum convergence criterion of at least  $10^{-4}$  is recommended for all flow field variables (Jorg et al., 2007).

### Evaluation

The evaluation of CFD dispersion models need to be assessed against wind tunnel experiments, tracer experiments or a real case application with measured air pollution concentrations. Each of the following evaluation cases have been studied in this thesis: evaluation against wind tunnel in Chapter 2, against real measured concentrations of  $\text{NO}_x$  and PM in Chapter 3 and against a tracer experiment in Appendix C.

A number of metrics are used to evaluate the performance of air quality models (Derwent et al., 2010; Jorg et al., 2007). The correlation coefficient  $R^2$  is one of them, although Derwent et al. 2010 suggested that additional statistical parameters should be used in conjunctions with the  $R^2$ . In this thesis, the Factorial Bias (FB), Normalised Mean Square Error (NMSE) and the Factor of two (FAC2) were used for model evaluation. They are defined such that

$$\begin{aligned}
 -0.3 \leq FB &= \frac{\sum_{i=1}^N O_i - P_i}{0.5 \cdot \sum_{i=1}^N (O_i + P_i)} \leq 0.3 \\
 NMSE &= \frac{1}{N} \sum_{i=1}^N \frac{(O_i - P_i)^2}{\bar{O} \cdot \bar{P}} \leq 1.5 \\
 0.5 \leq FAC2 &= \frac{\bar{P}}{\bar{O}} \leq 2
 \end{aligned} \tag{2.21}$$

where  $N$  is the number of observations,  $O_i$  are the measured (reference) values and  $P_i$  are the predicted modelled values.

#### 2.3.4 Tree modelling

In this thesis, the National Tree Map<sup>TM</sup> (NTM) Crown Polygon produced by LiDAR data from Bluesky was used in the tree database to map individual trees or closely grouped tree crowns (Bluesky, 2014). Trees and bushes over 3 m in height were included in the database. The NTM<sup>TM</sup> provided a canopy top height but did not provide the canopy base height. Current literature has described the use of an

assumed canopy base height of 1/3 of the canopy top height which is the same assumption as that used in the wind tunnel experiment studies (Gromke et al., 2008). Figure 2.5 shows an example of a idealised trees as viewed by the CFD model.

Here, the Leaf Area Density (LAD in  $\text{m}^2 \text{m}^{-3}$ ) is assumed to be constant across the canopy, however further work is intended to improve the modelling of trees with the integration of varying LAD (see Future Work section in Chapter 8).

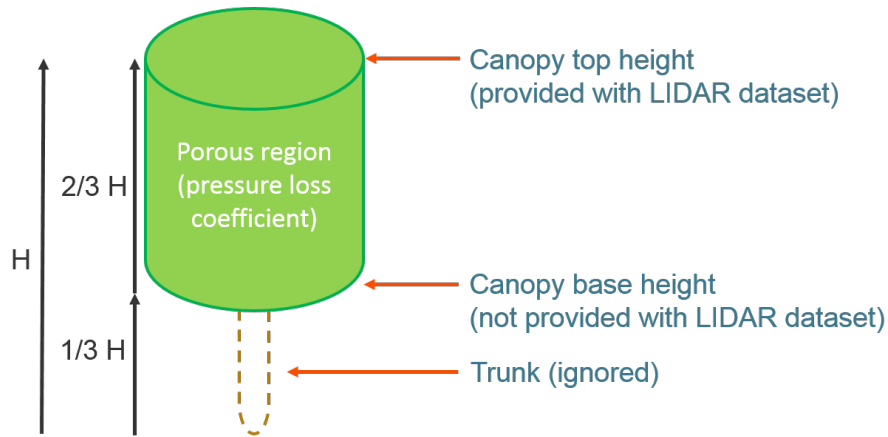


Figure 2.5: Assumption made for modelling tree: an average tree profile with a constant LAD over height.

Other studies have recommended the tree porosity (LAD) to change as a function of height (Hofman et al., 2016), but this approach requires a detailed LIDAR information for each individual tree which was not available here. In order to model their aerodynamic effects, trees were treated as a porous media (e.g. (Buccolieri et al., 2011; Vranckx et al., 2015)) by adding a momentum source ( $S$ ) variable to the cells occupied by the tree canopy such that:

$$S = -\lambda \left( \frac{1}{2} \rho u |u| \right), \quad (2.22)$$

where  $S$  is the momentum source loss ( $\text{Pa m}^{-1}$ ),  $\lambda$  is the inertial resistance factor or pressure loss coefficient ( $\text{m}^{-1}$ ),  $\rho$  is the fluid density ( $\text{kg m}^{-3}$ ) and  $u$  the fluid velocity ( $\text{m s}^{-1}$ ).

In the case of modelling the air pollution deposition on trees, the deposition inside the tree crown cells was parametrised as a sink term applied at each Eulerian step. The sink term is directly integrated inside the scalar dispersion equation (see Eq. 2.27). The scalar dispersion is calculated once the wind fields have been computed.

Without restriction on the courant number (which can be used to limit the number of cells on which the pollutant dispersed within one iteration), the assumption can be taken that one model iteration is equal to one second. The deposition inside the tree crown cells can then be expressed such that

$$\frac{\Delta C(t)}{\Delta t} = C(t-1) \times LAD \times Vd \quad (2.23)$$

where  $\Delta C(t)$  is the change in particles concentration via deposition in an Eulerian forward step ( $\text{kg m}^{-3}$ ),  $\Delta t$  is equal to one second (one model iteration),  $C(t-1)$  is the particles concentration ( $\text{kg m}^{-3}$ ),  $LAD$  is the Leaf Area Density ( $\text{m}^2 \text{m}^{-3}$ ) and  $Vd$  is the deposition velocity ( $\text{m s}^{-1}$ ).

In the rest of the thesis, the aerodynamic dispersive effects of trees will be assumed to come from the difference between a tree-free city and a city with trees (without deposition on trees enabled). The amount of deposition on trees will be calculated as the difference between a city with trees without and with deposition on trees enabled (see Figure 2.6).

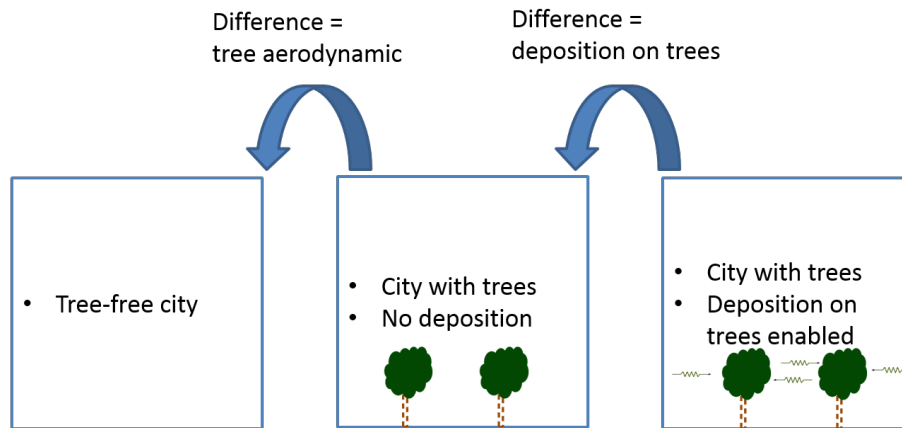


Figure 2.6: Calculations of the aerodynamic and deposition effects of trees.

### 2.3.5 CFD software platform

The CFD simulations presented in this thesis were performed using the OpenFOAM (Open Field Operation and Manipulation) open source software platform (freely available at <http://www.openfoam.com>). OpenFOAM has a large range of academic and commercial users, such as for wind farm applications (Barthelmie et al., 2010), naval architecture design (Jasak, 2009), combustion processes (Kassem et al., 2011),

etc. For ABL flow simulations, OpenFOAM has been shown to produce results as satisfactory as the commercial version Fluent (Balogh et al., 2012). Modelling the effect of trees has also been the object of recent studies in OpenFOAM (Vranckx and Vos, 2013; Vranckx et al., 2015).

## 2.4 Model evaluation against wind tunnel measurements

### 2.4.1 Wind tunnel description

Data to evaluate the model was taken from the CODASC wind tunnel experiments (CODASC, 2014). Additional information on the wind tunnel setup can be found in Gromke (2011) and Gromke and Ruck (2012). The experiment consisted of an isolated street canyon with trees and a ratio of width over height (W/H) of 1, at a scale of 1:150 (Figure 2.7a, b and c). Two lines of buildings of length 180 m, height 18 m, and width 18 m were separated by a street of width 18 m.

The approaching flow generated in the wind tunnel, from left to right along the  $x$  axis (Figure 2.7a), was designed to reproduce an atmospheric boundary layer flow that follows a power law such that:

$$\frac{U(z)}{U_H} = \left(\frac{z}{H}\right)^\alpha, \quad (2.24)$$

The reference velocity of  $U_H = 4.70 \text{ m s}^{-1}$  was taken at the building roof height  $H$  of 120 mm (18 m in real scale) with  $\alpha = 0.30$ . The surface roughness of the wind tunnel was  $z_0=0.0033$ . The approaching flow direction was set to 3 directions from the  $x$  axis:  $0^\circ$ ,  $45^\circ$  and  $90^\circ$  (Figure 2.7a). The wall A corresponds to the leeward side and the wall B to the windward side of the street canyon (Figure 2.7a). The modelled trees were placed in the centre of the street canyon. The tree canopy height is equal to the building height (18 m in full scale) and the canopy base height is equal to a third of the canopy height (6 m in full scale) as shown in Figure 2.7b. The wind tunnel pressure loss coefficient of the tree vegetation was  $\lambda = 200 \text{ m}^{-1}$  (around  $1.6 \text{ m}^{-1}$  in real scale) (Gromke et al., 2008). The gas tracer used in the wind tunnel experiment was sulphur hexafluoride ( $\text{SF}_6$ ) and its concentration was measured by Electron Capture Detection (ECD) at a distance of 5 mm (0.042 H) from the walls A and B. It was emitted at a constant emission rate  $Q_i$  ( $\text{m}^2\text{s}^{-1}$ ) by

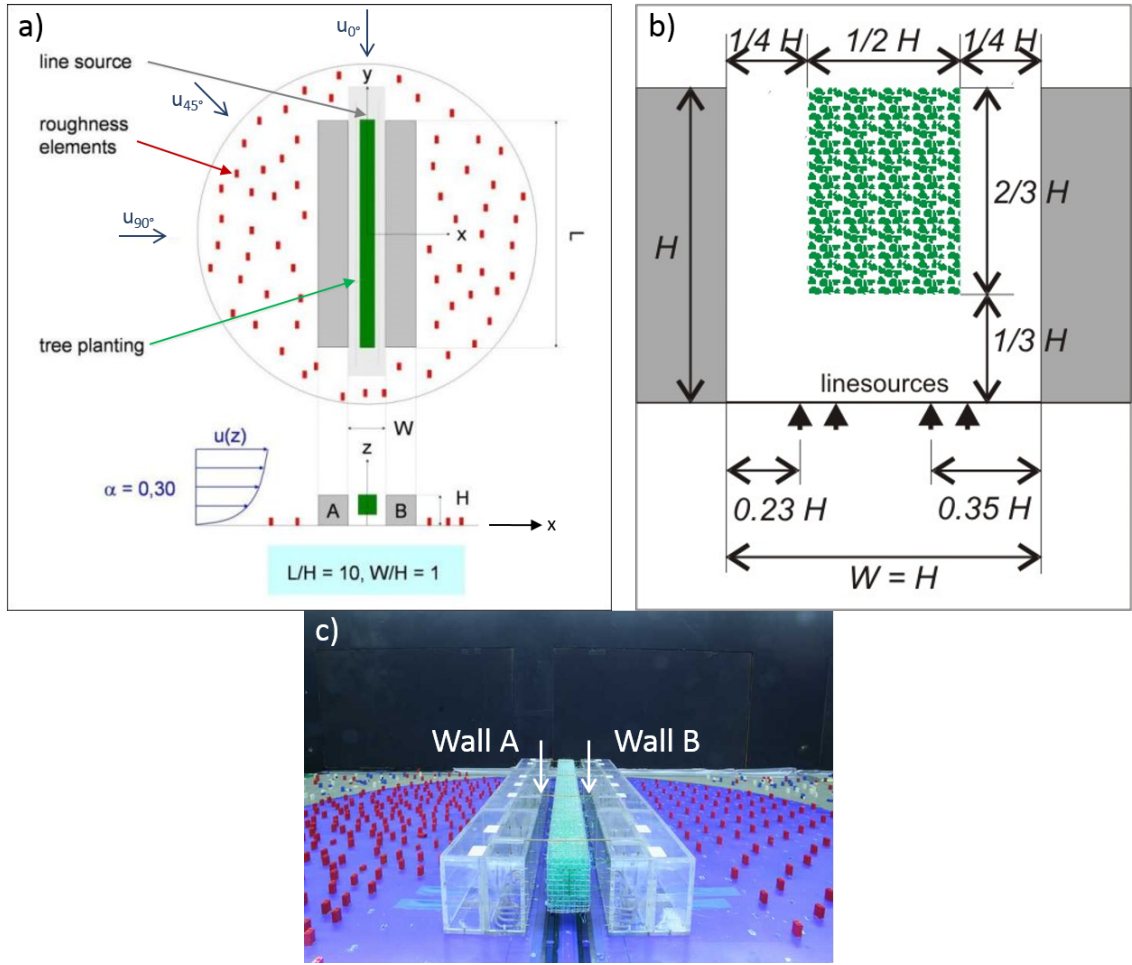


Figure 2.7: a) Sketch of the wind tunnel experiment. b) Dimensions of the street canyon. c) Wind tunnel model of idealised street canyon with trees (adapted from CODASC 2014).

4 line sources situated in the middle of the street canyon of length 1200 mm (180 m in real scale) as shown of Figure 2.7b). The concentrations was only measured at the walls inside the canyons (no data are available for the ground, roof and inside the canyon). The measured concentration  $c_m$  has been normalised to the normalised concentration  $c^+$  as

$$c^+ = \frac{c_m H U_H}{Q_l}. \quad (2.25)$$

### 2.4.2 CFD parametrisation for the wind tunnel

A base model was developed in the OpenFOAM software to reproduce the wind-tunnel experimental data. The model parametrisation presented in this section is

## 2.4 Model evaluation against wind tunnel measurements

---

CFD PARAMETERS	UNITS
Mesh type	Hexahedral
Number of cells	644 000
Residual convergence	$10^{-6}$
Smallest grid size along the x axis ( $\Delta x_{min}$ )	0.06 H
Smallest grid size along the y axis ( $\Delta y_{min}$ )	0.06 H
Smallest grid size along the z axis ( $\Delta z_{min}$ )	0.05 H
Street canyon height (H) and width (W)	120 mm
Minimum distance between walls and domain boundaries	30 H
Free stream velocity ( $U_{ref}$ )	$4.70 \text{ m s}^{-1}$
Frictional velocity ( $U^*$ )	$0.52 \text{ m s}^{-1}$
Roughness height ( $k_s$ )	0.0033 m

Table 2.1: Summary of the CFD parametrisation for the wind tunnel.

summarised in Table 2.1. The model is compliant with the COST Action 732 (European Cooperation in the field of Scientific and Technical Research) recommendations in respect to CFD simulation of flows in urban environments (Jorg et al., 2007). A hexahedral mesh with a total number of 644,000 cells was used for the simulations. A maximum expansion ratio lower than 1.3 was applied between two consecutive cells. The smallest grid size is  $\Delta x_{min} = 0.06 \text{ H}$  in the x direction,  $\Delta y_{min} = 0.06 \text{ H}$  in the y direction and  $\Delta z_{min} = 0.05 \text{ H}$  in the z direction. This corresponds to at least 16 cells in the x and y directions and 20 cells in the z direction in the street canyon. The overall blockage ratio reaches a maximum value of 2.6% for a  $90^\circ$  wind inclination and is therefore below the 3% recommended threshold (Jorg et al., 2007). A residual convergence of  $10^{-6}$  was used for all field variables. A similar mesh was used with 3 different inlet and outlet boundary conditions to simulate the 3 different wind directions at  $90^\circ$ ,  $45^\circ$  and  $0^\circ$  as shown in Figures 2.8a, b and c respectively. The minimum distance between the inlet plane and the first building and the minimum distance between the outflow plane and the closest building wall were set to 30 H. The same velocity profile as used in the wind tunnel was also used for the inflow boundary condition. The vertical profiles were setup based on the wind tunnel experiment, according to Eq. 2.20 for  $\epsilon$  and Eq. 2.26 for  $k$ .

$$k = \frac{U^{*2}}{\sqrt{C_\mu}} \left(1 - \frac{z}{\delta}\right), \quad (2.26)$$

The frictional velocity ( $U^*$ ) had a given value of  $0.52 \text{ m s}^{-1}$  in this wind tunnel experiment, the Karman's constant ( $K$ ) = 0.4, the vertical co-ordinate ( $z$ ) is in

## 2.4 Model evaluation against wind tunnel measurements

meters and the boundary layer depth ( $\delta$ ) = 0.96 m (Gromke et al., 2008).

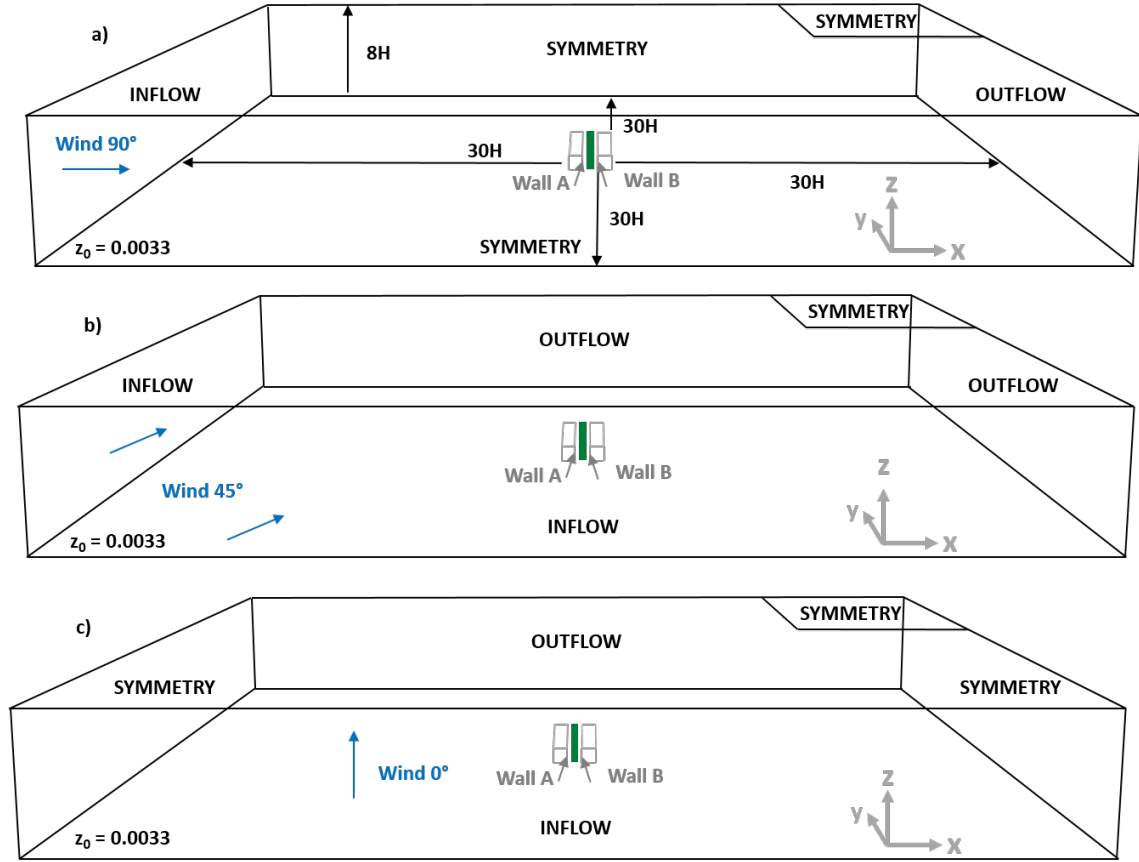


Figure 2.8: Geometry and boundary conditions used for the simulation of an idealised street canyon (of aspect ratio  $W/H=1$ ). a) For a wind direction of  $90^\circ$ . b) For a wind direction of  $45^\circ$ . c) For a wind direction of  $0^\circ$ . Wide buffer conditions are used around the buildings to allow the inflow wind to change directions.

The top boundary condition was setup as a symmetry condition. A wall function was used for the ground to reproduce the wind tunnel surface roughness. This was assigned with a roughness height with the same value as the surface roughness value of  $k_s = 0.0033$  m. Using a lower  $k_s$  with the same value as the surface roughness is not an ideal fit, but it allows a better horizontal resolution near the wall (Blocken et al., 2007). In the same wind tunnel modelling case, Gromke et al. (2008) have shown that using a  $k_s$  of 0.0033 m leads the inlet velocity profile to a reasonable and acceptable change. A turbulent Schmidt number ( $S_{ct}$ ) of 0.5 was used as recommended by Gromke and Blocken (2015a). A no-slip condition was used to model the velocity at the solid walls. The rest of the boundary conditions are shown in Figure 2.8 depending on the wind direction.

To model the pollution dispersion from road sides, pollutants emitted were considered as a passive scalar (non-reactant and not changing the property of the flow carrying them) using a scalar transport equation. This assumption is valid as long as the modelled pollutant is considered inert during the modelling experiment without being affected by chemical reactions and as long as its concentrations does not exceed a certain threshold which can modify the flow property (then difference in the flow and pollutant molar mass can create buoyancy convection).

The pollution was dispersed using a scalar transport equation taking into account the turbulent diffusivity as:

$$\frac{\partial C}{\partial t} + \Delta(UC) = \Delta^2 ((D + K)C) + Q + S, \quad (2.27)$$

where  $C$  is the transported scalar,  $U$  is the fluid velocity,  $D$  is the diffusion coefficient ( $\text{m}^2 \text{s}^{-1}$ ),  $K$  is the eddy diffusion coefficient ( $\text{m}^2 \text{s}^{-1}$ ),  $Q$  represents a source emission ( $\text{kg m}^{-3} \text{s}^{-1}$ ) and  $S$  a sink term, usually caused by deposition ( $\text{kg m}^{-3} \text{s}^{-1}$ ). The eddy diffusion coefficient can be expressed as:  $K = \mu_t / Sc_t$  where  $\mu_t$  is the eddy viscosity or turbulent viscosity ( $\text{m}^2 \text{s}^{-1}$ ) and  $Sc_t$  is the turbulent Schmidt number.

### 2.4.3 CFD comparison with wind tunnel measurements

#### CFD results for a tree-free street canyon

To compare the observed concentrations obtained using CFD against the wind tunnel (WT) measurements, normalised concentrations were used according to Equation 2.25. Figure 2.9 shows the normalised concentrations of the tracer at the walls of an empty street canyon for the 3 wind directions of  $0^\circ$ ,  $45^\circ$  and  $90^\circ$  for both the WT and the CFD experiments. Overall, the trend observed in the experimental data is reproduced in the CFD model. In four cases, (specifically  $0^\circ$  wind at wall A and B,  $45^\circ$  wind at wall A and  $90^\circ$  at wall B), the CFD closely reproduces the concentrations observed in the WT. In two cases ( $45^\circ$  wind at wall B and  $90^\circ$  at wall A), the CFD reproduces the trend of the results observed in the WT with a slight change of concentration. This is as expected because RANS simulations usually underpredict shear layer gradient in space (e.g. Hanjalí (1999)) and do not represent turbulent structures as well as reality. This could lead to a slight discrepancy of concentrations observed between the CFD and the WT.

## 2.4 Model evaluation against wind tunnel measurements

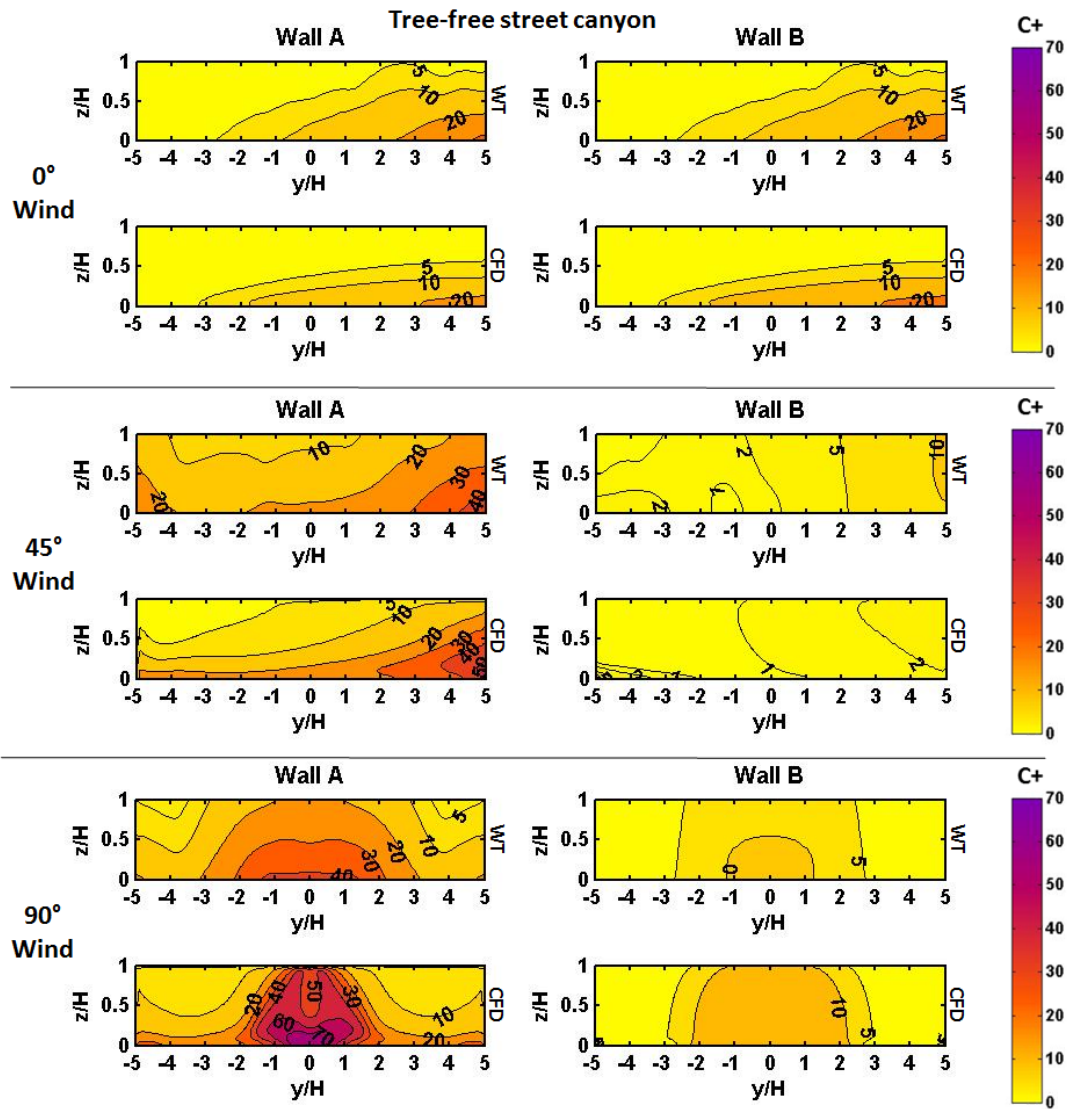


Figure 2.9: Normalised concentration ( $C^+$ ) at the walls of an empty street canyon for 3 wind directions of  $0^\circ$ ,  $45^\circ$  and  $90^\circ$ , for wind tunnel (WT) and simulated (CFD) experiments. Wind angles of incidence for the street canyon are defined in Figure 2.7. Wind tunnel concentrations data were collected up to the street canyon height ( $z/H = 1$ ) which explains why data are not shown above this height.

### CFD results for a street canyon filled with trees

Figure 2.10 shows the normalised concentrations at the walls of the street canyon filled with porous trees for 3 wind directions of  $0^\circ$ ,  $45^\circ$  and  $90^\circ$ . As for the empty street canyon case in Figure 2.9, the overall trend observed in the experimental data is reproduced in the CFD for most cases. For a  $45^\circ$  wind direction at wall

## 2.4 Model evaluation against wind tunnel measurements

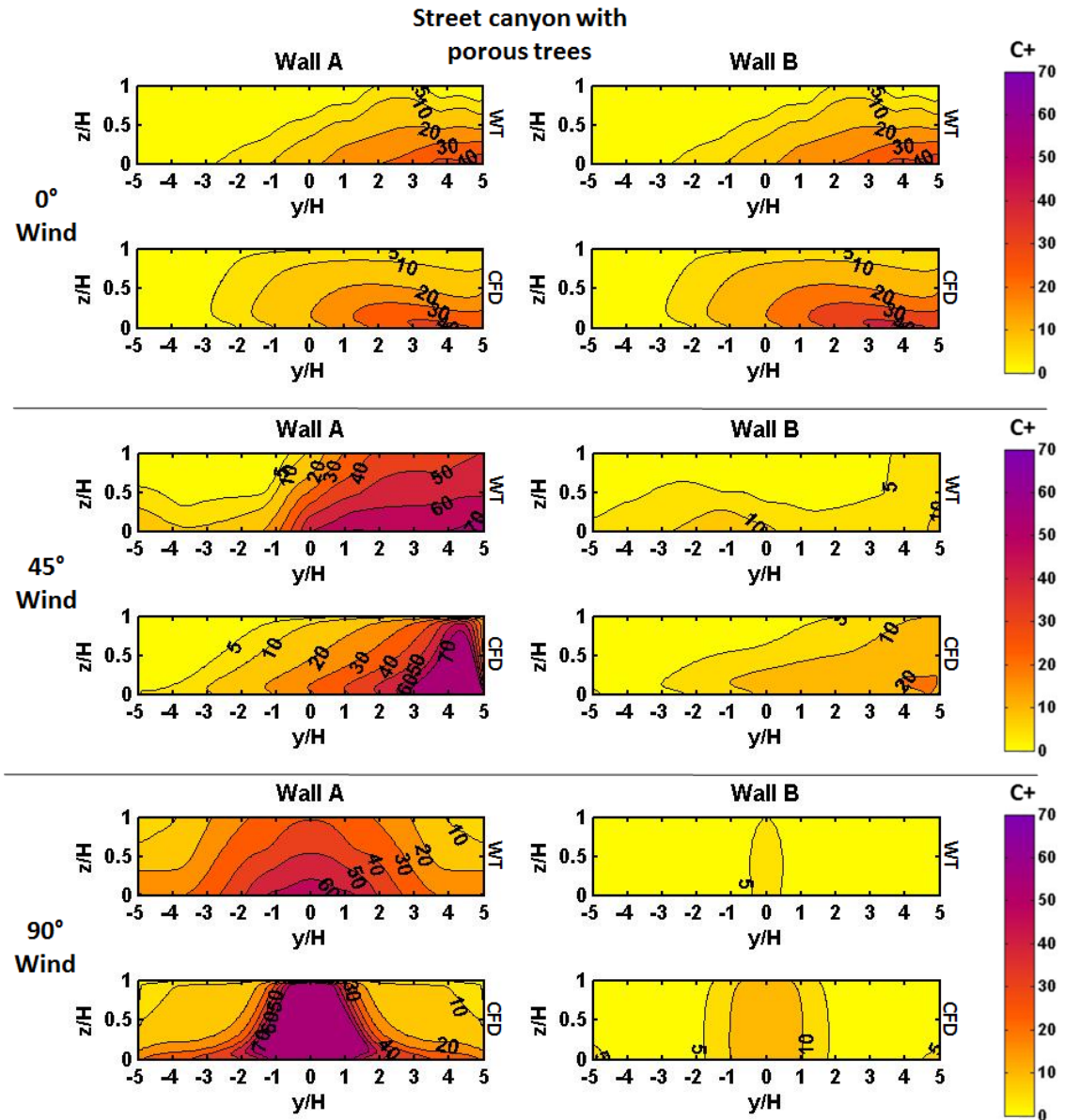


Figure 2.10: Normalised concentration ( $C^+$ ) for wind tunnel (WT) and simulated (CFD) experiments at the walls of a street canyon filled with porous tree for 3 wind directions of  $0^\circ$ ,  $45^\circ$  and  $90^\circ$ . Wind tunnel data were collected up to the street canyon height ( $z/H = 1$ ) which explains why data are not shown above this height.

A, the concentration of the tracer is greater on the right of canyon for  $3 \leq y/H \leq 5$  in the CFD. An underestimation of the shear layer down-wind of the wall could explain the decrease in dispersion and the greater concentrations observed in the CFD model in this case. This underestimation might be due to the failure of the CFD model to completely reproduce turbulence in the centre of the canyon. For

a  $90^\circ$  wind direction at wall A in the centre of the canyon, between  $-2 \leq y/H \leq 2$  concentrations were in fact overestimated in the CFD. Further studies must be conducted in order to evaluate the performance of tree modelling using CFD.

### Grid sensitivity analysis

To ensure that the results observed were independent from the grid resolution, a grid sensitivity analysis was performed as follows. The mesh resolution was decreased by a factor of 1.5 and then compared to the hexahedral mesh previously used (section 2.4.2). The subsequent decrease in the number of cells from 644,000 to 212,000 showed that the modelled concentrations were almost constant over the two meshes and thus grid-independent. This analysis was performed for a wind direction of  $90^\circ$  which corresponds to a wind blowing perpendicularly to the street canyons. The grid analysis was conducted for both tree-free and porous street canyon. The normalised concentrations were plotted in Figure 2.11 to quantify the changes between the two meshes. The centre of the canyon is a complex area to model; errors can be attributed to flow discrepancies (see section 2.4.3) and the grid size can affect the way errors propagate (Figure 2.11, top left). On the whole, the normalised concentrations stay the same between the two meshes which gives weight to the fact that the results are grid-independent.

### Statistical analysis between the wind tunnel and CFD experiments

	Wall A			Wall B		
Wind direction	$0^\circ$	$45^\circ$	$90^\circ$	$0^\circ$	$45^\circ$	$90^\circ$
$R^2$ (tree-free case)	0.94	0.90	0.85	0.94	0.61	0.97
$R^2$ (porous tree case)	0.95	0.80	0.87	0.95	0.49	0.92

Table 2.2: Correlation factors ( $R^2$ ) for normalised concentrations between CFD and wind tunnel measurements.

Table 2.2 summarises the performance of the CFD simulation in respect to the wind tunnel experiment through correlation analyses. The correlation factor  $R^2$  was calculated between the CFD and the wind tunnel measurements, and found to be above 0.80 for most cases. Nevertheless, a  $45^\circ$  wind direction at wall B has a lower correlation factor of 0.61 for the tree-free street canyon and 0.49 for the street canyon with trees.

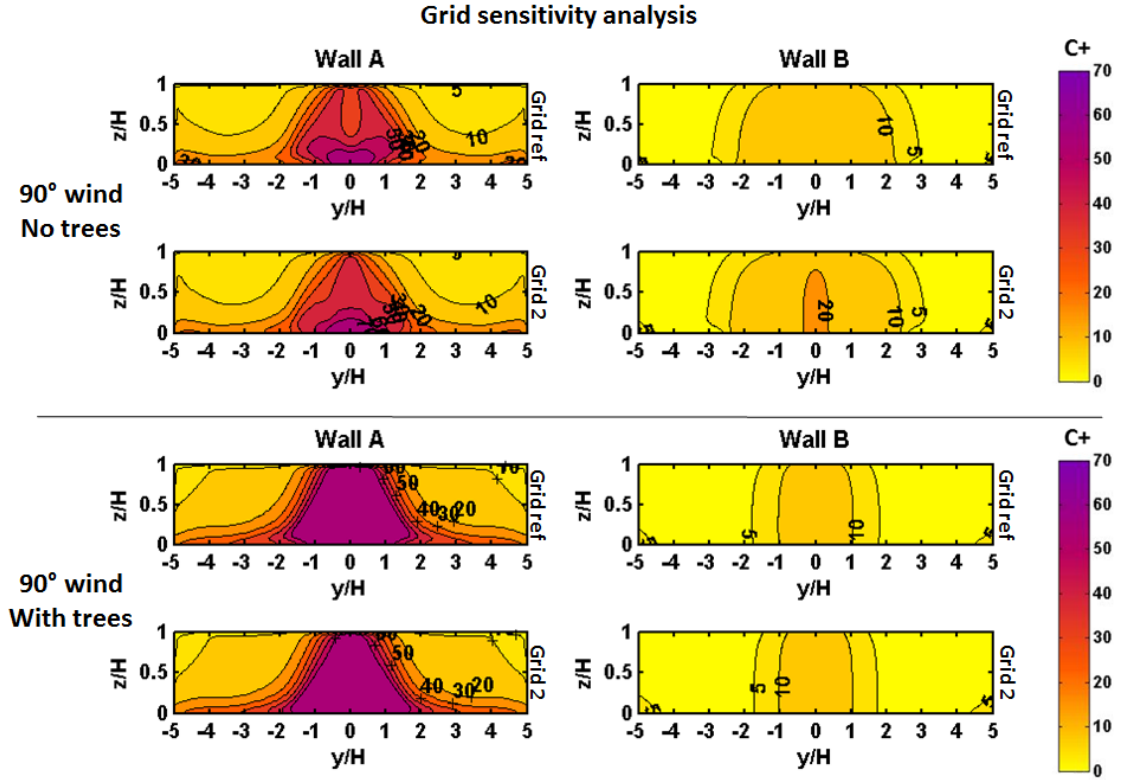


Figure 2.11: Comparison of the reference grid with a grid decreased by a factor of 1.5 (grid 2). Wind tunnel data were collected up to the street canyon height ( $z/H = 1$ ) which explains why data are not shown above this height.

Three other statistical measures were also calculated: the fractional bias (FB), the normalised mean square error (NMSE), the fraction of predictions within a factor of two of observations (FAC2).  $C_o$  is the observed concentration from the wind tunnel and  $C_p$  is the predicted concentration from the CFD. The acceptable ranges for these criteria according to COST 732 (Jorg et al., 2007) are  $-0.3 \leq FB \leq 0.3$ ,  $NMSE \leq 1.5$  and  $0.5 \leq FAC2 \leq 2$  (see FB, NMSE and FAC2 definitions in section 2.3.3).

Figure 2.12 shows the NMSE, FAC2 and FB values for an empty street canyon and for a street canyon filled with porous trees. For a tree-free street canyon, FB is slightly above the range for a  $0^\circ$  wind direction on the walls A and B owing to a slight underestimation of the concentration in the CFD. The tree-free case for a  $45^\circ$  wind direction at wall B is outside the satisfactory ranges. This discrepancy of concentration between CFD and WT was also seen before and has been made apparent in Figure 2.9.

## 2.4 Model evaluation against wind tunnel measurements

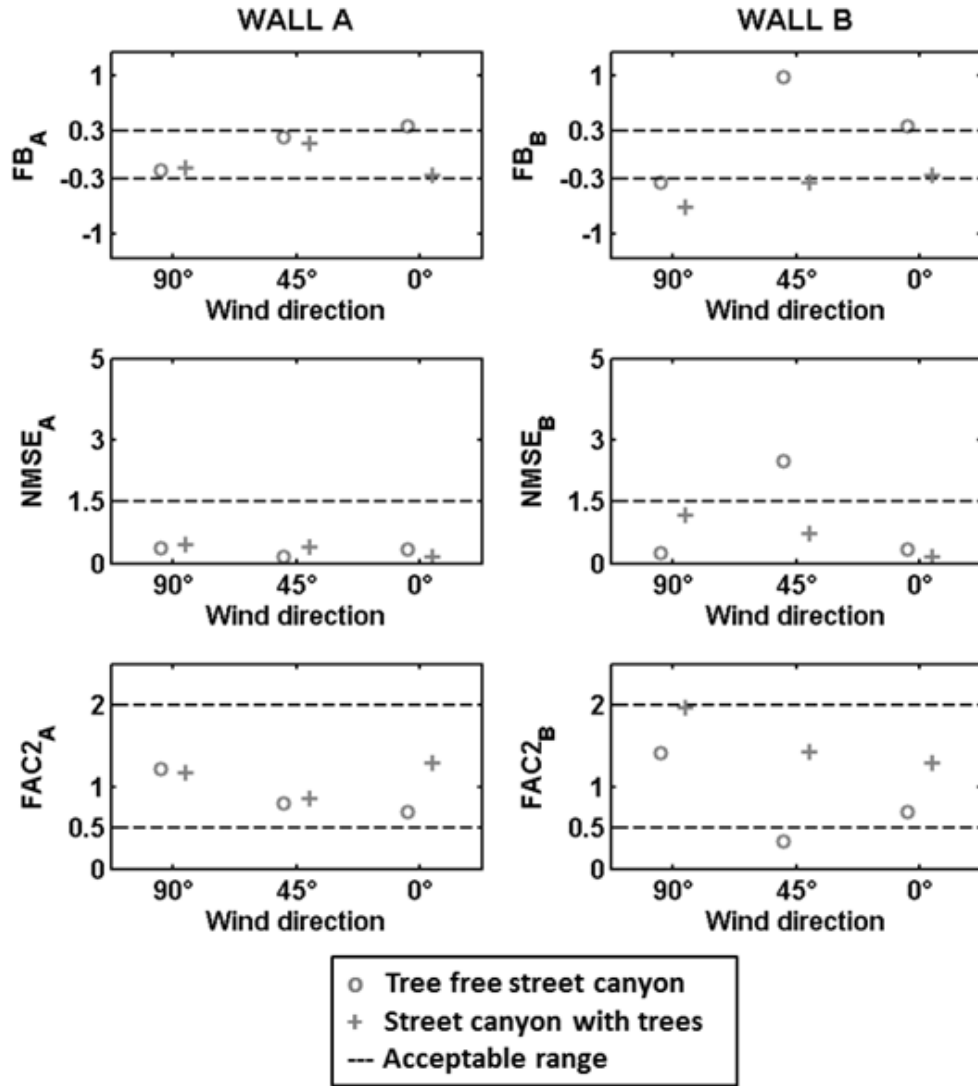


Figure 2.12: Statistical analysis of the CFD against wind tunnel measurements.

		Wall A			Wall B		
		Wind direction	0°	45°	90°	0°	45°
Tree-free street canyon	WT	7.1	18.4	19.7	7.1	3.7	5.3
	CFD	4.9	14.7	24	4.9	1.3	7.6
	<b>CFD - WT</b>	<b>-2.2</b>	<b>-3.7</b>	<b>4.3</b>	<b>-2.2</b>	<b>-2.4</b>	<b>2.3</b>
Street canyon with trees	WT	9.7	31.0	32.7	9.7	5.3	2.7
	CFD	12.6	26.6	38.4	12.6	7.6	5.3
	<b>CFD - WT</b>	<b>2.9</b>	<b>-4.4</b>	<b>5.7</b>	<b>2.9</b>	<b>2.3</b>	<b>2.6</b>

Table 2.3: Wall average normalised concentration  $C^+$  comparison between the WT experiment and CFD for a tree-free street canyon and a street canyon with trees.

To sum up, the CFD results are statistically well within the criteria limits except in one particular case (45° wind direction at wall B). By looking at the wall average concentration in Table 2.3, the CFD is actually closer in this particular case to the WT than for other cases that are statistically inside the criteria range (for example at wall A with a 45° and 90° wind direction). As the concentration values are low at wall B (between 10 and 1), it tends to increase the uncertainty in the statistical parameters (fractions with small denominators). From Table 2.3, the percentage uncertainty of CFD modelling compared to WT can be given by  $(\text{CFD-WT})/\text{WT} \times 100$ . The average CFD model uncertainty on both walls at the 3 wind directions is then of 35% for a tree-free street canyon and of 38% for a street canyon with trees which is comparable to an earlier study findings (Vranckx and Vos, 2013). As also described in previous studies, trees increase average pollutant concentrations locally inside a street canyon (Gromke et al., 2008).

## Chapter 3

# Air quality affected by trees in real street canyons: the case of Marylebone neighbourhood in central London

*This Chapter has been published in Urban Forestry and Urban Greening (Jeanjean et al., 2017) and Dr Riccardo Buccolieri (Universita del Salento, Italy) has contributed to the supervision of this work.*

### 3.1 Introduction

Many municipalities have shown a renewed interest in “urban forestry” by incorporating green space and vegetation into the urban environment (Manso and Castro-Gomes, 2015). Urban greening usually refers to urban design elements such as trees and other plants in parks, sidewalks or elsewhere, employed for recreation or aesthetic improvement of a city. In recent years, researchers have also been looking into potential benefits of green space and vegetation to address air quality concerns (Gallagher et al., 2015; Li et al., 2016). The use of vegetation in the urban environment has been reported to bring about many benefits, including lower energy use, reduced air pollution and greenhouse gas emissions, protection from harmful exposure to ultraviolet rays, decreased storm water runoff, potential reduced pavement maintenance (Roy et al., 2012; Hsieh et al., 2016), improved well-being of the urban population (White et al., 2013; van den Berg et al., 2015) and reduced traffic noise

levels (Kalansuriya et al., 2009).

Specifically, trees can reduce various pollutants found in the urban environment, such as particulate matter (PM), nitrogen oxides ( $\text{NO}_x$ ), sulphur dioxide ( $\text{SO}_2$ ), carbon monoxide (CO) and ground-level ozone ( $\text{O}_3$ ) (Janhäll, 2015).

Although particle deposition on plant surfaces removes pollutants from the atmosphere, thus reducing their concentration, it also should be noted that trees themselves act as obstacles to airflow decreasing air exchange and leading to larger pollutant concentrations when the source of pollution is inside the same ventilated compartment (e.g. street canyon) as the trees. Several experimental and modelling studies on the effects of trees on urban air quality have been performed in the recent literature (see reviews by Janhäll 2015 and Gallagher et al. 2015). Challenges and strategies for urban green-space planning in compact cities have also been proposed (Haaland and van den Bosch, 2015). Most studies mainly focus either on the aerodynamic or deposition effects of trees, showing that both dispersion and deposition related to vegetation are significant. These areas should be combined further before any action is taken in urban planning (Janhäll, 2015).

Within this context, the objectives of the present study are twofold. The first objective is to evaluate a CFD dispersion model of  $\text{NO}_x$  and  $\text{PM}_{2.5}$  to account for the aerodynamic effects of trees in combination with the deposition effects for  $\text{PM}_{2.5}$ . This allows a comprehensive evaluation of the effects of trees on pollution dispersion. The second objective of this research is to apply the developed methodology to investigate the combined effects of trees on dispersion in a real scenario, i.e. in the Marylebone neighbourhood in central London. CFD results are compared with concentration data from monitoring stations available from the UK Automatic Urban and Rural Network (AURN) (DEFRA, 2014b). Several meteorological conditions have been chosen based on data retrieved from the London City Airport weather station, paying particular attention to the prevalent wind speeds and directions.

## 3.2 The study site

### 3.2.1 Description of geometry and trees

Marylebone is an affluent inner-city area of central London (UK), located within the City of Westminster. It is characterised by major streets on a grid pattern such as Marylebone Road, one of the busiest roads of central London, with smaller mews

between the major streets. The area is characterised by a geometry typical of the architecture of many European cities with several street canyons (Di Sabatino et al., 2010). Marylebone Rd is also characterised by a street canyon configuration, with an aspect ratio (height over width) near unity (Nikolova et al., 2016).

It experiences high pollution episodes due to the passage of more than 80,000 vehicles per day on Marylebone Rd and regular traffic congestion (Crosby et al., 2014; Charron et al., 2007). This makes it one of the most polluted sites in the UK, with an average NO<sub>2</sub> concentration of 94 µg m<sup>-3</sup> in 2014, according to the AURN measurements. Pollutant concentration thresholds are regularly exceeded up to 35 times a year above the European recommended threshold of 200 µg m<sup>-3</sup> (Charron et al., 2007).

Roads, buildings and trees data were integrated to reconstruct a 3-dimensional (3D) area around the study area. Roads and buildings data were taken by Ordnance Survey which is the UK governmental mapping agency. The National Tree Map<sup>TM</sup> (NTM) Crown Polygon produced by Bluesky International Ltd. was used to represent individual trees or closely grouped tree crowns. Trees and bushes over 3 m in height were included in the database. An overview of the study area can be seen in Figure 3.1. The NTM<sup>TM</sup> product provides a canopy top height but does not however provide a canopy base height. Therefore, a canopy base height of 1/3 of the canopy depth was assumed, as is commonly done in current literature (e.g. Gromke et al. 2008).

### 3.2.2 Description of the cases investigated

Several cases have been simulated in this chapter (see Table 3.1). Wind data for the year 2014 was retrieved from the London City Airport weather station (EGLC, available at <https://www.wunderground.com>), every 30 minutes with a wind direction accuracy of 10°. The station is located around 15 km west of the monitoring site. In 2014, the recorded average wind speed was 4.3 m s<sup>-1</sup> at 10 m above the ground and the prevalent wind direction was South-West (see Figure 3.2). Specifically, 4 wind speeds and 15 wind directions were selected, i.e. every 30° in the range 270° to 180°, and every 15° in the range 180° to 270°, the latter being the prevailing wind direction range used in the study area.

Leaf-free trees (winter, referred to as CB), trees with half-grown leaves (spring and autumn, referred to as CT1) and trees with fully grown leaves (summer, referred to as CT2) were investigated for each wind speed and direction. Scenarios CT1 and

### 3.2 The study site



Figure 3.1: Area of interest around the Marylebone monitoring site in London, UK. M stands for Marylebone, GP for Gloucester Place and BS for Baker Street. (a) GoogleEarth overview (b) 3D model of the scene using roads and buildings from Ordnance Survey UK and tree data from Bluesky International Ltd.

CT2 have been modelled with different porosities (see Table 3.3 for further details). Overall, 4 wind speeds, 15 wind directions, 3 different tree profiles and 2 pollutant species were simulated, giving a total of 360 individual simulations.

### 3.2 The study site

Table 3.1: Scenarios investigated with different types of trees, seasons and meteorological data simulated.

Name	Trees	Season	Wind speed (m s <sup>-1</sup> )	Wind direction (°)
CB (Case of Buildings only)	Leaf-free	winter	3	0; 30; 60; 90; 120; 150; 180; 195; 210; 225; 240; 255; 270; 300; 330
CT1 (Case of Trees 1)	Half-grown leaves	spring & autumn	5	
			7	
			9	
CT2 (Case of Trees 2)	Fully grown leaves	summer		

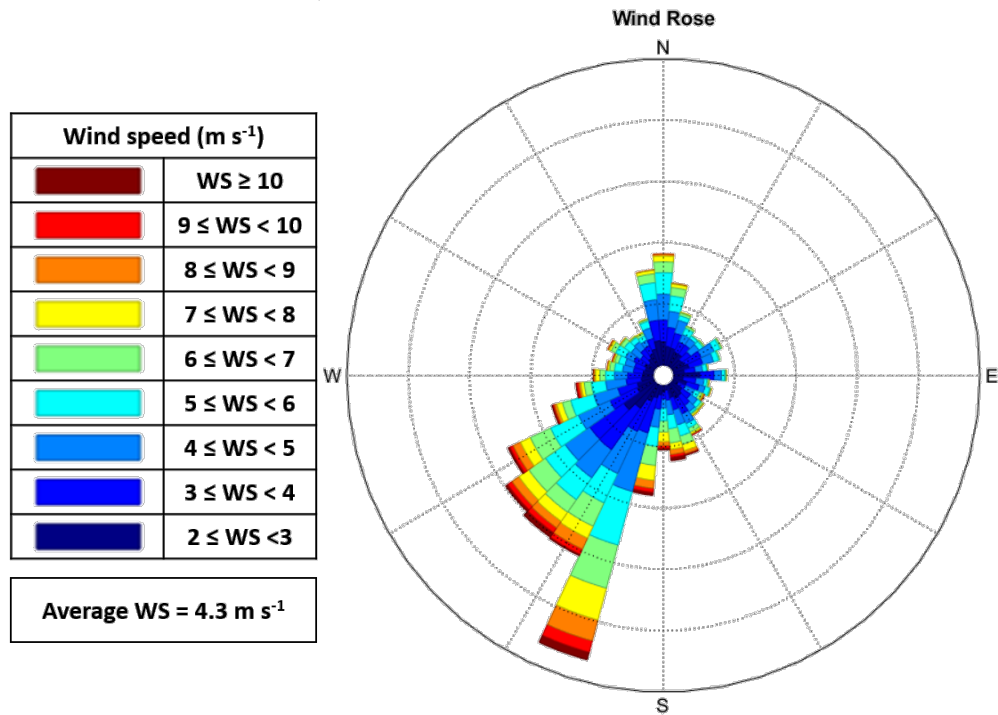


Figure 3.2: Wind Rose showing the wind directions (°) and wind speeds during the year 2014 in London (data: London City Airport weather station). The wind speed and direction were recorded every 30 minutes with a resolution of 10°.

The year 2014 has been chosen as a reference year in this study for pollutant concentrations as it provides a recent annual baseline to investigate the interaction between trees and the atmosphere. Although excluded here, the investigation of this relationship over time leaves room for further research.

### 3.2.3 Description of traffic data and pollutant concentration analysis

Estimated annual average daily flows from the Department for Transport were used to estimate road emissions of nitrogen oxides ( $\text{NO}_x$ ) and particulate matter ( $\text{PM}_{2.5}$ ) around the monitoring site. These typical daily flows were translated into road emissions using the Emissions Factors Toolkit (EFT) from the Department for Environment, Food & Rural Affairs (DEFRA, 2016). Emissions were produced for the average London vehicle fleet profile and are reported in Table 3.2.

Table 3.2: Calculated  $\text{NO}_x$  and  $\text{PM}_{2.5}$  emissions from annual average daily flows (AADF, annual averaged number of vehicles per 24h). M stands for Marylebone Rd traffic counts, GP for Gloucester Place and BS for Baker Street.

	Marylebone (M)		A41 - Gloucester Place (GP)		A41 - Baker Street (BS)	
<b>AADF</b>	M1 =	78880	GP1 =	13530	BS1 =	13813
	M2 =	78827	GP2 =	15627	BS2 =	10583
	M3 =	79528				
<b><math>\text{NO}_x</math> emissions</b> ( $\text{mg m}^{-1} \text{s}^{-1}$ )	M1 =	0.69	GP1 =	0.10	BS1 =	0.11
	M2 =	0.67	GP2 =	0.12	BS2 =	0.08
	M3 =	0.69	Average =	<b>0.11</b>	Average =	<b>0.10</b>
	Average =	<b>0.68</b>				
<b><math>\text{PM}_{2.5}</math> emissions</b> ( $\text{mg m}^{-1} \text{s}^{-1}$ )	M1 =	0.031	GP1 =	0.005	BS1 =	0.005
	M2 =	0.030	GP2 =	0.006	BS2 =	0.004
	M3 =	0.031	Average =	<b>0.006</b>	Average =	<b>0.005</b>
	Average =	<b>0.031</b>				

To calculate pollutant concentrations in Marylebone Rd from the AURN station (identification MY1), hourly measurements from the year 2014 were collected and distributed into classes depending on wind speed, wind direction and seasonality. In order to match this hourly measure of pollution, only the hourly wind data was used. Specifically, the averages reported for each wind direction were repeated for each wind speed (3; 5; 7 and 9  $\text{m s}^{-1}$ ) across the 3 modelled seasons (winter, spring & autumn and summer, see Table 3.1).

To compare model outputs with monitored data for Marylebone Rd, an urban background concentration was added to the modelled data for each case investigated. The closest urban background monitoring station in central London away from Marylebone Rd is located in Russell Square (DEFRA monitoring site identification: CLL2). Similar to what was done for AURN station concentration data, hourly measurements from the year 2014 were distributed into classes depending on

### 3.3 The study site

---

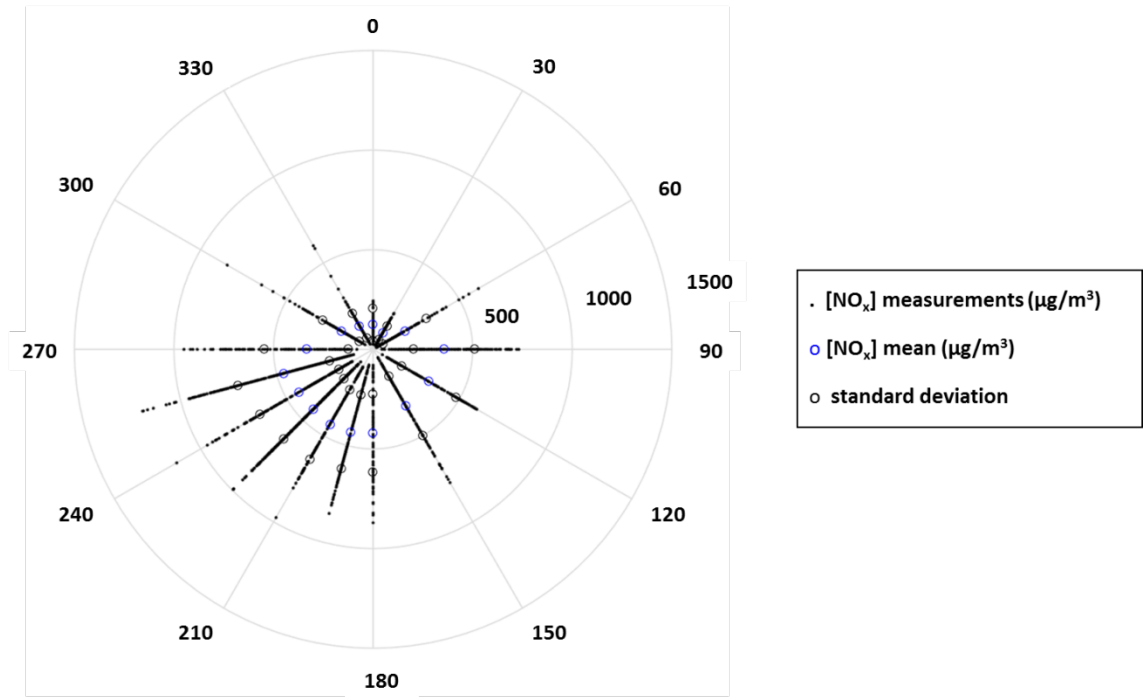


Figure 3.3: Example of the wind rose plot showing the method used to average hourly  $\text{NO}_x$  data over wind directions, here corresponding to the urban background pollution measured in Russell Square for the winter season at a wind speed of  $5 \text{ m s}^{-1}$ .

wind speeds and wind directions as shown in Figure 3.3.

The final modelled concentration for each case was then obtained as follows:

$$\text{Model}(WS, WD, season) = (\text{BKD}(WS, WD, season) + \text{RC}(WS, WD)), \quad (3.1)$$

where BKD is the urban background concentration and RC is the road contribution. The concentration obtained from model simulations remains the same across the seasons, whereas background and monitored data were variable across the seasons. It is worth noting that the annual average daily traffic flow assumption used in this study does not take into account all the temporal variations across the change of traffic during day and night, weekdays and weekend and so on, as the spread of traffic is averaged for a typical day.

## 3.3 CFD modelling

### 3.3.1 Flow modelling set-up

As it is the case in this thesis, wind flow calculations were performed under the steady-state simpleFOAM solver for incompressible, isothermal and turbulent flows. This steady-state solver is based on the Reynolds-Averaged Navier–Stokes (RANS) with the standard  $k$ – $\epsilon$  closure model (Launder and Spalding, 1974). The governing equations were discretised with second order upwind scheme.

Best practice guidelines were followed to build the computational domain (Franke et al., 2007). The maximum reported height in the domain is a building height ( $H$ ) of 63 m. The computational domain was built with its boundaries placed more than 15  $H$  away from the modelled area (Figure 3.4). The top of the computational domain was set to 570 m, which corresponds to 8  $H$ . A maximum expansion ratio between two consecutive cells was kept below 1.3. With an average building height of 12 m across the modelled area, the overall blocking ratio was kept below 1% inclination and is therefore below the 3% recommended threshold.

A hexahedral mesh of more than 4 million cells was used. A high mesh resolution of 0.5 m in the vertical direction close to the bottom of the computational domain was chosen with less than 1 m in order to ensure proper flow modelling at pedestrian height (Blocken, 2015). A cell size of 1.25 m along the X and Y axis was applied for the buildings, trees and roads. This resolution allows more than 10 cells to be present across the main street canyon to ensure proper flow modelling (Figure 3.5). The boundary conditions were chosen to reflect an atmospheric boundary layer. Single inlet and outlet conditions were used for Northern, Eastern, Southern and Western winds using the 4 sides of the outer domain. The mean velocity boundary flow and the turbulent dissipation were set up to follow a logarithmic law using the “atmBoundaryLayerInletEpsilon” (Eq. 2.20) and “atmBoundaryLayerInletVelocity” (Eq. 2.19) utilities in OpenFOAM.

As recommended by the Cost Action 732 best practice guidelines (Franke et al., 2007), the top of the domain was set as a symmetry plane. The wind atmospheric boundary layer was set to reach the wind speed at a height of 10 m to match with the wind measurements’s height. A surface roughness of  $z_0 = 0.10$  m was set for the ground, which corresponds to sparse, large obstacles (WMO, 2008). This surface roughness is set to account for the presence of parked car, bus stop and so on across the modelled scene. A residual convergence of  $10^{-5}$  was used for all field

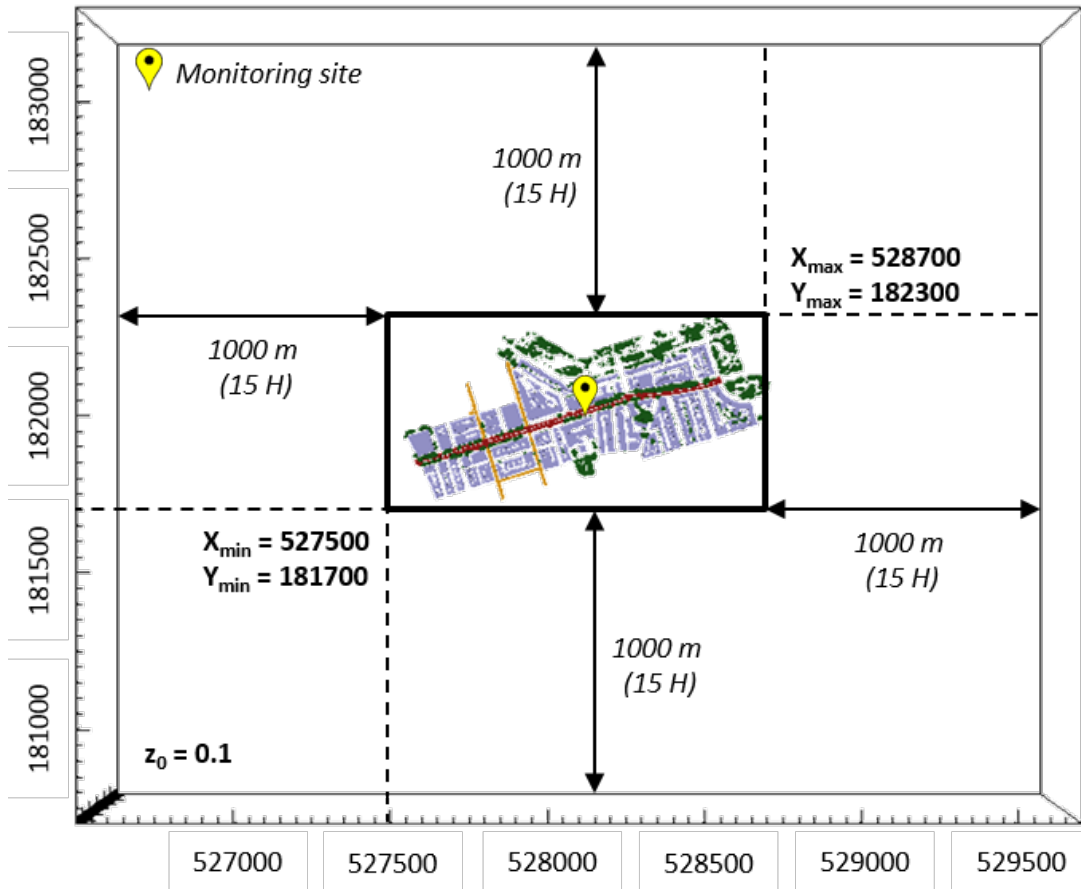


Figure 3.4: Modelled area of interest inside the CFD OpenFOAM software. Coordinates are in British National Grid (UK coordinate system expressed in metres). Wide buffer conditions are used around the buildings to allow the inflow wind to change directions.

variables and of  $10^{-4}$  for the pressure. For the scalar transport simulation (pollutant dispersion), a residual convergence of  $10^{-6}$  was reached. The simulation time per unique wind condition was 3 days on average on a single core running with a RAM of 8 GB.

### 3.3.2 Gaseous pollutant modelling set-up

The gaseous pollution dispersion was modelled as described in Eq. 2.27. A  $Sc_t$  value of 0.5 was used, which gave the best model agreement when compared to wind tunnel data (Chapter 2) which agrees with previous studies (Gromke and Blocken, 2015b). The zones for the road cells were selected up to 1.5 m height for pollution emission.

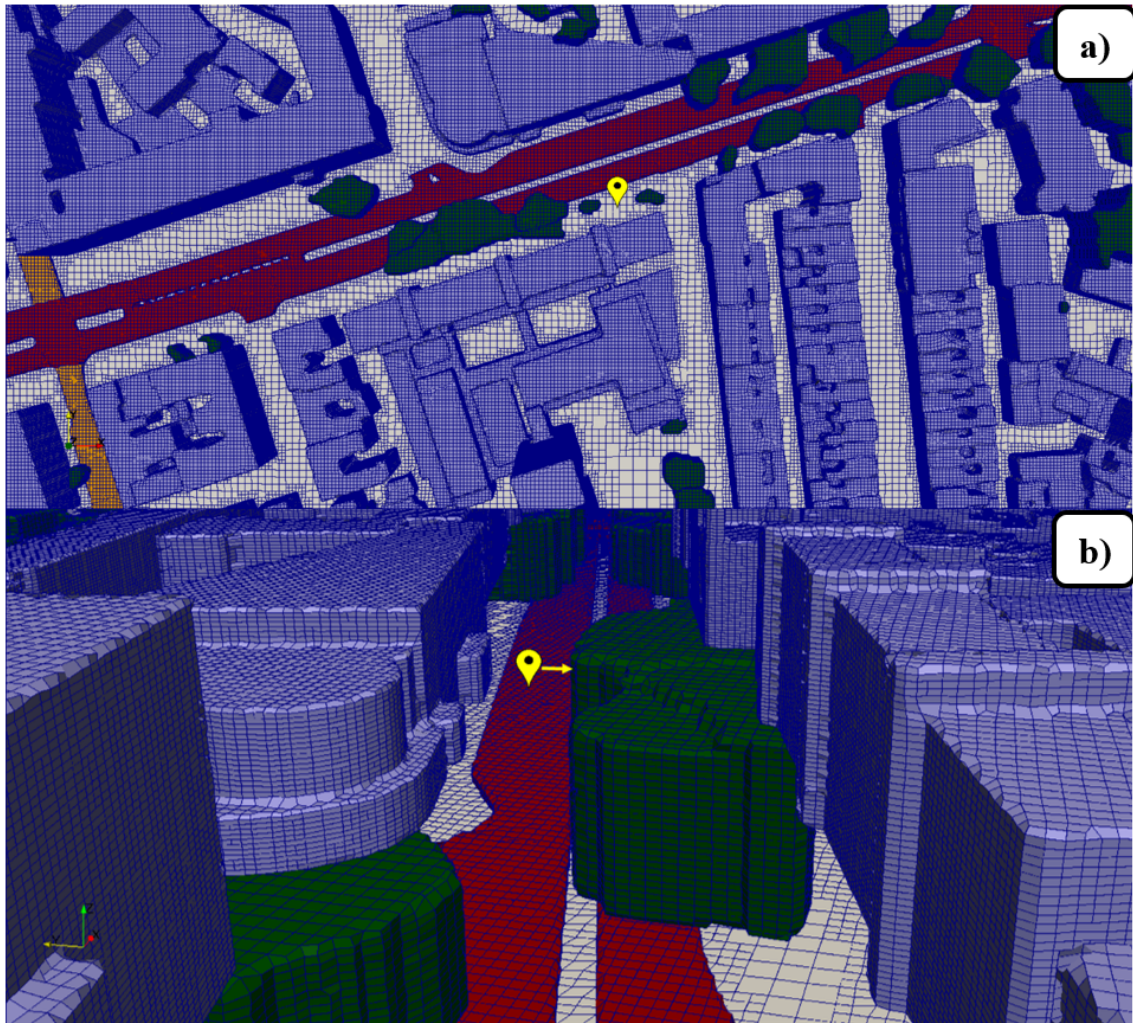


Figure 3.5: (a) View from the top and (b) View from the street canyon of the mesh used to carry out the CFD simulations. A maximum resolution of 1.25 m was used across the X and Y axis and 0.5 m along the Z axis.

### 3.3.3 Modelling the effects of trees

For the aerodynamic effects, trees were modelled as porous bodies following the same approach as used in Chapter 2 (Eq. 2.22).

With the assumption of a homogeneous spread of tree species across South East England and London, it can be estimated that London has 80.3% deciduous trees and 19.7% coniferous trees (Forestry-Commission, 2013b). Only deciduous trees were considered in this study as they are predominant in London. The *Platanus x hispanica*, commonly called *London plane*, is the species mainly present in Marylebone Rd. For the summer season, an average drag coefficient of  $C_d = 0.25$  for

### 3.4 CFD modelling

---

the tree canopy was used with an average LAD of  $1.6 \text{ m}^2 \text{ m}^{-3}$ , which is consistent with that estimated via ceptometer measurements by (Sabatino et al., 2015). The pressure loss coefficient of trees is expressed as

$$\lambda = C_d A, \quad (3.2)$$

where  $C_d$  is a fixed drag coefficient and  $A$  is the Leaf Area Density (LAD).

The final pressure loss coefficient  $\lambda$  was then equal to  $0.4 \text{ m}^{-1}$  in summer. With a LAD of  $0 \text{ m}^2 \text{ m}^{-3}$  in winter, the drag of the trees was neglected for this season. With the growth and fall of leaves in spring and autumn respectively, the model used the lower end of the LAD value of  $1.06 \text{ m}^2 \text{ m}^{-3}$  with a similar drag coefficient of  $C_d = 0.25$  leading to a pressure loss coefficient of  $0.26 \text{ m}^{-1}$ . Table 3.3 summarises the pressure loss coefficients used across all 4 seasons.

Table 3.3: Pressure loss coefficients of trees ( $\lambda$ ) of the modelled area across the seasons.

Season	Spring & Autumn	Summer	Winter
<b>Pressure loss coefficient of trees <math>\lambda</math> (<math>\text{m}^{-1}</math>)</b>	0.26	0.4	0
<b>Leaf Area Density LAD (<math>\text{m}^2 \text{ m}^{-3}</math>)</b>	1.06	1.6	0

As shown in Table 3.4, the range of dry deposition velocities in the literature is very wide. Deposition velocities are highly dependent on the vegetation species as well as the various particle diameters (size distribution) constituting  $\text{PM}_{2.5}$ . Although an average deposition velocity can be challenging to estimate, an intermediate value of  $0.64 \text{ cm s}^{-1}$  for  $\text{PM}_{2.5}$  was used for modelling the deposition of this pollutant on trees. The deposition inside the tree crown cells was parametrised as described in Eq. 2.23.

Table 3.4: Literature values of deposition velocities of  $\text{PM}_{2.5}$  on vegetation.

Pollutant species	Deposition velocity on vegetation ( $\text{cm s}^{-1}$ )	(Author, year)
<b><math>\text{PM}_{2.5}</math></b>	0.02 (lower end)	(Peters and Eiden, 1992)
	0.64 (intermediate)	(Pugh et al., 2012)
	30 (higher end)	(White and Turner, 1970)

## 3.4 Results and discussion

In this section, modelled results are first compared with monitored data to evaluate CFD simulations. Then data obtained from both simulations and observations are used to evaluate the effects of trees on concentration levels of  $\text{NO}_x$  and  $\text{PM}_{2.5}$  at the monitoring site in the study area. Particular attention is paid to the relative contribution of aerodynamic and deposition effects for all the wind directions and speeds summarised in Table 3.1. Finally, CFD simulations are used to provide a comprehensive evaluation of concentration levels and of the effects of trees over the whole study area, which is not possible for data monitored at a single point.

### 3.4.1 Comparison between simulations and 4 m height surface data monitored in the Marylebone site

Wind roses comparing monitored and modelled data for the Marylebone site are shown in Figure 3.6 for a wind speed of  $5 \text{ m s}^{-1}$ , which is close to the yearly average wind speed observed in the area. Overall the Figure 3.6 shows that the shape generated by pollution concentrations is similarly reproduced by the model. It can be noted that for the wind direction equal to  $225^\circ$  in the absence of trees (CB in wintertime), the modelled data is out of range. This is not observed in the presence of trees (CT1 and CT2). A reason for this shift in the results could be the fact that trees are not modelled for the winter season, which is also the case with other CFD studies. In reality however, tree trunks and branches are still present in winter suggesting that a model parameterisation for winter trees (without leaves) is needed for the CFD model.

An underestimation of  $\text{NO}_x$  concentrations for winds parallel to Marylebone Rd street canyon, i.e. Easterly and Westerly winds, is in agreement with findings from previous studies suggesting that CFD models usually underestimate concentrations for winds parallel to street canyons with trees (Gromke and Blocken, 2015b).

As for  $\text{PM}_{2.5}$ , the model overestimated concentrations by 30 to 40%, which corresponds to the average model accuracy (see chapter 2). A reason for this overestimation could be the assignment of too large a value for either the road emissions or the calculated urban background. It is worth noting that the urban background has a greater influence on  $\text{PM}_{2.5}$  concentrations of about 67%, with Marylebone road emissions contributing to 33% of total  $\text{PM}_{2.5}$  (Charron and Harrison, 2005).

To assess the overall model performance, several standard metrics have been

### 3.4 Results and discussion

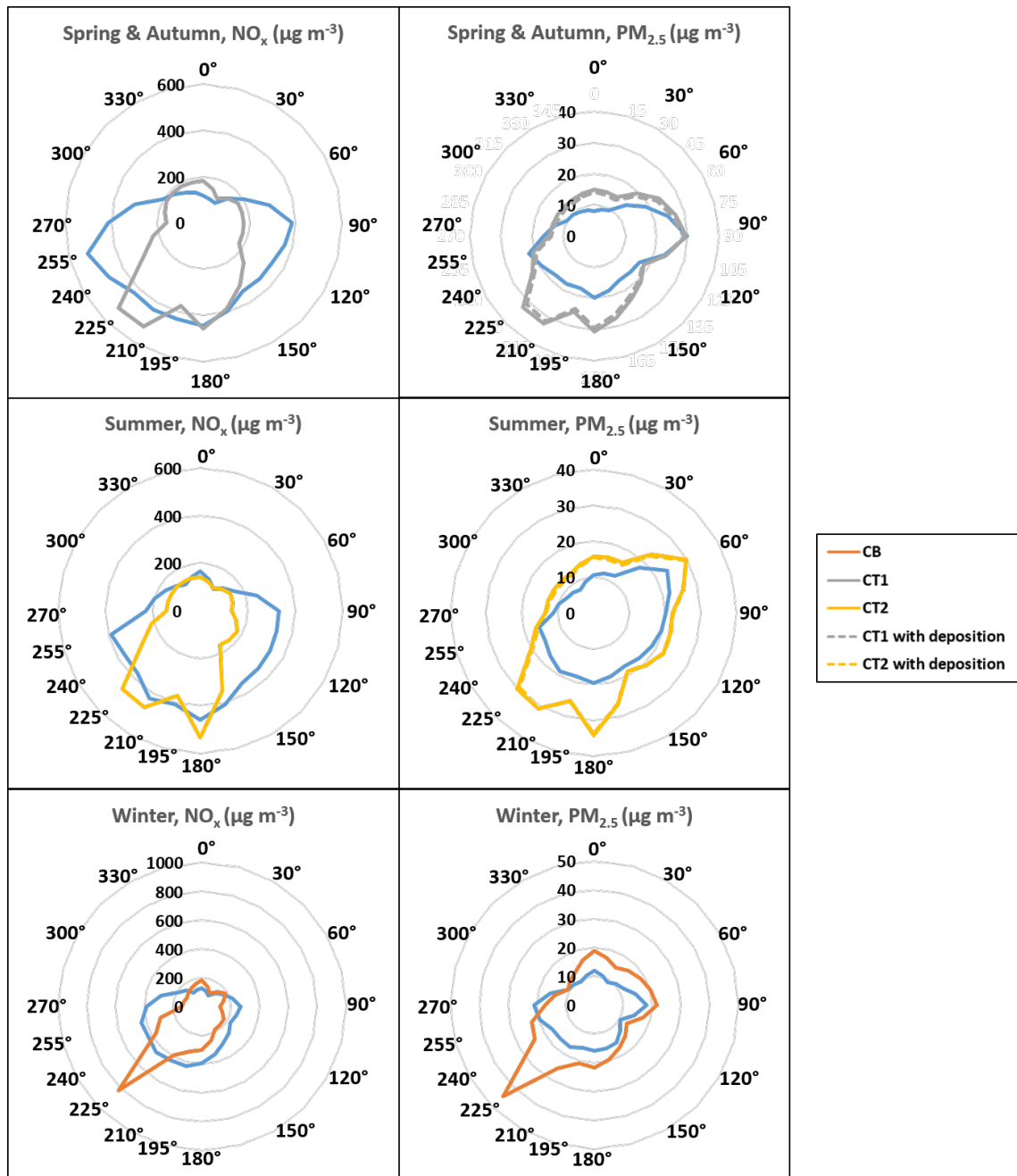


Figure 3.6: Wind rose plots comparing modelled  $\text{NO}_x$  and  $\text{PM}_{2.5}$  for the cases CB (orange), CT1 (grey) and CT2 (yellow) against monitored data by Marylebone AURN site (blue) at a wind speed of  $5 \text{ m s}^{-1}$ . The width of the wind rose plots is not fully reproduced by the CFD model for  $\text{NO}_x$ , which could be caused by the  $\text{Sct}$  of 0.5 used here which could increase dispersion for wind directions parallel to the street canyon.

calculated; namely the normalised mean square error (NMSE), the fraction of predictions within a factor of two for observations (FAC2) and the fractional bias (FB). According to COST Action 732 (Franke et al., 2007), the recommended criteria are:  $NMSE \leq 1.5$ ;  $FAC2 \geq 0.5$ ;  $-0.3 \leq FB \leq 0.3$ . Results of the statistical analysis are presented in Figure 3.7. Overall it can be noted that NMSE and FAC2 are within the acceptable range. FB is out of range for a few modelled cases, especially for high wind speeds for  $NO_x$  and low wind speeds for  $PM_{2.5}$ . The FB indicator gives information about overestimation (negative values) or underestimation (positive values). As pointed out previously, this indicator shows that  $NO_x$  values are underestimated by the model and  $PM_{2.5}$  values are overestimated.

It is worth emphasising that the buildings database employed in this study has an accuracy of 20 cm to 50 cm, but does not include roof shapes. Most of the features of buildings were thus accurately reconstructed, with the exception of roof shape which could introduce significant changes in the wind flow in street canyon studies (Yazid et al., 2014). The analysis of statistical data suggests that FB is highly dependent on wind speed, higher wind speeds employed in the CFD simulations tend to exacerbate this issue.

Overall, Figure 3.6 and Figure 3.7 show a satisfactory model performance in terms of the essential features of the mean concentrations and support the investigation of the effects of trees on air quality in the study area.

#### 3.4.2 The influence of trees under different wind directions

To investigate the aerodynamic and deposition effects of trees under different wind directions, the following section focuses purely on traffic emissions of  $PM_{2.5}$ . As discussed in the previous subsection, the analysis of wind roses and the statistical metrics showed that the wind direction of  $225^\circ$  was not reproduced correctly by the model, therefore this wind direction was removed from the analysis below.

Table 3.5 shows the influence of wind direction on  $PM_{2.5}$  concentrations emitted by traffic for a wind speed (WS) of  $5 \text{ m s}^{-1}$ , without urban background concentrations. In the table total percentages (%) are calculated in comparison with seasonal average concentrations of  $PM_{2.5}$  as follows:

$$Total(\%) = 1 - \frac{[MesSA](WS) - [ModSA](WS)}{[MesSA](WS)}, \quad (3.3)$$

where  $[MesSA]$  is the measured seasonal average of  $PM_{2.5}$  concentrations and  $[ModSA]$

### 3.4 Results and discussion

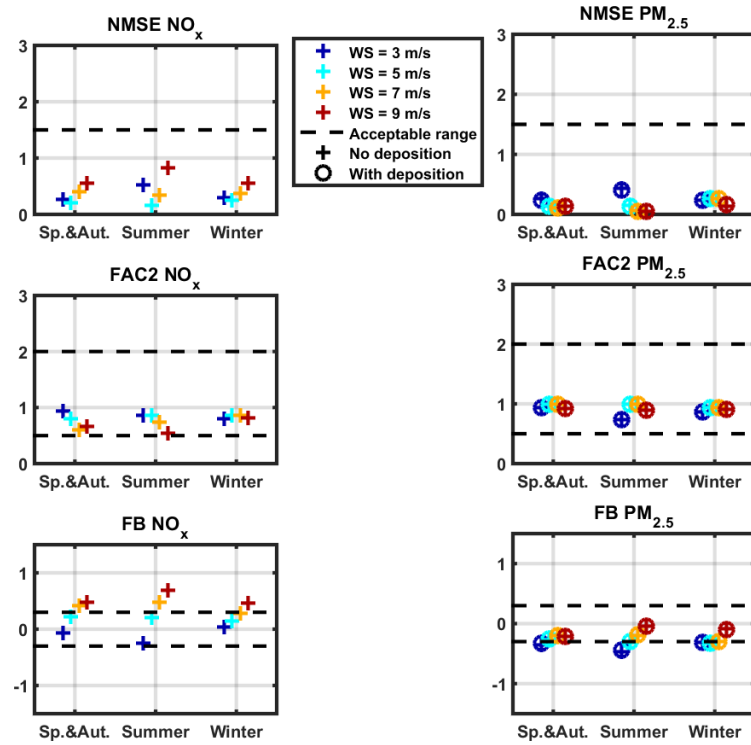


Figure 3.7: Statistical analysis of modelled pollutant concentrations when compared to the monitored data for the Marylebone site.

is the modelled seasonal average of  $PM_{2.5}$  concentrations.

Generally, Table 3.5 shows that trees were found to trap air pollution at the Marylebone monitoring site by 6.98% in spring and autumn and by 7.45% in summer. These increases in  $PM_{2.5}$  concentrations are equivalent to an increase of about  $1.2 \mu\text{g m}^{-3}$ , which shows that the aerodynamic effects are fairly similar over the leaf seasons. The deposition effects were found to be around 4 times less important than the aerodynamic effects, with reductions of 1.45% in spring and autumn and 2.08% in summer. More deposition was found over summer than in spring and autumn, as a greater leaf area density offers more surfaces for deposition (Steffens et al., 2012).

It should be noted that for wind directions of  $60^\circ$ ,  $240^\circ$  and  $255^\circ$ , which are parallel to Marylebone Rd street canyon, the aerodynamic effects of trees decreased street concentrations. This conclusion supports previous results in real scenarios which report a 12% increase in concentration for winds perpendicular to the street canyon and a 16% decrease for parallel winds (Amorim et al., 2013a).

### 3.4 Results and discussion

Table 3.5: Influence of wind direction on PM<sub>2.5</sub> concentrations emitted by traffic at the Marylebone monitoring station, for a wind speed of 5 m s<sup>-1</sup>, without urban background concentrations. Total percentages (%) are calculated in comparison with seasonal average concentrations of PM<sub>2.5</sub>, corresponding to the wind speed of 5 m s<sup>-1</sup>. The 225° wind direction was not included in the calculation as the results were not satisfactory when compared to measurements. Highlighted numbers correspond to wind directions which result in a beneficial reduction in air pollution because of the aerodynamic dispersion of trees. Aerodynamic and deposition effects are calculated as shown in Fig. 2.6.

WD (°)	WD probability (%)	Aerodynamic dispersion of trees (µg m <sup>-3</sup> )		Tree deposition (µg m <sup>-3</sup> )	
		Spring & autumn	Summer	Spring & autumn	Summer
0	11.52	0.82	0.28	-0.16	-0.16
30	6.19	1.60	1.70	-0.39	-0.54
60	5.99	-0.98	-0.83	-0.21	-0.30
90	10.63	1.83	2.13	-0.003	-0.003
120	5.12	0.33	0.80	-0.01	-0.01
150	5.40	6.27	0.44	-0.34	-0.02
180	4.36	7.63	11.69	-0.53	-0.68
195	6.87	2.59	3.78	-0.44	-0.74
210	6.14	6.57	4.80	-0.31	-0.41
240	6.97	-3.09	-2.90	-0.25	-0.37
255	13.66	-3.24	-2.69	-0.38	-0.53
270	5.49	1.56	2.10	-0.20	-0.29
300	6.65	2.41	2.45	-0.30	-0.44
330	5.01	0.07	0.09	-0.01	-0.02
<b>Total average (µg m<sup>-3</sup>)</b>		<b>1.19</b>	<b>1.16</b>	<b>-0.25</b>	<b>-0.32</b>
<b>Total average (%)</b>		<b>6.98</b>	<b>7.45</b>	<b>-1.45</b>	<b>-2.08</b>

#### 3.4.3 The influence of trees under different wind speeds

Table 3.6 shows the effects of trees on PM<sub>2.5</sub> concentrations for different wind speeds. Results show that the effectiveness of trees in altering street concentrations is greater at lower wind speeds. At a wind speed of 3 m s<sup>-1</sup>, trees increase road emission concentrations by 16.74% in summer, whilst providing a beneficial decrease of 3.43% via deposition. The dispersive effect of trees were subsequently much lower at a wind speed of 9 m s<sup>-1</sup>, with road emission concentrations increasing by 3.70%. Dispersion and deposition did not however decrease at the same rate across the different wind speeds, suggesting that the effects of trees were not linear with wind speed changes.

The ability of trees to increase turbulent dispersion accounts for their beneficial aerodynamic effects (see Chapter 5 and Chapter 6). However, little turbulent

### 3.4 Results and discussion

---

dispersion occurs at lower wind speeds because trees act as obstacles to wind flow, explaining the greater wind-trapping ability of trees at lower wind speeds. This finding is in agreement with a previous experimental study (Sabatino et al., 2015). An explanation for greater deposition effects occurring at lower wind speeds could be due to the fact that more time is left for the suspended particles to deposit on leaves. In addition, less dispersion occurs at lower wind speeds, which increases concentrations of pollution therefore leading to greater deposition flux.

Table 3.6: Influence of wind speed on aerodynamic dispersion and deposition of trees on PM<sub>2.5</sub> concentrations emitted by traffic at the Marylebone monitoring site.

	WS (m s <sup>-1</sup> )	Aerodynamic dispersion		Deposition		Total effects	
		S. & A.	Summer	S. & A.	Summer	S. & A.	Summer
<b>3</b>	( $\mu\text{g m}^{-3}$ )	2.16	2.84	-0.43	-0.58	1.73	2.26
	(%)	10.80	16.74	-2.13	-3.43	8.67	13.31
<b>5</b>	( $\mu\text{g m}^{-3}$ )	1.19	1.16	-0.25	-0.32	0.94	0.84
	(%)	6.98	7.45	-1.45	-2.08	5.53	5.37
<b>7</b>	( $\mu\text{g m}^{-3}$ )	0.26	0.23	-0.13	-0.19	0.13	0.04
	(%)	1.82	1.77	-0.87	-1.47	0.95	0.3
<b>9</b>	( $\mu\text{g m}^{-3}$ )	0.17	0.38	-0.09	-0.14	0.08	0.24
	(%)	1.71	3.70	-0.88	-1.34	0.83	2.36

#### 3.4.4 Discussion

##### Effects of trees at the Marylebone measurement station

The analysis of CFD results and data monitored at the Marylebone measurement station shows that trees should be considered as a mitigation measure, preferably for streets which are parallel to the prevailing winds. However, trees also exacerbate trapping for wind directions perpendicular to the street canyon orientation and tree planting would not improve air pollution in this situation. This supports previous findings which have shown an increase in street canyon pollution concentrations for perpendicular winds (see for example Gromke et al. 2008; Buccolieri et al. 2011; Wania et al. 2012) and demonstrates that local meteorology should be taken into account for tree planting policies.

In the CFD model employed in this study, no effect of trees has been taken into account when the LAD was supposed to be zero (CB case in winter), i.e. branches and trunks were neglected. Here results suggest that the remains of trunks and branches or possibly the presence of pine trees which are evergreen, seem to play a role in winter. In fact, for a particular wind direction (225°) a significant discrepancy

between modelled and monitored data was found for the CB case (buildings only) and not for the other cases with trees (CT1 and CT2).

#### **Overall effects of trees on pedestrians in Marylebone Rd**

To investigate the overall effects of trees on pedestrians, CFD concentrations were sampled across the whole of Marylebone Rd on a regular 2 m grid at a pedestrian height of 1.5 m (see concentrations of  $PM_{2.5}$  in Figure 3.8). The aerodynamic effects of trees were found to be similar for both  $PM_{2.5}$  and  $NO_x$ , the only difference being in terms of the value of the emissions emitted by them.

Street concentrations of  $PM_{2.5}$  can be seen in Figure 3.8a without the effect of trees and in Figure 3.8b with trees, the concentrations being averaged for Figure 3.8a,b across prevailing winds (using the prevailing winds probability in Table 3.5). The introduction of trees in the street slightly changes the distribution of concentrations, particularly of hotspots, which subsequently appear to be more spread out. The aerodynamic effects of trees (Figure 3.8c) is quite heterogeneous in that trees can either decrease or increase concentrations at pedestrian height. The pollution-trapping ability of trees is particularly important around the monitoring site. A reason for this increase might be the high number of trees towards the East of the monitoring site which act as a barrier to the prevailing winds coming from the South West. This has the effect of reducing wind velocities and therefore increasing pollution concentrations. Changes in  $PM_{2.5}$  via deposition on trees (Figure 3.8d) are less important than the aerodynamic effects in terms of magnitude.

When considering the effects of trees across the whole street, the aerodynamic dispersion of trees was actually found to decrease street pollution concentrations by 1.11% in spring and autumn and 0.65% in summer (Table 3.7). In addition, it was observed that the loss of  $PM_{2.5}$  via deposition on trees was greater than the aerodynamic effects when considering the whole street, with 2.87% loss in spring and autumn and 4.58% in summer. In most of the wind directions, trees were found to increase concentrations. In the special case of Marylebone Road, where prevailing winds are parallel to the street canyon, more weight is given to favourable wind directions, as illustrated by Table 3.7. The resultant weighted effect of trees also happen to be beneficial for pedestrians. This suggests that results found for a single measurement point location (Table 3.6) are not necessarily representative of the overall effects of trees and can lead to erroneous conclusions (at least in this case).

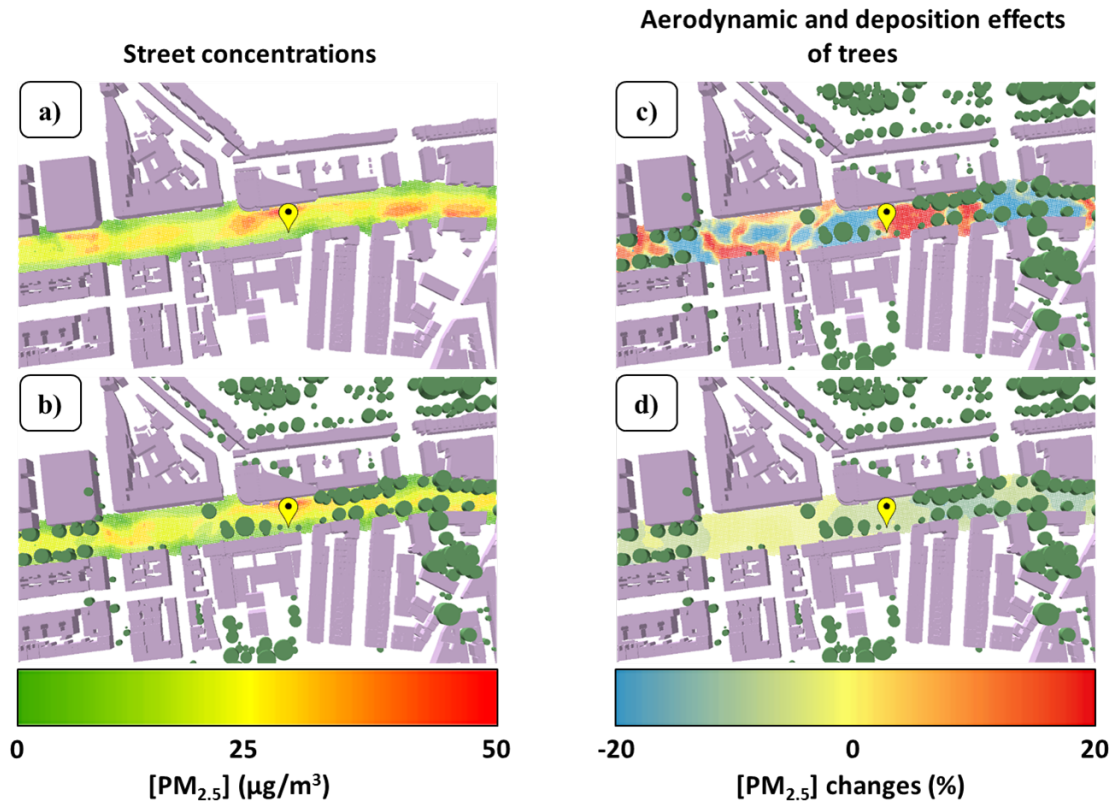


Figure 3.8: Street effects of trees in Marylebone Rd at pedestrian height over prevailing wind directions assuming a homogeneous spread of traffic. (a) Modelled  $\text{PM}_{2.5}$  concentrations without trees (CB). (b) Modelled  $\text{PM}_{2.5}$  concentrations with trees in summer (CT2). (c) Aerodynamic effects of trees in summer (%). (d) Loss of  $\text{PM}_{2.5}$  via deposition on trees in summer.

Note that the weight of the wind directions is very important in Table 3.7. For instance if the wind directions probability was assumed to be homogeneous (here 7.1% for the 14 wind directions), the aerodynamic dispersive effects of trees would be positive (meaning that trees would trap pollution) with  $0.18 \mu\text{g m}^{-3}$  (1.04%) in spring and autumn and  $0.42 \mu\text{g m}^{-3}$  (2.74%) in summer. The effects would be less important on the tree deposition, with  $-0.45 \mu\text{g m}^{-3}$  (-2.67%) in spring and autumn and  $-0.66 \mu\text{g m}^{-3}$  (-4.23%) in summer.

### 3.4 Results and discussion

Table 3.7: Effect of trees on average street concentrations of PM<sub>2.5</sub> emitted by traffic, for a wind speed of 5 m s<sup>-1</sup>, without urban background concentrations. Total percentages (%) are calculated in comparison with seasonal average concentrations of PM<sub>2.5</sub> corresponding to the wind speed of 5 m s<sup>-1</sup>. The 225° wind direction was not included in the calculation as the results were not satisfactory when compared to measurements. Highlighted numbers correspond to wind directions for which trees aerodynamic dispersion is beneficial.

WD (°)	WD probability (%)	Aerodynamic dispersion of trees (µg m <sup>-3</sup> )		Tree deposition (µg m <sup>-3</sup> )	
		Spring and autumn	Summer	Spring and autumn	Summer
0	11.52	3.51	3.85	-0.35	-0.51
30	6.19	1.86	2.14	-0.42	-0.64
60	5.99	-5.98	-6.66	-0.73	-1.02
90	10.63	-3.94	-4.75	-0.55	-0.78
120	5.12	2.00	1.33	-0.26	-0.37
150	5.40	-3.54	3.24	-0.16	-0.31
180	4.36	3.38	3.15	-0.22	-0.30
195	6.87	3.26	3.02	-0.20	-0.29
210	6.14	3.08	2.81	-0.27	-0.43
240	6.97	-1.84	-2.66	-0.82	-1.11
255	13.66	-4.24	-4.83	-0.85	-1.20
270	5.49	-2.84	-3.34	-0.55	-0.80
300	6.65	4.22	4.32	-0.59	-0.88
330	5.01	3.57	4.28	-0.39	-0.56
<b>Total (µg m<sup>-3</sup>)</b>		<b>-0.19</b>	<b>-0.10</b>	<b>-0.49</b>	<b>-0.71</b>
<b>Total (%)</b>		<b>-1.11</b>	<b>-0.65</b>	<b>-2.87</b>	<b>-4.58</b>

### 3.5 Conclusions

Dispersion of traffic emissions ( $\text{NO}_x$  and  $\text{PM}_{2.5}$ ) in a real neighbourhood were investigated by means of monitored data and CFD simulations. Analyses were performed to clarify the relative contribution of both aerodynamic and deposition effects of trees on pollutant concentrations at pedestrian level for several wind speeds and directions. Several conclusions were achieved from this study:

- the aerodynamic effects of trees prevailed over the deposition effects for all the cases investigated at the Marylebone monitoring site. As a consequence, the worst effects of trees with respect to air quality was found for lower wind speeds, since the turbulent mixing was inhibited;
- this study confirms previous findings that the street air quality is altered by trees, with increases of 7% for typical meteorological conditions at the monitoring site, and an additional benefit of 2% reduction of  $\text{PM}_{2.5}$  via deposition;
- while perpendicular winds lead to larger pollution concentrations in street canyons in the presence of trees, the effects of trees under parallel winds have been shown to be beneficial for air quality;
- when considering the average effects of trees on pedestrians, a beneficial reduction of 0.65% due to aerodynamic effects was found in summer, with an additional 4.58% reduction via deposition loss. This shows the importance of the local meteorology, as both wind direction and wind speed distribution have a critical impact on the overall trees effect. The above findings suggest that there is a crucial need for research to provide effective tree-planting policy advice for urban planners. This could lead to substantial air quality improvements depending on the interaction of trees with local meteorological conditions and building arrangements.

# Chapter 4

## The effectiveness of trees to disperse road traffic emissions in Leicester

*This Chapter has been published in Atmospheric Environment (Jeanjean et al., 2015).*

### 4.1 Introduction

During the last decade, a number of studies have shown the importance of vegetation in the urban environment (see for example Buccolieri et al. (2011), Mochida et al. (2008)) with regards to air pollution. Vegetation has been shown to be both beneficial and harmful. For instance, the presence of vegetation has been shown to be beneficial by decreasing the pollutant concentration *via* deposition on trees, leaves and other green infrastructures. Pugh et al. (2012) have shown that using "green walls" in street canyons can decrease pollutant concentrations as much as 40% for NO<sub>2</sub> and 60% for PM<sub>10</sub>. However, vegetation may also increase pollutant concentration in street canyons by blocking the wind circulation and via chemistry. The studies of Pugh et al. (2012) and Vos et al. (2013), in agreement with other studies, illustrate that tree-planting can increase pollutant concentration locally in street canyons where the levels of traffic emissions are high. Another approach was proposed by the European ATMOSYS project which looked into a range of different vegetation settings at different wind directions in a street canyon (Vranckx and Vos, 2013). In this study, trees were found to have an annual increase of 0.2% to 2.6% for

PM<sub>10</sub> and 1% to 13% for elementary carbon depending on the type of vegetation. On the city scale, some studies have shown the beneficial effect of trees that remove particles by deposition (Donovan et al., 2005). But few of these studies have looked at the dispersive impact of vegetation on the city scale.

This thesis chapter aims to investigate the effectiveness of trees at dispersing road traffic concentrations on a city scale. As previously, CFD simulations have been performed with the OpenFOAM software platform using the k- $\epsilon$  model. The CFD results were evaluated against data from the CODASC wind tunnel study (CODASC, 2014). A 3D database of buildings and trees was derived from airborne LIDAR data, and then integrated into the study on a flat  $2 \times 2$  km area around the City Centre of Leicester. Idealised deciduous trees were modelled as porous bodies using a momentum sink for the velocity. The dispersion of fixed traffic emissions was simulated for a tree-free city (city without trees), and for a city with trees for 12 wind directions. Although the assumption that the volume of urban space occupied by trees in tree-free city is negligible, this is not very close to reality. However, removing the trees in the modelling stage is a useful way of specifically studying their dispersive impact on air pollution.

## 4.2 Development of the CFD model for the Leicester urban area

### 4.2.1 Description

The study area for this work is the City of Leicester, which is located in the East Midlands region of the UK (latitude of  $52.63^\circ$ , longitude of  $-1.13^\circ$ ). In 2011, the population of Leicester was 329,600, making it around the tenth largest city in the UK. Leicester periodically fails to meet its European regulatory limits for urban air pollution concentrations (Evan, 2011). To develop a model for the city, a 3D LIDAR dataset of the buildings was made by Infoterra in 2007 at resolution of 25 cm. This was combined with a road map from the same year provided by Leicester City Council. The road map includes major junctions and omits the residential roads that have low traffic volumes (see Figure 4.1). The National Tree Map<sup>TM</sup> (NTM) Crown Polygon produced by Bluesky was used in the tree database to represent individual trees or closely grouped tree crowns (Bluesky, 2014). Trees and bushes over 3 m in height were included in the database. The NTM<sup>TM</sup> provided a canopy



Figure 4.1: Overview of the  $2 \text{ km} \times 2 \text{ km}$  area of interest in Leicester showing the LIDAR data of the buildings, the road map and the national tree map (NTM<sup>TM</sup>) from Bluesky.

top height but did not provide the canopy base height. While the results presented in this thesis chapter are promising, it is worth noting that limitations in current literature have necessitated the use of an assumed canopy base height of  $1 / 3$  of the canopy top height which is the same assumption as that used in the wind tunnel experiment (Gromke et al., 2008). The impact of other canopy base ratios such as  $1 / 4$  or  $1 / 5$  on the results were not investigated here which leaves room for further

research.

Figure 4.1 shows the  $2 \times 2$  km area of interest in Leicester used for the CFD simulations. The city centre is highlighted in the centre of the figure with the inner ring road around it. The traffic distribution was assumed to be constant across all roads (in pink) as the main focus of the study was the effectiveness of trees in dispersing traffic emission. Although not considered here, traffic turbulence can affect the dispersion of vehicular emissions (Jicha et al., 2000), the enhancement in kinetic energy usually affects the lower parts of the streets (Vachon et al., 2002). Using the ArcScene software, the total area covered by trees (in light green) was found to be  $0.46 \text{ km}^2$  which represents 11.5% of the modelled area with an average canopy height of 10.6 m. The total area covered by buildings was found to be  $1.2 \text{ km}^2$  which represents 29% of the modelled area with an average building height of 10 m. The idealised tree canopy modelling is detailed in the following section. The annual UK average wind speed of  $4.6 \text{ m s}^{-1}$  was chosen for the CFD simulation, which is similar to the yearly average wind speed in Leicester.

In summary, to assess the impact of trees on the dispersion of traffic emissions, two scenarios were modelled. The first scenario was run without trees, over a series of different wind directions. The second scenario ran with the same conditions as the first but with the inclusion of trees. A statistical analysis was then performed to compare the two scenarios and assess the impact of trees, with the finding that trees generally increase the dispersion of pollutants by 7% at pedestrian height.

### 4.2.2 Numerical modelling

Several assumptions were made to adapt the CFD model to city scale modelling. The same CFD modelling approach as previously used in the wind tunnel was also used for wind flow and pollutant dispersion calculations (see section 2.4.2). The traffic emissions were considered as a passive non-reactant scalar dispersed without buoyancy, the  $S_{ct}$  was kept with a value of 0.5. The same traffic volume was used for all roads with an arbitrary value of  $1 \mu\text{g s}^{-1} \text{ m}^{-2}$ , the concentration being normalised at the post-processing stage. The simulations were performed every  $30^\circ$  leading to a total of 12 different wind directions:  $0^\circ$ ,  $30^\circ$ , ...,  $300^\circ$  and  $330^\circ$ .

Figure 4.2 a) shows the total size of the computational domain of  $5 \times 5 \text{ km}$  ( $25 \text{ km}^2$ ). The area of interest was situated at the centre of the computational domain with a size of  $2 \times 2 \text{ km}$  ( $4 \text{ km}^2$ ). The tallest building in the area of interest is the Cardinal Telephone Exchange tower with a height ( $H_{max}$ ) of 84 m. The domain

boundaries were placed at more than  $17 H_{max}$  in each direction from the urban area of interest to allow the computation of different wind directions. The domain height was set up to 500 m which corresponds to  $6 H_{max}$ . With a built zone length of 2 km maximum and of average height 10 m, the built area is estimated at a maximum of  $19,300 \text{ m}^2$ . The blockage ratio of the built area was estimated at 0.77% which is below the recommended 3% (Jorg et al., 2007).

The same meshing method as the wind tunnel was used and adapted to the city scale with an average building height ( $H$ ) of 10 m. The total number of cells used numbered 3.2 million. The buildings and trees were assigned a cell size of  $0.132 x/H \times 0.132 y/H \times 0.112 z/H$ . The choice of mesh in this section may be coarser than the one used in the wind tunnel experiment. The cells that intersected the road location below a height of 1.5 m were selected for the traffic emission. Figure 4.2 b) shows an overview of the mesh.

With finite volume methods, the grid needs to be fine enough to capture important physical features such as shear layers and vortices. The mean velocity boundary flow ( $u(z)$ ) and the turbulent dissipation were set up to follow a logarithmic law using the `ABLInletVelocity` and `ABLInletEpsilon` utilities in OpenFOAM (Eq. (2.19) and (2.20)).

A residual convergence of  $10^{-5}$  was used for all the residuals. For the scalar dispersion, the same number of time steps was used for all the simulations to allow them to finish at the exact same time from which the dispersion started.

For modelling the idealised tree canopy, the same approach as the wind tunnel was used (see section 2.4.2). The same tree modelling technique was also used in the European ATMOSYS project (Vranckx and Vos, 2013). The pressure loss coefficient induced by trees is expressed in a real case as in Eq. 3.2.

Leicester has 81% deciduous trees (Forestry-Commission, 2013a) and 19% coniferous trees (Forestry-Commission, 2013b). Only deciduous trees were considered because as they are predominant in Leicester. Lalic and Mihailovic (2004) have shown that for deciduous trees, the average LAD through the canopy can be approximated to be between  $1.06$  and  $2.18 \text{ m}^2 \text{ m}^{-3}$ . From previous studies, the drag coefficient can be estimated to be between  $0.1 \leq C_d \leq 0.3$  for most types of vegetation (Katul et al., 2004). Therefore, the canopy pressure loss coefficient can be assumed to lie between  $0.11 \leq \lambda \leq 0.65$ . An average drag coefficient of  $C_d = 0.25$  for the tree canopy was used with an average LAD of  $1.6 \text{ m}^2 \text{ m}^{-3}$  leading to a final pressure loss coefficient ( $\lambda$ ) of  $0.4 \text{ m}^{-1}$ . In winter, the drag of the trees would be

smaller owing to a greater contribution from the trunk and branches, with a LAD of  $0 \text{ m}^2 \text{ m}^{-3}$ . Spring and autumn are a bit more complicated with the growth and fall of leaves, respectively. These special cases are not covered in this thesis chapter which focuses on trees with a fully developed LAD, best match by trees in the summer month. This thesis chapter works on the assumption that idealised trees have the same LAD during each month in the summer, in order to get the maximum impact from the vegetation on pollution dispersion. The variation in observed trend in pollution dispersion according to other seasons and trees species leaves room for future research.

## 4.3 City scale CFD results and discussion

### 4.3.1 Comparison of a tree-free city to a city with trees

In total, 24 CFD simulations were performed: 12 for the tree-free city and 12 for the city with porous trees, both at a wind speed of  $4.7 \text{ m s}^{-1}$  and for wind direction every  $30^\circ$ . The outputs were sampled regularly every 10 m leading to a sampling grid of  $200 \times 200$  pixels. It was found that changing the sampling method, either by sampling at specific locations along the road sides or by increasing the sampling resolution, did not have a significant impact on the results ( $< 10\%$  for altitudes under 10 m). The simulation outputs were sampled at 8 different altitudes of 1.5, 4, 8, 12, 20, 30 and 50 m to explore changes in concentration variation with height. The velocity and the eddy viscosity fields were also sampled. If the sample location was inside a building, a no data value (NaN) was attributed to it.

#### Impact of trees on pollutant concentration

To compare the scalar concentration of a tree-free city to a city with trees, the normalised Relative Deviation (RD)  $\Delta C^*(z)$  at the domain height  $z$  was defined. To construct a unique normalised scalar concentration difference  $\Delta C^*$  such as in Figure 4.3, multiples simulations results from different wind directions were aggregated (see Appendix B) such that

$$\Delta C^*(z) = \sum_{wd=1}^N \Delta C^*(wd, z) \cdot P(wd), \quad (4.1)$$

where  $N$  is the number of wind directions (here 12),  $\Delta C^*(wd, z)$  the scalar concentration at the  $wd$  specific wind direction and height  $z$  and  $P(wd)$  the percentage contribution of the wind direction  $wd$ . For example in the case of uniformly averaged wind directions,  $P(wd) = 1 / N = 1 / 12 = 8.3\%$ . In the case of prevailing wind directions, the percentage contribution of the wind directions are non-uniform (see Table 4.1). At a given wind direction, the normalised concentrations difference between a tree-free city and a city with trees was defined such that

$$\Delta C^*(wd, z) = \sum_{i,j} \frac{[C_{tree}(wd, i, j, z)] - [C_{notree}(wd, i, j, z)]}{C_0(wd, z)} \cdot 100, \quad (4.2)$$

where  $z$  is the height in meters,  $[C_{tree}(wd, i, j, z)]$  is the scalar concentration of the  $(i, j)$  pixel of a city with trees at the height  $z$  and wind direction  $wd$ ,  $[C_{notree}(wd, i, j, z)]$  is the scalar concentration of the  $(i, j)$  pixel of a tree-free city at the height  $z$ , and  $C_0(wd, z)$  is the averaged scalar concentration of a tree-free city at the height  $z$  and wind direction  $wd$ .  $\Delta C^*$  is the normalised RD scalar concentration in%.

Figure 4.3 shows the dispersive effect of trees on air pollutant concentrations from road sides averaged uniformly over 12 wind directions. Trees significantly increase concentrations in deep street canyons, as seen in Leicester City Centre. Nevertheless, in an open terrain configuration (outside of the City Centre), trees have a beneficial effect on air pollutant concentrations. A decrease of 0 to 20% is seen in most places and an even greater decrease is seen along road sides. A first consideration would be that trees planted outside densely built-up areas along roads and outside street canyons generally decrease pollutant concentrations. Figure 4.3 also suggests that trees change pollutant concentrations in their surrounding streets and not only in the street where they were planted. This is particularly true in the City Centre, where some streets demonstrate an increase in concentrations without trees being present. The reason for which trees increase pollutant concentrations in a downwind street could be due to a diminution of the wind flow speed. This preliminary finding would benefit from further CFD street canyon modelling to reinforce this idea.

To investigate these changes of concentration caused entirely by the tree dynamics,  $\Delta C^*$  was averaged at 8 different altitudes and plotted in Figure 4.4 a). It was quite surprising to find that  $\Delta C^*$  had a negative value. It was expected that greater concentrations would be found for the CFD simulations with trees, therefore giving a positive  $\Delta C^*$  for those heights. This means that trees decrease the scalar concentration for heights lower than 20 to 30 m, depending on the wind direction.

### 4.3 City scale CFD results and discussion

---

Figure 4.4 b) shows the number of sampling points associated with a specific  $\Delta C^*$ . Greater deviation is observed at smaller altitudes. These observations suggest that trees raise the scalar concentration vertically, as positive  $\Delta C^*$  concentrations are found above 30 m.

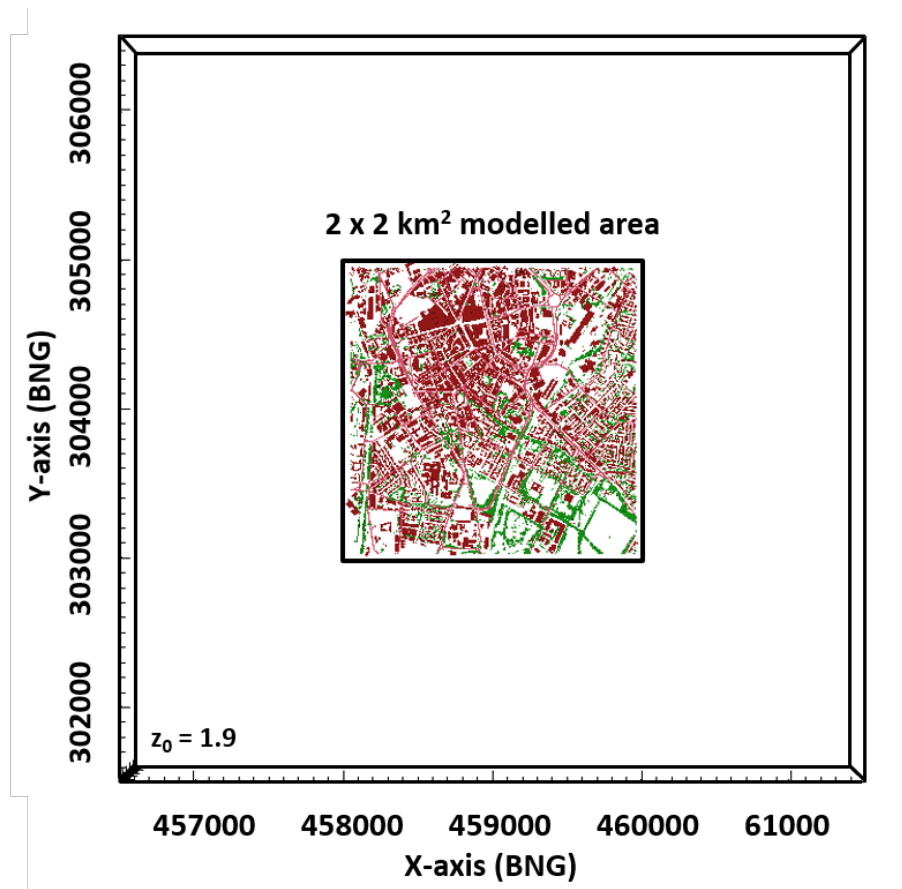
To explain these changes in concentration, other simulation parameters have been studied including the mean velocity ( $U$  in  $\text{m s}^{-1}$ ), the vertical velocity ( $Uz$  in  $\text{m s}^{-1}$ ) and eddy viscosity ( $nut$  in  $\text{m}^2 \text{s}^{-1}$ ) according to:

$$\Delta U(wd, z) = \sum_{i,j} [U_{tree}(wd, i, j, z) - U_{notree}(wd, i, j, z)], \quad (4.3)$$

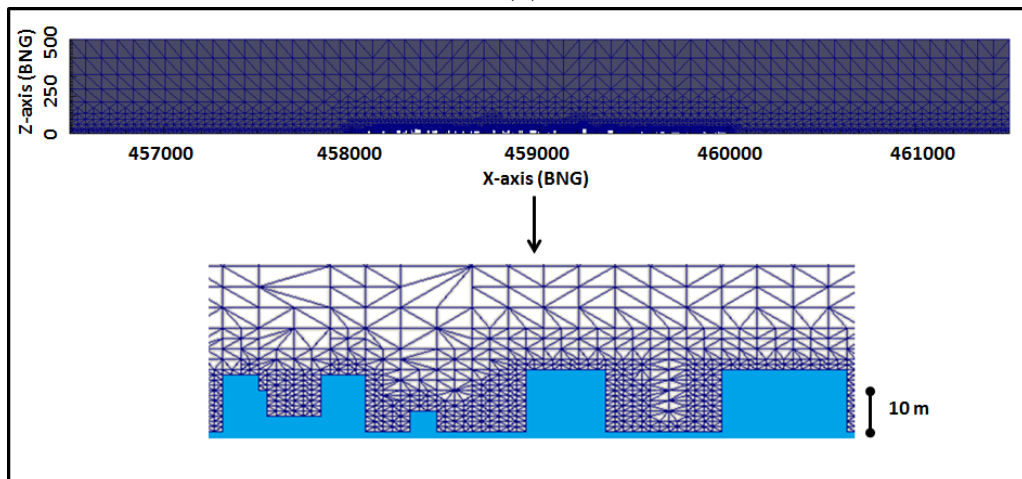
$$\Delta Uz(wd, z) = \sum_{i,j} [Uz_{tree}(wd, i, j, z) - Uz_{notree}(wd, i, j, z)], \quad (4.4)$$

$$\Delta nut(wd, z) = \sum_{i,j} [nut_{tree}(wd, i, j, z) - nut_{notree}(wd, i, j, z)], \quad (4.5)$$

Regarding the mean velocity  $U$ , it can be seen that trees decrease the velocity difference at all heights ( $\Delta U < 0$ ) as seen in Figure 4.5 a. The histogram in Figure 4.5 b also shows clearly that most of the pixels have a negative  $\Delta U$ . It is worth noting that  $\Delta U$  decreases at a maximum of around 10-12 m, which corresponds to the average canopy height of 10.6 m.



(a)



(b)

Figure 4.2: Area of interest loaded into the paraView software, axes in British National Grid (BNG). (a) Overview from the top of the domain. (b) Mesh overview from the side of the domain with a zoom on a street canyon. Wide buffer conditions are used around the buildings to allow the inflow wind to change directions.

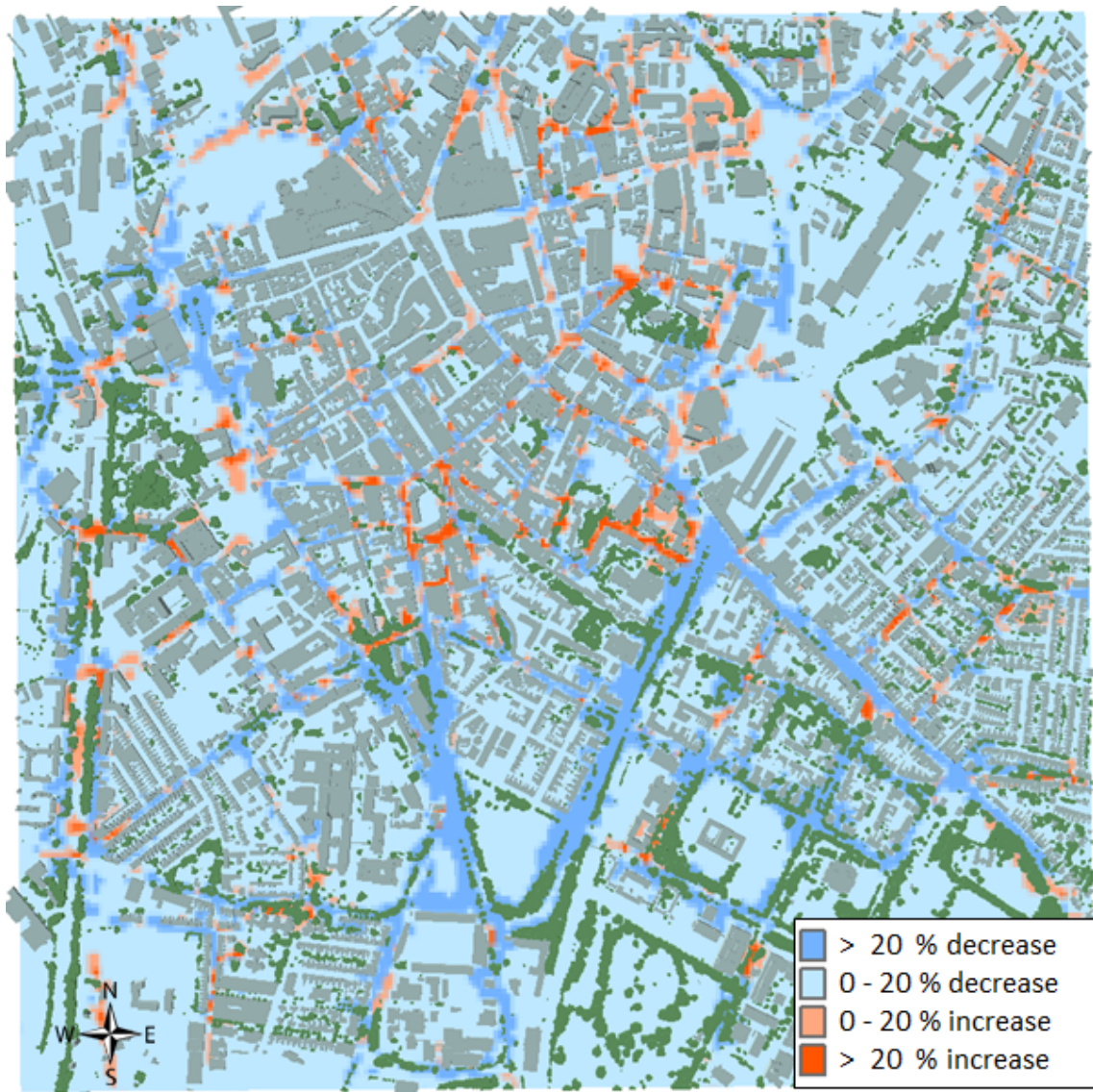
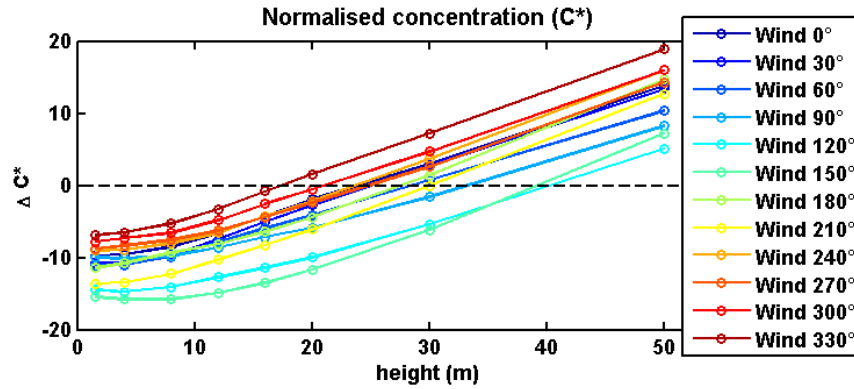
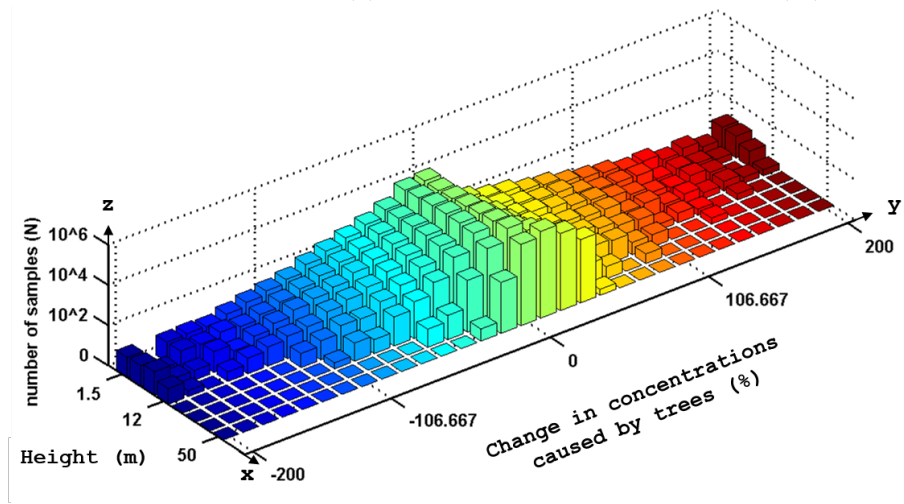


Figure 4.3: Modelling output of the normalised scalar concentration difference  $\Delta C^*$  at a height of 1.5 m averaged uniformly over 12 wind directions. Trees increase traffic concentrations in street canyons but show a beneficial decrease of concentrations in open terrain configurations.



(a) Plot of the average difference (%) in pollutant concentration depending on the wind direction ( $^{\circ}$ ) and height within the domain (m).



(b) Change of concentrations caused by trees (in % along y axis) at different domain height (x axis). The z axis represents the number of pixels from Figure 4.3 associated to a change of concentrations.

Figure 4.4: Difference in pollutant concentrations (%) induced by trees across the whole domain. Negative normalised concentrations indicate a decrease in pollutant concentrations and positive normalised concentrations indicate an increase. (a) Trees decrease pollutant concentrations at heights under 20-30 m and increase them at greater heights. (b) Greatest deviation in pollutant concentrations were observed at lower heights.

### **Impact of trees on the mean velocity**

Regarding the vertical velocity  $U_z$ , it can be seen that trees increase this parameter ( $\Delta U_z > 0$ ) as the height increases (Figure 4.6a). Greater vertical wind velocities would explain a decrease of concentration as the concentration follows the vertical path of the wind. The vertical velocity increases less for wind directions between  $120^\circ$  and  $180^\circ$  than other wind directions. This is likely to be due to greater eddy viscosity seen in more rural landscapes such as in the south of the area of interest (see Figure 4.1).

### **Impact of trees on the vertical velocity**

Regarding the eddy viscosity ( $\nu_{t}$ ), it can be seen that trees increase this parameter progressively from the ground up to a height of 30 m (see Figure 4.7). The eddy viscosity corresponds to the modeled turbulent eddies which means that trees increase turbulence ( $\Delta \nu_{t} > 0$ ) in this case. An increase in turbulence would cause greater mixing and thereby increase the concentration dispersion. Moreover, it is worth noting that the wind directions with the greatest increase in turbulence (wind directions between  $120^\circ$  and  $180^\circ$  in Figure 4.7 a) also showed the lowest increase in vertical turbulence (Figure 4.1 a) and the greatest reduction in concentration (Figure 4.4 a). This suggests that turbulence has a large impact on reduction in concentration than by an increase in vertical velocity.

### **Impact of trees on the turbulence**

However, the smallest reduction of concentration induced by trees is observed for the wind directions of  $300^\circ$  and  $330^\circ$ . A densely built-up area can be seen on the top left of the study area with a small presence of trees, which could explain the lower amount of mixing by turbulence for these wind directions.

### **4.3.2 Effectiveness of trees depending on the prevalent wind direction**

Figure 4.8 shows the prevalent wind directions for the city of Leicester averaged for the year 2013. The probability of a given wind direction is shown in Table 4.1. The prevalent wind directions in Leicester exist mainly between  $180^\circ$  and  $210^\circ$  which corresponds to Southerly and South Westerly winds. The probabilities of

### 4.3 City scale CFD results and discussion

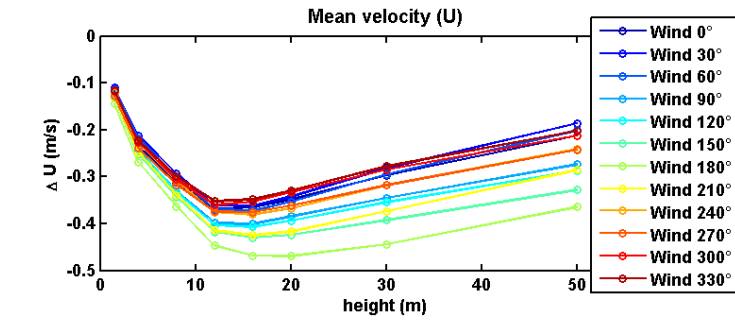
---

Wind direction (+ / - 15 °)	0°	30°	60°	90°	120°	150°
Probability (%)	7.0	6.7	5.8	7.2	7.2	8.3
Wind direction (+ / - 15 °)	180°	210°	240°	270°	300°	330°
Probability (%)	16.6	13.4	9.4	7.5	5.4	5.5

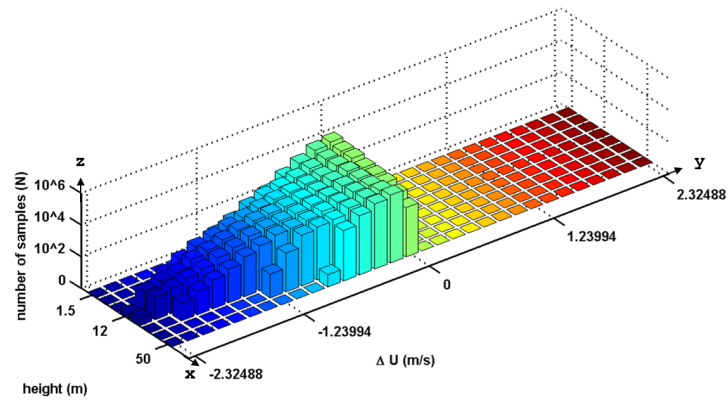
Table 4.1: Probability of the wind direction in Leicester from a local weather station. The probabilities have been aggregated every 30 ° ( + / - 15 ° around each wind direction).

these prevailing wind directions have been used to investigate the impact on the average scalar concentration difference  $\Delta C^*$ . This was previously calculated at a constant wind speed of 4.7 m s<sup>-1</sup> as compared to a uniformly averaged  $\Delta C^*$  with the same weight for each wind direction. It can be seen in Figure 4.9 that by using the observed wind direction distribution, the  $\Delta C^*$  is reduced from 10.5% to 7% at a height of 1.5 m. Then the  $\Delta C^*$  decreases at greater altitudes. This suggests that the way trees are positioned within a city impacts their effectiveness to disperse road traffic emissions.

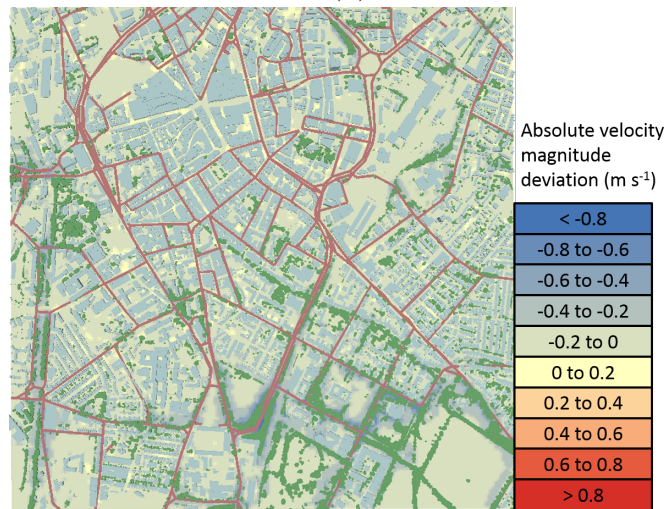
### 4.3 City scale CFD results and discussion



(a)



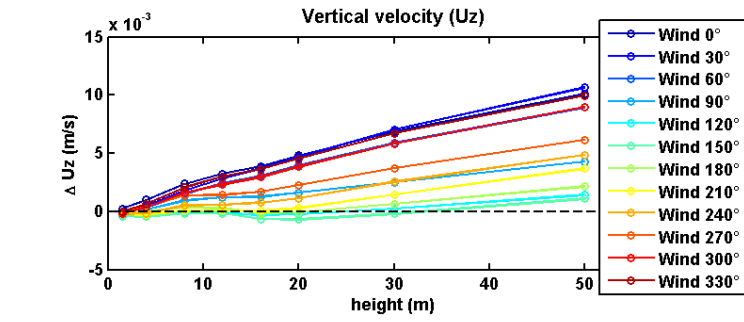
(b)



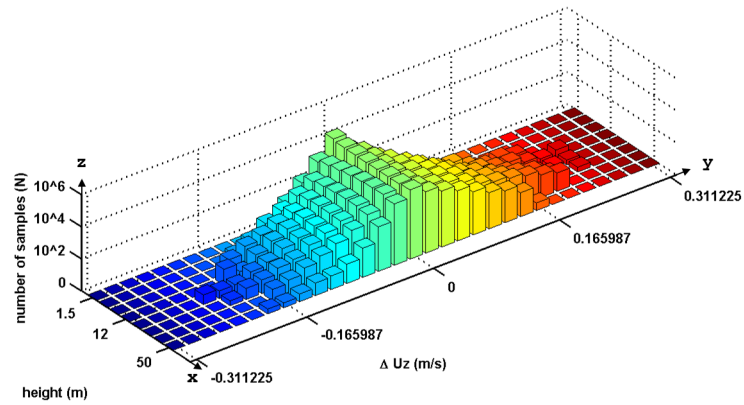
(c)

Figure 4.5: Difference in velocity ( $\text{m s}^{-1}$ ) induced by trees across the whole domain. (a) Plot of the difference in velocity ( $\text{m s}^{-1}$ ) depending on the wind direction ( $^\circ$ ) and height within the domain (m). Trees reduce the wind velocity across the domain with the greatest decrease observed at 12-15 m (corresponding to the average canopy height). (b) Distribution of difference in velocity ( $\text{m s}^{-1}$ ) averaged uniformly over 12 wind directions. Greatest deviation in velocity was observed around 12-15 m. (c) Map of the difference in velocity ( $\text{m s}^{-1}$ ) averaged uniformly over the 12 wind directions at  $z = 1.5$  m.

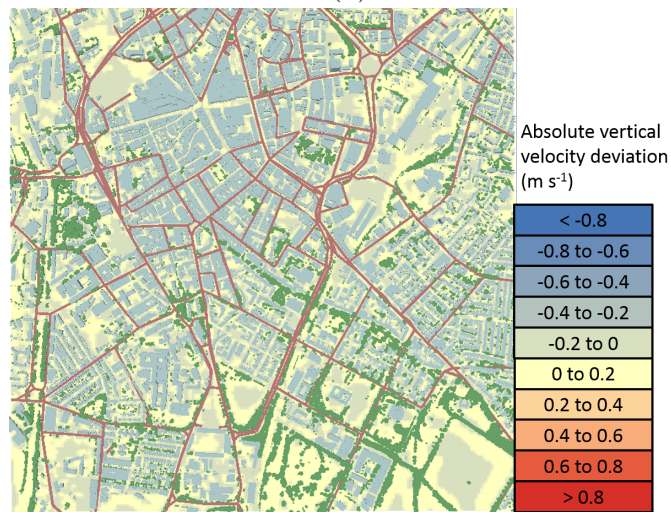
### 4.3 City scale CFD results and discussion



(a)



(b)



(c)

Figure 4.6: Difference in vertical velocity ( $\text{m s}^{-1}$ ) induced by trees across the whole domain. (a) Plot of the vertical velocity difference ( $\text{m s}^{-1}$ ) depending on the wind direction ( $^\circ$ ) and height within the domain (m). Trees show a minor increase vertical velocities ( $0\text{-}5 \cdot 10^{-3} \text{ m s}^{-1}$ ). (b) Distribution of difference in vertical velocity ( $\text{m s}^{-1}$ ) uniformly averaged over 12 wind directions ( $x$  axis), height ( $y$  axis) and a number of CFD sampled points. The distribution of difference in vertical velocities is roughly constant over the heights of the domain. (c) Map of the difference in vertical velocity ( $\text{m s}^{-1}$ ) averaged uniformly over the 12 wind directions at  $z = 1.5 \text{ m}$ .

### 4.3 City scale CFD results and discussion

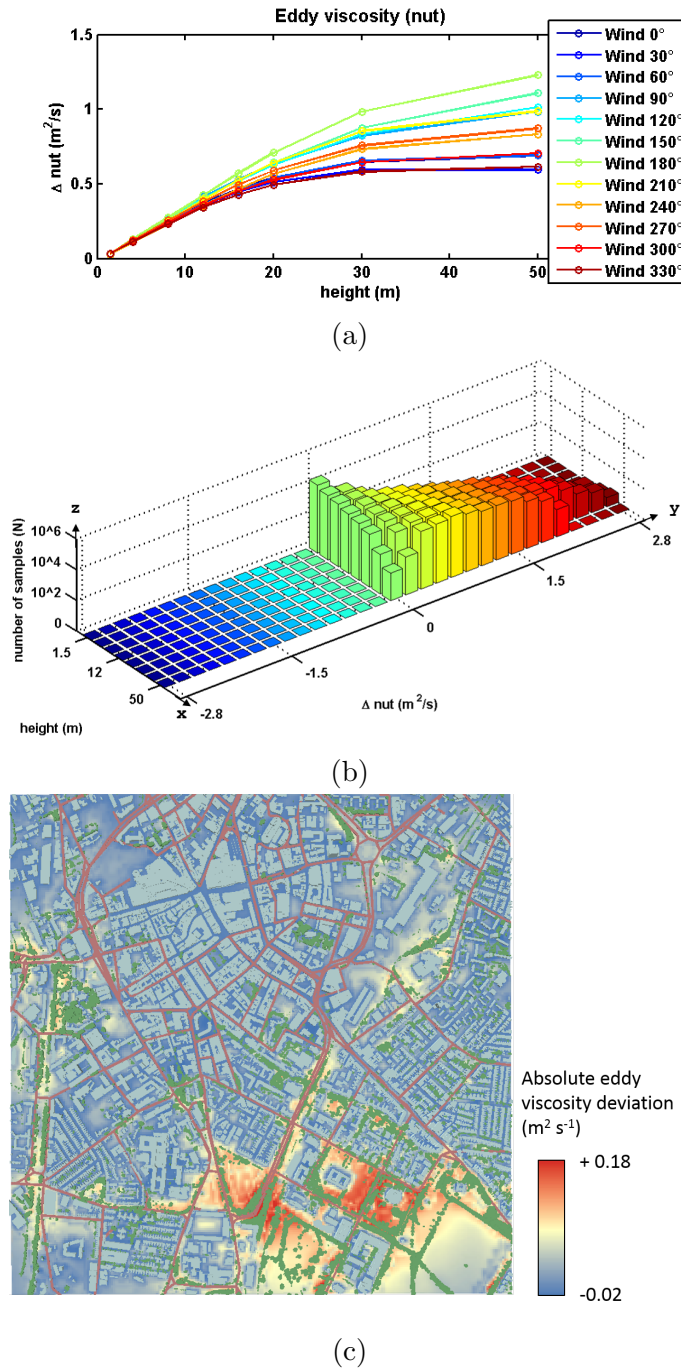


Figure 4.7: Difference in eddy viscosity difference ( $\text{nut} - \text{m}^2 \text{s}^{-1}$ ) induced by trees across the whole domain. (a) Plot of the eddy viscosity difference ( $\text{m}^2 \text{s}^{-1}$ ) depending on the wind direction ( $^\circ$ ) and height within the domain (m). Trees are showing to increase turbulence, especially at heights over 20 m. (b) Distribution of difference in eddy viscosity ( $\text{m}^2 \text{s}^{-1}$ ) uniformly averaged over 12 wind directions ( $x$  axis), height ( $y$  axis) and a number of CFD sampled points. The distribution of eddy viscosity difference shows that trees are only increasing turbulence. (c) Map of the difference in eddy viscosity ( $\text{m}^2 \text{s}^{-1}$ ) averaged uniformly over the 12 wind directions at  $z = 1.5$  m.

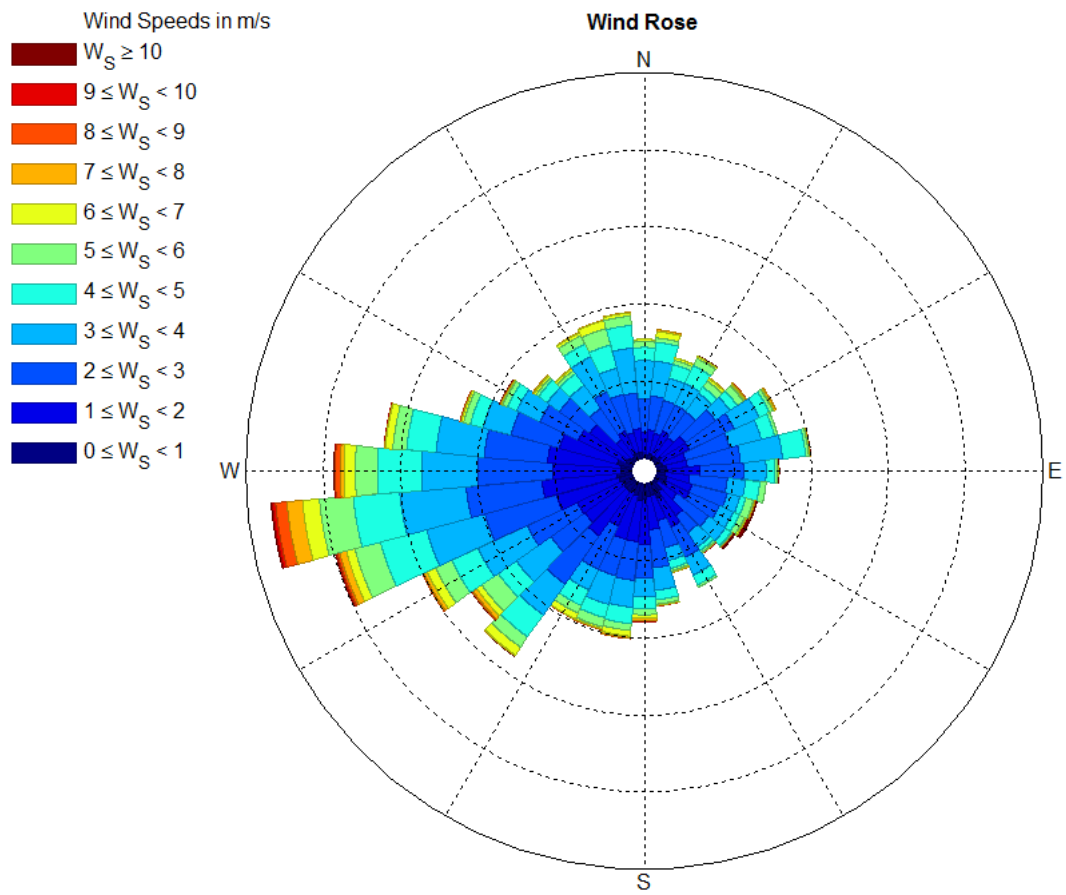


Figure 4.8: Yearly wind rose of the wind speed and direction in Leicester, averaged every hour from an anemometer placed on a 10 m mast in Leicester (data acknowledgement: Leicester City Council, 2013).

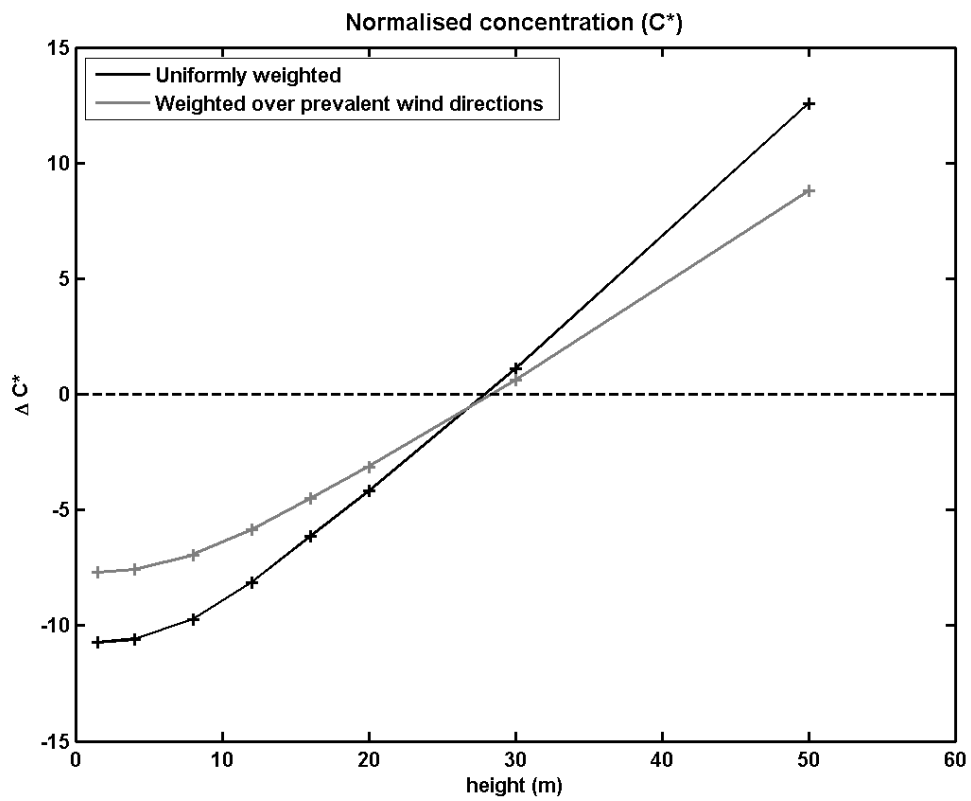


Figure 4.9: Impact of the prevalent wind on the modelled average scalar concentration difference  $\Delta C^*$  induced by trees: comparison of a uniform average over 12 wind directions with an average depending on the wind direction probability.

## 4.4 Conclusions

Arbitrary scenarios of dispersion for road traffic emissions were compared between a tree-free city and a city with idealised trees in CFD simulations. The effect of the trees on the dynamics of air flow was considered, other processes involving tree chemistry or deposition were not investigated but remain open to further research. In this thesis chapter, all idealised deciduous trees are assumed to have the same porosity value of  $0.4 \text{ m}^{-1}$ . Compared to wind tunnel measurements, the average CFD model uncertainty is 35% for a tree-free street canyon and 38% for a street canyon with trees, which is comparable to previous CFD studies.

The results suggest that trees are beneficial from a purely dynamic point of view, as they decrease the concentration of traffic emissions by 7% on average at pedestrian height. This decrease is primarily a result of an increase in turbulence that in turn increases the mixing of traffic emissions. Trees are less effective in deep street canyons as they tend to trap emissions, which can be seen in the City Centre of Leicester. Reduction is most effective when trees are placed in open areas, upwind from the emissions. The turbulence caused appears to propagate downwind where it increases the mixing of emissions.

The results in this thesis chapter on city scale modelling of pollution dispersion using CFD pave the way for future work by using data from traffic emissions and ambient pollutant concentrations in multiple locations. Such a study would require a detailed traffic model, a dense representative network of sensors, a degree of tree speciation knowledge, parametrisation of LAD, and ideally would be carried out over a full annual cycle. This novel study highlights this active area of research and hopes to provide a combination of local and regional scale models in order to assess the impact of trees in urban planning.

# Chapter 5

## The effectiveness of urban trees and grass on PM<sub>2.5</sub> reduction via dispersion and deposition in Leicester

*This Chapter has been published in Atmospheric Environment (Jeanjean et al., 2016).*

### 5.1 Introduction

Road traffic emissions contribute to up to 66% of particulate matter with aerodynamic diameter less than 2.5  $\mu\text{m}$  (PM<sub>2.5</sub>) (Sundvor et al., 2012). An excess of inhaled particulate matters can present adverse health effects such as premature death, lung cancer, cardiovascular disease and asthma attacks among health outcomes (Kim et al., 2015). The World Health Organisation recommends that PM<sub>2.5</sub> concentrations should not exceed the guideline value of 10  $\mu\text{g m}^{-3}$  as a yearly average and 25  $\mu\text{g m}^{-3}$  as a daily average (WHO, 2006). Most of the European population (85%) lives above these recommended levels of PM<sub>2.5</sub> (Guerreiro et al., 2013). In developing countries such as China, these thresholds are sometimes exceeded by an order of magnitude (Chan and Yao, 2008). Urban vegetation and green barriers have been shown to offer passive mitigation for air pollution (Gallagher et al., 2015; Li et al., 2016; Tong et al., 2016; Al-Dabbous and Kumar, 2014; Morakinyo and Lam, 2015). Regional scale modelling studies have shown a modest impact of trees

on particle deposition with less than a few percent reduction (Tallis et al., 2011; Beckett et al., 1998; Nowak et al., 2006; Selmi et al., 2016). However, at the street canyon scale, modelling studies suggest that green walls can decrease pollutant concentrations as much as 40% for NO<sub>2</sub> and 60% for PM<sub>10</sub> (Pugh et al., 2012). Vegetation barriers were also shown to reduce pedestrian exposure on ultrafine particles up by 37% under realistic wind conditions (Al-Dabbous and Kumar, 2014). There are also other benefits of urban green spaces, in that they contribute to the well being of the urban population (White et al., 2013) and road side vegetation also regulates the traffic noise level of busy streets (Kalansuriya et al., 2009). Vegetation can sometimes have adverse effects. Urban trees have been shown to increase pollutant concentrations in some street canyon configurations, as they modify the street canyon roughness properties changing the wind flow behaviour (Gromke et al., 2008; Buccolieri et al., 2011; Wania et al., 2012; Vos et al., 2013; Salmond et al., 2013; Gromke and Blocken, 2015a). However, for winds parallel to street canyons, urban trees have been found to decrease road traffic emissions (Amorim et al., 2013a; Abhijith and Gokhale, 2015). When looking at the global city scale, Barnes et al. (2014) have demonstrated that the urban surface has a direct impact on the dispersion of air pollution with pollutant concentrations increasing with lower surface roughness. This result has been confirmed in a modelling study around the City of Leicester where the aerodynamic effects of trees have been shown to decrease pollutant concentrations owing to an increase in turbulence production (Jeanjean et al., 2015). Recent reviews have pointed out that very little has been done attempting to integrate both the aerodynamics and deposition effects of trees on a city scale (Janhäll, 2015; Salmond et al., 2016), only a few studies focus on this aspect at the street canyon scale (Vos et al., 2013; Vranckx et al., 2015; Steffens et al., 2012), and not the city scale. The objective of this chapter is to study both the aerodynamics and deposition effects of trees and grass on road traffic emitted PM<sub>2.5</sub>. The study focuses on the City of Leicester in the United Kingdom over a total 2 × 2 km area (4 km<sup>2</sup>) using real 3D trees, grass, roads and 3D buildings data. The simulations were performed using a Computational Fluid Dynamics (CFD) model, previously evaluated against available wind tunnel measurements (Jeanjean et al., 2015). The impact of each individual model components such as buildings, trees and grass on PM<sub>2.5</sub> reduction were individually studied. The atmospheric lifetime of PM<sub>2.5</sub> ranges from days to week whereas PM<sub>10</sub> lasts for a few hours to days (Gugamsetty et al., 2012). This translates into a settling velocity of around 0.5 cm s<sup>-1</sup> for PM<sub>10</sub> which

is an order of magnitude larger than a factor than the  $\text{PM}_{2.5}$  settling velocity of  $0.02 \text{ cm s}^{-1}$  (Lapple, 1961).

## 5.2 Experimental

### 5.2.1 Model description

The same model setup as explained in the previous chapters is used here. The computational grid was modified to take into account the grass surface (see Figure 5.1). Guidelines in respect to CFD simulation of air flow in urban environments provided in the COST Action 732 (European Cooperation in the field of Scientific and Technical Research) was used to parameterise the CFD model (Franke et al., 2007).

To develop a model for the City of Leicester, a 3D LIDAR dataset of the buildings was constructed in 2007 with a resolution of 25 cm (see developed city model in Figure 5.1). This was combined with a road map from the same year provided by Leicester City Council. The road map includes major junctions and omits residential roads that have low traffic volumes. The traffic in this chapter was assumed to be uniform across all roads with an arbitrary  $\text{PM}_{2.5}$  road emission value of  $190 \mu\text{g s}^{-1} \text{ m}^{-1}$ , which roughly led to an average ground concentration of  $44 \mu\text{g m}^{-3}$  at a wind speed of  $4.6 \text{ m s}^{-1}$ . The National Tree Map<sup>TM</sup> (NTM) Crown Polygon produced by Bluesky Ltd was used in the tree database to represent individual trees or closely grouped tree crowns (Bluesky, 2014). The areas covered by grass were obtained by downloading the *OS MasterMap Topography Layer* produced by the UK governmental mapping agency, Ordnance Survey. The grass was treated as a smooth surface with a surface roughness of 0.03 m according to the World Meteorological Organisation classification (WMO, 2008). The rest of ground surface between buildings was treated as a surface roughness of 0.10 m, which corresponds to large occasional obstacles. An idealised tree population was considered, which corresponds to the average tree profile encounters in the East Midlands region of the UK. The vertical distribution of leaf was kept constant which corresponds to the average tree LAD in Leicester, previously estimated at  $1.6 \text{ m}^2 \text{ m}^{-3}$  (Jeanjean et al., 2015). In regards to tree species management, studying the impact of vertical distribution of leaf for different tree species as well different canopy shapes leaves room for future research. The trees were modelled as a porous media which results in a perturbation of the



Figure 5.1: Leicester City  $2 \times 2$  km area of interest. (a) Aerial photography of Leicester City in summer 2007. Urban structures are predominant with some green spaces located at the South East of the city. (b) Aerial photography combined with the LIDAR data of the buildings, the road map, the national tree map (NTM<sup>TM</sup>) from Bluesky Ltd and the grass areas from the UK mapping agency (Ordnance Survey). (c) Mesh of the Leicester City area viewed from the CFD software OpenFOAM. More than 17 million cells were used with a resolution of 1 m for each individual building, 2 m for the trees and roads, and 4 m for the grass.

air flow and in removal of particles via deposition. To take into account an average wind profile, 12 wind directions were calculated every  $30^\circ$  and then aggregated into a single average of  $\text{PM}_{2.5}$  concentration. The impact of the wind speed was also investigated with simulations for a turbulent wind flow of  $4.6 \text{ m s}^{-1}$  (which corresponds to the average wind speed in the UK) and for a low wind speed of  $1 \text{ m}$

## 5.2 Experimental

$\text{s}^{-1}$  (which corresponds to a laminar flow, without turbulence). The mean velocity flow and the turbulent dissipation were set up to follow a logarithmic law to reflect an atmospheric boundary layer profile on the bounding edges of the computational domain. Five independent scenarios were modelled looking tree aerodynamics and deposition on trees, grass and buildings. These cases were compared against a reference scenario without any tree aerodynamics and deposition (see Table 5.1). To investigate areas with different tree and grass cover settings, the City of Leicester was divided into smaller subsets: city centre, suburbs, road sides and suburb road sides (see Figure 5.2). All reported values are at ground concentration of 1.5 m, to reflect the effect of tree at pedestrian height.

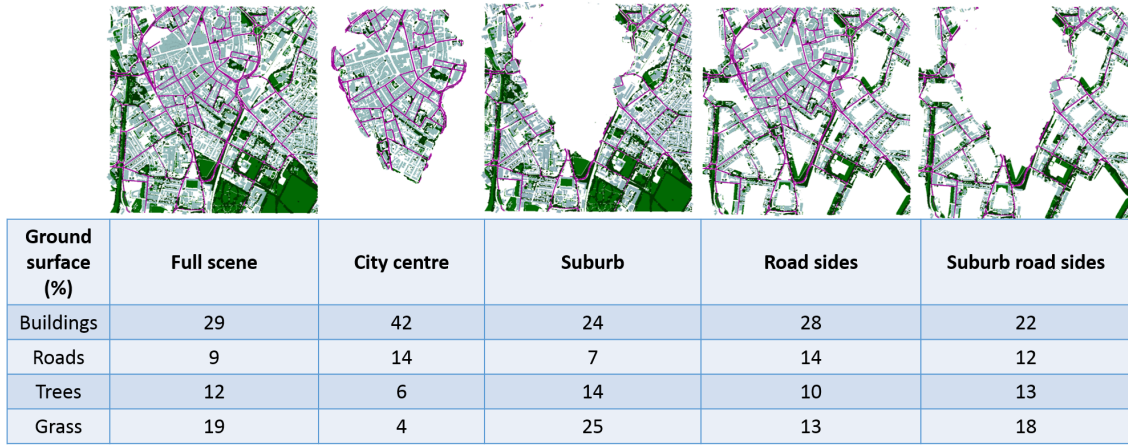


Figure 5.2: Subsets of Leicester city. These subsets were used to investigate the changes in  $\text{PM}_{2.5}$  and their relation to tree and grass ground surface fraction (%).

### 5.2.2 Deposition velocities

Scenario	Deposition velocity ( $\text{cm s}^{-1}$ )		
	Low	Average	High
1. Reference scenario: building aerodynamics	-	-	-
2. Building aerodynamics and deposition	-	$3.6 \times 10^{-3}$ (Roupsard et al., 2013)	-
3. Tree aerodynamics	-	-	-
4. Tree aerodynamics and deposition	0.02 (Peters and Eiden, 1992)	0.64 (Pugh et al., 2012)	30 (White and Turner, 1970)
5. Grass deposition	0.01 (Horbert et al., 1976)	0.64 (Pugh et al., 2012)	8 (Harrison et al., 1996)

Table 5.1: Set of modelled scenarios and associated deposition velocities.

### 5.3 Experimental

---

The model was enhanced with additional sink terms which take into account the deposition of  $PM_{2.5}$  on trees, grass and buildings using the same implementation method as Vranckx et al. (2015). The range of dry deposition velocities in the literature are very wide, as dry deposition velocities are highly dependent on the vegetation species and particle diameters (size distribution). As a single average deposition velocity would not be representative, the simulations were bounded by the lowest and highest published deposition (Litschke and Kuttler, 2008). For trees, the deposition velocities range from  $0.02 \text{ cm s}^{-1}$  for species such as Picea (Peters and Eiden, 1992) and Ficus (Freer-Smith et al., 2004) to  $30 \text{ cm s}^{-1}$  for the common Hazel (White and Turner, 1970). For grass, the dry deposition velocities range from  $0.01 \text{ cm s}^{-1}$  (Horbert et al., 1976) to  $8 \text{ cm s}^{-1}$  (Harrison et al., 1996). Although an average deposition velocity can be challenging to estimate, a conservative value of  $0.64 \text{ cm s}^{-1}$  chosen by Pugh et al. (2012) was used for trees and grass. Regarding building deposition, the dry deposition velocity of particles on cement of  $3.6 \times 10^{-3} \text{ cm s}^{-1}$  was used (Roupsard et al., 2013). The deposition inside the tree crown cells was parametrised as a sink term applied at each Eulerian step as described previously (Eq. 2.23).

Deposition on grass and buildings differ from trees as grass and buildings are represented as surfaces. The change in  $PM_{2.5}$  concentration via deposition on grass and buildings was expressed as

$$\frac{\Delta C(t)}{\Delta t} = C(t-1) \times Vd \times \frac{S}{V} (\times LAI_{grass}) \quad (5.1)$$

where  $\Delta C(t)$  is the change in particles concentration via deposition in an Eulerian forward step ( $\text{kg m}^{-3}$ ),  $C(t-1)$  is the particles concentration ( $\text{kg m}^{-3}$ ),  $S$  is the surface of grass ( $\text{m}^2$ ) and  $V$  the volume of the cells where the buildings or grass are present ( $\text{m}^3$ ). The leaf area index (LAI -  $\text{m}^2 \text{ m}^{-2}$ ) is an index used here to represent the total area of grass per meter square of ground occupied by grass. Urban grass areas have been parametrised in previous models with a LAI ranging between 1 to  $2 \text{ m}^2 \text{ m}^{-2}$  (Petroff and Zhang, 2010; Pugh et al., 2012). A LAI of  $1 \text{ m}^2 \text{ m}^{-2}$  was used for urban grass, which corresponds to the lower end range of LAI. In this chapter, no changes in aerodynamics resistance were considered for the deposition sink terms used in Eq. 2.23 and Eq. 5.1 which were kept constant across the two wind speeds of 1 and  $4.6 \text{ m s}^{-1}$ .

## 5.3 Results

### 5.3.1 Reduction by trees and grass

For a wind speed of  $4.6 \text{ m s}^{-1}$ , the aerodynamic effect of trees increases traffic-sourced concentrations in street canyons but shows a decrease in open terrain (Figure 5.3a). For a wind speed of  $1.0 \text{ m s}^{-1}$  (Figure 5.3b), no turbulent dispersion occurs under laminar conditions and trees are shown to significantly increase concentrations along the road sides. This effect occurs as trees are reducing the wind speed which then decreases the net dispersion. For deposition, trees decrease  $\text{PM}_{2.5}$  concentrations locally (close to where they are planted) and are more efficient when placed close to road sides where particle concentrations are greatest (Figure 5.3c,d). Relative changes (%) caused by deposition on trees are more important at a wind speed of  $4.6 \text{ m s}^{-1}$  and less insignificant at a wind speed of  $1 \text{ m s}^{-1}$  (see Figure 5.5, although absolute deviation in  $\mu\text{g m}^{-3}$  are likely to be more important at a wind speed of  $1 \text{ m s}^{-1}$ ). Like for deposition on trees, grass decreases  $\text{PM}_{2.5}$  concentrations locally and close to the road sides where particle concentrations are greatest (Figure 5.3e,f). Grass deposition shows similar results in terms of loss at both strong and low wind speeds. The change of  $\text{PM}_{2.5}$  by building deposition was less than 0.03% and is subsequently not detailed owing to its low impact on  $\text{PM}_{2.5}$  reduction.

#### Difference between mean and median values

The probability distribution of the changes in  $\text{PM}_{2.5}$  concentrations from Figure 5.3 are shown in Figure 5.4 to explore the reasons why differences between mean and median values were found. At a wind speed of  $4.6 \text{ m s}^{-1}$ , the mean and median values are similar (see Figures 5.4a, c & e). This can be explained by the fact that the standard deviation of the probability distribution are within the same order of magnitude that the mean values (see Figures 5.3a, c & e).

However, at a wind speed of  $1 \text{ m s}^{-1}$ , the mean and median are providing different results. For instance in Figure 5.4b, an arithmetic mean of 8% is compared to a negative median of -0.13%. A negative median means that here the tree aerodynamic dispersive effects have a beneficial impact in most point locations of the domain. A positive arithmetic mean shows that in Figure 5.4b trees are on average trapping vehicular emissions by 8% over the whole domain. An explanation for the difference can be explained by the fact that the changes in  $\text{PM}_{2.5}$  concentrations induced by trees are much larger at a wind speed of  $1 \text{ m s}^{-1}$  than at a wind speed of  $4.6 \text{ m s}^{-1}$ . The

low wind speed conditions exacerbates the tree effects leading to extremely large changes in  $\text{PM}_{2.5}$  concentrations. The larger spread in changes of concentrations causes then the standard deviation to be almost an order of magnitude greater than the mean values (see Figures 5.3b, d & f), which explains the difference between mean and median values.

The model results in Figure 5.5 show that the aerodynamic effects of trees prevails over the tree and grass deposition. Although the dispersive effects can appear important, similar results are found in the literature with a 12% increase in concentration for winds perpendicular to the street canyon and a 16% decrease for parallel winds (Amorim et al., 2013a). Other studies measured an overall reduction in black carbon concentration by 12% downwind of trees by combining dispersion and deposition, which is comparable to the results presented in Figure 5.5 (Brantley et al., 2014). In Figure 5.5, the model estimation of deposition on trees and grass depositions is shown to be highly dependent on the choice of the deposition velocities (see Table 5.1). For a wind speed of  $4.6 \text{ m s}^{-1}$ , observed depositions was greater for trees, (with a reduction of 2.5%) than for grass, (with a reduction of 0.8%), over the full scene. The aerodynamic dispersion induced by trees reduces  $\text{PM}_{2.5}$  concentrations by 11% over the full scene and up to 14% for the suburbs where the tree population is larger. This result is consistent with our previous work, where trees promote air turbulence which has a regional beneficial impact (Jeanjean et al., 2015) with the addition that trees increase the probability of particle deposition significantly more than on shorter vegetation like grass (Chen et al., 2016). For a wind speed of  $1 \text{ m s}^{-1}$ , trees were found to increase  $\text{PM}_{2.5}$  concentrations by 8% over the full scene. In the model settings, a wind speed of  $1 \text{ m s}^{-1}$  is considered laminar and therefore no turbulent dispersion occurs which explains why trees trap traffic emissions at pedestrian height as they decrease the wind flow (Jeanjean et al., 2015). Deposition on trees was negligible (less than 1%) over the full scene whereas deposition on grass was greater (1.7%). The model error was smaller for a wind speed of  $1 \text{ m s}^{-1}$ , which suggests that uncertainties in the model increase as the wind speed increases.

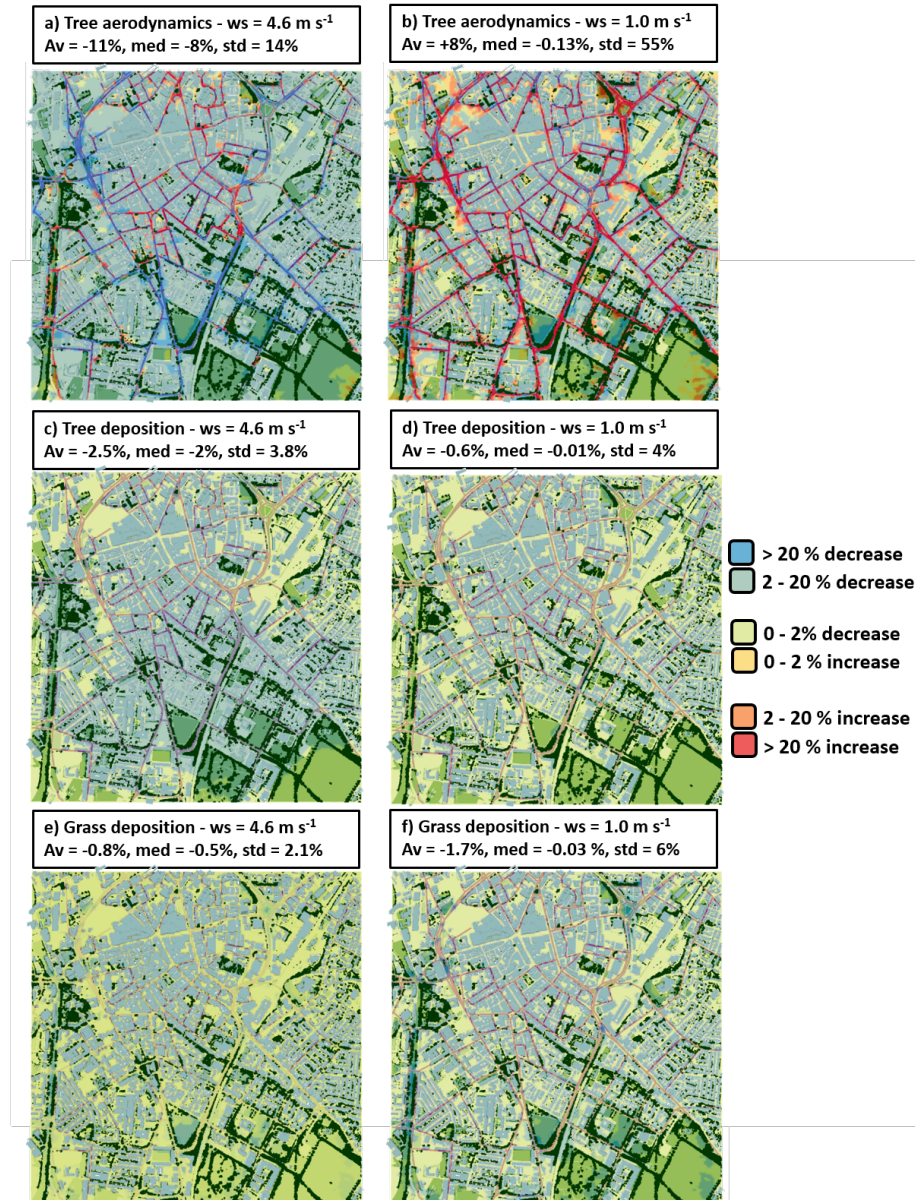


Figure 5.3: Modelling output of the spatial change of  $\text{PM}_{2.5}$  concentrations emitted from road sides at a height of 1.5 m. Tree aerodynamic effects for (a) a wind speed of  $4.6 \text{ m s}^{-1}$  and (b)  $1.0 \text{ m s}^{-1}$ . Tree deposition (aerodynamic effects of trees removed) calculated for an average deposition velocity of  $V_d = 0.64 \text{ cm s}^{-1}$  for (c) a wind speed of  $4.6 \text{ m s}^{-1}$  and (d)  $1.0 \text{ m s}^{-1}$ . Grass deposition calculated for an average deposition velocity of  $V_d = 0.64 \text{ cm s}^{-1}$  for (e) a wind speed of  $4.6 \text{ m s}^{-1}$  and (f)  $1.0 \text{ m s}^{-1}$ . Av is defined as average, med as median and std as standard deviation.

### 5.3.2 Generalisation between PM reduction and vegetation cover

#### Tree cover and $\text{PM}_{2.5}$ reduction

The data in Figure 5.6 suggest that a linear relation can be approximated between the tree ground surface fraction (%) and the  $\text{PM}_{2.5}$  reduction. By combining linear

### 5.3 Results

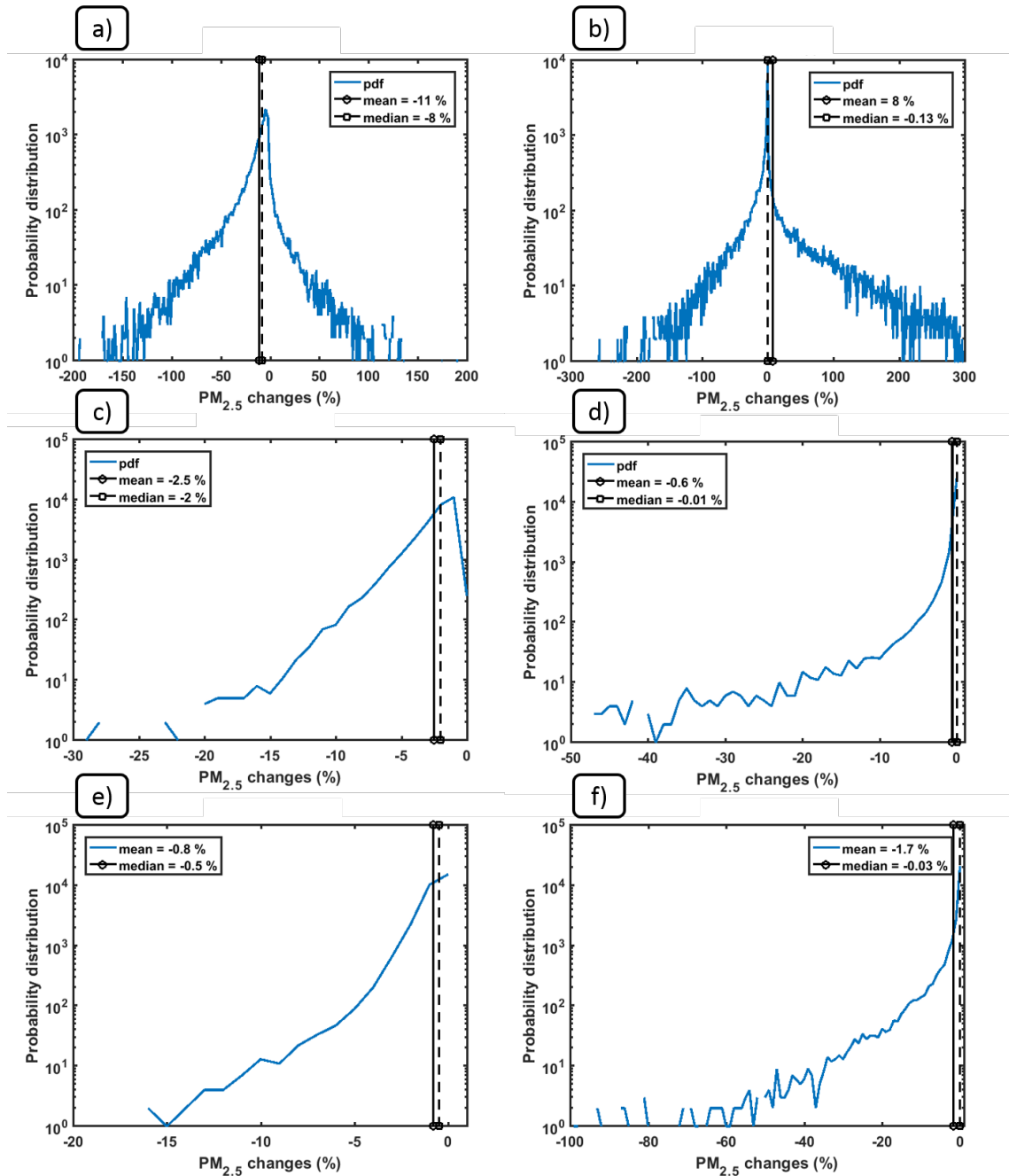


Figure 5.4: Probability distribution of the spatial change of PM<sub>2.5</sub> concentrations emitted from road sides at a height of 1.5 m (results from Figure 5.3). Tree aerodynamic effects for (a) a wind speed of 4.6 m s<sup>-1</sup> and (b) 1.0 m s<sup>-1</sup>. Tree deposition (aerodynamic effects of trees removed) calculated for an average deposition velocity of  $V_d = 0.64$  cm s<sup>-1</sup> for (c) a wind speed of 4.6 m s<sup>-1</sup> and (d) 1.0 m s<sup>-1</sup>. Grass deposition calculated for an average deposition velocity of  $V_d = 0.64$  cm s<sup>-1</sup> for (e) a wind speed of 4.6 m s<sup>-1</sup> and (f) 1.0 m s<sup>-1</sup>.

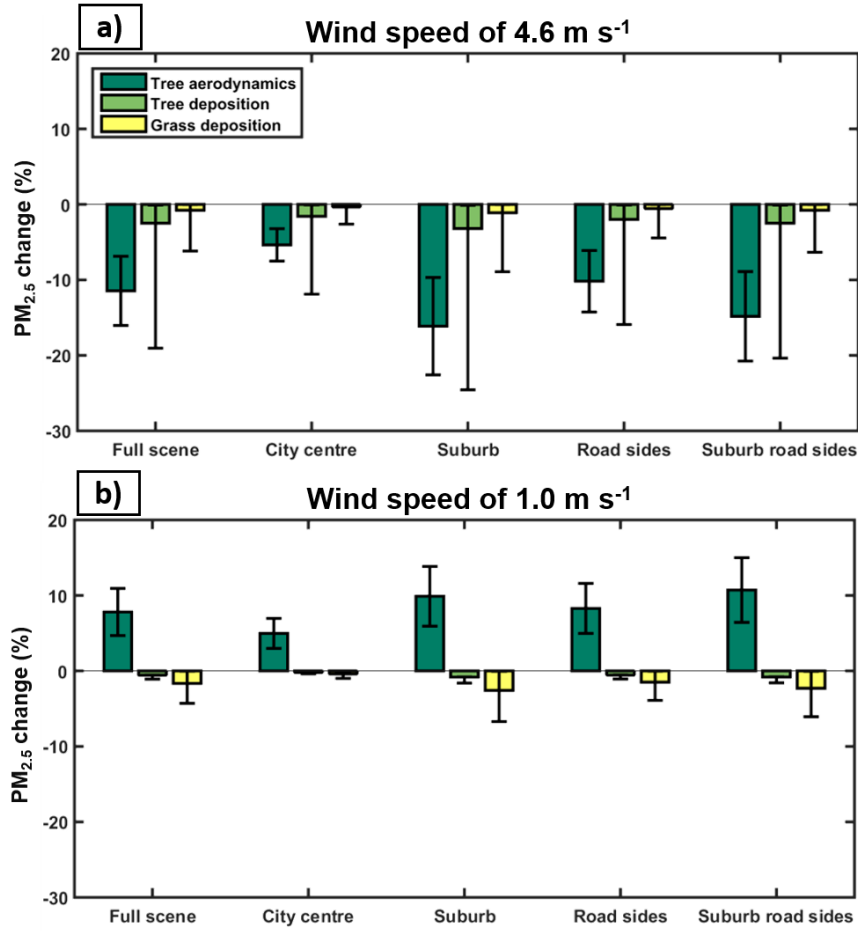


Figure 5.5: Modelled averaged change in traffic-emitted  $PM_{2.5}$  concentrations induced by the tree aerodynamics, tree deposition and grass deposition for (a) a wind speed of  $4.6 \text{ m s}^{-1}$  and (b) a wind speed of  $1.0 \text{ m s}^{-1}$  (Note that grass is a consistent deposition sink).

coefficients, an equation was formed to predict what the reduction in  $PM_{2.5}$  would be, depending on the tree ground surface cover, such that

$$\Delta PM_{2.5}(\%) = X (K_{t_1} + K_{t_2} (V_{dtrees})^\alpha)$$

$$\begin{aligned} \text{Changes in } PM_{2.5} \text{ caused by trees } (\%) &= \text{Ground fraction of trees } (\%) \times \\ &(\text{Aerodynamic coefficient} + \text{Deposition loss coefficient} \times \\ &(\text{deposition velocity})^\alpha) \end{aligned} \quad (5.2)$$

where  $X$  is the tree ground surface cover (%),  $K_{t_1}$  is the aerodynamic coefficient,

### 5.3 Results

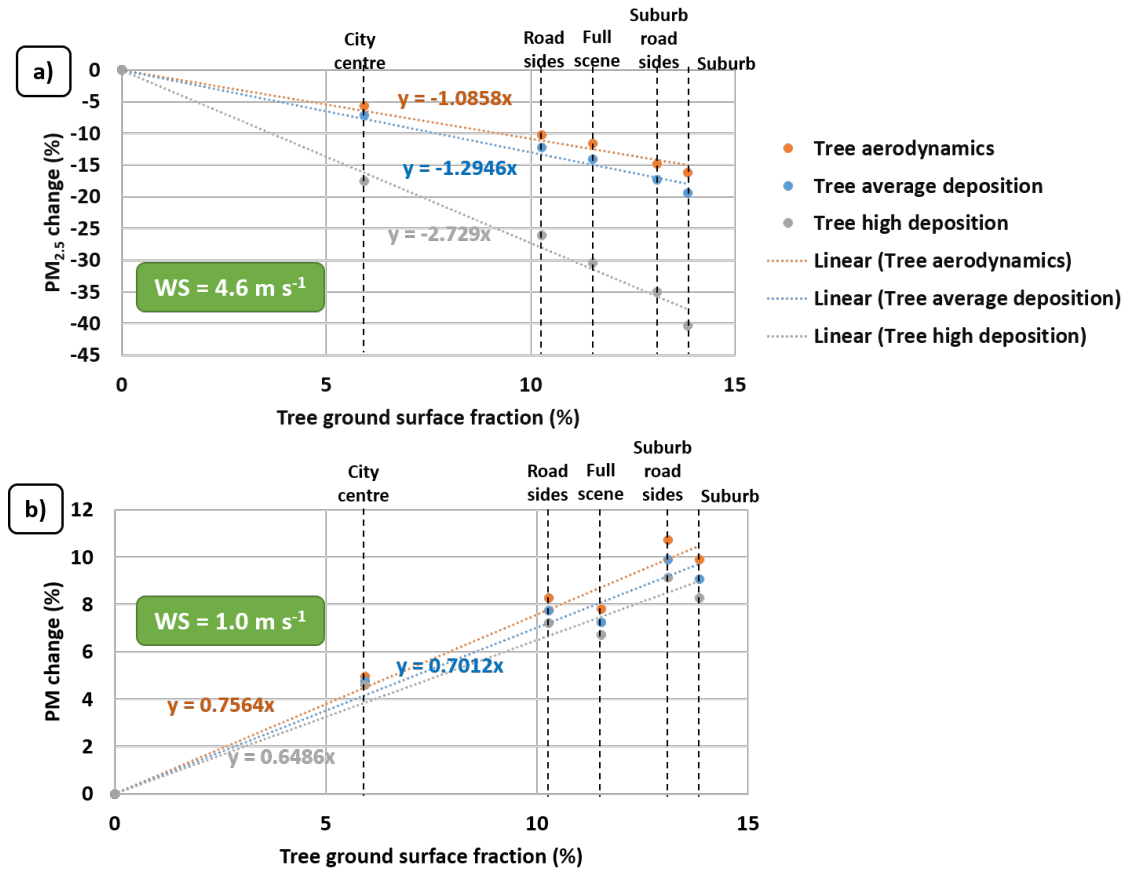


Figure 5.6: Relation between the tree ground surface fraction (%) and the  $\text{PM}_{2.5}$  reduction with the associated first order linear regression coefficients. The tree aerodynamics were included for the tree average ( $V_d = 0.64 \text{ cm s}^{-1}$ ) and high deposition ( $V_d = 30 \text{ cm s}^{-1}$ ) calculation (see choice of  $V_d$  in Table 5.1). The different spatial subsets of Leicester city are detailed in Figure 5.2.

$K_{t_2}$  is the deposition coefficient,  $V_{d_{trees}}$  is the tree deposition velocity and  $\alpha$  is a power law coefficient. Derived coefficients from this work are summarised in Table 5.2 and their comparison against initial CFD modelling results are shown in Figure 5.8. The use of the arithmetic mean is well spread in the literature to measure change in concentrations difference caused by the effects of trees or vegetation on air pollution concentrations (e.g. Gromke and Blocken 2015a; Amorim et al. 2013a; Santiago et al. 2016) and the use of median is less common. The linear regression coefficients were therefore derived based on the arithmetic mean and not median. It is interesting to note the nature of these linear relationships given the spatial inhomogeneity in any given sub-class of the city. It seems to suggest a level of robustness for predicting city-wide effects from simple models.

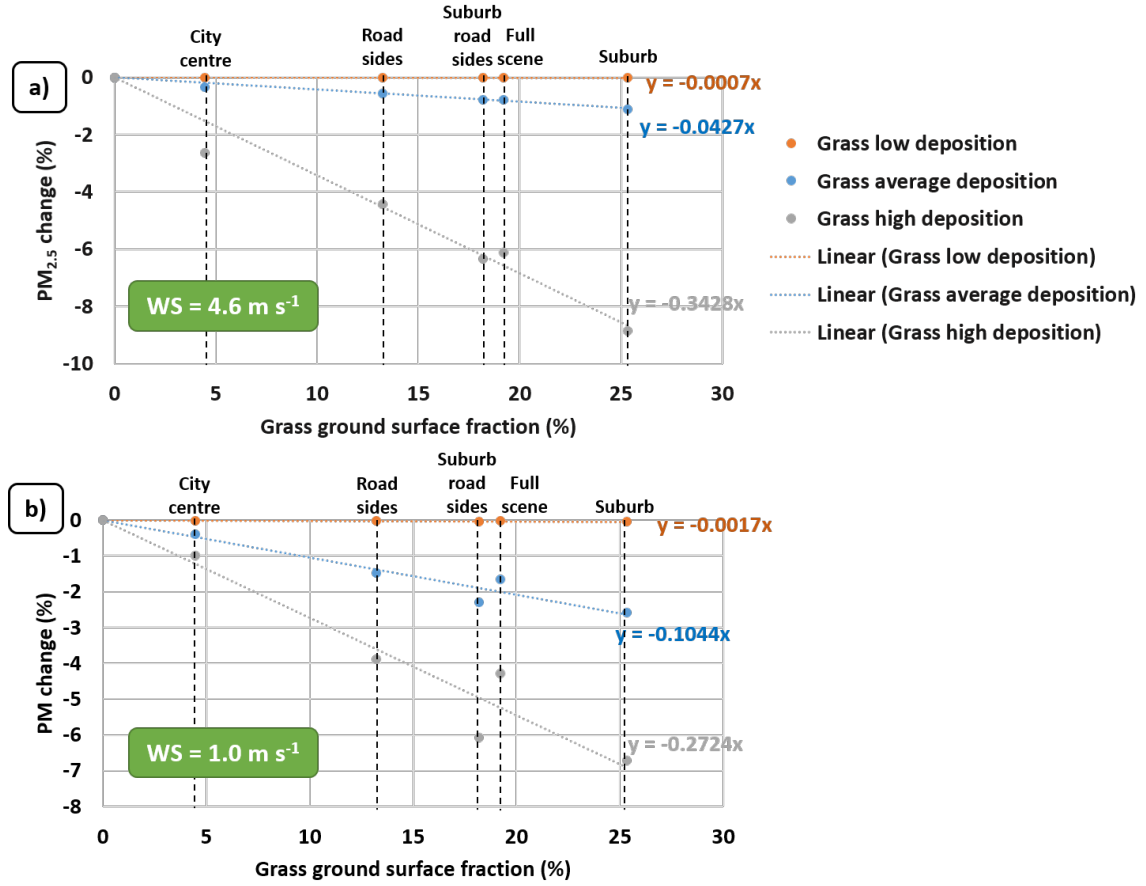
Grass cover and  $PM_{2.5}$  reduction

Figure 5.7: Relation between the grass ground surface fraction (%) and the  $PM_{2.5}$  reduction with the associated first order linear regression coefficients. The  $PM_{2.5}$  deposition on grass were calculated for low ( $0.01 \text{ cm s}^{-1}$ ), average ( $0.64 \text{ cm s}^{-1}$ ) and high ( $8 \text{ cm s}^{-1}$ ) deposition velocities. The different spatial subsets of Leicester city are detailed in Figure 5.2.

As with the case of trees, a similar linear relation can be approximated between the grass ground surface fraction (%) and the  $PM_{2.5}$  reduction (see Figure 5.7). By combining these linear coefficients, an equation was built to predict what the reduction in  $PM_{2.5}$  would be, depending on the grass ground surface cover, such that

$$\Delta PM_{2.5}(\%) = K_g X V_{d_{grass}} \quad (5.3)$$

where  $X$  is the grass ground surface cover (%),  $K_g$  is the aerodynamic coefficient,  $K_{t_2}$  is the deposition coefficient,  $V_{d_{grass}}$  is the grass deposition velocity and  $\alpha$  is a

power law coefficient. Derived coefficients are summarised in Table 5.2. In contrast to the relationship for tree (Eq. 5.2), the data in Figure 5.7 suggest a greater effect of spatial inhomogeneity particular at higher deposition velocities.

Wind speed (m s <sup>-1</sup> )	K <sub>t<sub>1</sub></sub>	K <sub>t<sub>2</sub></sub>	α	K <sub>g</sub>
4.6	-1.09	-3.12	0.53	-4.2
1.0	0.76	-0.13	0.16	-6.3

Table 5.2: Coefficients of PM<sub>2.5</sub> reduction at different wind speeds expressed in Eq. 5.2 and Eq. 5.3.

### Tree and grass relations evaluation against initial model results

Figure 5.8 shows a comparison of the predicted reduction of PM<sub>2.5</sub> by trees or grass using the simple linear representations (Eq. 5.2 and Eq. 5.3) against the full CFD results (see Figure 5.5), plotted across a range of ground surface fractions and deposition velocities.

The linear relations (Eq. 5.2 and Eq. 5.3) are based on the following assumptions. Each tree has been modelled as the average of the tree population of Leicester (Jeanjean et al., 2015). The dispersive effects of trees was calculated with a zero background concentration of PM<sub>2.5</sub> (road emissions were the only source). Eq. 5.2 and Eq. 5.3 are dependent on the wind speed and they have been derived at only two wind speeds of 4.6 and 1.0 m s<sup>-1</sup>. At this stage, applying the relationship to other wind speeds would require re-running a large set of simulations. The coefficients were also calculated for ground surface fraction of vegetation, going up to 25% for grass and 15% for trees. For vegetation cover greater than these, the proposed relation has not been verified but may be a topic for further research. Exploring the applicability of these relations on other cities is also something that could be considered for future work. For example, it was shown that deposition on trees is of minor importance in Northern countries owing to the short time of the leaf season, which would change the relations coefficients (Setälä et al., 2013).

### 5.3.3 Wind speed dependence

Owing to the very high computational resources needed to run the CFD model over different wind speeds, only two wind speeds were performed in this chapter.

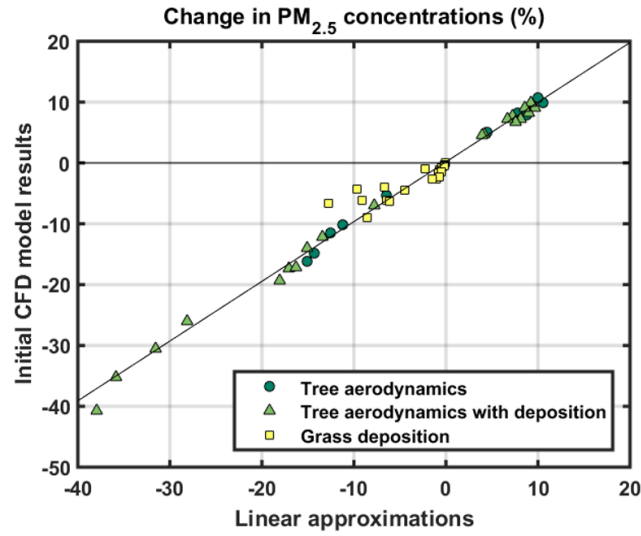


Figure 5.8: Comparison of change in  $\text{PM}_{2.5}$  concentrations (%) between the initial CFD model results (expressed in Figure 5.5) at pedestrian height and estimated changes through two linear relations (Eq. 5.2 and Eq. 5.3) based on trees and grass ground surface fraction (%). The aerodynamics of trees were added into the tree deposition calculation. 24 CFD cases (12 wind directions at two wind speeds) are compared to derived the relations.

Wind speed ( $\text{m s}^{-1}$ )	1	2	3	4	5
$K_{t1}$	0.76	0.25	-0.27	-0.78	-1.30
$K_{t2}$	-0.13	-0.96	-1.8	-2.6	-3.5
$\alpha$	0.16	0.27	0.37	0.47	0.57
$K_g$	-6.3	-5.7	-5.1	-4.6	-4.0

Table 5.3: Coefficients of the  $\text{PM}_{2.5}$  reduction relations linearly interpolated from Table 5.2 between the wind speeds of 1 and  $4.6 \text{ m s}^{-1}$ .

Although a crude simplification, it was supposed that the change observed with wind speed is linear between the two wind speeds of 1 and  $4.6 \text{ m s}^{-1}$ . Therefore the initial coefficients from Table 5.2 were linearly interpolated (see Table 5.3). Using the previous relations (Eq. 5.2 and Eq. 5.3), the change of wind speed on the tree and grass deposition was investigated. From these estimations, Figure 5.9a) shows that trees start to be beneficial for a wind speed of  $2.5 \text{ m s}^{-1}$  when considering the tree aerodynamics and  $2.0 \text{ m s}^{-1}$  when considering both the tree aerodynamics and deposition. As seen previously, the  $\text{PM}_{2.5}$  deposition on grass has much less impact on  $\text{PM}_{2.5}$  concentrations than trees. Although it needs more CFD simulations at different wind speeds to be confirmed, it appears in Figure 5.9b) that the ideal wind

### 5.3 Results

speed for the deposition on tree is  $3 \text{ m s}^{-1}$ . This could be understood as at low wind speed ( $1 \text{ m s}^{-1}$ ), not enough flux of pollutant is brought to the tree and at high wind speed the flux of pollutant passes quickly inside the tree and settle less.

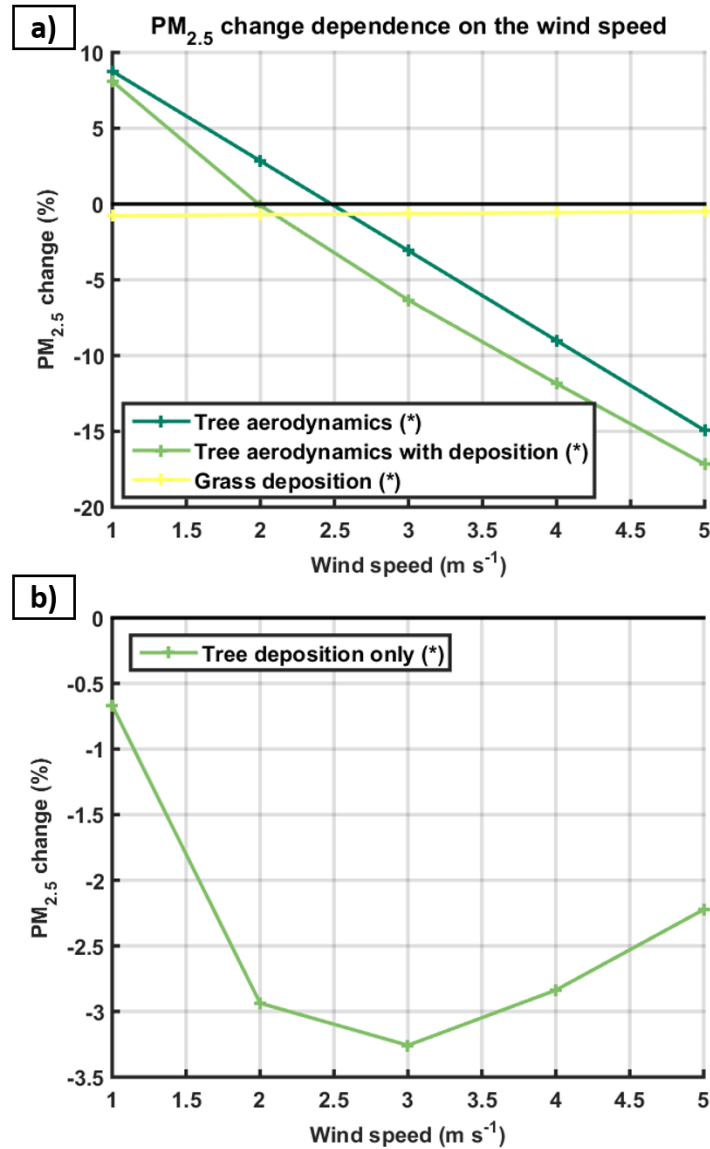


Figure 5.9:  $\text{PM}_{2.5}$  change dependence on the wind speed over Leicester City. (a) Tree aerodynamics, tree aerodynamics with deposition and grass deposition dependence on the wind speed (b) Tree deposition dependence on the wind speed (\*)  $\text{PM}_{2.5}$  estimated from linear relations (Eq. 5.2 and Eq. 5.3) with a linear interpolation between the two reference wind speeds of  $1$  and  $4.6 \text{ m s}^{-1}$ .

### 5.3.4 Net flux of trees and grass in the summer season over Leicester

In this chapter, the seasonality of spring and autumn was not investigated, as it requires further modelling of tree profiles with growing or falling leaves. The tree profile used here corresponds to tree with fully grown leaves mainly present during the summer season in England (21<sup>st</sup> June to 21<sup>st</sup> September). The net flux of trees and grass in the summer season over Leicester was estimated using half hourly wind measurement from the East Midlands Airport weather station, located 30 km North of Leicester City. From these measurements, the average wind speed in Leicester City was  $4.0 \text{ m s}^{-1}$  during the summer 2014. Based on these assumptions, the average net flux of tree and grass on  $\text{PM}_{2.5}$  concentration emitted by traffic was estimated to be a 9.0% reduction from the tree aerodynamics, 2.8% reduction from the deposition on trees and 0.6% reduction from the deposition on grass.

Local measurements of urban background concentrations of  $\text{PM}_{2.5}$  in 2014 in Leicester City as part of the Automatic Urban and Rural Network (AURN) monitored by the UK Department for Environment, Food and Rural Affairs (DEFRA, 2014a) had an average concentration of  $13.3 \mu\text{g m}^{-3}$ . Using this average leads to an overall deposition of  $\text{PM}_{2.5}$  of  $11.8 \text{ t year}^{-1}$  ( $2.9 \text{ t year}^{-1} \text{ km}^{-2}$ ) on trees and  $2.5 \text{ t year}^{-1}$  ( $0.6 \text{ t year}^{-1} \text{ km}^{-2}$ ) on grass.

A previous study looking at the same scene over Leicester concluding that tree were reducing road traffic emissions by 7% at a wind speed of  $4.6 \text{ m s}^{-1}$  (Jeanjean et al., 2015). In this present study, a reduction of 11.5% was found (see Figure 5.9a)). The main difference from the previous study mainly resides in the difference of surface roughness which was altered by the introduction of grass, treated here as a smoother surface than in the previous model set-up. This shows that results from CFD modelling studies shall be treated with caution as they are highly dependent on the boundary conditions and are limited by their modelling accuracy (being here 40%).

## 5.4 Discussion and links with previous studies

### 5.4.1 Comparison with the i-Tree model

To compare the decrease in particulate matter concentrations by deposition on trees, the model results were then compared with values calculated under the UFORE

model (i-Tree dry deposition module) (Escobedo and Nowak, 2009). The UFORE model has been used across a wide ranges of studies to characterise the impact of trees on  $\text{PM}_{10}$  deposition (e.g. (Nowak et al., 2006; Tallis et al., 2011; Baumgardner et al., 2012)) and  $\text{PM}_{2.5}$  deposition (Nowak et al., 2013). In the UFORE model, the reduction in particulate matter concentrations is calculated over the whole boundary layer. The results in Figure 5.10 show the changes in  $\text{PM}_{2.5}$  provided by the CFD model at a wind speed of  $4.6 \text{ m s}^{-1}$ . Although the Earth boundary layer height is typically 1 to 2 km (Seidel et al., 2010; Garratt, 1994), the maximum height of the simulation domain used here was 500 m as the main focus of the study was the dispersion and deposition of road traffic emissions. When averaging across the whole height, a reduction of 0.25% was found for the deposition on trees and 0.03% for grass averaged across the whole domain height. The estimated removal of  $\text{PM}_{2.5}$  by deposition on trees is in the same order of magnitude than provided by Nowak et al. (2013), where the average improvement of air quality by urban trees was reported to range between 0.05% to 0.24% across 10 major US cities. It is worth noting that comparing to steady state CFD model, the UFORE model integrates more temporal variation such as meteorology (changes in wind speed, direction, boundary layer) and measurements of  $\text{PM}_{2.5}$  concentrations over time. Nonetheless, CFD simulations have the ability to provide spatial information to see where particulate matter concentrations are decreased. In Figure 5.10, it can be seen that tree and grass have the greatest effect close to the ground and that there effects decrease with height. This suggests that trees have a lot more effects locally than on a larger scale. This finding agrees with recent empirical studies that have empirically demonstrated a reduction in PM close to green spaces (e.g. Irga et al. 2015).

### 5.4.2 Urban tree management

One of the main question arising from this work is how trees can best be used for air quality improvement, combining both their aerodynamic and deposition effects. A suggestion coming from this modelling work is that in this case study, for average wind speeds greater than  $2 \text{ m s}^{-1}$  the more trees the better for both aerodynamic dispersion and deposition of  $\text{PM}_{2.5}$  in an urban environment. It is important to note that the maximum tree cover used here was 20%, findings could be altered for greater tree cover. As aerodynamic effects are the most important, trees species that are planted in urban environment shall not only be chosen based on their deposition

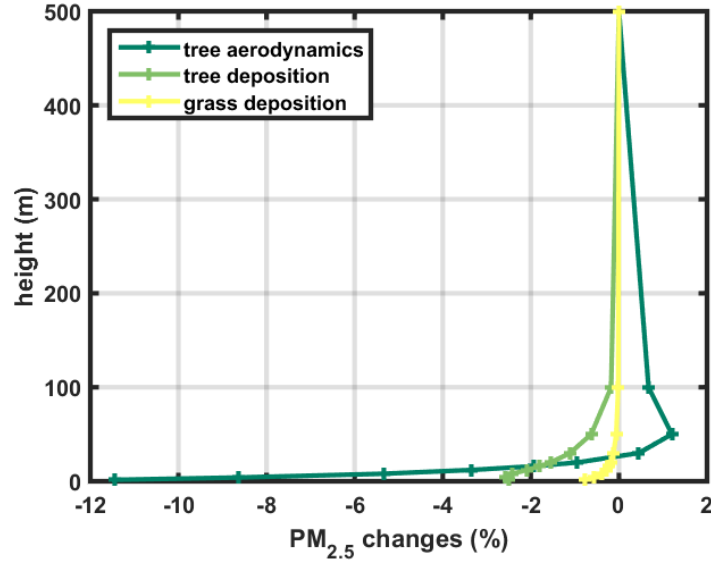


Figure 5.10: CFD results of changes in  $\text{PM}_{2.5}$  across the whole height of the simulation domain for a wind speed of  $4.6 \text{ m s}^{-1}$ . All relative reductions (%) were calculated using the average ground concentrations of the reference scenario (see Table 5.1) as denominator.

capability. Trees species with high LAD and high deposition are the best to enhance deposition but they shall at the same time favour aerodynamic dispersion. For cities with low average wind speeds (less than  $2 \text{ m s}^{-1}$ ), trees were shown to increase  $\text{PM}_{2.5}$  concentrations. In this special cases tree species shall be chosen to decrease as little as possible the wind speed to avoid trapping pollution. As shown by Tiwary et al. (2009), it was found that trees have more abilities to decrease particulate matter concentrations than grass.

Another question arising is where shall trees be planted in cities. Although street canyon trees would be the most effective for particulate matter deposition as exposed to greater concentrations (Tallis et al., 2011), previous studies have shown that the aerodynamic effect of trees would end up trapping road emissions in this situation (Gromke et al., 2008; Buccolieri et al., 2011; Wania et al., 2012). However, most of these studies have looked at perpendicular wind directions which exacerbates tree trapping effects in street canyons. Amorim et al. (2013a) found that for perpendicular wind directions trees are actually beneficial. The present study results suggest that street canyon trees could actually be beneficial, depending on the prevailing wind direction, wind speed, street canyon and surrounding building geometries.

## 5.5 Conclusion

The model results show that there is a direct relationship between changes in  $\text{PM}_{2.5}$  concentration and the trees and grass ground surface cover. This suggests that there is level of geometry independence combining buildings and trees that is dominated by the aerodynamics of trees. In terms of urban planning, the linear relationship observed (Eq. 5.2 and Eq. 5.3) provides a tool to monitor the effectiveness of green infrastructure on the local scale, at pedestrian height. Although only computed for 2 wind speeds, the aerodynamic effects of trees show that dispersion appears to be more important than deposition. Working on removing street pollution via dispersion will prove to be as or even more efficient than deposition technologies.

In Leicester City Centre, the overall global decrease in particle concentrations when considering trees and grass deposition together, is very limited, with 2.8% reduction from the deposition on trees and 0.6% reduction from the deposition on grass. The aerodynamics effect has a much stronger effect, owing a 9.0% reduction during summer time in Leicester City. Results found in this chapter suggest that reducing the road emissions by 10%, equivalent to one vehicle in 10, will have the same effect as all the combined green infrastructure in Leicester City Centre. Regarding the decrease of background particles (non-road emissions, which is not studied here), the literature shows as well that the deposition on vegetation is limited to less than a few percent decrease (Tallis et al., 2011; Beckett et al., 1998; Nowak et al., 2006).

Green infrastructures are beneficial but they do not represent a solution to completely remove air pollution from cities. The tree and grass species of a city could lead to very different reduction in  $\text{PM}_{2.5}$  from a few percent to almost 20% as suggested by the results. These reductions would only occur during the leaf-period (non-winter period), although for a temperate city like Leicester some trees and hedges are evergreen. It is clear that green infrastructure has a role to play at a city scale but only when co-ordinated with understanding of local implementation and traffic planning.

Because of the steady flow produced by the CFD model, it shall be noted that time dependent effects such as fluctuations in wind speed or direction, solar heating or chemical reactions were not reproduced by the simulations.

## Chapter 6

# Ranking current and prospective NO<sub>2</sub> mitigation strategies: a modelling investigation in Oxford Street, London

*Dr John Gallagher (Bangor University, UK) has produced the life-cycle analysis used in this Chapter which is currently under review in Environmental Pollution.*

### 6.1 Introduction

Road traffic emissions are the largest contributors of NO<sub>x</sub> emissions in the urban environment (Mattai et al., 2008). They account for 40% of the total European NO<sub>x</sub> emissions (Sundvor et al., 2012) and contribute between 47% and 53% of emissions in London (TFL, 2012; Mattai et al., 2008). Epidemiological studies have provided evidence of the adverse health effects of outdoor air pollution (WHO, 2013), linking it to various cardiovascular and respiratory hospital admissions in London (Samoli et al., 2016). The specified European directives on NO<sub>2</sub> concentrations give a limit value with an annual mean value of 40 µg m<sup>-3</sup> and an hourly value of 200 µg m<sup>-3</sup> with 18 permitted exceedances each year. However, these limit values are regularly exceeded throughout Europe (Guerreiro et al., 2012) and in London the hourly limit value was exceeded 60 times in the Marylebone area in 2013 (DEFRA, 2015). Personal exposure to NO<sub>2</sub> pollution in London is greatest at peak traffic times, which typically coincides with peak pedestrian and cyclist commuter times (Kaur

et al., 2007). Therefore, mitigating air pollution to reduce personal exposure for urban populations is an important consideration for authorities.

A number of pollution mitigation strategies exist to control air pollution in the urban environment. McNabola et al. (2013) defines these options as; (i) controlling the quantity of pollution (g) which can be achieved with congestion charging (Kelly et al., 2011), (ii) controlling the emission intensity ( $\text{g km}^{-1}$ ) which can be achieved with carbon tax (Galinato and Yoder, 2010) and (iii) controlling source-receptor pathways ( $\text{kg m}^{-3}$ ) which can be achieved with passive control measures (McNabola, 2010). Each control mechanism provides its own benefits and challenges with respect to improving air quality in the urban environment.

Focusing on controlling source-receptor pathways in the urban environment, current techniques for reducing  $\text{NO}_2$  rely on improving the aerodynamic dispersion of  $\text{NO}_2$  (Jeanjean et al., 2015, 2016), depositing  $\text{NO}_2$  on a surface or a combination of these two methods (Morakinyo and Lam, 2016; Janhäll, 2015).

The focus of this chapter is to compare different  $\text{NO}_2$  mitigation strategies which promote dispersion and deposition in the urban environment. A number of street canyon modelling studies have previously been performed, but there are limited findings that directly compare the impact of these dispersion and deposition strategies under the same conditions. The different mitigation strategies examined include trees, photocatalytic paint and the introduction of solid barriers, as investigated in the case of Oxford Street in London (UK), a real street canyon. The performance of each strategy will be evaluated and ranked based on its impact on improving air quality and associated life cycle costs of implementation and maintenance. Furthermore, how pollutant concentrations are affected at both child and adult exposure heights is explored, and a final focused assessment for improving air quality in hotspot zones is undertaken.

## 6.2 Methods

### 6.2.1 Case study: Oxford Street, London

Oxford Street is located in central London within the City of Westminster which extends between the two tube stations of Oxford Circus Station and the Marble Arch Station (see Figure 6.1). Oxford St, with numerous shopping centres and food-halls is one of the busiest street in central London.

### Street layout

Buildings data were taken from Ordnance Survey which is the UK governmental mapping agency. The average building height for the modelled scene was calculated to be 15 m and ranked between a few meters up to 59 m. Oxford Street length is 1.2 km and its width was estimated to be 20 m, giving an average width over height ratio (W/H) of 1.33, which corresponds to a deep street canyon configuration (Oke, 1988) and makes it an ideal street canyon location to model different techniques to mitigate NO<sub>2</sub> levels. The National Tree Map<sup>TM</sup> (NTM) Crown Polygon produced by Bluesky Ltd was used to represent individual trees or closely grouped tree crowns. Trees and bushes over 3 m in height were included in the database. An overview of the study area with trees can be seen in Figure 6.1. The NTM<sup>TM</sup> provided a canopy top height but did not provide the canopy base height. It is worth noting that limitations in current literature have necessitated the use of an assumed canopy base height of 1/3 of the canopy depth which is the same assumption as used in other studies (Gromke et al., 2008).

### NO<sub>x</sub> emission

The traffic volume of taxi and bus is important with more than 10 buses routes running along Oxford St. According to the automatic traffic counts provided by the UK Department for Transport (DFT, 2016), in 2014 more than 5000 buses travel daily through Oxford St and more than 6000 taxis. Using the daily average traffic counts, an average NO<sub>2</sub> road emissions of 60 µg m<sup>-1</sup> s<sup>-1</sup> was estimated using the Emissions Factors Toolkit (EFT) from the Department for Environment, Food & Rural Affairs (DEFRA, 2016). No background concentrations of NO<sub>2</sub> were modelled as the focus of this chapter is the mitigation of traffic emissions within the street canyon.

### Local meteorological conditions

In order to integrate local meteorological conditions, wind data from central London (London City airport) was used to determine the prevailing wind directions and the yearly average wind speed for London. London City airport is located closely to Central London, being less than 15 km away from Oxford Street. To take into account the spread in wind directions, 8 wind directions were simulated for each scenario at the average wind speed of 4.3 m s<sup>-1</sup> and weighted according to their

## 6.3 Modelled area dimensions

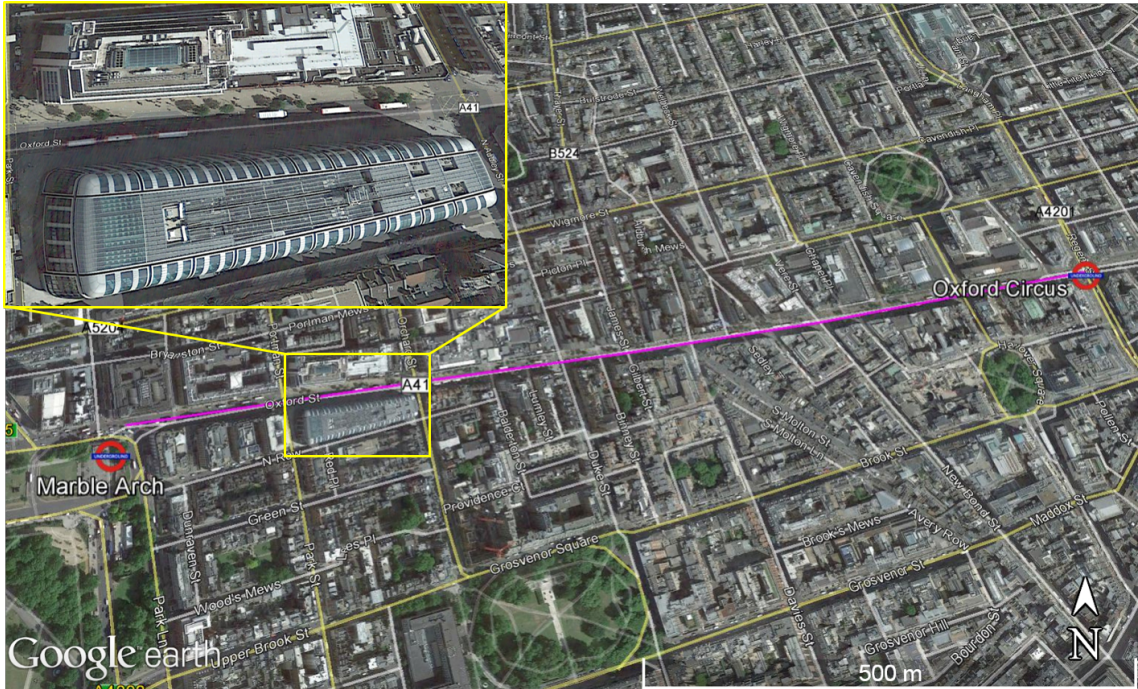


Figure 6.1: View from Google Earth of the area of interest corresponds to Oxford Street within the City of Westminster in London (UK). The modelled area extend on 1.2 km between the Marble Arch and Oxford Circus.

probability (see Figure 3.2). The wind data were recorded every 30 minutes.

### 6.2.2 CFD modelling

#### Computational grid

Best practice guidelines were followed to build the computational domain (Franke et al., 2007). The maximum reported height in the domain is a building height ( $H$ ) of 59 m. The computational domain was built with its boundaries placed more than  $15 H$  away from the modelled area (Figure 6.3).

## 6.3 Modelled area dimensions

The top of the computational domain was set to 500 m, which corresponds to  $7.5 H$  above the highest building. A maximum expansion ratio between two consecutive cells was kept below 1.3. With an average building heights of 15 m across the modelled area, the overall blocking ratio was kept below 1.2% inclination and is therefore below the 3% recommended threshold. A hexahedral mesh of 3 million

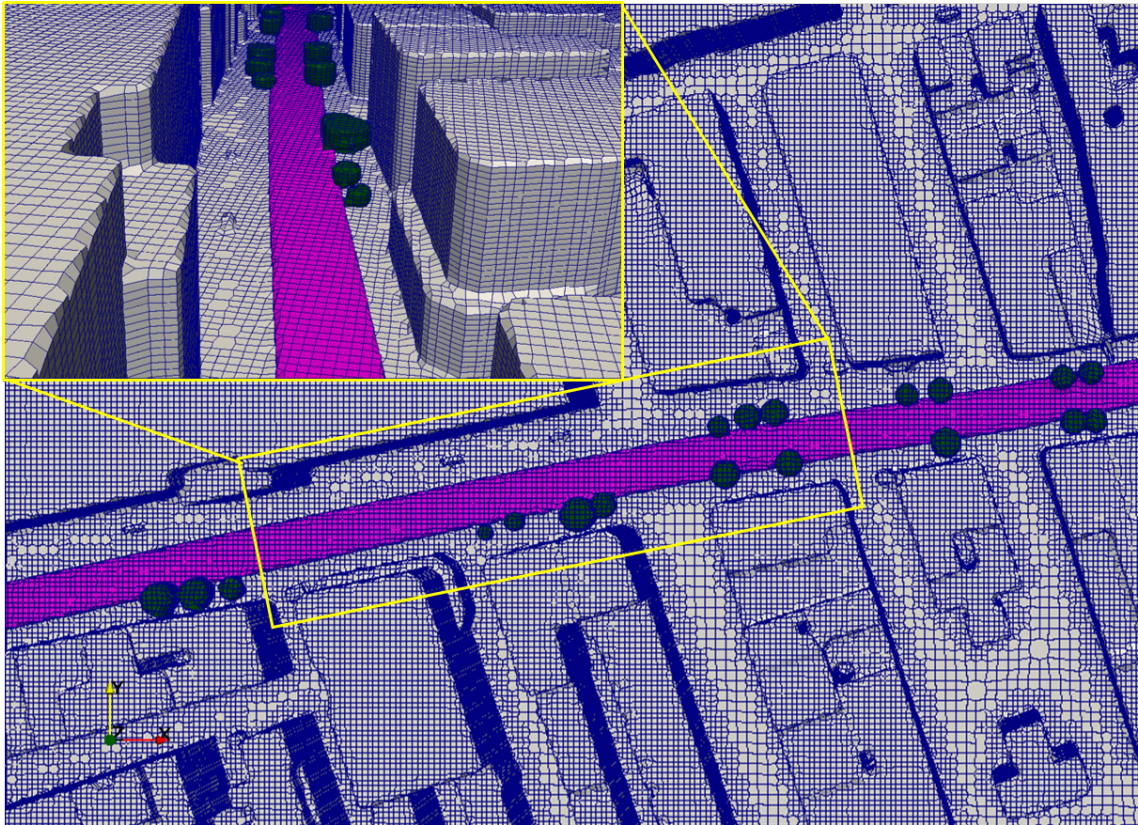


Figure 6.2: Mesh used to carry out the CFD simulations which contains 3 million cells. A maximum resolution of 1.0 m was used across the X and Y axis and 0.5 m along the Z axis.

cells was used. A mesh resolution of 0.5 m in the vertical direction close to the bottom of the computational domain was chosen ( $< 1$  m) to ensure proper flow modelling at pedestrian height (Blocken, 2015). A cell size of 1.2 m along the X and Y axis was applied for the buildings, trees and roads. This resolution allows more than 10 cells to be present across the main street canyon to ensure proper flow modelling (see Figure 6.1). For the solid barrier scenario, the mesh resolution was increased around barriers with a resolution of 0.5 m in the horizontal axis and 0.25 m vertically.

To assess the independence of the simulated wind speed and concentrations from the computational grid inside Oxford St canyon, a grid sensitivity analysis was performed (Figure 6.4). Wind speed and  $\text{NO}_2$  concentrations were compared between three different grid: a fine grid with a maximum cell resolution in the X Y Z directions of  $0.8 \times 0.8 \times 0.3$  m (6 million cells), an intermediate grid ( $1.2 \times 1.2 \times 0.5$  m, 3 million cells) and a coarse grid ( $2.4 \times 2.4 \times 1$  m, 600 thousand cells). The agree-

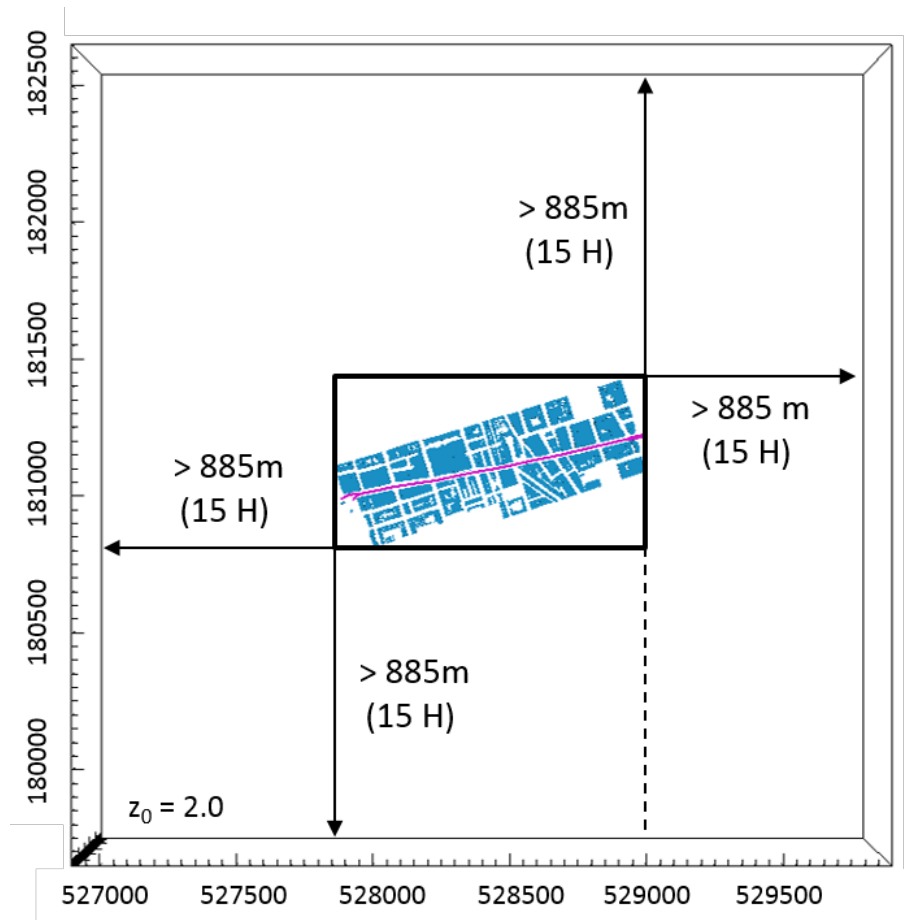


Figure 6.3: Modelled area of Oxford Street view from inside the CFD OpenFOAM software. Coordinates are in British National Grid (UK coordinate system expressed in meter). Wide buffer conditions are used around the buildings to allow the inflow wind to change directions.

ment between the intermediate and fine grid show that the simulated wind speeds and  $\text{NO}_2$  concentrations are independent from the grid used, although a few deviation are observed for a some points at high  $\text{NO}_2$  concentrations. More differences are observed between the intermediate and the coarse grid, which can be explained by the fact that the coarse grid is not compliant with the COST guidelines (not enough cells in the centre of the canyon to ensure a proper flow vorticity). As the coarse grid would be too inaccurate to use, the simulations were performed on the intermediate grid.

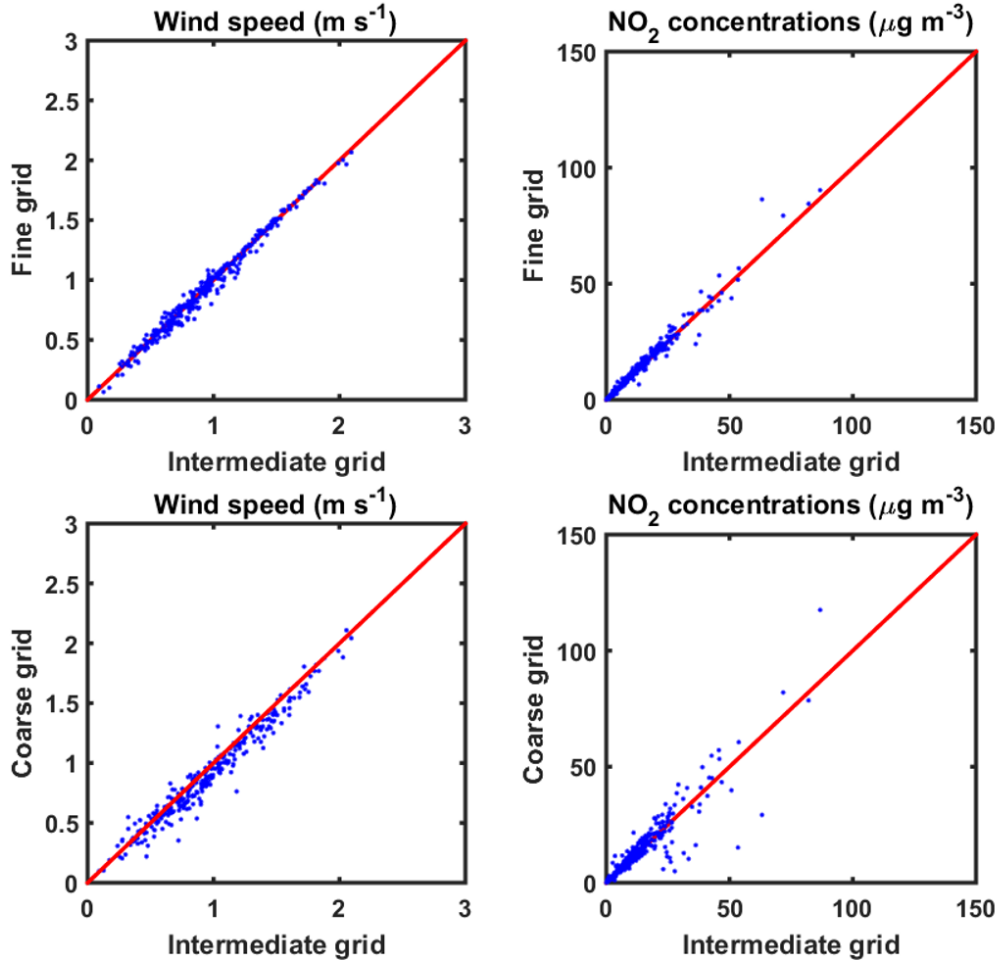


Figure 6.4: Grid sensitivity analysis inside Oxford Street canyon, 100 points were sampled across the whole street at heights spreading between 1 to 20 m.

## 6.4 Grid sensitivity analysis

### Flow calculation

As it is the case in the rest of this thesis, the simpleFOAM steady-state solver utility of OpenFOAM for incompressible, isothermal and turbulent flow was used. Second order upwind schemes were used. As recommended, the top of the domain was set as a symmetry plane (Franke et al., 2007). A surface roughness of  $z_0 = 2.0$  m was set for the ground, which corresponds to high rise buildings (WMO, 2008). For the wind flow calculation, a residual convergence of at least  $10^{-4}$  was reached for all field variables.

### **Gaseous dispersion calculation**

To model the NO<sub>2</sub> dispersion emitted from Oxford Street road, the previously defined transport equation was used (Eq. 2.27). The grid cells on the road were selected up to 1 m in height for emissions, as shown in Figure 6.2. Surface emissions source was adopted for this chapter to simulate traffic in the street. A  $Sc_t$  value of 0.5 was used, which gave the best model agreement when compared to wind tunnel data (Chapter 2) which agrees with previous studies (Gromke and Blocken, 2015b).

### **Trees and deposition modelling**

Regarding the aerodynamic effects, trees were modelled as porous bodies following the same approach as used in Chapter 2 (Eq. 2.22).

The deposition inside the tree crown cells was parametrised as a sink term applied at each Eulerian step as described previously (Eq. 2.23).

Deposition on photocatalytic paint differ from trees as grass and buildings are represented as surfaces. The change in PM<sub>2.5</sub> concentration via deposition on grass and buildings was expressed as described in Eq. 5.1. In this present case, no LAI (Leaf Area Index) are needed for the paint so a LAI of 1 is used.

### **Model limitations**

A RANS CFD model provides a steady state view of the reality, which corresponds to a fixed picture of the wind flow and pollutant concentrations. In real life, the wind is oscillating in strength and directions and pollutant concentrations are highly variable following wind and traffic presence. Traffic turbulence will also affect the way pollutants are dispersed within a street canyon. NO<sub>2</sub> is a reactive gas in a constant cycle of reactions with NO and O<sub>3</sub> (Barker, 1995), in this chapter the levels of NO<sub>2</sub> were supposed to be constant in the street canyon and kept as an average concentrations, without chemical reaction taken into account. This chapter also omits background concentrations of NO<sub>2</sub> to focus directly on the road emission. As each mitigation strategy is compared to a reference scenario, only relative concentrations are used and the background is therefore estimated to have little impact on the final results.

#### **6.4.1 Pollution mitigation strategies**

In total, six different scenarios were modelled and compared (see Figure 6.5).

- Scenario 1 corresponds to simulation of the empty street canyon of Oxford St. This scenario is taken as a reference to which each of the following scenarios will be compared to measure the change in NO<sub>2</sub> concentrations.
- Scenario 2 focuses on the integration of real porous trees inside the street canyon, as specified by the National Tree Map<sup>TM</sup>. Both aerodynamics and deposition effects were modelled. The upper limit of deposition velocity (Vd) of 0.21 cm s<sup>-1</sup> was used (Rondón et al., 1993), to see the maximum to which the trees could reduce NO<sub>2</sub> concentrations.
- Scenario 3 uses the same tree data from scenario 2 with the difference that the tree diameter was reduced almost by half to simulate the effects of narrow trees, as they have been suggested to be more effective than thick trees in improving local air quality (Janhäll, 2015).
- Scenario 4 considers the application of photocatalytic paint on building facades on each side of Oxford St. As for the tree scenario, the upper limit of deposition velocity (Vd) of 0.24 cm s<sup>-1</sup> was used (DEFRA, 2016), to determine the potential of photocatalytic paint in reducing NO<sub>2</sub> concentrations. This scenario does not consider the presence of windows or doors where the paint could not be applied and is therefore overestimating the painted surface (around 60 000 m<sup>2</sup>). To take into account the presence of doors and windows which are assumed to be uniformly spread along the street, results were halved supposing a 50% split between building facades where paint could be applied and non-paintable facades. The efficiency of the paint depending on UV radiation and the breakdown of NO<sub>2</sub> into HONO (Bedjanian and El Zein, 2012; Ndour et al., 2008), which can present adverse health effects for the lung functions (Beckett et al., 1995), were not explored in this study.
- Scenario 5 study the introduction of a solid barrier on each side of the Oxford St road. Its dimensions of 0.5 m (width) × 1 m (height) were based on previous studies examining wall height suitability as a passive control strategy (Gallagher et al., 2012; McNabola et al., 2009). Similarly to the tree scenario, the aerodynamics of the barrier inside the street canyon were modelled.
- Scenario 6 corresponds to solid barrier painted with photocatalytic paint (deposition velocity (Vd) of 0.24 cm s<sup>-1</sup> (DEFRA, 2016)). The barriers have the same characteristics as in scenario 5.

- In scenario 7, solid barriers were coated with an innovative material with an enhanced deposition velocity of  $1 \text{ cm s}^{-1}$  for  $\text{NO}_2$ . The solid barriers have the same characteristics as in scenario 5. The material used to coat the solid barrier corresponds to deposition capabilities offered by the A9 material. This innovative material uses an alternative technology than photocatalytic paint.

### 6.4.2 Life cycle costing of mitigation strategies

In addition to the potential for these measures to mitigate pollution in the urban environment, the likelihood of their implementation is dependent on their economic costs. Therefore, a life cycle cost analysis is undertaken to compare both the environmental and economic performance of each strategy to mitigate  $\text{NO}_2$  concentrations.

A similar approach to that used by Churchill and Panesar (2013), to quantify the life cycle costs of using photocatalytic material on highway noise barriers to reduce pollutant concentrations, was adopted in this study. A 10-year period was considered for the life cycle cost analysis, which included the installation of each measure and its annual maintenance requirements. However, the disposal stage of the life cycle is excluded as each strategy is considered to last beyond this time-frame. In addition, the embodied burdens associated with each technology is omitted, but it is acknowledged that implementing each measure has an associated environmental impact. Details of the installation and maintenance costs used in the assessment for each measure is presented in Table 6.1.

An inflation rate of 2.5% was applied to annual maintenance costs in the calculation of the total life cycle costs for each mitigation measure.

The same estimates were used for calculating the life cycle cost of implementing these mitigation strategies in pollution hotspots in the street canyon.

## 6.5 Results

### 6.5.1 Ranking environmental performance of pollution mitigation measures

Environmental performance was calculated based on the percentage difference in mean concentrations between the reference scenario and each pollution mitigation measure. The results considered the differences at both average child (1.0 m) and

## 6.5 Results

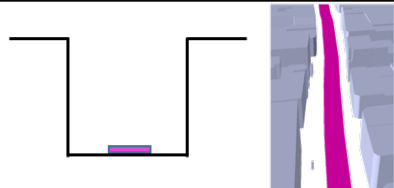
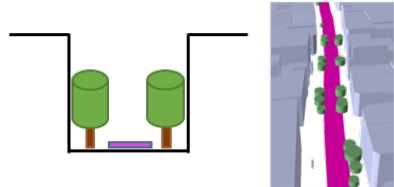
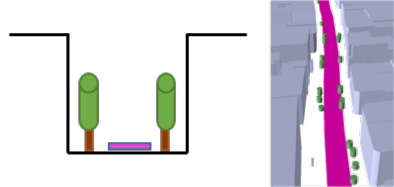
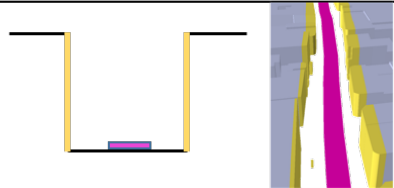
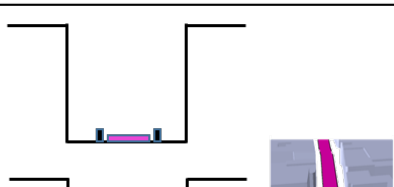
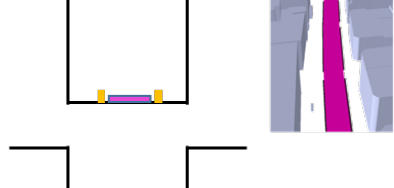
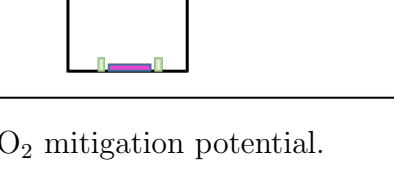
Scenario	Description	
1. Reference	Empty street canyon of Oxford St	
2. Existing tree	Tree using NTM™ specification (total of 50 trees) - on average 5.7 m wide x 5 m tall - total volume occupied by trees = 4000 m³ 2.1: Aerodynamics case ( $V_d = 0 \text{ cm s}^{-1}$ ) 2.2: Deposition case ( $V_d = 0.21 \text{ cm s}^{-1}$ )	
3. Narrow tree	Same tree height (as NTM™) but narrower width based on Janhäll (2015) suggestion - 3 m wide x 5 m tall - Total volume occupied by trees = 1000 m³ 3.1: Aerodynamics case ( $V_d = 0 \text{ cm s}^{-1}$ ) 3.2: Deposition case ( $V_d = 0.21 \text{ cm s}^{-1}$ )	
4. Painted buildings	Photocatalytic paint (pp) coated facades on each side of the street - 60 000 m² of painted wall (halved to 30 000 m² in results section to consider non-paintable door and window surfaces) 4.1: Deposition case ( $V_d = 0.24 \text{ cm s}^{-1}$ )	
5. Solid barrier	Solid barrier on each side of the road - 0.5 m wide x 1 m tall - 5300 m² of barrier (2.2 km of barrier) 5.1: Aerodynamics case ( $V_d = 0 \text{ cm s}^{-1}$ )	
6. Painted barrier	Same characteristics as solid barrier but painted with photocatalytic paint. 6.1: barrier aerodynamics with photocatalytic paint deposition ( $V_d = 0.24 \text{ cm s}^{-1}$ )	
7. Innovative barrier	Same characteristics as solid barrier but coated with innovative material. 7.1: barrier aerodynamics with artificial material deposition ( $V_d = 1.0 \text{ cm s}^{-1}$ )	

Figure 6.5: List of six scenarios examined for NO<sub>2</sub> mitigation potential.

adult (1.5 m) height. NO<sub>2</sub> simulations were averaged into a single average street concentration using eight wind directions weighted over London prevailing wind distribution. The results are presented in Table 6.2 and Figure 6.6.

- Scenario 2: The overall changes in NO<sub>2</sub> induced by existing trees at adult height was an overall 2.0% reduction: 1.6% reduction owing to enhanced dis-

## 6.5 Results

Table 6.1: Installation and maintenance costs for life cycle cost analysis of different NO<sub>2</sub> mitigation strategies (one-off installation cost; annual maintenance costs; all costs in Pound sterling). Prices were taken from the UK Forestry Commission for London trees and woodlands (Forestry-Commission, 2009).

Scenario	One-off installation costs	Annual maintenance costs
1. Reference	-	-
2. Existing trees planted in street <sup>1</sup>	£120 / tree	£10 per tree
3. Narrow trees planted in street <sup>1</sup>	£100 / tree	£10 per tree
4. Painted buildings <sup>2</sup>	£3.15 / m <sup>2</sup>	£3.15 / m <sup>2</sup>
5. Solid barrier <sup>3</sup>	£125 / m	£2 / m
6. Painted barrier	£133 / m	£5.95 / m
7. Innovative barrier <sup>4</sup>	£150 / m	£2 / m

<sup>1</sup> Plant standard and narrow trees along footpath cost £120 and £100 per tree, respectively (cost includes trees, labour and ground excavation for planting); annual pruning of trees estimated cost of £10 per tree.

<sup>2</sup> £6 per litre of TiO<sub>2</sub> paint, 1 litre of paint for 7.5 m<sup>2</sup>; labour, equipment and materials estimated at £3 per m<sup>2</sup> for painting surfaces; re-application or cleaning of TiO<sub>2</sub> surface annually estimated at 50 % of initial cost.

<sup>3</sup> One metre high, material and construction costs for 0.5 m deep solid wall estimated at £125 per m length of wall; annual maintenance includes washing faces of clean wall estimated at £2 per m length of wall.

<sup>4</sup> The wall is constructed with innovative artificial NO<sub>2</sub> deposition material. Estimated to add an additional 20 % to the cost of constructing solid barrier wall; Same annual maintenance requirements and costs to solid barrier.

persion and an additional 0.4% owing to deposition effects. The aerodynamics dispersion effects diminish when considering the pedestrian zones, meaning that tree dispersion is more effective over roads. The deposition of NO<sub>2</sub> on trees was calculated using the upper end of deposition velocities values (0.21 cm s<sup>-1</sup>), which indicates that even using a high estimate for deposition, the aerodynamic dispersion prevails over deposition which supports previous study results (Jeanjean et al., 2016). Deposition reduction was slightly greater over pedestrian zones (0.5%) than road zones (0.4%), as deposition occurs where trees are planted (over pedestrian zones).

- Scenario 3: In pedestrian zones, the overall changes in NO<sub>2</sub> induced by narrow trees was 1.0%: 1.0% increase due to dispersion and an additional negligible 0.005% decrease when considering deposition effects (at 1.5 m height). The volume of narrow trees (1000 m<sup>3</sup>) was one quarter of the existing trees (4000 m<sup>3</sup>), which suggests that deposition effects occur non linearly as the reduction via deposition was 0.5% for the existing trees.

- Scenario 4: With reductions between 0.4% over road zones and 0.8% over pedestrian zones, photocatalytic paint slightly reduce NO<sub>2</sub> levels. Reductions are greater towards the painted wall where the deposition occurs, which benefits directly the pedestrian, whereas, less reduction was observed towards the middle of the street canyon over the road zone. Deposition values are likely to be optimistic as an upper limit value for the deposition velocity of 0.24 cm s<sup>-1</sup> was used (DEFRA, 2016).
- Scenario 5: From the results obtained in Figure 6.6, it can be seen that the main element driving NO<sub>2</sub> using the solid barrier is enhanced dispersion, which increases canyon concentrations by 38.3% when considering the road zones at 1.5 m. When considering the pedestrian zones, the solid barrier actually helps reducing NO<sub>2</sub> concentration with a 10.1% decrease at 1.0 m height and 4.4% decrease at 1.5 m height.
- Scenario 6: The solid barriers coated with photocatalytic paint decrease NO<sub>2</sub> concentrations by an additional 2 - 3% in addition to the aerodynamic effects observed for the solid barriers.
- Scenario 7: Deposition loss of 7 - 10% are found for innovative barriers, which is more than 3 times the deposition values found for painted barriers. This result suggests that using material with enhanced deposition capability increases NO<sub>2</sub> reductions via deposition. Deposition velocity needs to be significant (here 1.0 cm s<sup>-1</sup>) to have a non negligible impact.

### 6.5.2 Spatial visualisation

Figure 6.7 shows the aerodynamic effects of existing trees, narrow trees and solid barriers averaged over the prevailing wind directions. It can be seen that the structure of NO<sub>2</sub> changes between existing and narrow trees are similar, although for narrow trees the changes are less extreme. For the case of solid barrier aerodynamic, the trapping over road areas can clearly be seen over the street. Note that a trapping effect means that here NO<sub>2</sub> will take longer to escape the street canyon location (essentially caused by lower wind speeds), which therefore leads to greater concentrations.

The Figure 6.8 illustrates the changes of NO<sub>2</sub> in terms of deposition on trees, photocatalytic paint and innovative material. In contrary to the heterogeneous

## 6.5 Results

Table 6.2: Relative differences in concentrations for different NO<sub>2</sub> mitigation strategies (represented as percentage reductions (-) or increases (+) to reference concentrations). Samples were taken all across Oxford St on a regular 2 x 2 m grid at both children height (1.0 m) and adults height (1.5 m).

Scenario	Height	Pedestrian zone			Road zone		
		Dispersion	Deposition	Total	Dispersion	Deposition	Total
2. Existing tree	1.0 m	-0.6	-0.5	-1.1	-1.8	-0.3	-2.1
	1.5 m	-0.5	-0.4	-0.9	-1.6	-0.4	-2.0
3. Narrow tree	1.0 m	0.9	≈0.0	0.9	0.2	≈0.0	0.2
	1.5 m	1.0	-0.01	1.0	0.3	≈0.0	0.3
4. Painted buildings	1.0 m	-	-0.8 <sup>1</sup>	-0.8 <sup>1</sup>	-	-0.4 <sup>1</sup>	-0.4 <sup>1</sup>
	1.5 m	-	-0.8 <sup>1</sup>	-0.8 <sup>1</sup>	-	-0.4 <sup>1</sup>	-0.4 <sup>1</sup>
5. Solid barrier	1.0 m	-10.1	-	-10.1	45.5	-	45.5
	1.5 m	-4.4	-	-4.4	38.3	-	38.3
6. Painted barrier	1.0 m	-10.1	-2.1	-12.2	45.5	-2.8	42.7
	1.5 m	-4.4	-2.1	-6.5	38.3	-2.2	36.1
7. Innovative barrier	1.0 m	-10.1	-7.4	-17.5	45.5	-9.9	35.6
	1.5 m	-4.4	-7.3	-11.7	38.3	-7.7	30.6

<sup>1</sup> Deposition values halved to consider half of the building wall surface non-paintable (presence of doors and windows).

Table 6.3: Summary of Table 6.2 over the full street. Only trees and photocatalytic paint have a positive effect over the full street.

Scenario	Height	Full Street		
		Dispersion	Deposition	Total
2. Existing tree	1.0 m	-1.26	-0.39	-1.65
	1.5 m	-1.11	-0.40	-1.51
3. Narrow tree	1.0 m	0.52	≈0	0.52
	1.5 m	0.62	≈0	0.62
4. Painted buildings	1.0 m	0	-0.58	-0.58
	1.5 m	0	-0.58	-0.58
5. Solid barrier	1.0 m	20.48	0	20.48
	1.5 m	19.10	0	19.10
6. Painted barrier	1.0 m	20.48	-2.49	18.0
	1.5 m	19.10	-2.16	16.93
Innovative barrier	1.0 m	20.48	-8.78	11.71
	1.5 m	19.10	-7.52	11.57

## 6.5 Results

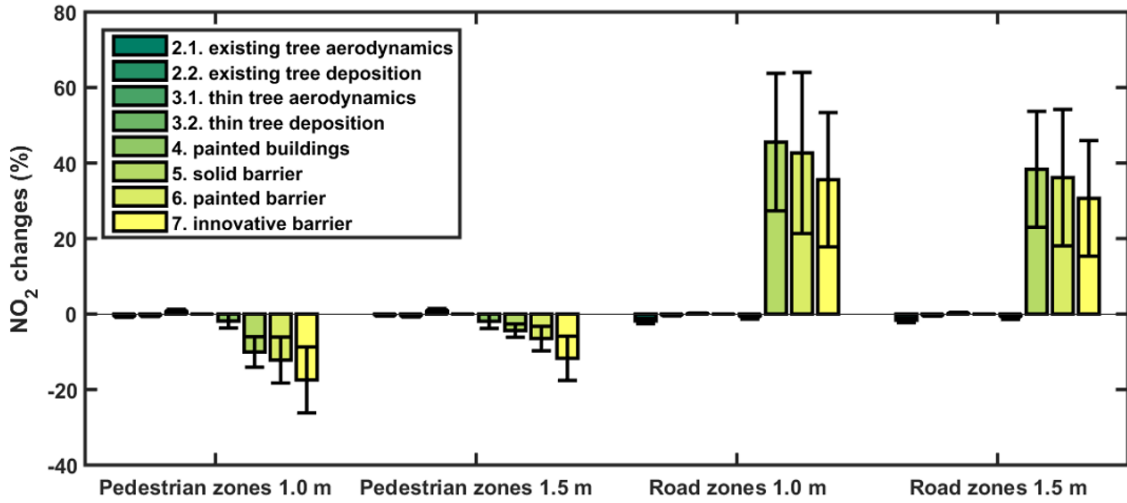


Figure 6.6: Relative difference in NO<sub>2</sub> concentrations in comparison to an empty street canyon (scenario 1). Samples were taken all across Oxford St on a regular  $2 \times 2$  m grid at both 1.0 and 1.5 m height. Error bars correspond to the model accuracy of 40%.

spread of the aerodynamic effects, it can be seen that NO<sub>2</sub> changes are clearly localised for deposition reductions. The amount of surface available for deposition is critical as for narrow trees almost no sign of deposition are found whereas for existing trees reduction via deposition can be seen towards the middle of Oxford St. However, even if large surface of buildings are painted, the deposition of NO<sub>2</sub> appears to be limited in the scenario 4. A possibility could be that the painted walls are located too far away from the road source so little concentration of NO<sub>2</sub> are exposed to the surface of paint. The values of deposition velocities seem as well to be an important parameter as deposition reductions are much greater for innovative barriers ( $V_d = 1.0 \text{ cm s}^{-1}$ ) than for painted barriers ( $V_d = 0.24 \text{ cm s}^{-1}$ ).

### 6.5.3 Ranking life cycle costs of pollutant mitigation measures

Based on the estimated costs for the installation and annual maintenance, Figure 6.9 presents the life cycle costs of each pollution mitigation measure for the next ten years. The findings illustrate the significant differences in initial installation and annual maintenance costs for each pollutant mitigation measure over the 10-year period in Oxford Street. Prices were taken from the UK Forestry Commission for London trees and woodlands (Forestry-Commission, 2009). The cost of trees as a

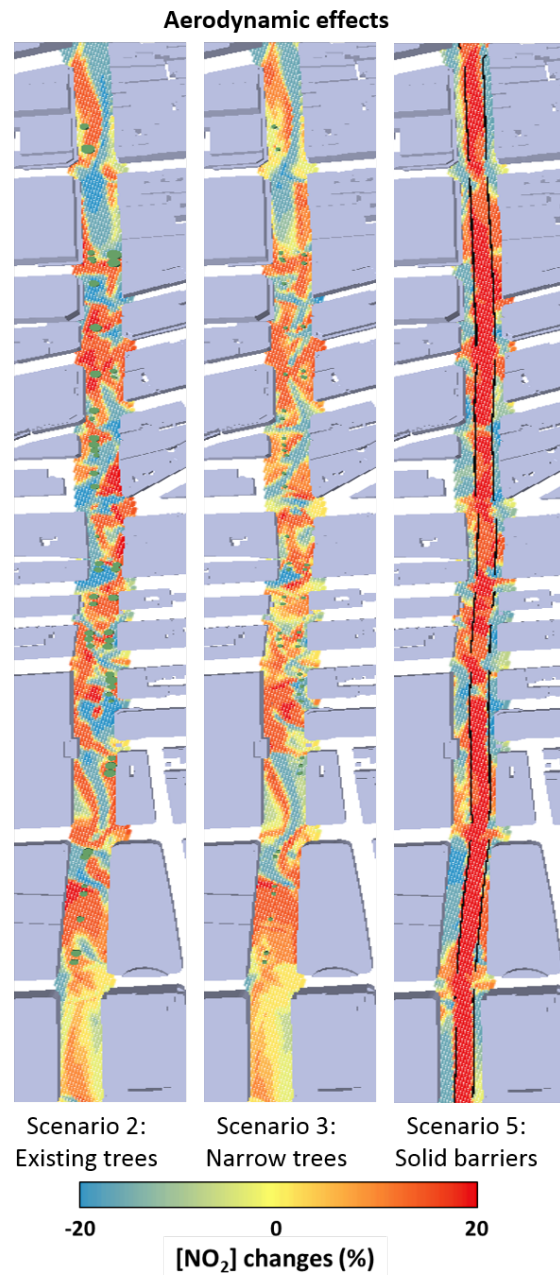


Figure 6.7: Aerodynamic effects of existing trees (Sc. 2), narrow trees (Sc. 3) and solid barriers (Sc. 5) on vehicular emissions of NO<sub>2</sub> in Oxford St. The position of trees can be seen in Sc. 2 and Sc. 3.

pollution mitigation measure was the least expensive of all scenarios, with initial planting and annual maintenance estimated at £21.5k and £23.5k depending on tree type. The cost of installing solid barriers with or without the use of an innovative material to enhance NO<sub>2</sub> deposition, were ten to fifteen times more expensive



## 6.5 Results

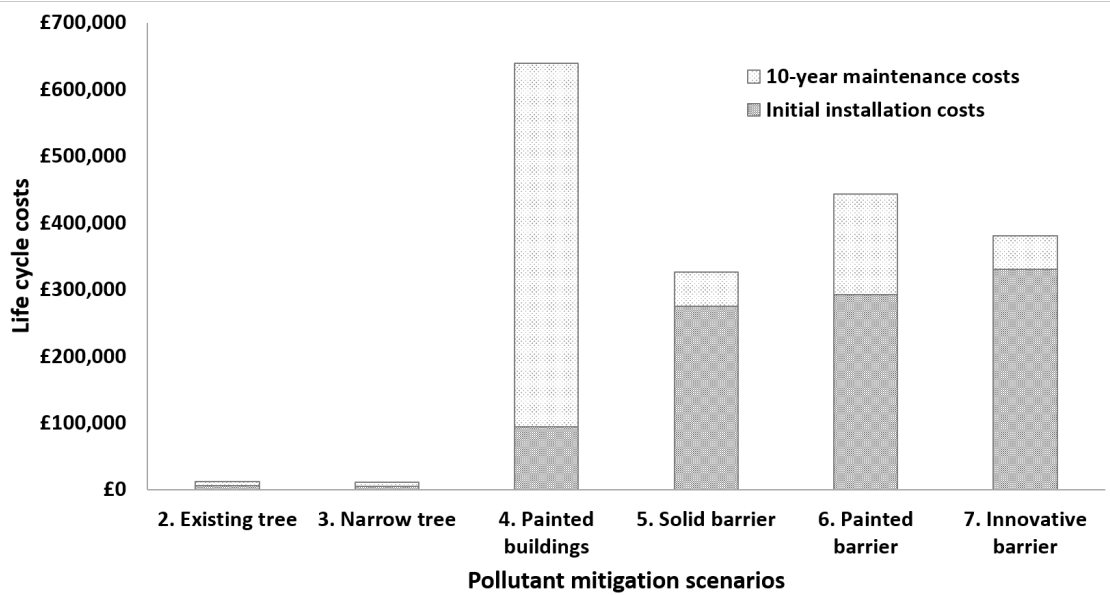


Figure 6.9: Life cycle costs of scenarios considered as feasible pollution mitigation measures in Oxford Street.

The initial application of photocatalytic paint in the street plus the cost of annual cleaning or reapplication of paint on building surfaces was estimated £623k, thirty times more expensive than trees and three to four times more expensive than the solid barriers.

The results presented in this Chapter were highly dependent on street geometry (aspect ratio), as demonstrated by the differences in results from the hotspot analysis. Local meteorological conditions, specifically the wind direction in the street canyon was also found to have a significant impact on the modelling results (see Chapter 3), where the aerodynamic effects of each mitigation strategy may differ depending on the orientation of the wind towards the street canyon. However, deposition reductions were found to be similar across the range of modelled wind directions. In modern cities with similar grid street patterns, these modelling results could potentially be extrapolated to assess the impact of a mitigation strategy over the entire city. However, as street geometry is variable within the neighbourhoods in London and other typical European cities, further research is required to extrapolate these results.

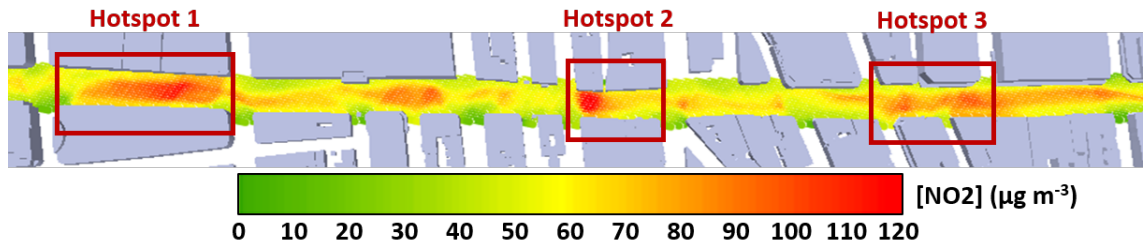


Figure 6.10: Hotspots locations in Oxford St for the reference scenario 1. Wind directions were averaged over the prevailing winds.

### 6.5.4 Mitigation at pollution hotspots

Instead of applying mitigation strategies throughout the whole street, another approach considered focusing on mitigating pollution hotspots. Figure 6.10 illustrates the average  $\text{NO}_2$  concentrations for the reference scenario and identifies three hotspot locations in the street canyon. The different mitigation strategies previously used (see Figure 6.5) were then considered in these areas. The combined mitigation results for these hotspots, which accounts for 25% of the full length of the street, presents reductions of 0.49% for painted buildings, 4.2% for solid barrier aerodynamic, 4.7% for painted barrier and 6.1% for innovative barrier. The aerodynamic effects of solid barrier are very similar to the results obtained for full street mitigation (4.2% decrease instead of 4.4%). Deposition reductions are around 4 times lower for hotspots mitigation (0.5% and 2.1% for painted barrier and innovative barrier instead of 1.9% and 7.3%), which shows that deposition effects are dependent on the amount of available surfaces of paint or material which covers 25% of the original street length. Figure 6.11 illustrates these changes of  $\text{NO}_2$  across the whole of Oxford St.

#### Hotspot 1

Hotspot 1 has a width over height ratio ( $W / H$ ) of 1. Reductions of 0.6% were found for painted buildings. Aerodynamic effects of solid barriers decrease  $\text{NO}_2$  by 31.9%. Additional reductions via deposition of 1.4% and 4.9% were found for painted barriers and innovative barriers.

### Hotspot 2

Hotspot 2 has a width over height ratio ( $W / H$ ) of 1.1. Reductions of 0.7% were found for painted buildings. Aerodynamic effects of solid barriers decrease  $\text{NO}_2$  by 27.0%. Additional reductions via deposition of 1.4% and 5.0% were found for painted barriers and innovative barriers.

### Hotspot 3

Hotspot 3 has a width over height ratio ( $W / H$ ) of 1.25. Reductions of 0.4% were found for painted buildings. Aerodynamic effects of solid barriers decrease  $\text{NO}_2$  by 16.8%. Additional reductions via deposition of 1.1% and 4.0% were found for painted barriers and innovative barriers.

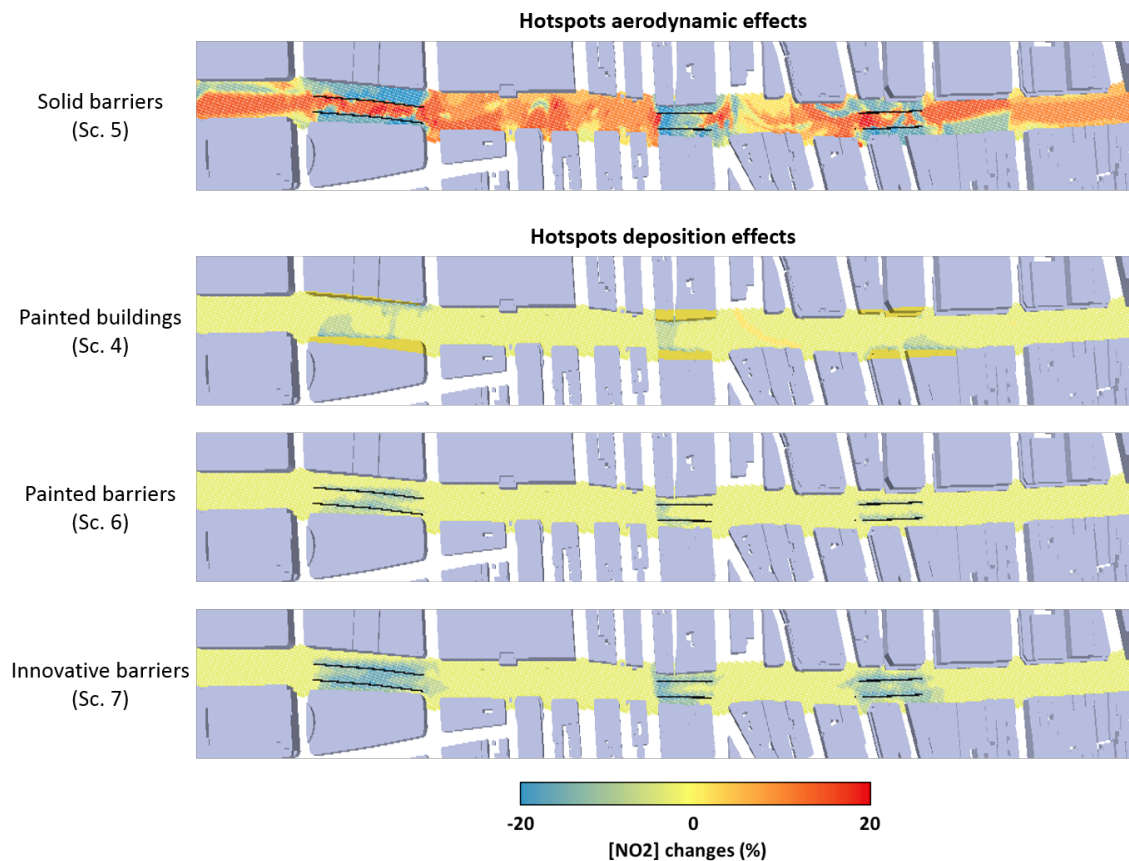


Figure 6.11: Aerodynamic and deposition effects of hotspot mitigation strategies on vehicular emissions of  $\text{NO}_2$  in Oxford St.

## 6.6 Discussion

### 6.6.1 Mitigation strategies strengths and weaknesses

In addition to being an affordable option compared to other mitigation strategies (see Figure 6.9), planting trees offers reductions in  $\text{NO}_2$ , through both aerodynamic dispersion and deposition, for all street users, such as pedestrians, cyclists and drivers. The deposition on trees extend to other air pollutants, such as particulate matter for  $\text{PM}_{2.5}$  (Nowak et al., 2013) and  $\text{PM}_{10}$  (Nowak et al., 2006). There are also other benefits of urban trees, in that they contribute to the well being of the urban population (White et al., 2013) and road side vegetation also regulates the traffic noise level of busy streets (Kalansuriya et al., 2009). The setbacks of a tree planting policy is that some streets might not be suitable for trees. Local meteorology must also be taken into account, here prevailing winds are parallel to the street orientation. Previous studies have shown that the aerodynamic effects of trees would end up trapping road emissions for perpendicular winds (Gromke et al., 2008; Buccolieri et al., 2011; Wania et al., 2012), which exacerbates tree trapping effects in street canyons.

The results of the narrow tree scenario showed that narrow trees actually increase trapping of pollutants within the street canyon, whereas the opposite was expected with greater aerodynamics dispersion than for existing tree (Janhäll, 2015). A reason could be the difference of context between, the previous study of Janhäll (2015) considered the use of regularly planted trees in avenues whereas the work done in this chapter corresponds more to sparse and randomly planted trees. This suggests the possibility of an existing threshold of tree cover that should be met in order to have a positive effects from trees.

Solid barrier strategies have very positive effects for pedestrians but present adverse effects for cyclists and drivers, as they trap air pollution over road zones. Thus, it is worthwhile improving their performances with paint and with innovative material which will introduce  $\text{NO}_2$  reductions via deposition. The option of green walls was not explored here, although they offer deposition capabilities for both  $\text{NO}_2$  and particulate matter. However, their maintenance costs are very important (Perini and Rosasco, 2013) and may negatively affect their ranking in comparison with other strategies.

### 6.6.2 Pedestrian areas vs on-road pollution

If the protection of pedestrian areas is the first priority of city planners, the suggested most beneficial mitigation strategy would be the installation of solid barriers an order of magnitude greater than the other scenarios. Deposition to the solid barrier could help decrease NO<sub>2</sub> with an additional 2 - 3% added with the use of photocatalytic paint and 7 - 10% with the use of innovative material. The installation of this strategy shall be made with the awareness that this would imply increased exposure for road users, such as cyclists and drivers (up to 38.3% increase at pedestrian height).

When considering on-road pollution, the most profitable scenario that decreases NO<sub>2</sub> are existing trees. The dispersive effect of trees are 4 times more effective than deposition reductions, showing that increasing aerodynamic dispersion over traffic zones has a direct benefit. Tree presents the interesting trade-off of being beneficial to pedestrians as well.

### 6.6.3 Child vs adult exposure

Children and the elderly, are more likely to be affected by air pollutants than healthy adult individuals (Brunekreef and Holgate, 2002). In general, the trends given by the scenarios are very similar for adults and children (see Table 6.2). As pedestrians, children would spend most of their time walking on footpaths rather than on roads, except when crossing. When crossing roads (road zones), the use of the solid barrier would be more adverse for children than for adults. However, crossing a road represents a shorter time period of an individual commute so it is likely the overall net exposure would be positive.

These results suggest that the adoption of the mitigation strategies would benefit children more than adults in all scenarios.

### 6.6.4 Full street vs hotspots

Limited available financial resources will be one of the main challenges faced by city planners wanting to improve air pollution within busy streets. Therefore, applying a mitigation strategy only within hotspots reduces the price of photocatalytic paint and solid barriers by a factor of 4 (25% of the street length). The identification of hotspots appears to be the critical step to undertake. Hotspots could be mapped by combining modelling and mobile measurements of air pollution.

Hotspot mitigation has the advantage of being very effective within deep street canyon. Inside mitigated hotspot street canyons, solid barrier aerodynamic effects (16.8 - 31.9%) are at least 4 times more effective than for results over the whole street (4.4%). Deposition effects of painted buildings (0.4 - 0.7%), painted barrier (1.1 - 1.4%) and innovative barrier (4.0 - 5.0%) are similar to the results obtained in the case of a full street mitigation. Consequently, mitigating hotspots where the pollution levels are the greatest provides a cost-effective alternative to reducing personal exposure.

It shall be noted that the application of mitigation strategies may create new hotspots, such as increased concentrations over road zones in the case of solid barriers. Although useful in hotspots, dispersion remains a temporary mitigation measure as the air pollutants are not removed from the urban environment.

### 6.6.5 Ranking mitigation strategies

To find which mitigation strategy was best in terms of environmental performance and life cycle costs, the ranking of the mitigation strategy was based on the amount of spending (in £k) necessary to decrease NO<sub>2</sub> levels by 1%. If a mitigation strategy was shown to increase concentrations, no final rank (-) was attributed. Existing tree

Table 6.4: Ranking of mitigation strategies based on both their cost and ability in decreasing NO<sub>2</sub> concentrations (over pedestrian zone at 1.5 m height).

Scenario	£k per 1 % NO <sub>2</sub> reduction	Rank
2. Existing tree	13.0	1
3. Narrow tree	∞	-
4. Painted buildings	798.5	5
5. Solid barrier	74.0	4
6. Painted barrier	68.1	3
7. Innovative barrier	25.7	2

arrives in 1<sup>st</sup> positions, this position being arbitrary as the existing trees are already planted. Nevertheless, it shows that planting trees can actually be the preferred mitigation strategy for busy urban avenues. Trees being the most affordable option between the studied strategies, chapter findings suggest that planting trees shall be carefully considered in both developed and developing countries, taking into account local meteorology.

Owing to their enhanced deposition performance, the solid barriers coated with innovative material are the most profitable of the solid barrier solutions (rank 2),

followed by painted barrier (rank 3) and solid barrier (rank 4). The less profitable strategy corresponds to the painted buildings (rank 5), having a too important cost to be competitive with the other mitigation strategies.

Despite combined dispersion and deposition reductions, the findings of this chapter suggest that mitigation strategies do not remove the problem of pollution. It is worth noting that in polluted cities the urban background (not considered here) can be a large contributor in terms of air pollution, which would decrease the efficiency of mitigation strategies presented here.

## 6.7 Conclusions

Trees are appearing as the most cost-effective mitigation strategy in terms of costs related to their environmental impact. There is a crucial need from the research field to find an effective tree planting policy in street canyons. Owing to their attractive costs, efficient tree planting policy could benefit both developed and developing countries. As found in this study, trees are beneficial when prevailing winds are parallel to the street canyon orientation, which shows the importance of taking local meteorology into account.

For streets in which tree planting is not suitable, which could be for street orientations perpendicular to prevailing winds, innovative barriers are appearing an attractive alternative. Aerodynamic benefits of solid barrier would translate to other traffic emitted pollutants such as particulate matters. Improving solid barrier surfaces with innovative material or photocatalytic paint to decrease NO<sub>2</sub> levels via deposition has been shown to be a cost-effective action when considering both environmental and economic perspectives.

Painted building facades with photocatalytic paint as been shown to have a cost too great in order to be competitive with the other mitigation strategies.

# Chapter 7

## Conclusion

### 7.1 Model evaluation and performance

Steady state dispersion models do not fully reproduce the wind flow as they do not capture time-dependent fluctuations which occur within the ABL (changes in wind speed, wind direction, etc.). Therefore, special attention was paid in the evaluation of the CFD simulations. A first evaluation exercise was made against a wind tunnel experiment (see Chapter 2). The overall average accuracy of the CFD model was found to be between 30 to 40%. In Chapter 3, simulations of  $\text{NO}_x$  and  $\text{PM}_{2.5}$  concentrations were compared to a measurement station in Marylebone Rd, London. Overall, it was found that the statistical parameters used to assess the model were satisfactory. Most of statistical parameters were within acceptable ranges, except for the FB which was sometimes found out of range. The FB indicated an underestimation of  $\text{NO}_x$  concentrations and an overestimation of  $\text{PM}_{2.5}$  concentrations by the model. These two evaluation exercises support previous studies which found that CFD models were suitable for modelling trees as porous bodies. A final evaluation study was done over a landfill site in Appendix C, where a similar model accuracy of 30 to 40% was found between measured and modelled tracer concentrations.

### 7.2 The use of trees as a mitigation strategy

Until now, previous modelling studies (Gromke et al., 2008; Buccolieri et al., 2011, 2009) primarily focused on wind directions perpendicular to street canyons, which exacerbate the trapping effect of trees. This thesis identified that if prevailing winds were parallel to street canyons, the overall effects of trees can become beneficial

(depending on the street geometry). The density of trees within street canyons also seemed to be an important factor. Chapter 6 highlighted that reducing the tree density (from existing trees to narrower trees), switched the beneficial effects of trees from reducing pollution to trapping pollution. In contrast, Janhäll (2015) found that for large avenues densely populated with trees, reducing the tree cover brought about an improvement in air quality. These findings suggest the existence of a lower threshold of tree cover that needs to be met in order to have beneficial effects on air pollution. Alternatively, reducing tree cover might be considered for a dense population of trees within a deep street canyon when prevailing winds are perpendicular to the street orientation.

The modelling results of the effects of trees on air pollution dispersion are extremely heterogeneous across a city, making a clear pattern not easily identifiable. This suggests that the effect of trees on air pollution should be considered at different scales, both local and city-wide. At a city-wide scale, Chapter 4 and Chapter 5 show that the modelled dispersive effect of trees is beneficial (between 7 and 9% improvement). Aerodynamic dispersion were found to be even greater than the loss of air pollution via deposition. When comparing different sections of Leicester City, it was found that the greater the number of trees, the better the reduction in air pollution, noting that tree cover up to 20% was modelled. This suggests that every single tree has an effect on air pollution dispersion, not only the ones in street canyons.

When compared to other mitigation strategies as in the case of  $\text{NO}_2$ , trees were found to be the most attractive solution in terms of both environmental and economic perspectives. Nevertheless, it was found that other mitigation strategies such as solid barriers, could be used in street canyons where planting trees would not be suitable, such as when prevailing winds are perpendicular to street canyons. Solid barriers as mitigation strategies were found to be particularly effective in pollution hotspots, which are usually located in the deeper street canyons.

The decision on whether to plant trees or not should be based on air quality as well as other factors. Published studies usually focus on a single aspect of urban vegetation such as air quality, the improvement of social well-being, the reduction of traffic noise, etc. The choice of tree species could also be an important factor when considering the leaf seasons, as well as the emissions of BVOCs (which enhance the production of ozone).

In summary, clear guidelines on the use of trees as a mitigation strategy could

not be fully identified. At this stage, it can be imagined that trees planted upwind of a hotspot could enhance turbulent mixing and have an equivalent effects to trees planted within hotspots. These conclusions do not seem to apply for other mitigation strategies such as solid barriers, which are found to have clear, distinctive effects in spatial locations, such as between footpath and road zones. This thesis represents an important step towards understanding these processes.

## 7.3 Future work

### 7.3.1 Improved tree modelling

The following section details a possibility of future improvements of tree modelling.

#### **Varying LAD over height**

Idealised trees were modelled, with a constant leaf area density. However, it is known that the LAD of trees changes over height (e.g. Lalic and Mihailovic 2004). In order to integrate a more advanced modelling of the tree LAD, further research needs to be conducted to find an average profile that could be used in the modelling. Tree pruning (pollarding) for example can make a significant difference to the LAD.

#### **Tree species**

The determination of species would bring a more accurate view of the split between deciduous, evergreen leaf trees and coniferous trees. This would additionally provide further information on the LAD variation over height which varies depending on the tree species. The benefit would be particularly obvious in the simulation of the winter season, where all trees are currently neglected in the CFD model.

#### **Trunk and branches**

The omission of trees in the winter season lead to erroneous simulations for a particular wind direction (see Chapter 3), suggesting that winter parameterisation for trees could be developed by the integration of trunk and branches. For instance, the use of a Plant Area Index (PAD) instead of LAD was recently suggested (Hofman et al., 2016).

### **Tree shape**

The modelled tree shape is currently identical from the bottom to the top of the canopy (see previous Figure 2.5), suggesting that the tree shape could be improved. Trees usually have a larger canopy base height which decreases with height. Pine trees have very different shapes with the canopy base height potentially starting higher up. A knowledge of tree species would be needed in order to adjust the tree shape according to the species.

### **Dependence of the deposition velocities on wind speeds**

In the present thesis, average values of deposition velocities were used, without taking into account the effect of wind speed. Other tree models, such as the i-Tree model, are using deposition velocities which are dependent on the wind speed (Nowak et al., 2013). As deposition velocity values have been published by these models across a range of wind speeds, a likely future update of the CFD model will be the integration of variable deposition velocities based on the wind speed (e.g. empirical equation of Vong et al. 2010 in Chapter 1).

## **7.3.2 Other model improvements**

### **Land surface temperature**

It has been mentioned previously that a branch of CFD studies have been focusing on the simulation of urban heat islands affecting the wind flow (Chapter 2). The ENVI-MET model has particularly been used for this kind of application, as illustrated in Figure 7.1 by Ketterer and Matzarakis (2015). Urban vegetation tends to be cooler than surrounding buildings which affects the formation of urban heat islands. The modelling of the dispersion of vehicular emissions, when considering both urban vegetation and urban heat island effects, is an emerging research area and could potentially be studied. This would imply the simulation of a buoyant flow to model the change of air density based on temperature. The land surface temperature (LST) could be estimated using the same approach as Ketterer and Matzarakis (2015), using Physiological Equivalent Temperature (PET) of materials and vegetation. Note LES have been shown to be suitable for the study of urban heat islands (e.g. Tomlinson et al. 2013).

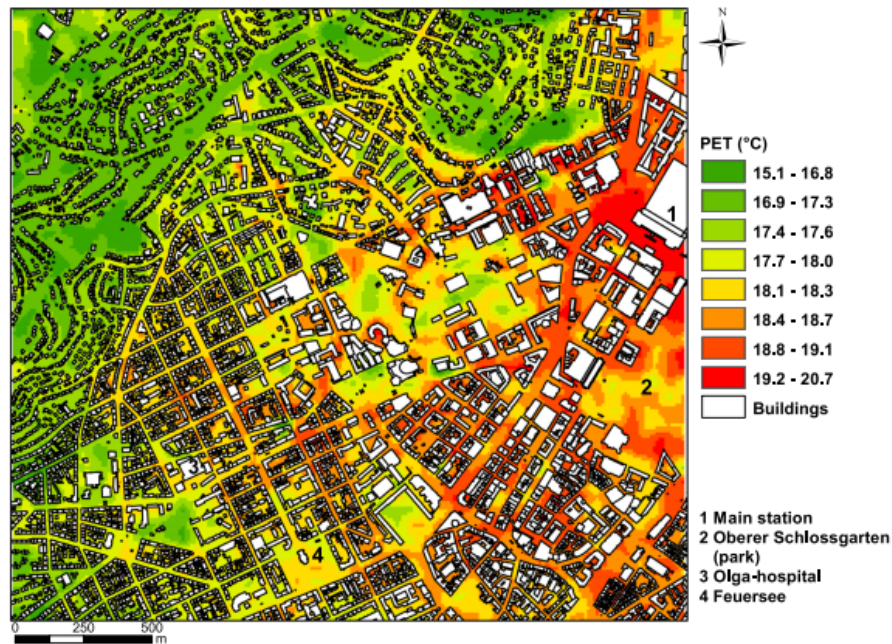


Figure 7.1: Example of urban land surface temperature integration in a CFD model (Ketterer and Matzarakis, 2015).

### Pedestrian exposure

A final work could be a deeper analysis of pedestrian exposure towards road pollution. This thesis mainly focused on the study of averaged air pollution map whereas other indicators could be used to measure the exposure of pedestrians. Modelled concentrations could for example be plotted as a function of pedestrian itineraries, leading to greater understanding of the urban vegetation impact on sensitive groups of the population, such as the young, elderly or asthmatics.

### 7.3.3 The role of CFD in the development of future mitigation strategies

Air pollution mitigation strategies are expensive to deploy, the larger the scale of the mitigation the larger the cost. The design of an existing city can hardly be changed instantaneously, the disruption caused by moving road junctions or modifying roof tops as an answer to air quality is hard to justify. This leads to the assumption that future mitigation strategies are likely to be applied in particular hotspot locations, such as busy street canyons, schools, hospitals, etc.

The role of CFD lies in its ability to simulate the effects of a mitigation strategy.

Other fields have shown the importance of using CFD simulations, such as the automotive and aerospace industries, for designing aerodynamically efficient car and plane shapes, or the wind turbine industry to investigate the best location of a wind farm. The same could be expected from the design of future streets that will integrate air pollution mitigation strategies.

It should be noted though that mitigation strategies are not the final answer to air pollution. Only a few percents of reduction in air pollution can be found with the use of mitigation strategies, the most beneficial actions being the aerodynamic dispersion of pollution from street levels. This dispersive effect diminishes during strong pollution episodes, as the pollution removed from the street will be replaced by background pollution. Therefore, mitigation strategies should be chosen according the city where they are meant to be deployed. Cities with average wind speeds greater than  $4 \text{ m s}^{-1}$  (such as London or Paris) would benefit for mitigation strategies that enhance aerodynamic dispersion whereas cities facing low wind speed conditions with less than  $2 \text{ m s}^{-1}$  (such as Milan in Italy or New Delhi in India) would rather benefit from mitigation strategies that favour deposition. So reducing emissions should stay as the main focus.

# Appendix A

## Derivations of the Navier-Stokes equations

### A.1 Mass conservation

The mass conservation principle applied to a control volume (CV) can be defined as: [Mass variation of CV] = [Mass entering the CV] - [Mass exiting the CV]

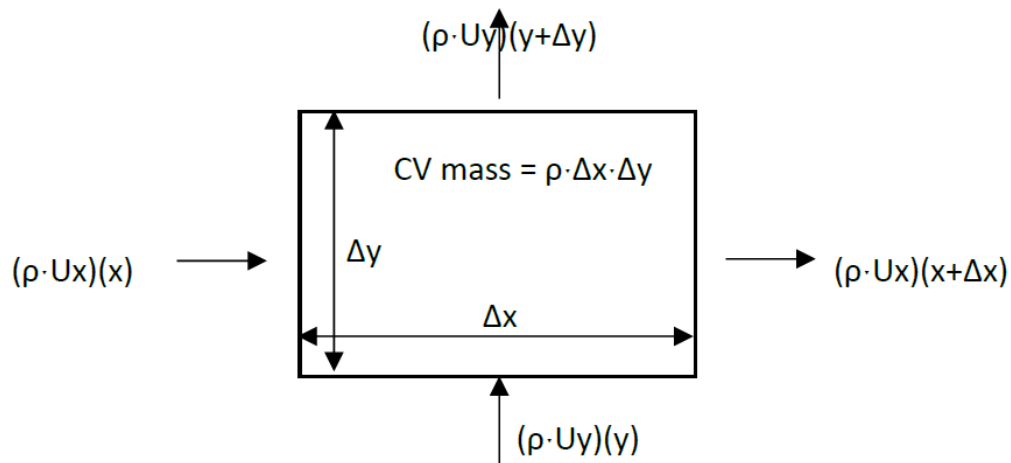


Figure A.1: Mass conservation principle applied to a control volume.

This leads to:

$$\frac{\partial(\rho \cdot \Delta x \cdot \Delta y)}{\partial t} = ((\rho \cdot Ux)(x) - (\rho \cdot Ux)(x + \Delta x)) \cdot \Delta y + ((\rho \cdot Uy)(y) - (\rho \cdot Uy)(y + \Delta y)) \cdot \Delta x \quad (\text{A.1})$$

Dividing by  $\Delta x \cdot \Delta y$  leads to:

$$\frac{\partial(\rho)}{\partial t} = \frac{(\rho \cdot Ux)(x) - (\rho \cdot Ux)(x + \Delta x)}{\Delta x} + \frac{(\rho \cdot Uy)(y) - (\rho \cdot Uy)(y + \Delta y)}{\Delta y} \quad (\text{A.2})$$

For a real function  $f(x)$ , the first order Taylor series expansion gives:

$$f(x + \Delta x) \approx f(x) + \frac{(f'(x))}{1!} \cdot \Delta x \quad (\text{A.3})$$

Therefore:

$$(\rho \cdot Ux)(x + \Delta x) = (\rho \cdot Ux)(x) + \frac{\partial(\rho \cdot Ux)}{\partial x \Delta x} \quad (\text{A.4})$$

Eq. A.2 can then be rearranged as:

$$\frac{\partial(\rho)}{\partial t} = \frac{-\partial(\rho \cdot Ux)}{\partial x} - \frac{\partial(\rho \cdot Uy)}{\partial y} \quad (\text{A.5})$$

Expressed in 3 dimensions, this equation is known as the conservation of mass (see Eq. 2.2):

$$\frac{\partial \rho}{\partial t} = \nabla \cdot (\rho \cdot U) \quad (\text{A.6})$$

## A.2 Momentum equation

The force-momentum principle applied to a control volume can be defined as: [Momentum variation in CV] = [Momentum entering the CV] – [Momentum exiting the CV] + [Forces applied to CV faces] + [Body forces within CV].

Following Fig. A.2, the force-momentum principle for the  $U_x$  component of the velocity can be expressed as:

$$\begin{aligned} \frac{\partial(\rho \cdot Ux)}{\partial t} \cdot \Delta x \cdot \Delta y &= ((\rho \cdot Ux \cdot Ux)(x) - (\rho \cdot Ux \cdot Ux)(x + \Delta x)) \cdot \Delta y \\ &+ ((\rho \cdot Ux \cdot Uy)(y) - (\rho \cdot Ux \cdot Uy)(y + \Delta y)) \cdot \Delta x \\ &+ ((P - \tau_{xx})(x) - (P - \tau_{xx})(x + \Delta x)) \cdot \Delta y \\ &- (\tau_{xy}(y) - \tau_{xy}(y + \Delta y)) \cdot \Delta x \\ &+ \rho \cdot g_x \cdot \Delta x \cdot \Delta y \end{aligned} \quad (\text{A.7})$$

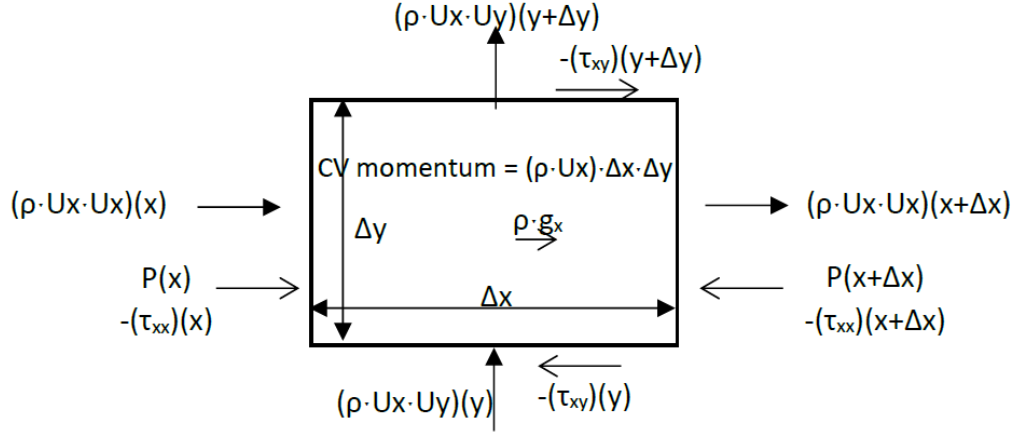


Figure A.2: Force-momentum principle applied to a control volume (here for the  $U_x$  component of the velocity).  $g_x$  represents any forces exterior to CV.

Dividing by  $\Delta x \cdot \Delta y$  leads to:

$$\begin{aligned}
\frac{\partial(\rho \cdot U_x)}{\partial t} &= \frac{(\rho \cdot U_x \cdot U_x)(x) - (\rho \cdot U_x \cdot U_x)(x + \Delta x)}{\Delta x} \\
&+ \frac{(\rho \cdot U_x \cdot U_y)(y) - (\rho \cdot U_x \cdot U_y)(y + \Delta y)}{\Delta y} \\
&+ \frac{P(x) - P(x + \Delta x)}{\Delta x} \\
&- \frac{\tau_{xx}(x) - \tau_{xx}(x + \Delta x)}{\Delta x} \\
&- \frac{(\tau_{xy}(y) - \tau_{xy}(y + \Delta y))}{\Delta y} \\
&+ \rho g_x
\end{aligned} \tag{A.8}$$

Using Taylor series first order expansion (see Eq. A.3), the  $U_x$  momentum equation becomes:

$$\begin{aligned}
\frac{\partial(\rho \cdot U_x)}{\partial t} &= \frac{-\partial(\rho \cdot U_x \cdot U_x)}{\partial x} - \frac{\partial(\rho \cdot U_x \cdot U_y)}{\partial y} \\
&- \frac{\partial(P)}{\partial x} + \frac{\partial\tau_{xx}}{\partial x} + \frac{\partial\tau_{xy}}{\partial y} + \rho \cdot g_x
\end{aligned} \tag{A.9}$$

## A.2 Momentum equation

---

In 3 dimensions, the Ux momentum equations becomes:

$$\begin{aligned} \frac{\partial(\rho \cdot Ux)}{\partial t} = & - \frac{\partial(\rho \cdot Ux \cdot Ux)}{\partial x} - \frac{\partial(\rho \cdot Ux \cdot Uy)}{\partial y} - \frac{\partial(\rho \cdot Ux \cdot Uz)}{\partial z} \\ & - \frac{\partial(P)}{\partial x} + \frac{\partial\tau_{xx}}{\partial x} + \frac{\partial\tau_{xy}}{\partial y} + \frac{\partial\tau_{xz}}{\partial z} + \rho \cdot g_x \end{aligned} \quad (\text{A.10})$$

The general form of the Navier-Stokes momentum equation can then be expressed as (same as Eq. 2.3):

$$\frac{\partial(\rho \cdot U)}{\partial t} + \nabla \cdot (\rho U U) = -\nabla P + \nabla \cdot \tau + \rho \cdot g \quad (\text{A.11})$$

For a Newtonian fluid (viscosity  $\mu=\text{constant}$ ) and assuming an incompressible flow (density  $\rho=\text{constant}$ ), the viscous stress can be considered linearly related to the strain rate. The expression for the strain rate tensor is:

$$\tau = \begin{bmatrix} 2\mu \frac{\partial Ux}{\partial x} & \mu \left( \frac{\partial Ux}{\partial y} + \frac{\partial Uy}{\partial x} \right) & \mu \left( \frac{\partial Ux}{\partial z} + \frac{\partial Uz}{\partial x} \right) \\ \mu \left( \frac{\partial Uy}{\partial x} + \frac{\partial Ux}{\partial y} \right) & 2\mu \frac{\partial Uy}{\partial y} & \mu \left( \frac{\partial Uy}{\partial z} + \frac{\partial Uz}{\partial y} \right) \\ \mu \left( \frac{\partial Uz}{\partial x} + \frac{\partial Ux}{\partial z} \right) & \mu \left( \frac{\partial Uz}{\partial y} + \frac{\partial Uy}{\partial z} \right) & 2\mu \frac{\partial Uz}{\partial z} \end{bmatrix} \quad (\text{A.12})$$

The incompressible Ux momentum equations becomes:

$$\begin{aligned} \rho \left( \frac{\partial Ux}{\partial t} + \frac{\partial(Ux \cdot Ux)}{\partial x} + \frac{\partial(Ux \cdot Uy)}{\partial y} + \frac{\partial(Ux \cdot Uz)}{\partial z} \right) = & - \frac{\partial P}{\partial x} + \rho \cdot g_x \\ + \frac{\partial}{\partial x} \left( 2\mu \frac{\partial Ux}{\partial x} \right) + \frac{\partial}{\partial y} \left( \mu \left( \frac{\partial Ux}{\partial y} + \frac{\partial Uy}{\partial x} \right) \right) + \frac{\partial}{\partial z} \left( \mu \left( \frac{\partial Ux}{\partial z} + \frac{\partial Uz}{\partial x} \right) \right) \end{aligned} \quad (\text{A.13})$$

The stress tensor terms can be rearranged as:

$$\begin{aligned} & \frac{\partial}{\partial x} \left( 2\mu \frac{\partial Ux}{\partial x} \right) + \frac{\partial}{\partial y} \left( \mu \left( \frac{\partial Ux}{\partial y} + \frac{\partial Uy}{\partial x} \right) \right) + \frac{\partial}{\partial z} \left( \mu \left( \frac{\partial Ux}{\partial z} + \frac{\partial Uz}{\partial x} \right) \right) \\ & = 2\mu \frac{\partial}{\partial x} \left( \frac{\partial Ux}{\partial x} \right) + \mu \frac{\partial}{\partial y} \left( \frac{\partial Ux}{\partial y} \right) + \mu \frac{\partial}{\partial y} \left( \frac{\partial Uy}{\partial x} \right) + \mu \frac{\partial}{\partial z} \left( \frac{\partial Ux}{\partial z} \right) + \mu \frac{\partial}{\partial z} \left( \frac{\partial Uz}{\partial x} \right) \\ & = \mu \frac{\partial^2 Ux}{\partial x^2} + \mu \frac{\partial^2 Uy}{\partial y^2} + \mu \frac{\partial^2 Uz}{\partial z^2} + \mu \frac{\partial}{\partial x} \left( \frac{\partial Ux}{\partial x} + \frac{\partial Uy}{\partial y} + \frac{\partial Uz}{\partial z} \right) \xrightarrow{0 \text{ (continuity equation)}} \\ & = \mu \frac{\partial^2 Ux}{\partial x^2} + \mu \frac{\partial^2 Uy}{\partial y^2} + \mu \frac{\partial^2 Uz}{\partial z^2} \end{aligned} \quad (\text{A.14})$$

The incompressible Ux momentum equations is then:

$$\begin{aligned} \rho \left( \frac{\partial U_x}{\partial t} + \frac{\partial(U_x \cdot U_x)}{\partial x} + \frac{\partial(U_x \cdot U_y)}{\partial y} + \frac{\partial(U_x \cdot U_z)}{\partial z} \right) \\ = -\frac{\partial P}{\partial x} + \rho \cdot g_x + \mu \left( \frac{\partial^2 U_x}{\partial x^2} + \frac{\partial^2 U_y}{\partial y^2} + \frac{\partial^2 U_z}{\partial z^2} \right) \end{aligned} \quad (\text{A.15})$$

The associated general form of the incompressible equation is:

$$\rho \frac{\partial U}{\partial t} = -\nabla P + \rho \cdot g + \mu \nabla^2 U \quad (\text{A.16})$$

Diving Eq. A.15 by  $\rho$  and assuming constant density gives:

$$\begin{aligned} \frac{\partial U_x}{\partial t} + \frac{\partial(U_x \cdot U_x)}{\partial x} + \frac{\partial(U_x \cdot U_y)}{\partial y} + \frac{\partial(U_x \cdot U_z)}{\partial z} \\ = -\frac{1}{\rho} \frac{\partial P}{\partial x} + \nu \left( \frac{\partial^2 U_x}{\partial x^2} + \frac{\partial^2 U_y}{\partial y^2} + \frac{\partial^2 U_z}{\partial z^2} \right) \end{aligned} \quad (\text{A.17})$$

Using the same notation as Eq. 2.6 (i = x and j = x, y and z):

$$\frac{\partial U_i}{\partial t} + \frac{\partial(U_i U_j)}{\partial x_i} = -\frac{1}{\rho} \frac{\partial P}{\partial x_i} + \nu \frac{\partial}{\partial x_i} \left( \frac{\partial U_i}{\partial x_j} \right) \quad (\text{A.18})$$

# Appendix B

## Wind averaged maps

### B.1 Wind averaged concentration maps

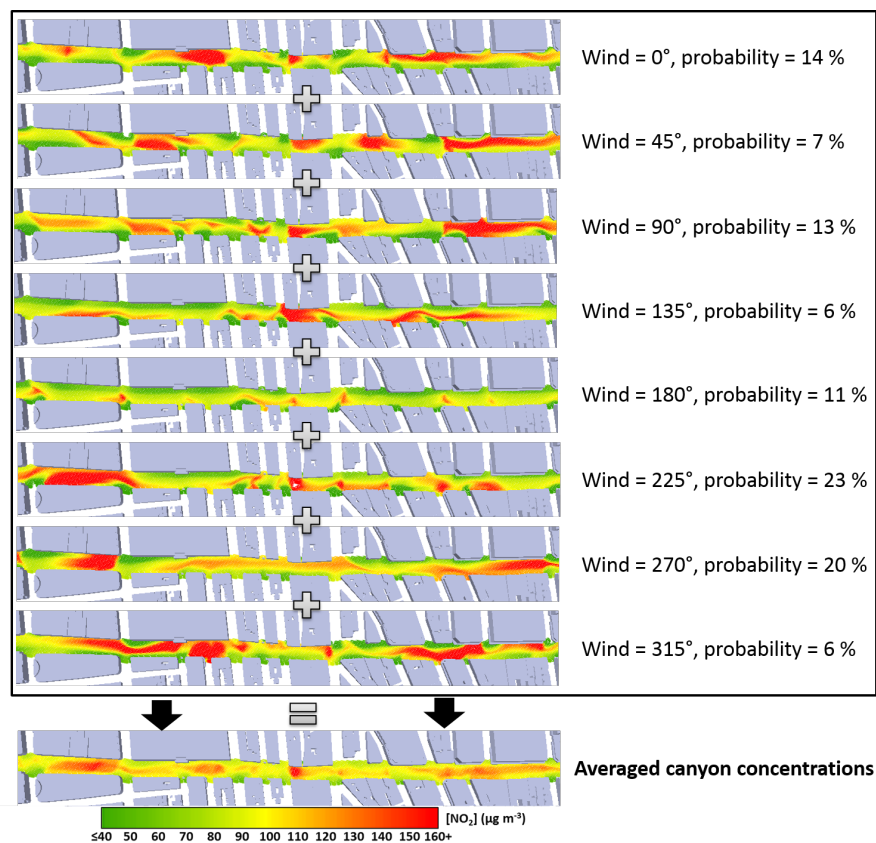


Figure B.1: Chronology followed to produce an averaged concentrations map (here NO<sub>2</sub> results from Chapter 6). 8 wind directions are averaged depending on the prevailing wind directions percentages and aggregated into a single average.

Fig. B.1 details the chronology of how each wind averaged maps are produced. Here 8 wind directions are averaged depending on the prevailing wind directions percentages and aggregated into a single average.

## **B.2 Wind averaged concentration difference maps**

### **B.2.1 Processing steps**

A similar methodology is followed to produce wind averaged concentration difference maps. For each wind direction, the modelling output of a city with trees is subtracted to a tree-free city (which can then be divided by the average scalar concentrations for the tree-free city for percentages calculation). This produces multiple difference maps for each wind directions which are then aggregated into a single averaged difference maps (see Fig. B.2).

### **B.2.2 Wind direction dependence**

This section reports the wind direction dependence on the normalised scalar concentrations difference (data from Chapter 4).

## B.2 Wind averaged concentration difference maps

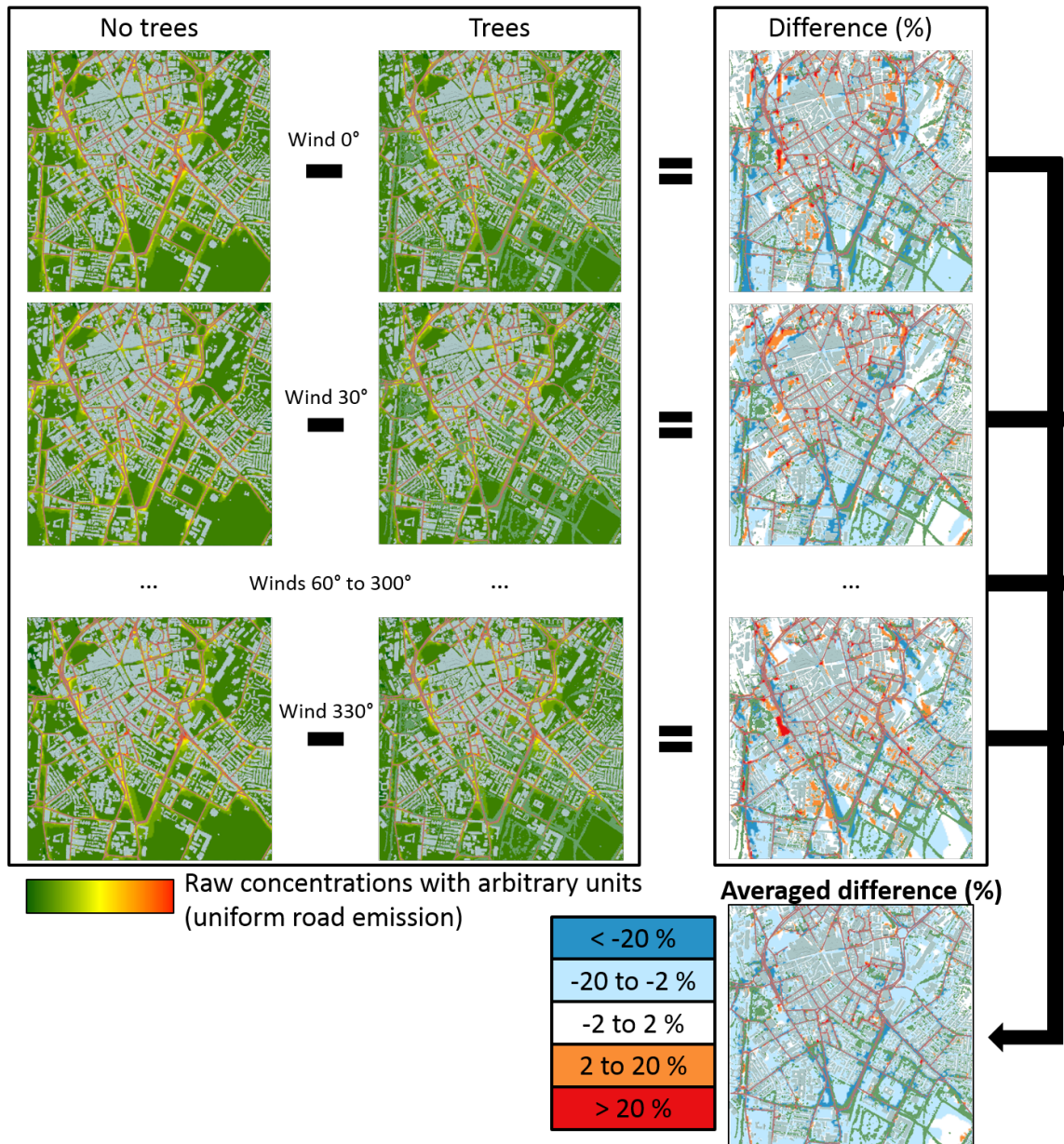


Figure B.2: Steps showing how are obtained average difference maps. Percentages difference are obtained by dividing the difference of a tree-free city with a city with trees by the average scalar concentrations for the tree-free city.

## B.2 Wind averaged concentration difference maps

---

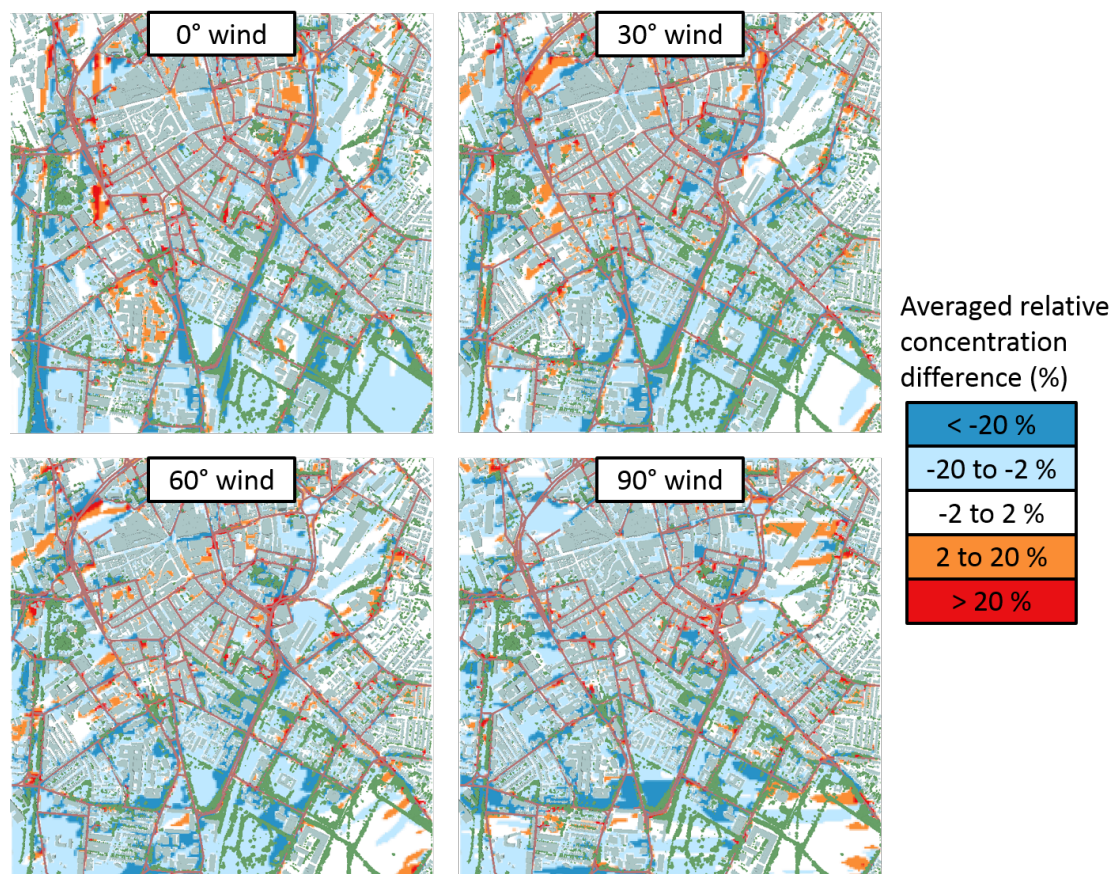


Figure B.3: Wind direction dependence on the normalised scalar concentrations difference (see Fig. B.6 for the averaged map). Here are shown the wind directions of  $0^\circ$ ,  $30^\circ$ ,  $60^\circ$  and  $90^\circ$ .

## B.2 Wind averaged concentration difference maps

---

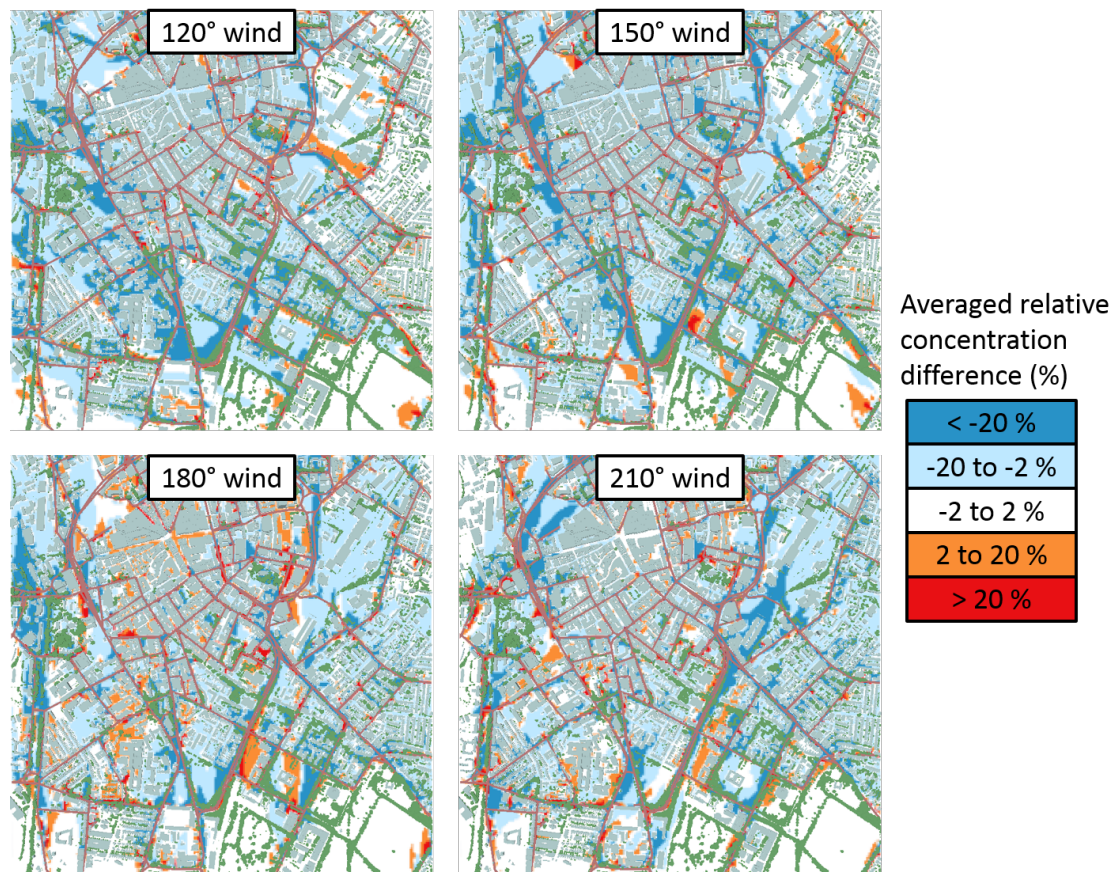


Figure B.4: Wind direction dependence on the normalised scalar concentrations difference (see Fig. B.6 for the averaged map). Here are shown the wind directions of 120°, 150°, 180° and 210°.

## B.2 Wind averaged concentration difference maps

---

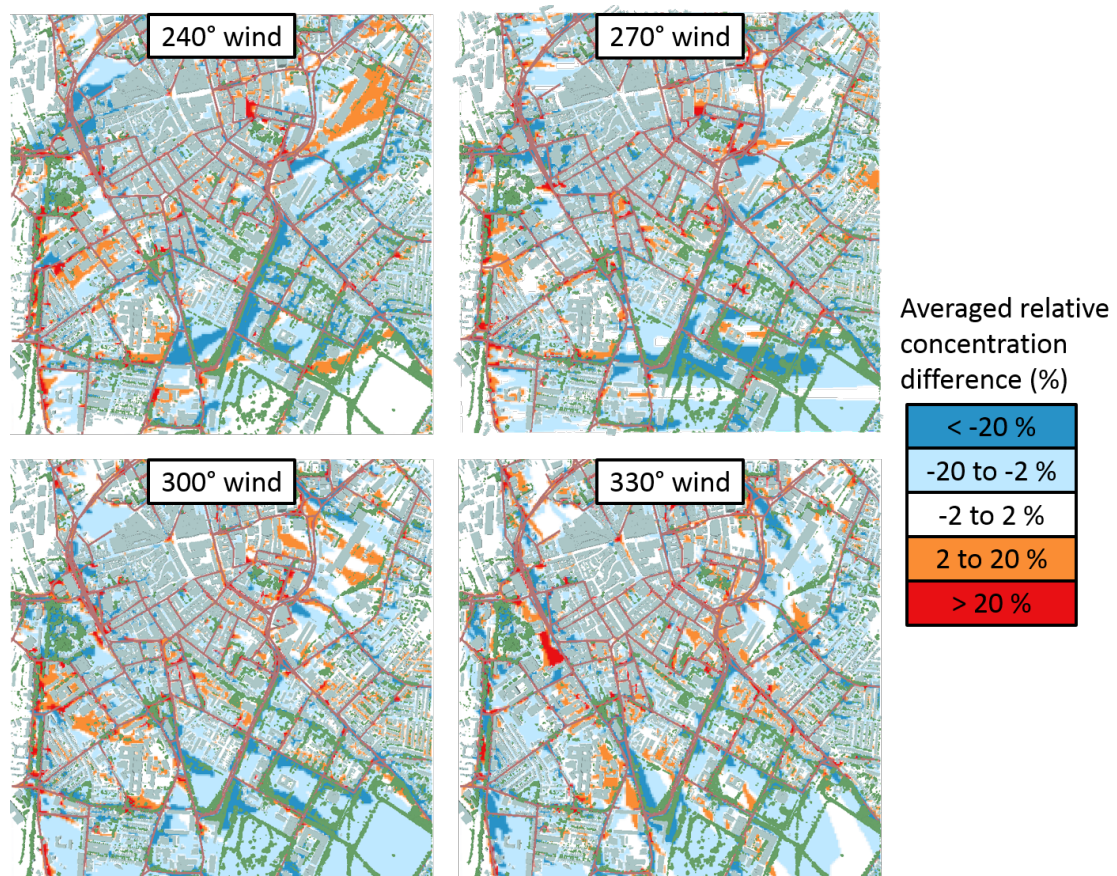


Figure B.5: Wind direction dependence on the normalised scalar concentrations difference (see Fig. B.6 for the averaged map). Here are shown the wind directions of 240°, 270°, 300° and 330°.

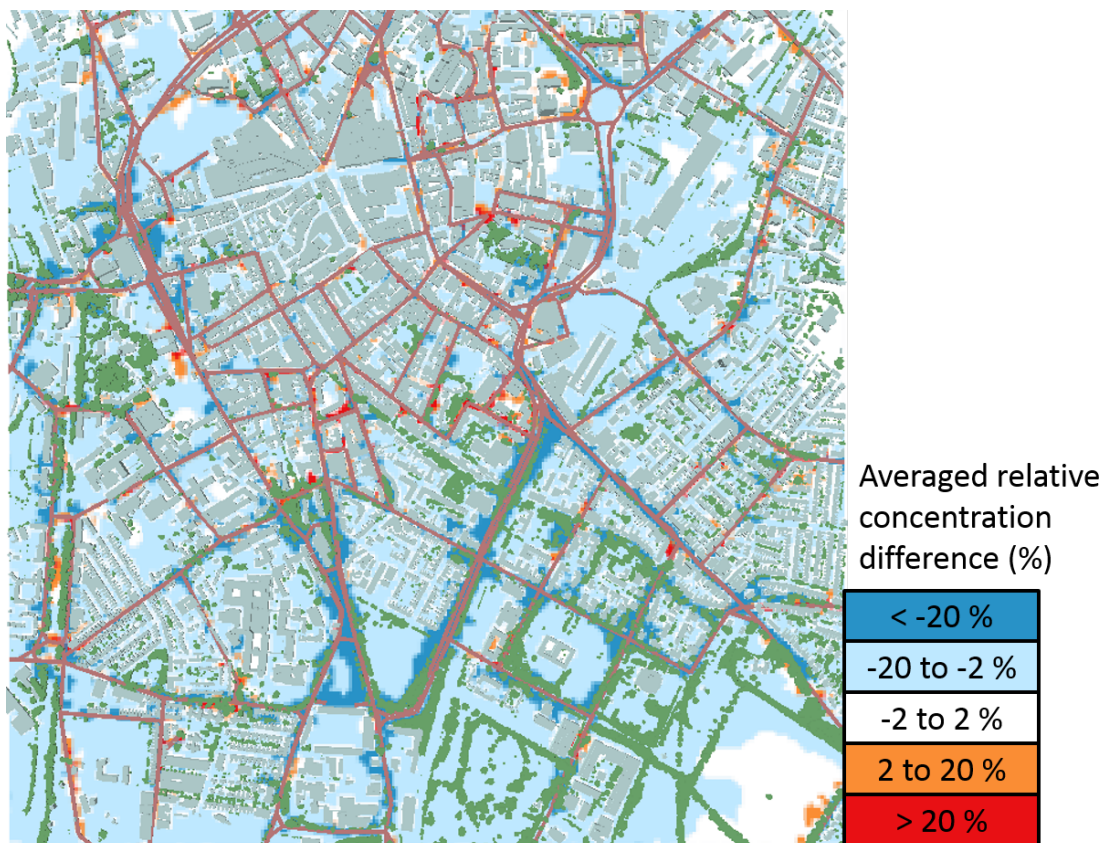


Figure B.6: Modelling output of the normalised scalar concentration difference  $\Delta C^*$  at a height of 1.5 m averaged uniformly over 12 wind directions (same Figure as Fig. 4.3).

# Appendix C

## Model real scale application and validation over a landfill site

*This work was made possible by the contributions of Dr James C Matthews, Dr Matthew D Wright, Dr Damien Martin and Prof Dudley Shallcross (University of Bristol, UK) for the tracer experiment. Dr David Hodgetts (University of Manchester, UK) realised the LIDAR site survey and Dr Grant Allen (University of Manchester, UK) supervised the whole project.*

Although the focus of this thesis is urban air quality, the scope was slightly extended to reproduce a tracer experiment over a landfill site in order to validate the CFD model in a real outdoor environment. A second objective was to assess the CFD model suitability of quantifying the methane that is being emitted from landfills. To evaluate the performance of the CFD dispersion model, a tracer release experiment of PMCH (perfluoromethylcyclohexane) was conducted. PMCH concentrations were measured and then compared to the concentrations simulated by the CFD model. This study was conducted by first distributing the wind into different classes of speeds and directions and then using these values to average a wide range of CFD simulations. A 1 m LIDAR (LIght Detection And Ranging) terrain model was used to build the 3D structure of the landfill site. The CFD model was able to reconstruct the measured PMCH concentrations with an overall model bias of 36 %.

### C.1 Introduction

Methane is an atmospheric greenhouse gas released from decomposing waste in landfill sites and is a well known contributor to global warming. Quantifying the landfill

methane emissions in the UK has been the object of recent attention of institutional bodies like the Department of Energy and Climate Change (DECC, 2015a,b).

A large range of gas dispersion models currently exist, including CFD and Gaussian models, each with their own strengths and limitations with regard to the variation in the temporal and spatial measurements required to model landfill emissions. These measurements of landfill emissions for instance can be obtained via eddy covariance (Lohila et al., 2007), enclosure (Czepiel et al., 1996), chamber grid (Börjesson et al., 2000; Sanci and Panarello, 2012), tracer experiment (Scheutz et al., 2011; Mønster et al., 2014) or a combination of these methods.

The complexity of the task of initially setting up the CFD simulation tends to make CFD less frequently used than Gaussian dispersion models. Nevertheless, CFD simulations have the advantage in that they can better deal with complex shapes like buildings, edges and uneven terrain. In this study for instance, modelling the topography of the landfill site which was situated in a pit, made CFD an ideal choice (Fig. C.1a). CFD dispersion models are usually used in the urban environment (Vardoulakis et al., 2003). Dispersion modelling studies over landfill sites have been limited, because CFD has traditionally been applied in urban environment contexts. Torno et al. (2011) show that a CFD model could be used to illustrate concentrations of dust particles in a landfill, using a high resolution terrain retrieved by LIDAR. However a clear idea of the performance and accuracy of CFD gas dispersion model over a landfill terrain has not been found in the literature.

The work presented in this chapter focuses on the validation of a CFD dispersion model over a landfill site by finely dividing wind speeds and directional distributions. The approach presented here uses multiple CFD simulations for a range of wind speeds (every 1 m/s) and directions (every  $7.5^\circ$ ) in order to estimate reliable simulated concentrations. To evaluate its performance, a tracer release experiment of PMCH ( $C_7H_{14}$ , perfluoromethylcyclohexane) was conducted. Measured tracer concentrations were then compared with simulated concentrations. The use of PMCH as a tracer gas has been established in the current literature (Martin et al., 2010a,b, 2011) which makes it suitable for the use of verification of the CFD model. PMCH was chosen as a tracer due to its low background concentration and ability to be detected in small volumes.

## C.2 Site description and survey

The landfill site on which the study is conducted is located near Ipswich in England, UK. The landfill overview from Bing Maps can be seen in Fig. C.1a. The digital surface model was obtained from a terrestrial LIDAR survey with a submeter accuracy for the global georeferencing. A more detailed summary of the use and processing of this kind of LIDAR data can be found in Hodgetts (2013). The resulting digital surface model was then resampled into a 1 m grid, which in turn was extended using a 5.0 m digital elevation model from the Ordnance Survey (the UK government agency responsible for topographic survey and mapping of Great Britain) to extend the studied area as shown in Fig. C.1b. The terrain was then exported as a 3 dimensional stl (STereoLithography) file. This file format is compatible with the CFD software and can be incorporated as a base terrain.

## C.3 Tracer release experiment

### C.3.1 Tracer release test

A gas tracer release was carried out on the 5<sup>th</sup> of August 2014, between 14:27 pm and 14:54 pm (GMT). The average temperature during the experiment was 293.1 K (20.1°C). PMCH was released from a point source with a constant emission rate of  $4.48 \times 10^{-5}$  g/s, from a gas mixture of 0.171% PMCH in air. The gas mixture was provided by F2 Chemicals Ltd (UK) and is certified to +/-5% accuracy. The location of the tracer emission was an Easting of 610866 and Northing of 250008 in British National Grid (BNG) coordinates, with a height of 0.5 m from the ground (see Fig. C.1a). The emission velocity from which the tracer gas was emitted was 1.2 m/s.

### C.3.2 Gas sampling

Gas samples were collected for 15 minutes during the tracer release (14:35 - 14:50 GMT) to gain concentrations of the plume during release. The sample time started 5 minutes after which the tracer release started. Wind speeds greater than 2 m/s limit the impact of the transport time on the result (the maximum distance between release point and measurement location is less than 500 m). Previous tracer campaigns (e.g. Martin et al. 2010a,b) sampled concentrations of gas during the

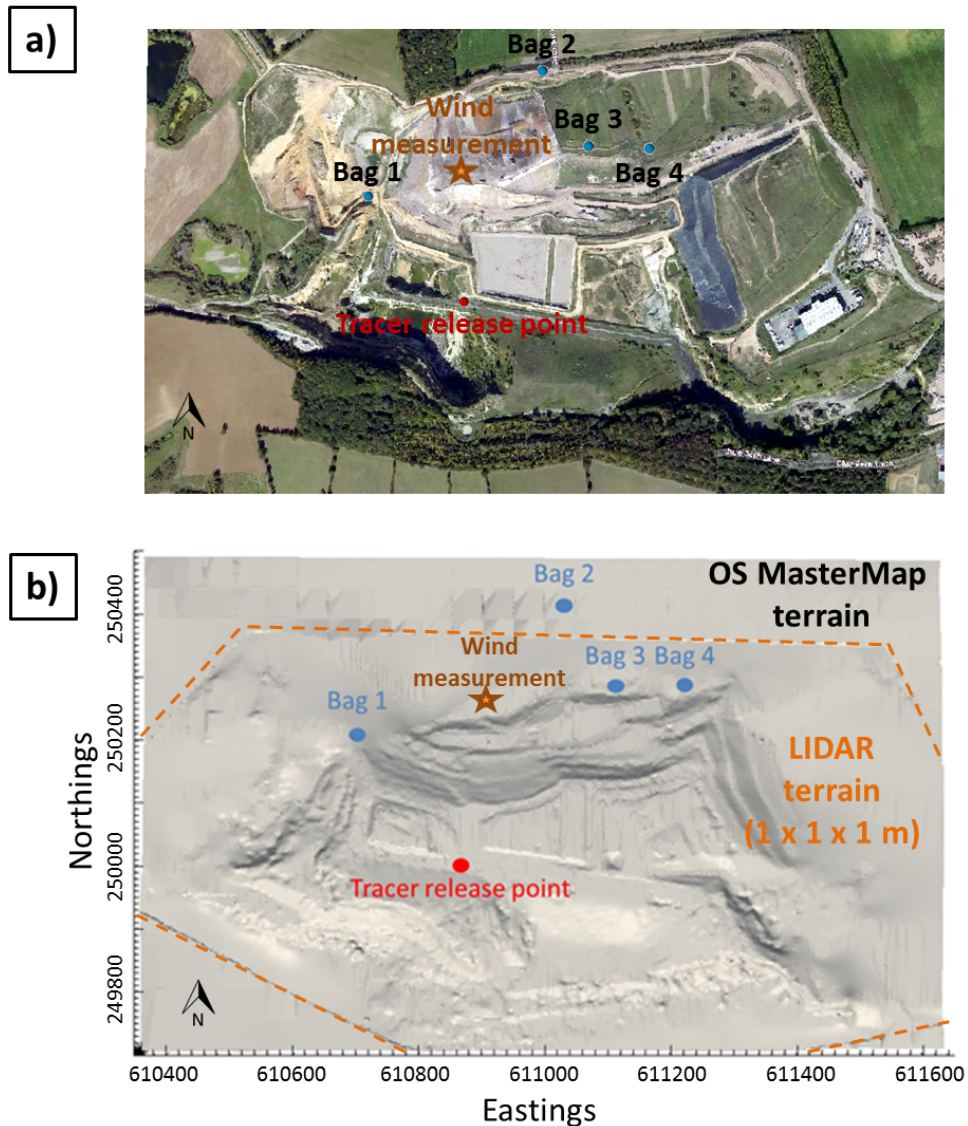


Figure C.1: (a) View of the landfill site (image credit: Bing Maps). (b) Combined LIDAR (1 m resolution) and OS MasterMAP terrain (50×50×5 m resolution) dataset used for the CFD simulations (British National Grid coordinates).

whole release and afterwards to catch the whole plume. In this study, the samples were retrieved during the plume release to simulate a sample of a continuous release as opposed to a ‘puff’ release (e.g. Wood et al. 2009; Martin et al. 2011). Four samples were then collected in Tedlar bags provided by SKC Ltd (UK) to measure the PMCH concentration in different locations. Samples of approximately 7.5 L were collected at a sampling rate of 0.5 litre per minute for the 15 minutes during the release, sampling the overall concentration over that time. The flow rate was

controlled by a mass flow controller to ensure a constant air flow. More details of the sampling system is available at the following references (Simmonds et al., 1995; Cooke et al., 2001). The sample pumps of the 4 sampling bags were programmed to start simultaneously with the help of timers which were accurate to within a second. The locations of the tracer release and the bag samples are shown in Fig. C.1b. The wind was from a Southerly direction during the experiment (see Fig. C.2), this explains the Northerly location of the sample bags from the release point.

### C.3.3 Wind monitoring

The wind speeds and directions were measured by sonic wind anemometer on the border of the landfill pit and at a height of 2.5 m (see Fig. C.1a,b). Wind measurements were taken 20 times per second. The wind speeds in the CFD model were then set-up to match the recorded wind speeds at the same height and location. When applied to urban environment, CFD simulations tend to be computationally demanding to run due to the increased complexity of the mesh (buildings, etc). They are therefore only performed for a limited number of wind speeds and wind direction, for instance every  $22.5^\circ$  (Santiago et al., 2013) or every  $45^\circ$  at 3 different wind speeds (Mumovic et al., 2006).

## C.4 CFD modelling

### C.4.1 Method

CFD simulations were performed under the OpenFOAM software platform. For calculating the wind flow, the Reynolds-averaged Navier-Stokes (RANS)  $k - \epsilon$  model was used. The CFD model used in this study has already been validated by being compared to wind tunnel measurements (Jeanjean et al., 2015) but has not been validated in real conditions over a complex terrain, which is the case in this study.

The mean velocity boundary flow ( $u(z)$ ) and the turbulent dissipation were set up to follow a logarithmic law using the `ABLIInletVelocity` and `ABLIInletEpsilon` utilities in OpenFOAM (Eq. (2.19) and (2.20)). The top boundary condition of the domain was setup as a symmetry condition. The inlets (representing the air going in the domain) and outlets (air going out of the domain) were adjusted depending on the simulated wind conditions. For example, to simulate a South Easterly wind, the two inlets would be the South and Eastern sides of the landfill domain and the

outlets would be the Northern and Western sides. A wall function was used for the ground to reproduce the landfill surface roughness. A roughness length value of 0.03 m was used to model the landfill terrain. This roughness length value corresponds to an open terrain with grass and a few isolated obstacles (WMO, 2008).

The total number of cells used for the simulation numbered 142 000. The boundaries used for the mesh are (in BNG, minimum to maximum): X=[610350 611650], Y=[249700 250500], Z=[0 500]. The initial cells of the domain were assigned a dimension of 30 m. The cells corresponding to the terrain (ground) were assigned a size of 7 m and were kept constant up to 30 m away from the ground. Their resolutions were then coarsened beyond 30 m with a maximum expansion ratio of 1.3. No data was found in the current literature to parameterise a mesh for CFD simulation over a landfill site, so the criterion for cell size was derived from previous CFD validation studies against wind tunnel measurements (Jeanjean et al., 2015). The turbulent Schmidt number ( $Sc_t$ ) is known to have an important impact on the dispersion and its value can be set between 0.3 to 1.3 (Tominaga and Stathopoulos, 2007). A model sensitivity analysis was performed and a  $Sc_t$  of 0.7 was found to give the most satisfactory results (see section C.5.4). The PMCH tracer emission rate was of  $4.48 \times 10^{-5}$  g/s. The units used in the CFD model for the PMCH concentrations were in  $g/m^3$ . In order to convert final concentrations to mixing ratios in ppqv the CFD modelled concentrations of PMCH were translated in a post processing stage such that

$$[PMCH](ppqv) = \left( \frac{[PMCH](g/m^3)}{M_{PMCH}m_{air}} \right) 10^{15} \quad (C.1)$$

where  $M_{PMCH} = 350$  g/mol is the molar mass of PMCH,  $m_{air}$  is the molar gaseous concentration of air which was estimated to 41 mol/m<sup>3</sup> with the experimental conditions and a scaling factor of  $10^{15}$  then translates the results into ppqv.

### C.4.2 Additional modification of the method incorporated in OpenFOAM

Even if the release was carried out at low concentrations, PMCH is a gas around 12 times more dense than air necessitating the need to model the effect of buoyancy on the tracer dispersion. Released as a 0.2 % mixture in air, the PMCH release gas would be at most 2.5 % more dense than standard air. To take into account the

buoyancy, the OpenFOAM solver buoyantBoussinesqSimpleFoam (governing equations defined in Miao et al. 2013) was used and modified for this study. Originally, the definition of buoyantBoussinesqSimpleFoam allowed it to be affected a change of temperature. In this study, the effect of temperature on the buoyancy was assumed to be negligible (temperature constant over the domain) and the concentration of PMCH was set to change the buoyancy of air locally. The change of air density related to PMCH concentrations was defined such that

$$\frac{1}{\rho} = \frac{\xi}{\rho_{PMCH}} + \frac{1 - \xi}{\rho_{air}} \quad (C.2)$$

where  $\rho$  is the modelled fluid density ( $\text{kg}/\text{m}^3$ ),  $\xi$  is the molar fraction of PMCH,  $\rho_{PMCH}$  is the density of PMCH ( $\text{kg}/\text{m}^3$ ) and  $\rho_{air} = 1.2 \text{ kg}/\text{m}^3$  is the density of air at  $20.1^\circ\text{C}$ . Note that here  $\xi$  is equal to  $10^{-15}$  which suggests that the change made on the density are negligible.

From this change in density the pressure is then corrected according to

$$p^* = p_{rgh} + \rho_k g h \quad (C.3)$$

with

$$\rho_k = 1.0 + \xi \left( \frac{\rho_{air}}{\rho_{PMCH}} - 1 \right) \quad (C.4)$$

where  $p^*$  is the modelled air pressure ( $p^* = p/\rho$  in  $\text{m}^2/\text{s}^2$ ),  $p_{rgh}$  is the dynamic pressure ( $\text{m}^2/\text{s}^2$ ),  $\rho_k$  is defined as the change of kinematic density in OpenFOAM,  $g$  is the gravity ( $\text{m}/\text{s}^2$ ) and  $h$  the height (m). Note that Eq. C.3 and Eq. C.4 are Favre averaged ( $\rho$ -normalised).

## C.5 Results

### C.5.1 Experimental wind conditions

Table C.1 and Fig. C.2 show the wind speed and wind directions observed during the experiment. The wind blew mainly at wind speeds between 2 and 5 m/s and from a Southerly direction.

In the case of an open terrain configuration, as for this study on the landfill site, the decreased complexity of the mesh allows an increase in the number of simulations. A first attempt was made to divide the wind directions every  $22.5^\circ$ ,

but the accuracy of the results was found to be limited (see Tab. C.4). The wind directions were then divided every  $7.5^\circ$  and the wind speeds were separated into 5 classes. The simulations were carried out with the average wind speed of the class (e.g. 2.5, 3.5, 4.5 and 5.5 m/s). The wind speeds below 2 m/s were not taken into account in the simulations as their percentages of occurrence were negligible. The simulations were then performed for wind directions every  $7.5^\circ$  between  $127.5^\circ$  and  $232.5^\circ$ . The wind directions outside this range were neglected (presence  $< 1\%$ ). These assumptions led to a total number of 60 simulations (15 wind directions and 4 different wind speeds).

Wind speed classes (m/s)	Percentage (%)
$0 \leq ws < 2$	Negligible
$2 \leq ws < 3$	18.7
$3 \leq ws < 4$	35.0
$4 \leq ws < 5$	30.5
$5 \leq ws$	15.8

Table C.1: Distribution of wind speed classes observed during the tracer experiment.

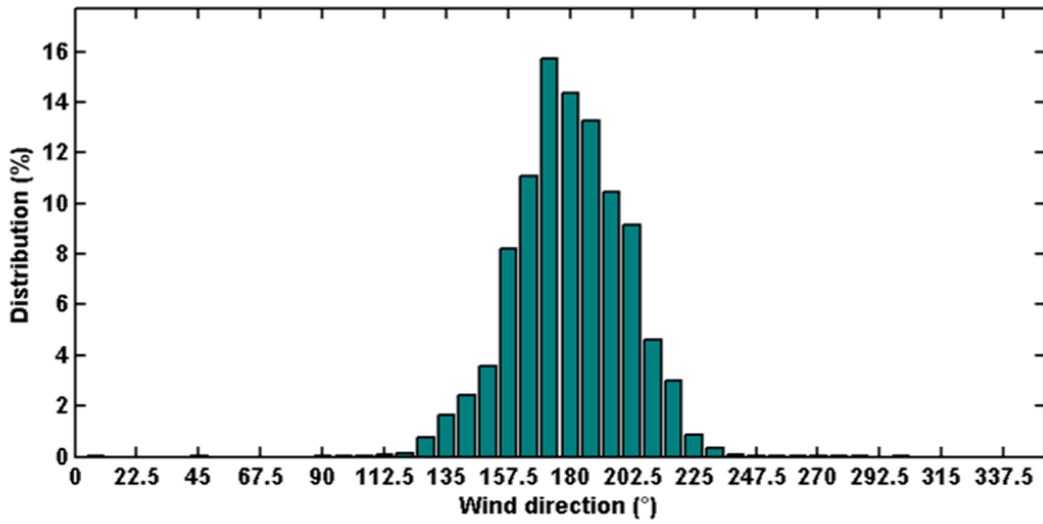


Figure C.2: Distribution of wind directions divided every  $7.5^\circ$  observed during the tracer experiment. 15 wind directions were simulated between  $127.5^\circ$  and  $232.5^\circ$ .

<b>Bags</b>	<b>Northing</b>	<b>Easting</b>	<b>Measured concentrations (ppqv)</b>
<b>B1</b>	250200	610680	177
<b>B2</b>	250431	611014	49
<b>B3</b>	250295	611103	44
<b>B4</b>	250292	611212	16

Table C.2: PMCH sample bags coordinates

### C.5.2 Measured gas concentration

A background PMCH concentration of 24.6 ppqv (parts per quadrillion) was measured before the experiment and this amount was subtracted from the samples. The error of the sample bags was estimated to be less than 1 ppqv, which corresponds to the analytical error from the laboratory measurements. The measured concentrations of each of the sample bags is reported in Tab. C.2.

### C.5.3 CFD simulated concentrations and comparison with the measured data

The CFD simulations of PMCH dispersion were weighted according to their individual wind speeds and directional distributions. The final results of PMCH ground concentrations are reported in Fig. C.3, the PMCH sample bags coordinates are reported in Table C.2.

The comparison summary between the measured PMCH concentrations is shown in Fig. C.4. Gaussian dispersion models usually have an accuracy of a factor of 2.0 (Hanna et al., 2007; Korsakissok and Mallet, 2009). The performances of the dispersion models can be increased with the use of CFD simulations (Buccolieri and Sabatino, 2011). The simulated tracer concentrations for bags 1,2 and 3 are within a factor of 2.0 (FAC 2) of the measurements, a factor of 2.0 meaning that the modelled concentrations are no more than twice or half of the measured concentrations. The sample bags are situated well within the modelled plume (Fig. C.3). For lower PMCH concentrations that are located on the side of the plume, the modelled uncertainty tends to be greater (bag 4).

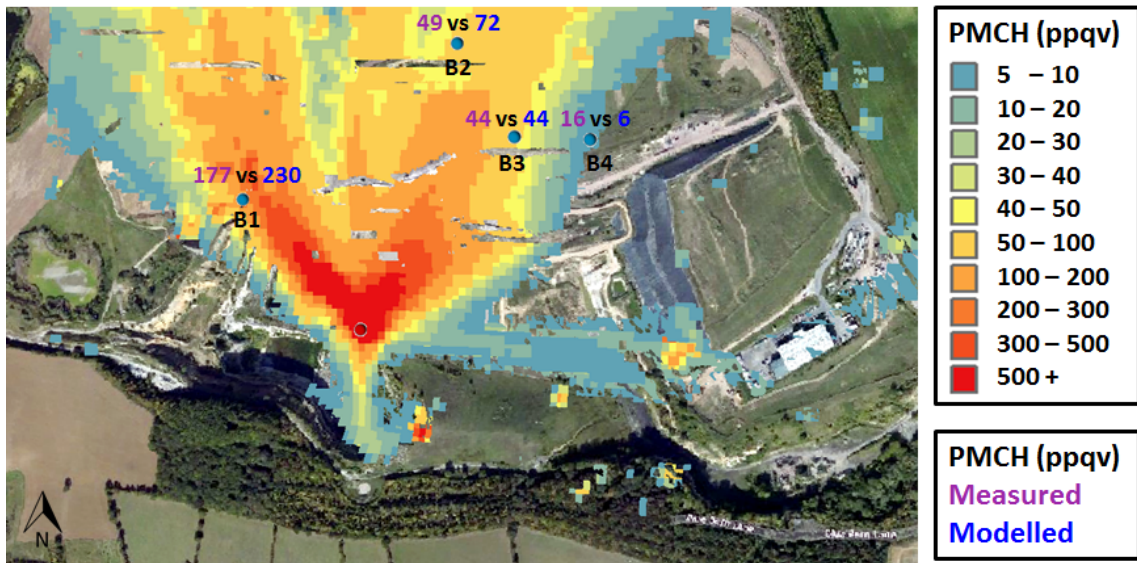


Figure C.3: PMCH modelled concentrations at ground level corresponding to the distributed wind classes of the tracer experiment. Measured tracer concentrations are compared to the modelled concentrations at each of the sampling locations (image credit: Bing Maps).

### C.5.4 Model sensitivity analysis

#### Impact of the turbulent Schmidt number

The  $Sc_t$  as expressed in Eq. 2.27 influences the modelled dispersion of the tracer by changing the eddy diffusion coefficient  $K$ . Lower  $Sc_t$  would increase  $K$  and then enhance the dispersion by turbulent transport. On the other hand, greater  $Sc_t$  would decrease the dispersion by turbulent transport. Tab. C.3 shows 4 model results produced for 4 different  $Sc_t$ . The difference between the modelled and measured tracer concentrations average across the 4 bags are very similar, ranging from a mean difference of 34.7 to 42.7 %.

Although the best results are observed for a  $Sc_t$  of 0.3 with a mean difference of 34.7 %, the choice of such a low  $Sc_t$  is not very common in the literature (Tominaga and Stathopoulos, 2007). It was then decided to use a  $Sc_t$  value of 0.7 in this study, which is in range with the values observed in other studies.

#### Impact of wind classes distribution

The impact of multiple wind directions (WD) and wind speeds (WS) between the measured and modelled tracer concentrations are shown in Tab. C.4. The reported

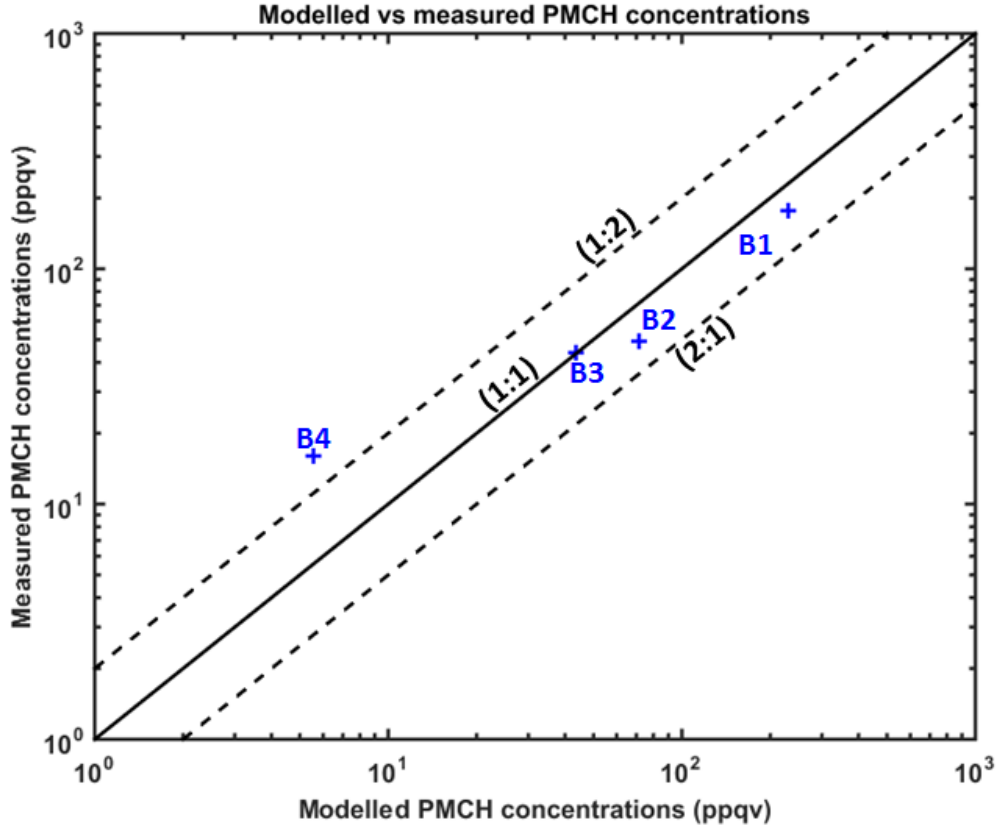


Figure C.4: Summary of measured PMCH concentrations compared to modelled PMCH concentrations. Errors of a factor of 2.0 (FAC2) are represented in dashed lines.

	Measured (ppqv)	Modelled							
		$Sc_t = 0.3$		$Sc_t = 0.5$		$Sc_t = 0.7$		$Sc_t = 1.0$	
		(ppqv)	dif. (%)						
<b>B1</b>	177	172.5	2.5	207.9	17.5	230.0	30.0	218.7	23.6
<b>B2</b>	49	50.5	3.1	58.7	19.9	71.8	46.5	75.1	53.3
<b>B3</b>	44	23.7	46	33.3	24.2	43.6	0.8	54.3	23.5
<b>B4</b>	16	2.1	87	3.0	81.2	5.6	65.2	4.7	70.3
	<b>mean dif.:</b>		<b>34.7</b>		<b>35.7</b>		<b>35.6</b>		<b>42.7</b>

Table C.3: Impact of the  $Sc_t$  on the modelled concentrations.

values have been averaged across the 4 bags. Better agreement are found by increasing the number of wind speeds and directions. Increasing the number of wind speed classes had a more limited impact on the modelling performance than increasing the number of wind directions. The worst model performance correspond to a single simulation with an average wind direction of  $180^\circ$  and a wind speed of 4.6 m/s.

## C.5 Results

---

By increasing the number of wind directions to 5 classes (wind distributed every  $22.5^\circ$  between  $135^\circ$  and  $225^\circ$ ), the average modelling error is improved by a factor of 2. The full wind distributions used in this studies (15 WD distributed every  $7.5^\circ$  between  $127^\circ$  and  $232^\circ$  and 4 WS modelled every 1 m/s) provide the best modelling performance with an average model error of 35.6 %. Note that a similar exercise was tried with the Gaussian dispersion model ADMS, which provided results similar to the CFD model using a non-buoyant solver.

	<b>1 WD 1 WS</b>	<b>5 WD 1 WS</b>	<b>5 WD 4 WS</b>	<b>15 WD 1 WS</b>	<b>15 WD 4 WS</b>
<b>Mean difference between modelled and measured tracer concentrations (%)</b>	98.0	51.7	51.3	38.6	35.6

Table C.4: Difference between modelled and measured tracer concentrations depending on the number of wind directions (WD) and wind speeds (WS).

## C.6 Conclusions

The approach taken uses wind speeds and directional distributions was successfully applied to reconstruct tracer concentrations during a 15 minute window. 60 CFD simulations were performed every  $7.5^\circ$  at 4 different wind speeds. Overall, the CFD model reconstruct the tracer concentrations with an accuracy of 36 %. A similar model accuracy was found in a previous CFD modelling study using the same dispersion model which was validated against wind tunnel measurements (Jeanjean et al., 2015). Using CFD as a tool to model landfill emissions is possible and could be used as a complementary method to tracer experiments in order to estimate gas fluxes from landfill. The CFD will produce dilution coefficients from the landfill depending on the wind speed and direction for any desired measurement locations. The measured concentrations will then be used to revert emissions sourced from the landfill site.

The CFD dispersion model was validated with a limited number of 4 sampling points using a single point source as an emission, which is not representative of a landfill surface. A further study with an increased number of sampling points would be beneficial. Ideally, the field data would have been made with different leaking points and with more measurements across different days. Even if limited, the experimental data still provide a useful validation dataset for a dispersion model. The presented CFD dispersion model has been shown to work over stable wind conditions. If this model happens to be used in combination with measurements made over a long period of time with stable and unstable wind conditions, data will need to be selected for the periods when the wind is stable to ensure proper performance.

# Bibliography

- Abhijith, K. and Gokhale, S.: Passive control potentials of trees and on-street parked cars in reduction of air pollution exposure in urban street canyons, *Environmental Pollution*, 204, 99–108, 2015.
- Al-Dabbous, A. N. and Kumar, P.: The influence of roadside vegetation barriers on airborne nanoparticles and pedestrians exposure under varying wind conditions, *Atmospheric Environment*, 90, 113–124, 2014.
- Amann, M., Bertok, I., Borcken-Kleefeld, J., Cofala, J., Hettelingh, J., Heyes, C., Holland, M., Kieseewetter, G., Klimont, Z., Rafaj, P., et al.: Policy scenarios for the revision of the thematic strategy on air pollution, IIASA, Vienna, 2013.
- Amorim, J., Rodrigues, V., Tavares, R., Valente, J., and Borrego, C.: CFD modelling of the aerodynamic effect of trees on urban air pollution dispersion, *Science of the Total Environment*, 461, 541–551, 2013a.
- Amorim, J. H., Valente, J., Cascão, P., Rodrigues, V., Pimentel, C., Miranda, A. I., and Borrego, C.: Pedestrian exposure to air pollution in cities: modeling the effect of roadside trees, *Advances in Meteorology*, 2013, 2013b.
- Anderson, J. D.: *Introduction to flight*, vol. 199, McGraw-Hill Boston, 2005.
- Arnfield, A. J.: Two decades of urban climate research: a review of turbulence, exchanges of energy and water, and the urban heat island, *International journal of climatology*, 23, 1–26, 2003.
- Baldauf, R., Thoma, E., Khlystov, A., Isakov, V., Bowker, G., Long, T., and Snow, R.: Impacts of noise barriers on near-road air quality, *Atmospheric Environment*, 42, 7502–7507, 2008.

## C.6 BIBLIOGRAPHY

---

- Balogh, M., Parente, A., and Benocci, C.: RANS simulation of ABL flow over complex terrains applying an enhanced  $k$ - $\epsilon$  model and wall function formulation: Implementation and comparison for Fluent and OpenFOAM, *Journal of wind engineering and industrial aerodynamics*, 104, 360–368, 2012.
- Barker, J. R.: *Progress and problems in atmospheric chemistry*, vol. 3, World Scientific, 1995.
- Barnes, M., Brade, T. K., Mackenzie, A. R., Whyatt, J., Carruthers, D., Stocker, J., Cai, X., and Hewitt, C.: Spatially-varying surface roughness and ground-level air quality in an operational dispersion model, *Environmental Pollution*, 185, 44–51, 2014.
- Barthelmie, R. J., Pryor, S. C., Frandsen, S. T., Hansen, K. S., Schepers, J. G., Rados, K., Schlez, W., Neubert, A., Jensen, L. E., and Neckelmann, S.: Quantifying the Impact of Wind Turbine Wakes on Power Output at Offshore Wind Farms, *Journal of Atmospheric and Oceanic Technology*, 27, 1302–1317, doi: 10.1175/2010JTECHA1398.1, 2010.
- Baumgardner, D., Varela, S., Escobedo, F. J., Chacalo, A., and Ochoa, C.: The role of a peri-urban forest on air quality improvement in the Mexico City megalopolis, *Environmental Pollution*, 163, 174–183, 2012.
- Beckett, K. P., Freer-Smith, P., and Taylor, G.: Urban woodlands: their role in reducing the effects of particulate pollution, *Environmental pollution*, 99, 347–360, 1998.
- Beckett, W. S., Russi, M. B., Haber, A. D., Rivkin, R. M., Sullivan, J. R., Tameroglu, Z., Mohsenin, V., and Leaderer, B. P.: Effect of nitrous acid on lung function in asthmatics: a chamber study., *Environmental Health Perspectives*, 103, 372, 1995.
- Bedjanian, Y. and El Zein, A.: Interaction of NO<sub>2</sub> with TiO<sub>2</sub> surface under UV irradiation: products study, *The Journal of Physical Chemistry A*, 116, 1758–1764, 2012.
- Blocken, B.: *Computational Fluid Dynamics for Urban Physics: Importance, scales, possibilities, limitations and ten tips and tricks towards accurate and reliable simulations*, *Building and Environment*, 91, 219–245, 2015.

## C.6 BIBLIOGRAPHY

---

- Blocken, B., Stathopoulos, T., and Carmeliet, J.: CFD simulation of the atmospheric boundary layer: wall function problems, *Atmospheric environment*, 41, 238–252, 2007.
- Bluesky: National Tree Map Specification, [http://www.emapsite.com/downloads/product\\_guides/NTM-Specification.pdf](http://www.emapsite.com/downloads/product_guides/NTM-Specification.pdf), 2014.
- Boonen, E. and Beeldens, A.: Recent Photocatalytic Applications for Air Purification in Belgium, *Coatings*, 4, 553–573, 2014.
- Börjesson, G., Danielsson, A., and Svensson, B. H.: Methane fluxes from a Swedish landfill determined by geostatistical treatment of static chamber measurements, *Environmental Science & Technology*, 34, 4044–4050, 2000.
- Brantley, H. L., Hagler, G. S., Deshmukh, P. J., and Baldauf, R. W.: Field assessment of the effects of roadside vegetation on near-road black carbon and particulate matter, *Science of the Total Environment*, 468, 120–129, 2014.
- Breuninger, C., Meixner, F., and Kesselmeier, J.: Field investigations of nitrogen dioxide (NO<sub>2</sub>) exchange between plants and the atmosphere, *Atmospheric Chemistry and Physics*, 13, 773–790, 2013.
- Brunekreef, B. and Holgate, S. T.: Air pollution and health, *The lancet*, 360, 1233–1242, 2002.
- Buccolieri, R. and Sabatino, S. D.: MUST experiment simulations using CFD and integral models, *International Journal of Environment and Pollution*, 44, 376–384, 2011.
- Buccolieri, R., Gromke, C., Di Sabatino, S., and Ruck, B.: Aerodynamic effects of trees on pollutant concentration in street canyons, *Science of the Total Environment*, 407, 5247–5256, 2009.
- Buccolieri, R., Salim, S. M., Leo, L. S., Di Sabatino, S., Chan, A., Ielpo, P., de Genaro, G., and Gromke, C.: Analysis of local scale tree–atmosphere interaction on pollutant concentration in idealized street canyons and application to a real urban junction, *Atmospheric Environment*, 45, 1702–1713, 2011.
- Carruthers, D., Holroyd, R., Hunt, J., Weng, W., Robins, A., Apsley, D., Thompson, D., and Smith, F.: UK-ADMS: A new approach to modelling dispersion in the

## C.6 BIBLIOGRAPHY

---

- earth's atmospheric boundary layer, *Journal of wind engineering and industrial aerodynamics*, 52, 139–153, 1994.
- Castillo, J. E.: *Mathematical aspects of numerical grid generation*, vol. 8, Siam, 1991.
- Chan, C. K. and Yao, X.: Air pollution in mega cities in China, *Atmospheric Environment*, 42, 1–42, 2008.
- Charron, A. and Harrison, R. M.: Fine (PM<sub>2.5</sub>) and coarse (PM<sub>2.5-10</sub>) particulate matter on a heavily trafficked London highway: sources and processes, *Environmental science & technology*, 39, 7768–7776, 2005.
- Charron, A., Harrison, R. M., and Quincey, P.: What are the sources and conditions responsible for exceedences of the 24h PM<sub>10</sub> limit value ( $50\mu\text{gm}^{-3}$ ) at a heavily trafficked London site?, *Atmospheric Environment*, 41, 1960–1975, 2007.
- Chen, L., Liu, C., Zou, R., Yang, M., and Zhang, Z.: Experimental examination of effectiveness of vegetation as bio-filter of particulate matters in the urban environment, *Environmental Pollution*, 208, 198–208, 2016.
- Churchill, C. J. and Panesar, D. K.: Life-cycle cost analysis of highway noise barriers designed with photocatalytic cement, *Structure and Infrastructure Engineering*, 9, 983–998, 2013.
- Chuwah, C., van Noije, T., van Vuuren, D. P., Stehfest, E., and Hazeleger, W.: Global impacts of surface ozone changes on crop yields and land use, *Atmospheric Environment*, 106, 11–23, 2015.
- Cimorelli, A. J., Perry, S. G., Venkatram, A., Weil, J. C., Paine, R. J., and Peters, W. D.: *AERMOD—Description of model formulation*, U. S. Environmental Protection Agency, 1998.
- CODASC: Concentration Data of Street Canyon, <http://www.ifh.uni-karlsruhe.de/science/aerodyn/CODASC.htm>, 2014.
- Cofala, J. and Klimont, Z.: Emissions from households and other small combustion sources and their reduction potential, International Institute of Applied Systems Analysis (IIASA), Austria, 2012.

## C.6 BIBLIOGRAPHY

---

- Cooke, K. M., Simmonds, P. G., Nickless, G., and Makepeace, A.: Use of capillary gas chromatography with negative ion-chemical ionization mass spectrometry for the determination of perfluorocarbon tracers in the atmosphere, *Analytical chemistry*, 73, 4295–4300, 2001.
- Crosby, C., Fullen, M. A., Booth, C., and Searle, D.: A dynamic approach to urban road deposited sediment pollution monitoring (Marylebone Road, London, UK), *Journal of Applied Geophysics*, 105, 10–20, 2014.
- Czepiel, P., Mosher, B., Harriss, R., Shorter, J., McManus, J., Kolb, C., Allwine, E., and Lamb, B.: Landfill methane emissions measured by enclosure and atmospheric tracer methods, *Journal of Geophysical Research: Atmospheres* (1984–2012), 101, 16 711–16 719, 1996.
- Dai, A.: Drought under global warming: a review, *Wiley Interdisciplinary Reviews: Climate Change*, 2, 45–65, 2011.
- Davis, L. W.: The effect of driving restrictions on air quality in Mexico City, *Journal of Political Economy*, 116, 38–81, 2008.
- DECC: Review of UK-specific GHG Emission Factors And Update of IPCC Default Emission Factors, Report, UK Department for Environment, Food & Rural Affairs (DEFRA), 2015a.
- DECC: UK Greenhouse Gas and Air Quality Pollutant Inventory Improvement Programme: Analysis of volumes of landfill gas flared in the UK between 1990 and 2013, Report, UK Department for Environment, Food & Rural Affairs (DEFRA), 2015b.
- DEFRA: Air Quality Plans for the achievement of EU air quality limit values for nitrogen dioxide (NO<sub>2</sub>) in the UK, Department for Environment, Food and Rural Affairs, 2011a.
- DEFRA: Air Quality Plan for the achievement of EU air quality limit values for nitrogen dioxide (NO<sub>2</sub>) in Leicester Urban Area (UK0011), 2011b.
- DEFRA: Automatic Urban and Rural Network, data files for Leicester University monitoring site, [https://uk-air.defra.gov.uk/data/flat\\_files?site\\_id=LECU](https://uk-air.defra.gov.uk/data/flat_files?site_id=LECU), 2014a.

## C.6 BIBLIOGRAPHY

---

- DEFRA: Automatic Urban and Rural Network, data files for Marylebone monitoring site, [https://uk-air.defra.gov.uk/data/flat\\_files?site\\_id=MY1](https://uk-air.defra.gov.uk/data/flat_files?site_id=MY1), 2014b.
- DEFRA: Air Quality Plan for the achievement of EU air quality limit value for nitrogen dioxide (NO<sub>2</sub>) in Greater London Urban Area (UK0001), Tech. rep., UK Department for Environment, Food and Rural Affairs (DEFRA), 2015.
- DEFRA: Emissions Factors Toolkit, <http://laqm.defra.gov.uk/review-and-assessment/tools/emissions-factors-toolkit.html>, 2016.
- DEFRA: Paints and Surfaces for the Removal of Nitrogen Oxides, Tech. rep., UK Department for Environment, Food and Rural Affairs (DEFRA), 2016.
- Denby, B., Douros, I., and Fragkou, L.: Modelling of Nitrogen Dioxide (NO<sub>2</sub>) for air quality assessment and planning relevant to the European Air Quality Directive, in: FAIRMODE, Forum for air quality modelling in Europe, Version, vol. 3, 2011.
- Derwent, D., Fraser, A., Abbott, J., Jenkin, M., Willis, P., and Murrells, T.: Evaluating the performance of air quality models, Report prepared for the UK Department for Environment, Food and Rural Affairs, 2010.
- Dewan, A.: Reynolds-Averaged Governing Equations and Closure Problem, in: Tackling Turbulent Flows in Engineering, pp. 43–48, Springer, 2011.
- DfT: Road Traffic Forecasts 2015, 2015.
- DfT: Traffic counts: street-level traffic data, [www.dft.gov.uk/traffic-counts/](http://www.dft.gov.uk/traffic-counts/), 2016.
- Di Sabatino, S., Kastner-Klein, P., Berkowicz, R., Britter, R., and Fedorovich, E.: The modelling of turbulence from traffic in urban dispersion models—Part I: theoretical considerations, *Environmental Fluid Mechanics*, 3, 129–143, 2003.
- Di Sabatino, S., Leo, L. S., Cataldo, R., Ratti, C., and Britter, R. E.: Construction of digital elevation models for a southern European city and a comparative morphological analysis with respect to Northern European and North American cities, *Journal of Applied Meteorology and Climatology*, 49, 1377–1396, 2010.
- Donovan, R. G., Stewart, H. E., Owen, S. M., MacKenzie, A. R., and Hewitt, C. N.: Development and application of an urban tree air quality score for photochemical

## C.6 BIBLIOGRAPHY

---

- pollution episodes using the Birmingham, United Kingdom, area as a case study, *Environmental science & technology*, 39, 6730–6738, 2005.
- EEA: European Union Emission Inventory Report 1990–2011 under the UNECE Convention on Long-Range Transboundary Air Pollution (LRTAP), 2011.
- EEA: Air quality in Europe - 2015 report, 2015.
- EPA: The benefits and costs of the Clean Air Act, 1970 to 1990, 1997.
- EPA: The Benefits and Costs of the Clean Air Act from 1990 to 2020, 2011.
- Escobedo, F. J. and Nowak, D. J.: Spatial heterogeneity and air pollution removal by an urban forest, *Landscape and urban planning*, 90, 102–110, 2009.
- European Commission: Air Quality Standards, <http://ec.europa.eu/environment/air/quality/standards.htm>, 2015.
- Evan, D.: Leicester City's Air Quality Action Plan 2011-2016, <http://www.leicester.gov.uk/EasysiteWeb/getresource.axd?AssetID=76740&type=full&servicetype=Attachment>, 2011.
- Finn, D., Clawson, K. L., Carter, R. G., Rich, J. D., Eckman, R. M., Perry, S. G., Isakov, V., and Heist, D. K.: Tracer studies to characterize the effects of roadside noise barriers on near-road pollutant dispersion under varying atmospheric stability conditions, *Atmospheric Environment*, 44, 204–214, 2010.
- Forestry-Commission: London Trees and Woodlands Standard Costs, [http://www.forestry.gov.uk/pdf/eng-lon-ltwgs-standard-costs-report-appendix.pdf/\\$FILE/eng-lon-ltwgs-standard-costs-report-appendix.pdf](http://www.forestry.gov.uk/pdf/eng-lon-ltwgs-standard-costs-report-appendix.pdf/$FILE/eng-lon-ltwgs-standard-costs-report-appendix.pdf), 2009.
- Forestry-Commission: National Forest Inventory: NFI preliminary estimates of quantities of broadleaved species in British woodlands, with special focus on ash, [http://www.forestry.gov.uk/pdf/NFI\\\_Prelim\\\_BL\\\_Ash\\\_Estimates.pdf/\\$FILE/NFI\\\_Prelim\\\_BL\\\_Ash\\\_Estimates.pdf](http://www.forestry.gov.uk/pdf/NFI\_Prelim\_BL\_Ash\_Estimates.pdf/$FILE/NFI\_Prelim\_BL\_Ash\_Estimates.pdf), 2013a.
- Forestry-Commission: National Forest Inventory: standing timber volume for coniferous trees in Britain, [http://www.forestry.gov.uk/pdf/FCNFI111.pdf/\\$FILE/FCNFI111.pdf](http://www.forestry.gov.uk/pdf/FCNFI111.pdf/$FILE/FCNFI111.pdf), 2013b.

## C.6 BIBLIOGRAPHY

---

- Franke, J., Hellsten, A., Schlunzen, K. H., and Carissimo, B.: Best practice guideline for the CFD simulation of flows in the urban environment, COST Office Brussels, 2007.
- Freer-Smith, P., El-Khatib, A., and Taylor, G.: Capture of particulate pollution by trees: a comparison of species typical of semi-arid areas (*Ficus nitida* and *Eucalyptus globulus*) with European and North American species, *Water, Air, and Soil Pollution*, 155, 173–187, 2004.
- Furbo, E.: Evaluation of RANS turbulence models for flow problems with significant impact of boundary layers, Master’s thesis, Uppsala University, 2010.
- Galinato, G. I. and Yoder, J. K.: An integrated tax-subsidy policy for carbon emission reduction, *Resource and Energy Economics*, 32, 310–326, 2010.
- Gallagher, J., Gill, L. W., and McNabola, A.: Optimizing the use of on-street car parking system as a passive control of air pollution exposure in street canyons by large eddy simulation, *Atmospheric environment*, 45, 1684–1694, 2011.
- Gallagher, J., Gill, L. W., and McNabola, A.: Numerical modelling of the passive control of air pollution in asymmetrical urban street canyons using refined mesh discretization schemes, *Building and Environment*, 56, 232–240, 2012.
- Gallagher, J., Baldauf, R., Fuller, C. H., Kumar, P., Gill, L. W., and McNabola, A.: Passive methods for improving air quality in the built environment: A review of porous and solid barriers, *Atmospheric Environment*, 120, 61–70, 2015.
- Garratt, J. R.: Review: the atmospheric boundary layer, *Earth-Science Reviews*, 37, 89–134, 1994.
- Gartmann, A.: CFD methods in the atmospheric roughness layer at different scales, Ph.D. thesis, University\_of\_Basel, 2012.
- Grantz, D., Garner, J., and Johnson, D.: Ecological effects of particulate matter, *Environment international*, 29, 213–239, 2003.
- Gromke, C.: A vegetation modeling concept for Building and Environmental Aerodynamics wind tunnel tests and its application in pollutant dispersion studies, *Environmental pollution*, 159, 2094–2099, 2011.

## C.6 BIBLIOGRAPHY

---

- Gromke, C. and Blocken, B.: Influence of avenue-trees on air quality at the urban neighborhood scale. Part II: Traffic pollutant concentrations at pedestrian level, *Environmental Pollution*, 196, 176–184, 2015a.
- Gromke, C. and Blocken, B.: Influence of avenue-trees on air quality at the urban neighborhood scale. Part I: Quality assurance studies and turbulent Schmidt number analysis for RANS CFD simulations, *Environmental Pollution*, 196, 214–223, 2015b.
- Gromke, C. and Ruck, B.: Influence of trees on the dispersion of pollutants in an urban street canyon—experimental investigation of the flow and concentration field, *Atmospheric Environment*, 41, 3287–3302, 2007.
- Gromke, C. and Ruck, B.: Pollutant concentrations in street canyons of different aspect ratio with avenues of trees for various wind directions, *Boundary-layer meteorology*, 144, 41–64, 2012.
- Gromke, C., Buccolieri, R., Di Sabatino, S., and Ruck, B.: Dispersion study in a street canyon with tree planting by means of wind tunnel and numerical investigations—evaluation of CFD data with experimental data, *Atmospheric Environment*, 42, 8640–8650, 2008.
- Gromke, C., Jamarkattel, N., and Ruck, B.: Influence of roadside hedgerows on air quality in urban street canyons, *Atmospheric Environment*, 139, 75–86, 2016.
- Guardian: Four of world’s biggest cities to ban diesel cars from their centres, <https://www.theguardian.com/environment/2016/dec/02/four-of-worlds-biggest-cities-to-ban-diesel-cars-from-their-centres>, 2016.
- Guerreiro, C., Larssen, S., de Leeuw, F., and Foltescu, V.: Air Quality in Europe: 2011 Report, EEA, 2011.
- Guerreiro, C., de Leeuw, F., Foltescu, V., et al.: Air Quality in Europe: 2012 Report, European Environment Agency (EEA), 2012.
- Guerreiro, C., de Leeuw, F., and Foltescu, V.: Air Quality in Europe: 2013 Report, EEA, 2013.

## C.6 BIBLIOGRAPHY

---

- Guerreiro, C., de Leeuw, F., Foltescu, V., and Horalek, J.: Air Quality in Europe: 2014 Report, EEA, 2014.
- Gugamsetty, B., Wei, H., Liu, C.-N., Awasthi, A., Hsu, S.-C., Tsai, C.-J., Roam, G.-D., Wu, Y.-C., and Chen, C.-F.: Source characterization and apportionment of PM<sub>10</sub>, PM<sub>2.5</sub> and PM<sub>0.1</sub> by using positive matrix factorization, *Aerosol Air Qual. Res.*, 12, 476–491, 2012.
- Haaland, C. and van den Bosch, C. K.: Challenges and strategies for urban green-space planning in cities undergoing densification: A review, *Urban Forestry & Urban Greening*, 14, 760–771, 2015.
- Hallquist, M., Wenger, J., Baltensperger, U., Rudich, Y., Simpson, D., Claeys, M., Dommen, J., Donahue, N., George, C., Goldstein, A., et al.: The formation, properties and impact of secondary organic aerosol: current and emerging issues, *Atmospheric Chemistry and Physics*, 9, 5155–5236, 2009.
- Han, X. and Naeher, L. P.: A review of traffic-related air pollution exposure assessment studies in the developing world, *Environment international*, 32, 106–120, 2006.
- Hanjali, K.: Second-Moment Turbulence Closures for CFD: Needs and Prospects\*, *International Journal of Computational Fluid Dynamics*, 12, 67–97, 1999.
- Hanjalic, K.: Closure models for incompressible turbulent flows, VKI Lecture Series, 2005, 2004.
- Hanna, S. R. and Britter, R. E.: Wind flow and vapor cloud dispersion at industrial and urban sites, vol. 7, John Wiley & Sons, 2010.
- Hanna, S. R., Hansen, O. R., and Dharmavaram, S.: FLACS CFD air quality model performance evaluation with Kit Fox, MUST, Prairie Grass, and EMU observations, *Atmospheric Environment*, 38, 4675–4687, 2004.
- Hanna, S. R., Brown, M. J., Camelli, F. E., Chan, S. T., Coirier, W. J., Kim, S., Hansen, O. R., Huber, A. H., and Reynolds, R. M.: Detailed simulations of atmospheric flow and dispersion in downtown Manhattan: An application of five computational fluid dynamics models, *Bulletin of the American Meteorological Society*, 87, 1713–1726, 2006.

## C.6 BIBLIOGRAPHY

---

- Hanna, S. R., Paine, R., Heinold, D., Kintigh, E., and Baker, D.: Uncertainties in air toxics calculated by the dispersion models AERMOD and ISCST3 in the Houston ship channel area, *Journal of Applied Meteorology and Climatology*, 46, 1372–1382, 2007.
- Hargreaves, D. and Wright, N. G.: On the use of the  $k$ - $\epsilon$  model in commercial CFD software to model the neutral atmospheric boundary layer, *Journal of Wind Engineering and Industrial Aerodynamics*, 95, 355–369, 2007.
- Harrison, R., Brimblecombe, P., Derwent, R., Dollard, G., Eggleston, S., Hamilton, R., Hickman, A., Holman, C., Laxen, D., and Moorcroft, S.: Airborne particulate matter in the United Kingdom, Third Report of the Quality of Urban Air Review Group, 1996.
- Heagle, A. S.: Ozone and crop yield, *Annual review of phytopathology*, 27, 397–423, 1989.
- Hereid, D. P. and Monson, R. K.: Nitrogen oxide fluxes between corn (*Zea mays* L.) leaves and the atmosphere, *Atmospheric Environment*, 35, 975–983, 2001.
- Hinds, W. C.: *Aerosol technology: properties, behavior, and measurement of airborne particles*, 1999.
- HoCEAC: Air quality: A follow up report, ninth report of Session 2010-12, <http://www.publications.parliament.uk/pa/cm201012/cmselect/cmenvaud/1024/1024.pdf>, 2011.
- Hodgetts, D.: Laser scanning and digital outcrop geology in the petroleum industry: a review, *Marine and Petroleum Geology*, 46, 335–354, 2013.
- Hofman, J., Bartholomeus, H., Janssen, S., Calders, K., Wuyts, K., Van Wittenberghe, S., and Samson, R.: Influence of tree crown characteristics on the local PM 10 distribution inside an urban street canyon in Antwerp (Belgium): A model and experimental approach, *Urban Forestry & Urban Greening*, 20, 265–276, 2016.
- Holland, S. P., Mansur, E. T., Muller, N. Z., and Yates, A. J.: Damages and Expected Deaths Due to Excess NO<sub>x</sub> Emissions from 2009 to 2015 Volkswagen Diesel Vehicles, *Environmental Science & Technology*, 50, 1111–1117, doi:10.1021/acs.est.5b05190, <http://dx.doi.org/10.1021/acs.est.5b05190>, 2016.

## C.6 BIBLIOGRAPHY

---

- Holman, C. and Consultants, B. C.: IAQM Guidance on the assessment of dust from demolition and construction, Institute of Air Quality Management, London, [www.iaqm.co.uk/text/guidance/construction-dust-2014.pdf](http://www.iaqm.co.uk/text/guidance/construction-dust-2014.pdf), 2014.
- Horbert, M., Vogt, K., and Angeletti, L.: Studies on the deposition of aerosols on vegetation and other surfaces, ORNL-tr-4314, 1976.
- Hsieh, C.-M., Jan, F.-C., and Zhang, L.: A simplified assessment of how tree allocation, wind environment, and shading affect human comfort, *Urban Forestry & Urban Greening*, 2016.
- Huang, R.-J., Zhang, Y., Bozzetti, C., Ho, K.-F., Cao, J.-J., Han, Y., Daellenbach, K. R., Slowik, J. G., Platt, S. M., Canonaco, F., et al.: High secondary aerosol contribution to particulate pollution during haze events in China, *Nature*, 514, 218–222, 2014.
- Invernizzi, G., Ruprecht, A., Mazza, R., De Marco, C., Močnik, G., Sioutas, C., and Westerdahl, D.: Measurement of black carbon concentration as an indicator of air quality benefits of traffic restriction policies within the ecopass zone in Milan, Italy, *Atmospheric Environment*, 45, 3522–3527, 2011.
- Irga, P., Burchett, M., and Torpy, F.: Does urban forestry have a quantitative effect on ambient air quality in an urban environment?, *Atmospheric Environment*, 120, 173–181, 2015.
- Jacob, D.: *Introduction to atmospheric chemistry*, Princeton University Press, 1999.
- Jacob, D. J. and Winner, D. A.: Effect of climate change on air quality, *Atmospheric environment*, 43, 51–63, 2009.
- Jacobs, C. T.: *Modelling of multiphase flows on adaptive unstructured meshes with applications to the dynamics of volcanic ash plumes*, Ph.D. thesis, Imperial College London, 2014.
- Janhäll, S.: Review on urban vegetation and particle air pollution—Deposition and dispersion, *Atmospheric Environment*, 105, 130–137, 2015.
- Jasak, H.: OpenFOAM: open source CFD in research and industry, *International Journal of Naval Architecture and Ocean Engineering*, 1, 89–94, 2009.

## C.6 BIBLIOGRAPHY

---

- Jeanjean, A., Monks, P., and Leigh, R.: Modelling the effectiveness of urban trees and grass on PM<sub>2.5</sub> reduction via dispersion and deposition at a city scale, *Atmospheric Environment*, 147, 1–10, 2016.
- Jeanjean, A., Buccolieri, R., Eddy, J., Monks, P., and Leigh, R.: Air quality affected by trees in real street canyons: The case of Marylebone neighbourhood in central London, *Urban Forestry & Urban Greening*, 22, 41–53, 2017.
- Jeanjean, A. P., Hinchliffe, G., McMullan, W., Monks, P. S., and Leigh, R. J.: A CFD study on the effectiveness of trees to disperse road traffic emissions at a city scale, *Atmospheric Environment*, 120, 1–14, 2015.
- Jicha, M., Pospisil, J., and Katolicky, J.: Dispersion of pollutants in street canyon under traffic induced flow and turbulence, in: *Urban Air Quality: Measurement, Modelling and Management*, pp. 343–351, Springer, 2000.
- Jimenez, J., Canagaratna, M., Donahue, N., Prevot, A., Zhang, Q., Kroll, J. H., DeCarlo, P. F., Allan, J. D., Coe, H., Ng, N., et al.: Evolution of organic aerosols in the atmosphere, *Science*, 326, 1525–1529, 2009.
- Jon, A.: Review of the UK Air Quality Index, A report by the Committee on the Medical Effects of Air Pollutant, [https://www.gov.uk/government/uploads/system/uploads/attachment\\_data/file/304633/COMEAP\\_review\\_of\\_the\\_uk\\_air\\_quality\\_index.pdf](https://www.gov.uk/government/uploads/system/uploads/attachment_data/file/304633/COMEAP_review_of_the_uk_air_quality_index.pdf), 2011.
- Jones, W. and Launder, B.: The prediction of laminarization with a two-equation model of turbulence, *International journal of heat and mass transfer*, 15, 301–314, 1972.
- Jorg, F., Antti, H., Heinke, S., and Bertrand, C.: COST Action 732 Report, [https://www.mi.uni-hamburg.de/fileadmin/files/forschung/techmet/cost/cost\\\_732/pdf/BestPractiseGuideline\\\_1-5-2007-www.pdf](https://www.mi.uni-hamburg.de/fileadmin/files/forschung/techmet/cost/cost\_732/pdf/BestPractiseGuideline\_1-5-2007-www.pdf), 2007.
- Kalansuriya, C., Pannila, A., and Sonnadara, D.: Effect of roadside vegetation on the reduction of traffic noise levels, *Proceedings of the Technical Sessions of the Institute of Physics Sri Lanka*, 25, 1–6, 2009.
- Kassem, H. I., Saqr, K. M., Aly, H. S., Sies, M. M., and Wahid, M. A.: Implementation of the eddy dissipation model of turbulent non-premixed combustion

## C.6 BIBLIOGRAPHY

---

- in OpenFOAM, *International Communications in Heat and Mass Transfer*, 38, 363–367, 2011.
- Katul, G. G., Mahrt, L., Poggi, D., and Sanz, C.: One-and two-equation models for canopy turbulence, *Boundary-Layer Meteorology*, 113, 81–109, 2004.
- Kaur, S., Nieuwenhuijsen, M. J., and Colville, R. N.: Fine particulate matter and carbon monoxide exposure concentrations in urban street transport microenvironments, *Atmospheric Environment*, 41, 4781–4810, 2007.
- Kelly, F., Anderson, H., Armstrong, B., Atkinson, R., Barratt, B., Beevers, S., Derwent, D., Green, D., Mudway, I., and Wilkinson, P.: The impact of the congestion charging scheme on air quality in London. Part 1. Emissions modeling and analysis of air pollution measurements., *Research Report (Health Effects Institute)*, 43, 5–71, 2011.
- Ketterer, C. and Matzarakis, A.: Comparison of different methods for the assessment of the urban heat island in Stuttgart, Germany, *International journal of biometeorology*, 59, 1299–1309, 2015.
- Kim, K.-H., Kabir, E., and Kabir, S.: A review on the human health impact of airborne particulate matter, *Environment international*, 74, 136–143, 2015.
- Knutson, T. R., McBride, J. L., Chan, J., Emanuel, K., Holland, G., Landsea, C., Held, I., Kossin, J. P., Srivastava, A., and Sugi, M.: Tropical cyclones and climate change, *Nature Geoscience*, 3, 157–163, 2010.
- Korsakissok, I. and Mallet, V.: Comparative study of Gaussian dispersion formulas within the Polyphemus platform: evaluation with Prairie Grass and Kincaid experiments, *Journal of applied meteorology and climatology*, 48, 2459–2473, 2009.
- Lalic, B. and Mihailovic, D. T.: An empirical relation describing leaf-area density inside the forest for environmental modeling, *Journal of Applied Meteorology*, 43, 641–645, 2004.
- Lapple, C.: Characteristics of particles and particle dispersoids, *Stanford Research Institute Journal*, 5, 94, 1961.
- Larsen, B., Gilardoni, S., Stenström, K., Niedzialek, J., Jimenez, J., and Belis, C.: Sources for PM air pollution in the Po Plain, Italy: II. Probabilistic uncertainty

## C.6 BIBLIOGRAPHY

---

- characterization and sensitivity analysis of secondary and primary sources, *Atmospheric Environment*, 50, 203–213, 2012.
- Lasek, J., Yu, Y.-H., and Wu, J. C.: Removal of NO<sub>x</sub> by photocatalytic processes, *Journal of Photochemistry and Photobiology C: Photochemistry Reviews*, 14, 29–52, 2013.
- Latza, U., Gerdes, S., and Baur, X.: Effects of nitrogen dioxide on human health: systematic review of experimental and epidemiological studies conducted between 2002 and 2006, *International Journal of Hygiene and Environmental Health*, 212, 271–287, 2009.
- Lauder, B. E. and Spalding, D.: The numerical computation of turbulent flows, *Computer methods in applied mechanics and engineering*, 3, 269–289, 1974.
- Leibensperger, E. M., Mickley, L. J., and Jacob, D. J.: Sensitivity of US air quality to mid-latitude cyclone frequency and implications of 1980–2006 climate change, *Atmospheric Chemistry and Physics*, 8, 7075–7086, 2008.
- Lenschow, P., Abraham, H.-J., Kutzner, K., Lutz, M., Preuß, J.-D., and Reichenbächer, W.: Some ideas about the sources of PM<sub>10</sub>, *Atmospheric Environment*, 35, S23–S33, 2001.
- Li, X.-B., Lu, Q.-C., Lu, S.-J., He, H.-D., Peng, Z.-R., Gao, Y., and Wang, Z.-Y.: The impacts of roadside vegetation barriers on the dispersion of gaseous traffic pollution in urban street canyons, *Urban Forestry & Urban Greening*, 17, 80–91, 2016.
- Litschke, T. and Kuttler, W.: On the reduction of urban particle concentration by vegetation—a review, *Meteorologische Zeitschrift*, 17, 229–240, 2008.
- Liu, C.-H. and Barth, M. C.: Large-eddy simulation of flow and scalar transport in a modeled street canyon, *Journal of Applied Meteorology*, 41, 660–673, 2002.
- Liu, F., Beirle, S., Zhang, Q., Dörner, S., He, K., and Wagner, T.: NO<sub>x</sub> lifetimes and emissions of cities and power plants in polluted background estimated by satellite observations, *Atmospheric Chemistry and Physics*, 16, 5283–5298, 2016.
- Lohila, A., Laurila, T., Tuovinen, J.-P., Aurela, M., Hatakka, J., Thum, T., Pihlatie, M., Rinne, J., and Vesala, T.: Micrometeorological measurements of methane and

## C.6 BIBLIOGRAPHY

---

- carbon dioxide fluxes at a municipal landfill, *Environmental science & technology*, 41, 2717–2722, 2007.
- Lundquist, J. K. and Chan, S. T.: Consequences of urban stability conditions for computational fluid dynamics simulations of urban dispersion, *Journal of applied meteorology and climatology*, 46, 1080–1097, 2007.
- MacKenzie, A. R., Harrison, R. M., Colbeck, I., and Hewitt, C. N.: The role of biogenic hydrocarbons in the production of ozone in urban plumes in southeast England, *Atmospheric Environment. Part A. General Topics*, 25, 351–359, 1991.
- Manso, M. and Castro-Gomes, J.: Green wall systems: A review of their characteristics, *Renewable and Sustainable Energy Reviews*, 41, 863–871, 2015.
- Martin, D., Nickless, G., Price, C., Britter, R., Neophytou, M., Cheng, H., Robins, A., Dobre, A., Belcher, S., and Barlow, J.: Urban tracer dispersion experiment in London (DAPPLE) 2003: field study and comparison with empirical prediction, *Atmospheric Science Letters*, 11, 241–248, 2010a.
- Martin, D., Price, C., White, I., Nickless, G., Petersson, K., Britter, R., Robins, A., Belcher, S. E., Barlow, J. F., Neophytou, M., et al.: Urban tracer dispersion experiments during the second DAPPLE field campaign in London 2004, *Atmospheric Environment*, 44, 3043–3052, 2010b.
- Martin, D., Petersson, K., and Shallcross, D.: The use of cyclic perfluoroalkanes and SF<sub>6</sub> in atmospheric dispersion experiments, *Quarterly Journal of the Royal Meteorological Society*, 137, 2047–2063, 2011.
- Mattai, J., Griffin, A., and Martinez, C.: London Atmospheric Emissions Inventory (LAEI) 2008 User Guide. Report Produced for the Greater London Authority (GLA), Tech. rep., Greater London Authority (GLA), 2008.
- McNabola, A.: New Directions: Passive control of personal air pollution exposure from traffic emissions in urban street canyons, *Atmospheric Environment*, 44, 2940–2941, 2010.
- McNabola, A., Broderick, B., and Gill, L.: Reduced exposure to air pollution on the boardwalk in Dublin, Ireland. Measurement and prediction, *Environment international*, 34, 86–93, 2008.

## C.6 BIBLIOGRAPHY

---

- McNabola, A., Broderick, B., and Gill, L.: A numerical investigation of the impact of low boundary walls on pedestrian exposure to air pollutants in urban street canyons, *Science of the total environment*, 407, 760–769, 2009.
- McNabola, A., O’Luanaigh, N., Gallagher, J., and Gill, L.: The development and assessment of an aspiration efficiency reducing system of air pollution control for particulate matter in building ventilation systems, *Energy and Buildings*, 61, 177–184, 2013.
- Menter, F. R.: Review of the shear-stress transport turbulence model experience from an industrial perspective, *International Journal of Computational Fluid Dynamics*, 23, 305–316, 2009.
- Miao, Y., Liu, S., Chen, B., Zhang, B., Wang, S., and Li, S.: Simulating urban flow and dispersion in Beijing by coupling a CFD model with the WRF model, *Advances in atmospheric sciences*, 30, 1663–1678, 2013.
- Mochida, A., Tabata, Y., Iwata, T., and Yoshino, H.: Examining tree canopy models for CFD prediction of wind environment at pedestrian level, *Journal of Wind Engineering and Industrial Aerodynamics*, 96, 1667–1677, 2008.
- Mønster, J. G., Samuelsson, J., Kjeldsen, P., Rella, C. W., and Scheutz, C.: Quantifying methane emission from fugitive sources by combining tracer release and downwind measurements—a sensitivity analysis based on multiple field surveys, *Waste management*, 34, 1416–1428, 2014.
- Morakinyo, T. E. and Lam, Y. F.: Simulation study of dispersion and removal of particulate matter from traffic by road-side vegetation barrier, *Environmental Science and Pollution Research*, pp. 1–14, 2015.
- Morakinyo, T. E. and Lam, Y. F.: Study of traffic-related pollutant removal from street canyon with trees: dispersion and deposition perspective, *Environmental Science and Pollution Research*, pp. 1–17, 2016.
- Mumovic, D., Crowther, J., and Stevanovic, Z.: Integrated air quality modelling for a designated air quality management area in Glasgow, *Building and environment*, 41, 1703–1712, 2006.

## C.6 BIBLIOGRAPHY

---

- Ndour, M., D'Anna, B., George, C., Ka, O., Balkanski, Y., Kleffmann, J., Stemmler, K., and Ammann, M.: Photoenhanced uptake of NO<sub>2</sub> on mineral dust: Laboratory experiments and model simulations, *Geophysical Research Letters*, 35, 2008.
- Nikolova, I., MacKenzie, A. R., Cai, X., Alam, M. S., and Harrison, R. M.: Modelling component evaporation and composition change of traffic-induced ultrafine particles during travel from street canyon to urban background, *Faraday discussions*, 2016.
- Nowak, D. J., Crane, D. E., and Stevens, J. C.: Air pollution removal by urban trees and shrubs in the United States, *Urban forestry & urban greening*, 4, 115–123, 2006.
- Nowak, D. J., Hirabayashi, S., Bodine, A., and Hoehn, R.: Modeled PM 2.5 removal by trees in ten US cities and associated health effects, *Environmental Pollution*, 178, 395–402, 2013.
- OECD: *Environmental Outlook to 2050: The Consequences of Inaction*, 2012.
- OECD: *Environmental Outlook to 2060*, 2016.
- Oke, T. R.: Street design and urban canopy layer climate, *Energy and buildings*, 11, 103–113, 1988.
- Omidvarborna, H., Kumar, A., and Kim, D.-S.: Recent studies on soot modeling for diesel combustion, *Renewable and Sustainable Energy Reviews*, 48, 635–647, 2015.
- Palacios, M., Núñez, L., Pujadas, M., Fernández-Pampillón, J., Germán, M., Sánchez, B., Santiago, J., Martilli, A., Suárez, S., and Cabrero, B.: Estimation Of NO<sub>x</sub> Deposition Velocities For Selected Commercial Photocatalytic Products, *WIT Transactions on The Built Environment*, 168, 729–740, 2015.
- Parra, M., Santiago, J., Martín, F., Martilli, A., and Santamaría, J.: A methodology to urban air quality assessment during large time periods of winter using computational fluid dynamic models, *Atmospheric Environment*, 44, 2089–2097, 2010.
- Perini, K. and Rosasco, P.: Cost–benefit analysis for green façades and living wall systems, *Building and Environment*, 70, 110–121, 2013.

## C.6 BIBLIOGRAPHY

---

- Perini, K., Ottel , M., Fraaij, A., Haas, E., and Raiteri, R.: Vertical greening systems and the effect on air flow and temperature on the building envelope, *Building and Environment*, 46, 2287–2294, 2011.
- Peters, K. and Eiden, R.: Modelling the dry deposition velocity of aerosol particles to a spruce forest, *Atmospheric Environment*, 26, 2555–2564, 1992.
- Petroff, A. and Zhang, L.: Development and validation of a size-resolved particle dry deposition scheme for application in aerosol transport models, *Geoscientific Model Development*, 3, 753–769, 2010.
- Philips, D. A.: Modeling scalar dispersion in urban environments, Ph.D. thesis, Stanford University, 2012.
- Pitsch, H.: Large-eddy simulation of turbulent combustion, *Annu. Rev. Fluid Mech.*, 38, 453–482, 2006.
- Pope, S. B.: *Turbulent flows*, Cambridge university press, 2000.
- Pugh, T. A., MacKenzie, A. R., Whyatt, J. D., and Hewitt, C. N.: Effectiveness of green infrastructure for improvement of air quality in urban street canyons, *Environmental science & technology*, 46, 7692–7699, 2012.
- Pye, J. M.: Impact of ozone on the growth and yield of trees: a review, *Journal of environmental quality*, 17, 347–360, 1988.
- Richardson, L. F.: *Weather prediction by numerical process*, Cambridge University Press, 1922.
- Riddle, A., Carruthers, D., Sharpe, A., McHugh, C., and Stocker, J.: Comparisons between FLUENT and ADMS for atmospheric dispersion modelling, *Atmospheric environment*, 38, 1029–1038, 2004.
- Rogge, W. F., Hildemann, L. M., Mazurek, M. A., Cass, G. R., and Simoneit, B. R.: Sources of fine organic aerosol. 3. Road dust, tire debris, and organometallic brake lining dust: roads as sources and sinks, *Environmental Science & Technology*, 27, 1892–1904, 1993.
- Rond n, A., Johansson, C., and Granat, L.: Dry deposition of nitrogen dioxide and ozone to coniferous forests, *Journal of Geophysical Research: Atmospheres*, 98, 5159–5172, 1993.

## C.6 BIBLIOGRAPHY

---

- Roupsard, P., Amielh, M., Maro, D., Coppalle, A., Branger, H., Connan, O., Laguionie, P., Hébert, D., and Talbaut, M.: Measurement in a wind tunnel of dry deposition velocities of submicron aerosol with associated turbulence onto rough and smooth urban surfaces, *Journal of Aerosol Science*, 55, 12–24, 2013.
- Roy, S., Byrne, J., and Pickering, C.: A systematic quantitative review of urban tree benefits, costs, and assessment methods across cities in different climatic zones, *Urban Forestry & Urban Greening*, 11, 351–363, 2012.
- Sabatino, S. D., Buccolieri, R., Pappacogli, G., and Leo, L. S.: The effects of trees on micrometeorology in a real street canyon: consequences for local air quality, *International Journal of Environment and Pollution*, 58, 100–111, 2015.
- Salim, S. M., Buccolieri, R., Chan, A., and Di Sabatino, S.: Numerical simulation of atmospheric pollutant dispersion in an urban street canyon: Comparison between RANS and LES, *Journal of Wind Engineering and Industrial Aerodynamics*, 99, 103–113, 2011.
- Salmond, J., Williams, D., Laing, G., Kingham, S., Dirks, K., Longley, I., and Henshaw, G.: The influence of vegetation on the horizontal and vertical distribution of pollutants in a street canyon, *Science of the Total Environment*, 443, 287–298, 2013.
- Salmond, J. A., Tadaki, M., Vardoulakis, S., Arbuthnott, K., Coutts, A., Demuzere, M., Dirks, K. N., Heaviside, C., Lim, S., Macintyre, H., et al.: Health and climate related ecosystem services provided by street trees in the urban environment, *Environmental Health*, 15, 95, 2016.
- Samara, C. and Voutsas, D.: Size distribution of airborne particulate matter and associated heavy metals in the roadside environment, *Chemosphere*, 59, 1197–1206, 2005.
- Samoli, E., Atkinson, R. W., Analitis, A., Fuller, G. W., Green, D. C., Mudway, I., Anderson, H. R., and Kelly, F. J.: Associations of short-term exposure to traffic-related air pollution with cardiovascular and respiratory hospital admissions in London, UK, *Occupational and environmental medicine*, pp. oemed–2015, 2016.
- Sanci, R. and Panarello, H. O.: CO<sub>2</sub> and CH<sub>4</sub> Flux Measurements from Landfills-A Case Study: Gualeguaychú Municipal Landfill, Entre Ríos Province, Argentina, INTECH Open Access Publisher, 2012.

## C.6 BIBLIOGRAPHY

---

- Santiago, J., Borge, R., Martin, F., de la Paz, D., Martilli, A., Lumbreras, J., and Sanchez, B.: Evaluation of a CFD-based approach to estimate pollutant distribution within a real urban canopy by means of passive samplers, *Science of The Total Environment*, 576, 46–58, 2017.
- Santiago, J. L., Martín, F., and Martilli, A.: A computational fluid dynamic modelling approach to assess the representativeness of urban monitoring stations, *Science of the total environment*, 454, 61–72, 2013.
- Santiago, J.-L., Martilli, A., and Martin, F.: On Dry Deposition Modelling of Atmospheric Pollutants on Vegetation at the Microscale: Application to the Impact of Street Vegetation on Air Quality, *Boundary-Layer Meteorology*, pp. 1–24, 2016.
- Scheutz, C., Samuelsson, J., Fredenslund, A. M., and Kjeldsen, P.: Quantification of multiple methane emission sources at landfills using a double tracer technique, *Waste Management*, 31, 1009–1017, 2011.
- Seidel, D. J., Ao, C. O., and Li, K.: Estimating climatological planetary boundary layer heights from radiosonde observations: Comparison of methods and uncertainty analysis, *Journal of Geophysical Research: Atmospheres*, 115, 2010.
- Seinfeld, J. H. and Pandis, S. N.: *Atmospheric chemistry and physics: from air pollution to climate change*, John Wiley & Sons, 2016.
- Selmi, W., Weber, C., Rivière, E., Blond, N., Mehdi, L., and Nowak, D.: Air pollution removal by trees in public green spaces in Strasbourg city, France, *Urban Forestry & Urban Greening*, 17, 192–201, 2016.
- Setälä, H., Viippola, V., Rantalainen, A.-L., Pennanen, A., and Yli-Pelkonen, V.: Does urban vegetation mitigate air pollution in northern conditions?, *Environmental Pollution*, 183, 104–112, 2013.
- Simmonds, P., O’Doherty, S., Nickless, G., Sturrock, G., Swaby, R., Knight, P., Ricketts, J., Woffendin, G., and Smith, R.: Automated gas chromatograph/mass spectrometer for routine atmospheric field measurements of the CFC replacement compounds, the hydrofluorocarbons and hydrochlorofluorocarbons, *Analytical Chemistry*, 67, 717–723, 1995.

## C.6 BIBLIOGRAPHY

---

- Smith, R., Fowler, D., Sutton, M., Flechard, C., and Coyle, M.: Regional estimation of pollutant gas dry deposition in the UK: model description, sensitivity analyses and outputs, *Atmospheric Environment*, 34, 3757–3777, 2000.
- Speak, A., Rothwell, J., Lindley, S., and Smith, C.: Urban particulate pollution reduction by four species of green roof vegetation in a UK city, *Atmospheric Environment*, 61, 283–293, 2012.
- Stavrakou, T., Müller, J.-F., Boersma, K., Kurokawa, J., Ohara, T., Zhang, Q., et al.: Key chemical NO<sub>x</sub> sink uncertainties and how they influence top-down emissions of nitrogen oxides, *Atmospheric Chemistry and Physics*, 13, 9057–9082, 2013.
- Steffens, J. T., Wang, Y. J., and Zhang, K. M.: Exploration of effects of a vegetation barrier on particle size distributions in a near-road environment, *Atmospheric Environment*, 50, 120–128, 2012.
- Stull, R. B.: An introduction to boundary layer meteorology, vol. 13, Springer Science & Business Media, 2012.
- Sullivan, P. P., McWilliams, J. C., and Moeng, C.-H.: A subgrid-scale model for large-eddy simulation of planetary boundary-layer flows, *Boundary-Layer Meteorology*, 71, 247–276, 1994.
- Sundvor, I., Balaguer, N., Mar Viana, X., Reche, C., Amato, F., and Mellios, G.: Road traffic’s contribution to air quality in European cities, ETC/ACM Technical Paper, 14, 1–74, 2012.
- Tai, A. P., Mickley, L. J., and Jacob, D. J.: Correlations between fine particulate matter (PM<sub>2.5</sub>) and meteorological variables in the United States: Implications for the sensitivity of PM<sub>2.5</sub> to climate change, *Atmospheric Environment*, 44, 3976–3984, 2010.
- Tallis, M., Taylor, G., Sinnett, D., and Freer-Smith, P.: Estimating the removal of atmospheric particulate pollution by the urban tree canopy of London, under current and future environments, *Landscape and Urban Planning*, 103, 129–138, 2011.

## C.6 BIBLIOGRAPHY

---

- TFL: Roads Task Force - Technical Note 21. What is air quality on the road network and how does this vary by road type, location and time of day?, Tech. rep., Transport for London (TFL), 2012.
- Tiwary, A., Sinnett, D., Peachey, C., Chalabi, Z., Vardoulakis, S., Fletcher, T., Leonardi, G., Grundy, C., Azapagic, A., and Hutchings, T. R.: An integrated tool to assess the role of new planting in PM 10 capture and the human health benefits: a case study in London, *Environmental pollution*, 157, 2645–2653, 2009.
- Tominaga, Y. and Stathopoulos, T.: Turbulent Schmidt numbers for CFD analysis with various types of flowfield, *Atmospheric Environment*, 41, 8091–8099, 2007.
- Tominaga, Y. and Stathopoulos, T.: CFD modeling of pollution dispersion in a street canyon: Comparison between LES and RANS, *Journal of Wind Engineering and Industrial Aerodynamics*, 99, 340–348, 2011.
- Tominaga, Y. and Stathopoulos, T.: CFD simulation of near-field pollutant dispersion in the urban environment: A review of current modeling techniques, *Atmospheric Environment*, 79, 716–730, 2013.
- Tomlinson, C., Prieto-Lopez, T., Bassett, R., Chapman, L., Cai, X.-M., Thornes, J., and Baker, C.: Showcasing urban heat island work in Birmingham—measuring, monitoring, modelling and more, *Weather*, 68, 44–49, 2013.
- Tong, Z., Baldauf, R. W., Isakov, V., Deshmukh, P., and Zhang, K. M.: Roadside vegetation barrier designs to mitigate near-road air pollution impacts, *Science of the Total Environment*, 541, 920–927, 2016.
- Torno, S., Toraño, J., Menendez, M., Gent, M., and Allende, C.: Prediction of particulate air pollution from a landfill site using CFD and LIDAR techniques, *Environmental fluid mechanics*, 11, 99–112, 2011.
- Trenberth, K. E.: Changes in precipitation with climate change, *Climate Research*, 47, 123–138, 2011.
- UNO: World urbanization prospects: the 2005 revision, United Nations Publications, 2011.
- Vachon, G., Louka, P., Rosant, J., Mestayer, P., and Sini, J.: Measurements of traffic-induced turbulence within a street canyon during the Nantes’ 99 experiment, *Water, Air and Soil Pollution: Focus*, 2, 127–140, 2002.

## C.6 BIBLIOGRAPHY

---

- van den Berg, M., Wendel-Vos, W., van Poppel, M., Kemper, H., van Mechelen, W., and Maas, J.: Health benefits of green spaces in the living environment: A systematic review of epidemiological studies, *Urban Forestry & Urban Greening*, 14, 806–816, 2015.
- van der Zee, S. C., Fischer, P. H., and Hoek, G.: Air pollution in perspective: Health risks of air pollution expressed in equivalent numbers of passively smoked cigarettes, *Environmental Research*, 148, 475–483, 2016.
- Vardoulakis, S., Fisher, B. E., Pericleous, K., and Gonzalez-Flesca, N.: Modelling air quality in street canyons: a review, *Atmospheric environment*, 37, 155–182, 2003.
- Viegas, J. M.: Making urban road pricing acceptable and effective: searching for quality and equity in urban mobility, *Transport Policy*, 8, 289–294, 2001.
- Vong, R. J., Vong, I. J., Vickers, D., and Covert, D. S.: Size-dependent aerosol deposition velocities during BEARPEX’07, *Atmospheric Chemistry and Physics*, 10, 5749–5758, 2010.
- Vos, P. E., Maiheu, B., Vankerkom, J., and Janssen, S.: Improving local air quality in cities: To tree or not to tree?, *Environmental Pollution*, 183, 113–122, 2013.
- Vranckx, S. and Vos, P.: OpenFOAM CFD simulation of pollutant dispersion in street canyons: Validation and annual impact of trees, [http://atmosys.eu/atmosys/faces/doc/ATMOSYS\\_Deliverable\\_9.2b\\_windtunnel\%20validation.pdf](http://atmosys.eu/atmosys/faces/doc/ATMOSYS_Deliverable_9.2b_windtunnel\%20validation.pdf), 2013.
- Vranckx, S., Vos, P., Maiheu, B., and Janssen, S.: Impact of trees on pollutant dispersion in street canyons: A numerical study of the annual average effects in Antwerp, Belgium, *Science of The Total Environment*, 532, 474–483, 2015.
- Wagner, C., Hüttl, T., and Sagaut, P.: Large-eddy simulation for acoustics, vol. 20, Cambridge University Press, 2007.
- Wallace, J. M. and Hobbs, P. V.: Atmospheric science: an introductory survey, vol. 92, Academic press, 2006.
- Wania, A., Bruse, M., Blond, N., and Weber, C.: Analysing the influence of different street vegetation on traffic-induced particle dispersion using microscale simulations, *Journal of Environmental Management*, 94, 91–101, 2012.

## C.6 BIBLIOGRAPHY

---

- Watkiss, P., Eyre, N., Holland, M., Rabl, A., and Short, N.: Impacts of air pollution on building materials, *POLLUTION ATMOSPHERIQUE*, pp. 139–154, 2001.
- Wayne, R. P.: *Chemistry of atmospheres*, New York, NY (United States); Oxford Univ. Press, 1993.
- White, E. and Turner, F.: A method of estimating income of nutrients in a catch of airborne particles by a woodland canopy, *Journal of Applied Ecology*, pp. 441–461, 1970.
- White, M. P., Alcock, I., Wheeler, B. W., and Depledge, M. H.: Would you be happier living in a greener urban area? A fixed-effects analysis of panel data, *Psychological Science*, 24, 920–928, 2013.
- WHO: WHO Air quality guidelines for particulate matter, ozone, nitrogen dioxide and sulfur dioxide: global update 2005: summary of risk assessment, Geneva: World Health Organization, 2006.
- WHO: Review of evidence on health aspects of air pollution: REVIHAAP project: final technical report, 2013.
- WHO: Ambient (outdoor) air quality and health, <http://www.who.int/mediacentre/factsheets/fs313/en/>, 2014.
- WHO: Global Urban Ambient Air Pollution Database (update 2016), [http://www.who.int/entity/phe/health\\_topics/outdoorair/databases/WHO\\_AAP\\_database\\_May2016\\_v3web.xlsx?ua=1](http://www.who.int/entity/phe/health_topics/outdoorair/databases/WHO_AAP_database_May2016_v3web.xlsx?ua=1), 2016.
- Wieringa, J.: Updating the Davenport roughness classification, *Journal of Wind Engineering and Industrial Aerodynamics*, 41, 357–368, 1992.
- Wilson, W. E. and Suh, H. H.: Fine particles and coarse particles: concentration relationships relevant to epidemiologic studies, *Journal of the Air & Waste Management Association*, 47, 1238–1249, 1997.
- WMO: *Guide to Meteorological Instruments and Methods of Observation*, Report, World Meteorological Organization (WMO), 2008.

- Wood, C. R., Barlow, J. F., Belcher, S. E., Dobre, A., Arnold, S. J., Balogun, A. A., Lingard, J. J., Smalley, R. J., Tate, J. E., Tomlin, A. S., et al.: Dispersion experiments in central London: the 2007 DAPPLE project, *Bulletin of the American Meteorological Society*, 90, 955–969, 2009.
- Xie, X., Huang, Z., and Wang, J.-s.: Impact of building configuration on air quality in street canyon, *Atmospheric Environment*, 39, 4519–4530, 2005.
- Yang, F., Gao, Y., Zhong, K., and Kang, Y.: Impacts of cross-ventilation on the air quality in street canyons with different building arrangements, *Building and Environment*, 104, 1–12, 2016.
- Yao, X., Lau, N., Chan, C., and Fang, M.: The use of tunnel concentration profile data to determine the ratio of NO<sub>2</sub>/NO<sub>x</sub> directly emitted from vehicles, *Atmospheric Chemistry and Physics Discussions*, 5, 12 723–12 740, 2005.
- Yazid, A. W. M., Sidik, N. A. C., Salim, S. M., and Saqr, K. M.: A review on the flow structure and pollutant dispersion in urban street canyons for urban planning strategies, *Simulation*, p. 0037549714528046, 2014.
- Zhu, T., Melamed, M., Parrish, D., Gauss, M., Klenner, L. G., Lawrence, M., Konare, A., and Lioussé, C.: WMO/IGAC impacts of megacities on air pollution and climate, World Meteorological Organization Report No. World Meteorological Organization (WMO) Global Atmosphere Watch (GAW) Report, 2012.